Chair of Energy Network Technology

Doctoral Thesis

Evaluating the integration of future e-mobility into distribution power networks

Dipl.-Ing. Bernd Thormann, BSc

February 2022

MONTANUNIVERSITÄT LEOBEN
www.unileoben.ac.at

AFFIDAVIT

I declare on oath that I wrote this thesis independently, did not use other than the specified sources and aids, and did not otherwise use any unauthorized aids.

I declare that I have read, understood, and complied with the guidelines of the senate of the Montanuniversität Leoben for "Good Scientific Practice".

Furthermore, I declare that the electronic and printed version of the submitted thesis are identical, both, formally and with regard to content.

Date 14.02.2022

Signature Author
Bernd Thormann

ABSTRACT

The transition towards e-mobility represents a crucial cornerstone to fulfill global and national climate protection regulations. However, the integration of future electric vehicles into the power system must be planned adequately to prevent grid restrictions in the upcoming years. On this account, the presented thesis initially examines the suitability of conventional grid simulation methods applied to identify future grid reinforcement needs. Considering static deterministic grid simulations, conventional approaches to model grid customers' electrical loads neglect temporal interdependences between different customer classes (e.g., households and electric vehicles). Furthermore, most approaches applied in the current state of research underestimate the grid customers' coincidence at the end of the grid's feeders. Consequently, future grid conditions caused by future electric vehicles, photovoltaic modules, or electric heat pumps are misjudged.

In addition, the presented thesis demonstrates how to accurately quantify future grid reinforcement measures and costs in a large-scale area. Due to the heterogeneity of real-life grids, the simulation of a few individually selected grids and the scaling of their results might lead to erroneous assessments. In fact, several thousand low-voltage grids must be simulated to quantify total grid reinforcement costs adequately. This thesis develops and presents a fully automated large-scale grid simulation tool to overcome the highlighted shortcomings. The developed tool allows the simulation of several thousand grid structures while keeping the required computing time adequate. Furthermore, it uses novel coincidence factors, modeled and validated in this thesis, to take temporal interactions between all customer classes into account. Thereby, future grid conditions are estimated correctly, and grid reinforcement costs are accurately quantified.

Besides identifying future grid restrictions, the presented thesis analyzes how various e-mobility use cases can be integrated into the existing distribution grid in a grid-friendly way. Considering electric vehicles charged at home or work, classic grid reinforcement measures can successfully be prevented by the analyzed voltage-controlled measures. However, limiting the available charging power, e.g., by implementing adequate charging tariffs, is the most effective measure to prevent future grid congestions. Furthermore, decentralized energy storage systems enable the grid-friendly supply of e-mobility use cases with strict schedules, e.g., electric busses, requesting high-power charging to fulfill their mobility needs.

Implementing the findings, tools, and methods acquired and developed in this work will increase the accuracy and the level of detail of future grid planning processes. Thereby, this thesis helps design the future power system more adequately to enable the integration of future e-mobility.

KURZFASSUNG

Die Elektrifizierung des Verkehrssektors stellt eine entscheidende Säule zur Erreichung der globalen und nationalen Klimaschutzziele dar. Die Integration zukünftiger Elektrofahrzeuge in das bestehende Stromnetz erfordert frühzeitige Planung, um zukünftigen Netzengpässen vorzubeugen.

Zu diesem Zweck untersucht die vorliegende Arbeit zunächst die Eignung konventioneller Simulationsmethoden zur Identifikation zukünftiger Netzauswirkungen. Herkömmliche Lastansätze, die in statisch-deterministischen Netzsimulationen zum Einsatz kommen, vernachlässigen die zeitliche Überlagerung unterschiedlicher Kundentypen (z. B. Haushalte und Elektrofahrzeuge). Zusätzlich unterschätzen sie die Gleichzeitigkeit der Netzkunden am Ende des Netzstrangs. Folglich werden zukünftige Netzengpässe, hervorgerufen durch zukünftige Netzkunden, falsch eingeschätzt. Darüber hinaus verdeutlicht die vorliegende Arbeit, wie zukünftige Netzverstärkungskosten in einem großflächigen Netzgebiet quantifiziert werden können. Aufgrund der hohen Heterogenität von Niederspannungsnetzen, kann die Simulation einiger weniger, individuell ausgewählter Netze und die Skalierung ihrer Ergebnisse zu einer Fehleinschätzung führen. Die Genauigkeit der Kostenabschätzung steigt jedoch mit zunehmender Anzahl der simulierten Netze.

Um den aufgezeigten Unsicherheiten entgegenzuwirken, wird im Rahmen dieser Arbeit ein vollautomatisiertes Netzberechnungstool präsentiert. Dieses ermöglicht die detaillierte Simulation mehrerer tausend Netze bei angemessener Rechenzeit. Mithilfe der im Rahmen dieser Arbeit entwickelten neuartigen Gleichzeitigkeitsfaktoren wird das zeitliche Zusammenspiel sämtlicher Kundentypen realistisch abgebildet.

Zusätzlich analysiert die vorliegende Arbeit zahlreiche Maßnahmen für eine netzschonende Netzintegration unterschiedlicher Use Cases der Elektromobilität: Netzgesteuerte Maßnahmen ermöglichen eine netzschonende Versorgung von Elektrofahrzeugen, die zu Hause oder am Arbeitsplatz laden. Die Begrenzung der verfügbaren Ladeleistung, z. B. durch entsprechende Ladetarife, stellt diesbezüglich jedoch die effektivste Maßnahme dar. Use Cases, die aufgrund ihrer strikten Zeitpläne hohe Ladeleistungen benötigen (z. B. Elektrobusse), lassen sich mithilfe dezentraler Energiespeichersysteme unter der Vermeidung klassischer Netzausbaumaßnahmen integrieren.

Die Anwendung der in dieser Arbeit gewonnenen Erkenntnisse, sowie entwickelter Tools und Methoden erhöht die Genauigkeit und den Detaillierungsgrad zukünftiger Netzplanungsprozesse. Damit trägt diese Arbeit dazu bei, das zukünftige Stromnetz angemessen zu gestalten, um die Integration der zukünftigen Elektromobilität zu ermöglichen.

FOREWORD

After finishing my master thesis, I got the chance to continue my research in e-mobility and its integration into the power system. So I began working at the chair of Energy Network Technology and started my PhD-thesis in December 2017. Since then, many people have supported me on this journey, whom I want to express my sincerest thanks.

I want to start with my supervisor and head of the chair of Energy Network Technology, Thomas. Thank you so much for giving me the opportunity to deal with this field of research by cooperating in several research projects and participating in many national and international conferences. Thereby, I learned a lot about scientific and independent working during the last four years. Moreover, I was lucky to establish new contacts in the field of e-mobility and power grids, from which I profited tremendously. I really enjoyed our professional discussions and chats in numerous PhD-Talks. The fact that we share the (almost) same idea of e-mobility made work so much easier for me.

My deepest thank to Anna. You helped me every time I had questions in the field of electrical engineering and power systems. In addition, our professional discussions really improved my scientific work and helped me overcome some obstacles on my journey. Sharing an office with you for almost a year was a great pleasure. Besides work, you have become a very important part of my life and supported me in many ways. You made my time at the chair of Energy Network Technology so much more fun.

Great thanks also to you, Julia. You supervised my master thesis and helped me to get accustomed to my work at the chair of Energy Network Technology. I enjoyed sharing an office room with you for most of the time and the chats about work-related and private things. Philipp, Wildfried, and Thomas, your scientific works helped me a lot during my journey and are a significant part of this thesis. I really appreciate the effort and spirit you have shown during your bachelor's and master's thesis! Many thanks to all my other colleagues, Jasmin, Rebekka, Elisabeth, Kerstin, Maedeh, Roberta, Vanessa, Lisa, Mahshid, Andreas, Christoph, Johannes, Matthias, Thomas, Paul, David, Peter, Christopher, Josef, and Nouman—I really enjoyed working with you.

Of course, special thanks to my parents, Karin and Helmut, for supporting me all the way during this time. You always knew how to cheer me up during challenging and stressful times. Huge thanks to my brother, Micha, who constantly challenged me with his way, way too intelligent, and hard-to-answer questions. Though, discussions with you helped me understand some aspects of my work even more clearly.

Thank you so much to all of you!

CONTENTS

NOMENCLATURE

Abbreviation

EV	Electric vehicle
DSO	Distribution system operator
MV	Medium voltage
LV	Low voltage
PV	Photovoltaic
HP	Heat pump
ESS	Energy storage system
DC	Direct current
AC	Alternating current

Indices

Indices	Description [Unit]
R‘	Specific resistance [Ω/km]
X‘	Specific inductance [Ω/km]
R	Total resistance [Ω]
X	Total inductance [Ω]
$\Delta\underline{U}$	Complex voltage deviation between a grid line’s sending- and receiving-end [V]
$\underline{U}_1$	Complex sending-end voltage [V]
$\underline{U}_2$	Complex receiving-end voltage [V]
U_t	Transverse voltage deviation between a grid line’s sending- and receiving-end [V]
U_l	Longitudinal voltage deviation between a grid line’s sending- and receiving-end [V]
ϑ	Phase angle between the sending- and receiving-end voltage [°]

I_a	Active current transmitted by a grid line [A]
I_r	Reactive current transmitted by a grid line [A]
P	Active power [W]
Q	Reactive power [var]
$S''_{s,node}$	Short-circuit apparent power at a node [VA]
$U_{Nom.}$	Nominal voltage [V]
c	Voltage factor [-]
Z_{node}	Impedance between a grid node and the power supply [Ω]
$\underline{U_i}$	Complex voltage at node i [V]
$\underline{I_i}$	Complex current injected at node i [A]
$\underline{\boldsymbol{Y}}$	Node admittance matrix [S]
$\underline{Y_{ij}}$	Complex admittance between node i and node j [S]
δ	Phase angle of voltage [°]
$\underline{S_i}$	Complex apparent power injected at a node [VA]
$\underline{P_i}$	Complex active power injected at a node [W]
Q_i	Complex reactive power injected at a node [var]
$\Delta\boldsymbol{P}$	Deviation between the targeted and calculated active power [W]
$\Delta\boldsymbol{Q}$	Deviation between the targeted and calculated reactive power [var]
ν	Iteration [-]
$\boldsymbol{x}$	Vector including all nodes' voltages and phase angles [V,°]
$\boldsymbol{J}$	Jacobi matrix [W/V, W/°, var/V, var/°]
NoC	Number of customers [-]
$P_{Aggregated}$	Aggregated active power [W]
$P_{cust.}$	Active power of grid customers [W]
S_{nom}	Nominal apparent power [VA]
S_{EV}	Apparent power of EV charging [VA]

S_{ESS}	Apparent power of ESS [VA]
$S_{Load,init}$	Initial apparent power of grid elements [VA]
$S_{max,therm}$	Maximum thermal apparent power of grid elements [VA]
P_{ESS}	Apparent power of ESS [W]
$\eta_{Discharging}$	Discharging efficiency of ESS [-]

LIST OF FIGURES

LIST OF TABLES

1 INTRODUCTION

The increase of greenhouse gas emissions within the last decades has unquestionably been the major driver of global warming and resulting climate- and environmental-related challenges [1]. In Europe, for example, more than a fourth of greenhouse gas emissions are caused by the traffic sector. Thereof, road transport accounted for 71.7 % in 2019, including passenger vehicles (43.5%), heavy-duty trucks and busses (18.8%), light-duty trucks (8.5%), and others (0.9 %). [2] In the European Green Deal [3], the European Commission defined multiple goals to decarbonize the traffic sector: Increasing transport's efficiency by forcing multimodal transport, removing fossil-fuel subsidies, and implementing more stringent CO_2-emission targets for vehicles. Considering the latter, passenger vehicles (- 37.5 % by 2030), vans (- 31 %), and trucks (- 30 %) must decisively reduce their greenhouse gas emissions [4, 5].

However, the achievement of these ambitious emission targets requires, among other things, enhancing the electrification of the traffic sector in the future. In fact, e-mobility has already been declared on the global [6] and European level [3] to be forced and promoted in the upcoming years. Therefore, monetary and non-monetary incentives should foster the share of registered electric vehicles (EVs) [7]. Furthermore, public charging infrastructure is implemented extensively (one million public charging points by 2025 [8]) to reduce range anxiety [9] and allow long-distance traveling with EVs [3]. All these measures combined will further raise the number of registered EVs in the following decades (Figure 1). Depending on Austria's political and economic framework conditions, between 21 – 27 % of passenger vehicles might be electrified by 2030 [10–14]. In 2050, the share of EVs in Austria might deviate between 52 – 100 % [10, 12, 13, 15].

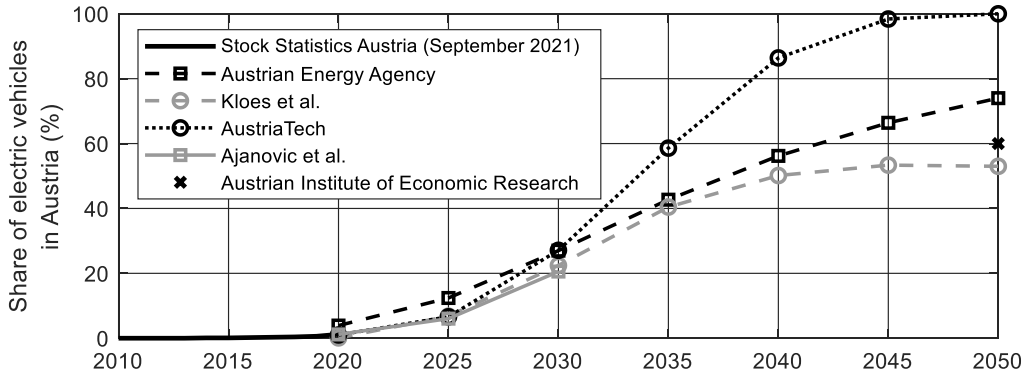

Figure 1: Actual and forecasted share of electric vehicles in Austria (own illustration based on [10–15])

While these trends contribute to the traffic sector's decarbonization, the supply of future EVs will unquestionably challenge the existing energy- and power system. As demonstrated in several studies, the charging of EVs will increase the energy demand in the upcoming years [16–18], e.g., between 14 - 16 % if all vehicles are electrified [19, 20]. Furthermore, these

amounts of energy must be supplied by local distribution networks. From the perspective of a distribution system operator (DSO), EVs represent new customers characterized by high nominal power (compared to existing customers) and high, challenging-to-predict energy demand [21]. As a result, their integration must comply with local grid conditions. Recent studies (e.g. [22–27]) demonstrate limited capacity on the medium- (MV) and low-voltage (LV) levels to integrate these new customers. **Hence, the integration of e-mobility into the power system must be planned at an early stage by prematurely identifying EV-induced grid restrictions.**

In addition to EVs, present-day distribution networks face new challenges due to the forced implementation of other domestic low-carbon technologies, e.g., photovoltaic (PV) modules and electric heat pumps (HP) [28]. PV modules feed power into the power system during midday hours based on the sun's daily course. The power demand of electric HPs, on the other hand, shows several peaks during the day, especially during winter [28, 29]. Hence, when planning the grid integration of future e-mobility, existing (e.g., households, commercial businesses) and future grid customers' temporal characteristics (e.g., PV modules, HPs) must be investigated together.

Besides the temporal aspect, the spatial development of future EVs, domestic PV modules, and HPs is crucial to identify future grid reinforcement measures. Suburban and rural areas are characterized by a high share of single- or two-family houses. Compared to multi-apartment residual buildings, they facilitate the installation of private charging infrastructure at home (the preferred location of charging [30–33]), domestic PV modules, or electric HPs. Hence, the transition towards those technologies will occur in large parts in suburban and rural areas [34–36]. **Both temporal and spatial criteria must be met to identify EV-induced grid restrictions. This can be done by performing detailed load flow simulations. Therefore, temporal interdependences between various customer classes and different grid regions' characteristics can be considered.**

In case of grid congestions, existing grid structures are usually extended or reinforced, e.g., by installing additional grid lines or by enhancing substations' capacities. However, those classic grid reinforcement measures often entail significant investment costs and lengthy processes [37]. Consequently, the future integration of additional EVs could be postponed or even inhibited. Furthermore, the timespan, most distribution grids require increased capacity is limited to a few hours per year [38]. Grid-relieving measures, e.g., implementing demand-side measures or energy storage systems (ESSs), might provide the required capacity during that period. Thus, the power grid can be designed for the most frequent grid conditions, and classic grid reinforcement measures can be reduced to a high extend. **Therefore, various grid-**

relieving measures must be examined as alternatives to classic grid reinforcements and included in future grid planning processes.

Besides private passenger vehicles, decarbonizing the traffic sector also requires the electrification of other vehicles classes. For example, numerous countries have already integrated electric busses into their public transportation system, above all China with a projected number of more than 1.3 billion busses in 2025 [39]. Several Austrian cities also operate electric busses for public transportation [40]. Furthermore, more and more taxies and car sharing vehicles have been electrified because of benefits in city transport compared to vehicles with an internal combustion engine (lower fuel costs, lower maintenance effort, and faster acceleration) [41, 42]. EVs are also applicable for last-mile delivery providers, e.g., retail or postal services [43], due to their constant mobility needs. Indeed, more and more last-mile delivery providers have already electrified their fleets (e.g., [44]). These trends demonstrate that the electrification of the transport sector includes several e-mobility use cases.

However, future e-mobility use cases differ considerably regarding vehicle specifics (e.g., specific energy consumption, battery capacity) and charging behavior (e.g., time and power of charging). Both represent crucial aspects for determining the EVs' future charging loads which the local power grid must supply. While EV manufacturers define vehicle specifics, the EVs' temporal charging behavior strongly depends on individual mobility patterns, including parking time (Figure 2), covered distances, and the number of trips.

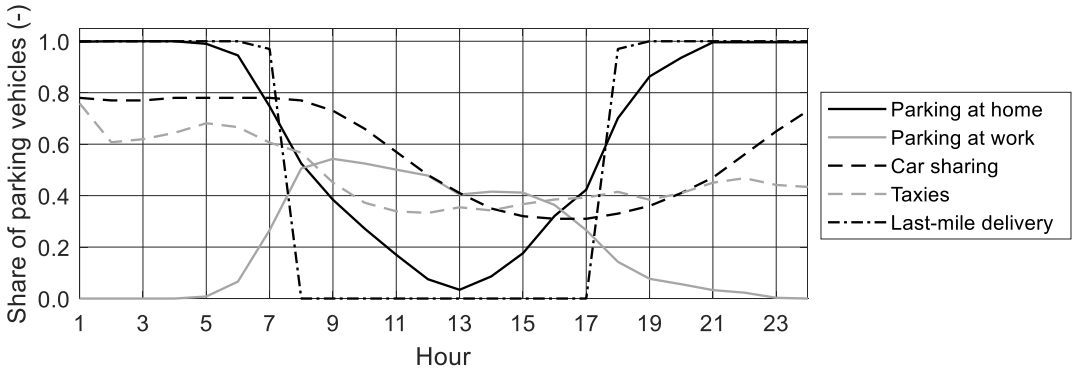

Figure 2: Time-resolved share of parking vehicles considering various e-mobility use cases [45]

The majority of private EVs, for example, are parked at home between 18:00 – 08:00 or at work during the day. Flexibility options, implemented to prevent classic grid reinforcement measures, must comply with mobility- and charging patterns of future EV use cases. For example, e-busses or last-mile delivery EVs impede demand-side measures to assure a fast onward journey. **On this account, the evaluation of grid-relieving measures must include various EV use cases and accurately predict their mobility patterns and charging behavior**.

2 STATE OF RESEARCH

As demonstrated in Chapter 1, the planning of integrating future e-mobility into the power system must include the following aspects:

- Identifying EV-induced grid restrictions using detailed load flow simulations (Chapter 2.1): Therefore, temporal interdependences between EVs, PV modules, and HPs (Chapter 2.1.1) as well as differences in grid regions (Chapter 2.1.2) should be considered
- Evaluating grid-relieving measures including various EV use cases' mobility- and charging patterns (Chapter 2.2)

The following chapters illustrate whether the current state of research fulfills the criteria mentioned above. Therefore, recent studies evaluating the integration of e-mobility into the power system are divided accordingly.

2.1 Identifying EV-induced grid restrictions using load flow simulations

2.1.1 Temporal interdependences between customer classes

Recent studies (e.g., [22, 23, 37, 38, 46–55]) have already analyzed the impacts of EVs, PV modules, or HPs on the present-day power system. However, they differ in the applied simulation method and how temporal interdependences between different customer classes are taken into account: Some studies determine potential grid bottlenecks based on time-series analyses [37, 48–51]. Thereby, temporal differences between EVs, PV modules, and HPs are included by using time-resolved profiles. Monte-Carlo simulations provide another possibility to estimate future grid restrictions and are applied by several works [38, 46, 47, 55]. Therefore, the power at each grid node is stochastically determined for numerous iterations based on statistical data [56]. As a result, temporal interactions between customers classes are considered based on their probability of occurrence. While time series analyses and Monte-Carlo simulations facilitate the consideration of temporal customer interdependences, they require the simulation of several time steps or iterations (Chapter 5.3.2). In contrast, static deterministic grid simulations, applied by several recent studies [22, 23, 53, 54, 57–59], allow much faster computation [60, 61]. In this simulation method, grid customers' aggregated load in the power grid is determined using coincidence factors [62, 63]. The coincidence factor takes temporal characteristics and interdependences between multiple grid customers into account. However, recent studies' coincidence factors only consider temporal interdependences individually within one customer class (e.g., households or EVs).

Temporal interactions between customer classes, such as EVs, HPs, and PV modules, are neglected in the current state of research using static deterministic grid simulations.

In addition, recent studies consider different grid elements in the power grid to determine grid customers' coincidence factors: While many studies (e.g., [22, 53]) neglect to define this detail, the majority of studies [23, 53, 57, 58] determine coincidence factors based on the number of grid customers supplied by the MV/LV substation. Others [22, 59] use the number of customers supplied by each feeder to estimate coincidence factors applied for load flow simulation. However, none of these studies takes grid customers' coincidence at the end of feeders into account.

2.1.2 Differences in grid regions

Besides the applied simulation method, the current state of research varies concerning the analyzed distribution networks and their region: Many recent works only analyze single distribution grids in urban [48, 51] and rural areas [46]. However, these studies exclude real-life housing types (e.g., family houses, multi-apartment residential buildings) and, thereby, their ability to integrate future EVs, PV modules, or HPs. Furthermore, most works neglect defining the analyzed grid region (e.g., [37, 47, 50]).

While the studies mentioned above analyze the impact of EVs on one grid respectively, others quantify EV-induced grid reinforcement measures in a large area, including several thousand LV grids. Therefore, they use two different methods: Most recent works [22, 23, 38, 54, 55] identify potential grid congestions in individually selected, representative grids based on load flow simulation. The selected grids' results are aggregated and scaled to the whole area of investigation. The other group of studies [53, 59] quantifies the total grid reinforcement needs by simulating each grid in the investigated area. Based on the different quantification methods applied in recent studies, their results substantially differ when considering the same scenario [55]. Hence, the current state of research misses a comparison of different quantification methods (scaling of individually selected grids' results or simulating all grids) and their impact on estimating future grid reinforcement costs.

2.2 Evaluating grid-relieving measures applied to mitigate EV-induced grid impacts

While research presented in Chapter 2.1 focuses on identifying EV-induced grid congestions, this chapter describes studies examining the suitability of grid-relieving measures to prevent them. However, the grid-friendly application of such options must comply with the particular e-mobility use case and its mobility- and charging patterns. Due to their long daily duration connected to the power grid, EVs charged at home (mainly during the night) or at work (mainly

during the day) allow for the control of charging processes. Thus, recent studies [64–71] primarily focus on demand response based on controlled charging (Chapter 5.4.4) regarding these use cases [72]. They either attempt to mitigate local grid congestions on the distribution level [64–69] or increase the share of charged energy generated by local PV [70, 71].

Furthermore, the prevention of voltage violations triggered by EVs charged at home or work is dealt with in previous research. Therefore, voltage-controlled reactive- [73, 74] or active power regulation [75–77] is implemented into EV charging infrastructure (Chapter 5.4.2). Thereby, the available charging power of EVs is adapted according to the actual voltage in the supplying distribution network. Other studies [78–81] combine those concepts with the control of charging processes to increase their effectiveness. Besides charging at home or work, the grid-dependent regulation of reactive charging power has been applied for public fast-charging of EVs [82, 83]. Several recent studies analyzed the potential of distribution transformers equipped with on-load tap-changers (Chapter 5.4.1) to prevent voltage violations on the LV level triggered by EVs charged at home [84] or elsewhere [85–87].

Besides investigating demand-side and voltage-controlled measures, several recent studies focus on decentralized ESSs to support EV charging (Chapter 5.4.3). They can be classified depending on the ESS's objective: Multiple works [88–93] investigate the potential of ESSs to minimize the operation costs of EV charging. Another study [94] tries to maximize the share of charged energy locally generated by renewable energy sources. However, most studies [95–106] investigate the implementation of decentralized ESSs to cover EV-induced peak loads according to classic peak shaving. The latter group can further be divided according to their analyzed e-mobility use case. They analyze ESS specifications required to supply public charging points [96–99, 104, 105], domestic charging at home [100, 101], e-bus charging [95, 106]. Some studies neglect defining the considered use case [102, 103].

However, most studies presented in this chapter consider only one particular use case. Although, none of these studies analyze the flexibility required to integrate electric last-mile delivery vehicles into present-day distribution networks preventing grid restrictions. In addition, recent works focus on one charging power of EVs, and a fixed number of available charging points, respectively. As a result, the correlations between the flexibility demand and the different use cases' mobility patterns, charging power, and the number of charging points are missing in the current state of research. Similarly, many studies in this regard focus on one particular measure (e.g., [65, 66, 73, 78]) to relieve stress from the LV grid. Hence, they neglect a direct comparison of possible stress mitigation measures. Furthermore, grid-relieving measures are primarily evaluated based on economic aspects [95, 97, 105, 106]. On the contrary, technical criteria have been neglected so far in the current state of research.

3 RESEARCH QUESTIONS

Chapter 1 demonstrates multiple criteria essential to plan the integration of future e-mobility into distribution grids: Firstly, temporal interdependences between grid customers and differences in grid regions must be considered when identifying EV-induced grid restrictions. Secondly, evaluating potential grid-relieving measures must consider various EV use cases' mobility and charging patterns. However, the current state of research (Chapter 2) often neglects these criteria. Hence, the following research questions unanswered by the current state of research should be addressed in this work.

According to Chapter 2, the described criteria and related research questions are divided into two fields: The first field of research deals with the **identification of EV-induced grid restrictions**. In this regard, modern-day grid planning primarily relies on numerical grid analyses based on load flow simulations (Chapter 5.3). However, as highlighted in Chapter 2.1, the following research questions in this field are unanswered in the current state of research:

1) How to realistically consider temporal interdependences between grid customers (e.g., EVs, PV modules, and HPs) using static deterministic load flow simulations?
2) How many coincidence factors (single, double, multiple) must be applied for each grid, and based on which grid elements should they be determined?
3) What is the qualitative correlation between the region (urban, suburban, rural) of the analyzed LV grids and their hosting capacity in terms of voltage violations and thermal congestions?
4) How many LV grids (in %) must be simulated to quantify future grid reinforcement costs in a large service area with adequate accuracy?
5) How to technically (required reinforcement measures) and economically (required costs) quantify future grid reinforcement needs?

The second field of research includes the **evaluation of grid-relieving measures** as a countermeasure to classic grid reinforcements. In this field, the following research questions are unanswered in the current state of research and addressed in the presented thesis:

6) Which grid-relieving measures are suitable for preventing classic grid reinforcement measures while complying with user behavior of EV use cases?
7) How must these measures be designed and operated to provide sufficient grid support depending on the supplying EV use case?
8) Can grid-relieving measures provide cost benefits compared to classic grid reinforcements? If so, can they still be operated at technical optima?

3.1 Structure of this work

The methodology applied to answer the highlighted research questions, including the papers' contribution to this work, is described in detail in Chapter 4. To ensure the required theoretical background, Chapter 5 summarizes the state-of-the-art in the fields of EV charging (5.1), the structure of the electricity system (5.2), load flow simulations (5.3), and grid-relieving measures (5.4).

Chapter 6 demonstrates the thesis' results for answering the research questions in both research fields: Identifying EV-induced grid restrictions (6.1) and evaluating the potential of grid-relieving measures (6.2). Chapter 7 provides a holistic discussion of acquired results and presents the conclusions derived from this thesis. Finally, Chapter 8 gives an outlook to further studies in this thesis' research fields.

Relevant journal and conference papers published during this dissertation can be found in Appendix A, including contribution statements. Appendix B lists additional conference papers and other scientific articles contributed to this work.

4 METHODOLOGY

The presented thesis gives answers to all research questions highlighted in Chapter 3. Therefore, it refers to the author's works published in three peer-reviewed journals and three conference papers (Appendix A). This chapter describes the applied methodology, the connection between published papers, and how they contribute to this thesis.

The methodology applied in this thesis can be divided into three parts illustrated in Figure 3: As the foundation for both research fields (identification of grid restrictions and evaluating the potential of grid-relieving measures), realistic charging profiles of different EV use cases are modeled based on real-life mobility patterns, measured charging curves, and EV specifics. Table 1 illustrates which e-mobility use cases are modeled and analyzed in the author's works. A detailed description of analyzed e-mobility use cases can be found in the respective papers.

Table 1: E-mobility use cases analyzed in this work and corresponding journal and conference papers

Use Case	Paper 1	Paper 2	Paper 3	CIRED 2019	NEIS 2019	IEWT 2021
Charging at home	✓		✓	✓	✓	
Charging at work	✓					
On-street public charging					✓	
Highway fast-charging		✓				✓
e-taxies						✓
e-car sharing						✓
e-busses		✓				✓
Electric last-mile delivery vehicles		✓				✓

The applied modeling approaches have been published in Paper 1 and 2 [29, 107]:

> THORMANN, B.; KIENBERGER, T., *Evaluation of Grid Capacities for Integrating Future E-Mobility and Heat Pumps into Low-Voltage Grids,* In: Energies 2020, 13, 5083. doi.org/10.3390/en13195083
>
> THORMANN, B.; PUCHBAUER, P.; KIENBERGER, T., *Analyzing the suitability of flywheel energy storage systems for supplying high-power charging e-mobility use cases*, In: Journal of Energy Storage 2021, 39, 102615, doi: 10.1016/j.est.2021.102615.

The second step is about the identification of potential grid restrictions caused by EV charging by performing numerical load flow simulations (Chapter 6.1). Therefore, novel coincidence factors are calculated based on the modeled time series. The author published this work in Paper 1.

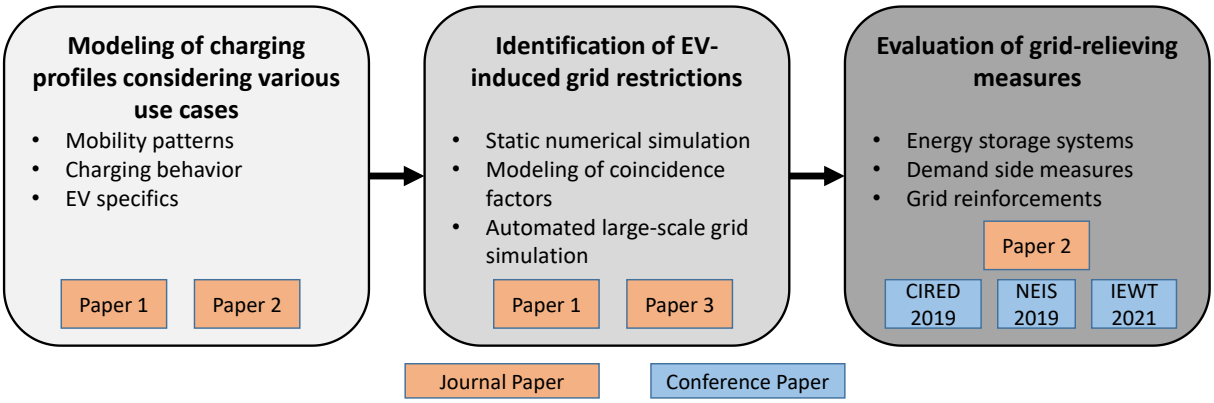

Figure 3: Methodology of this work including corresponding journal and conference papers

Furthermore, a fully automated large-scale grid simulation tool is developed to analyze several thousand grids and quantify future grid reinforcement needs. The developed tool is described and published in Paper 3 [108]:

> THORMANN, B.; KIENBERGER, T., *Estimation of Grid Reinforcement Costs Triggered by Future Grid Customers: Influence of the Quantification Method (Scaling vs. Large-Scale Simulation) and Coincidence Factors (Single vs. Multiple Application),* In: Energies 2022, 15, 1383, doi: 10.3390/en15041383

In addition, one journal- and three conference papers analyze the following flexibility options to mitigate EV-induced grid restrictions (Chapter 6.2) and give answers concerning their design: ESSs (NEIS 2019 [109], Paper 2 [107], IEWT 2021 [110]), as well as grid-controlled and demand-side measures (CIRED 2019 [111]). All these measures represent countermeasures to classic grid reinforcement measures (e.g., transformer- and line extensions).

5 THEORETICAL BACKGROUND

The following chapter provides the theoretical background necessary to put the presented work into context. Therefore, the state of the art regarding electric vehicles and their charging infrastructure is summarized (Chapter 5.1). Chapter 5.2 describes the structure of the current power system. The concept of load flow simulations to analyze and plan the power system is illustrated in Chapter 5.3. Finally, different measures to prevent conventional grid reinforcements are depicted (Chapter 5.4).

5.1 Electric vehicles and charging infrastructure

Although the electrification of vehicles started more than 180 years ago, it just accelerated in the past few years due to breakthroughs in lithium-ion technology and the increased attention regarding climate protection [112]. Per definition, the group of four-wheeled EVs includes all vehicles with one or more electric machines integrated into their drive unit. While battery EVs are powered only by the electric machine, hybrid EVs have an additional power source (e.g., an internal combustion engine) integrated into the vehicle. [113] The latter can be classified according to their drive train design (parallel, serial, or combined) or their degree of hybridization (micro, mild, full, or plug-in hybrid). From all EVs mentioned above, only battery and plug-in hybrid EVs allow the recharging of their battery via an external power source, e.g., the power grid. [114] While the power system must supply both types of EVs, the market share of plug-in hybrid EVs will likely decrease in the upcoming years in favor of battery EVs [115]. Hence, only four-wheeled battery EVs are considered in this thesis and, from now on, consistently termed EV.

Today, electric versions of many vehicle classes (e.g., busses [116], trucks [117], vans [118], passenger vehicles [119, 120]) are available on the market. However, those substantially differ in their vehicle specifics: While today's passenger EVs and e-vans provide a battery capacity between 17.6 - 95 kWh [121] and 33 - 79 kWh [118, 122–125], e-busses (85 - 550 kWh) [126] and e-trucks (343 - 540) [117, 127, 128] can store a higher amount of energy. This is indeed necessary, due to a significantly higher specific energy demand: 0.147 – 0.240 kWh/km [121] and 0.250 – 0.530 kWh/km [129] considering passenger EVs and e-vans, 1.160 – 1.990 kWh/km [130] considering e-busses and 0.980 – 1.440 kWh/km [131, 132] considering e-trucks.

Theoretically, EV charging can be done via the conventional (domestic) power socket. However, in most cases, EVs are charged via a charging station to allow for higher charging power and shorten the required duration of charging. Most public charging stations provide two or more charging points (connection of one EV), enabling the simultaneous charging of

multiple EVs [115]. Since the EV's battery requires direct current (DC) to be recharged, power electronics convert alternating current (AC) from the power grid into DC. AC/DC and DC/DC inverters are either integrated into the EV (AC charging) or into the charging infrastructure (DC charging) [115]. However, some existing EV models do not support DC charging and only use AC charging [133].

Furthermore, state-of-the-art EV models vary in their possible charging power and their number of phases used for AC charging. While some EV models only support one- or two-phase AC charging with a charging power of 3.7 or 7.4 kVA, the general trend is towards three-phase AC charging with 11 kVA up to 43 kVA. Single-phase charging of EVs can result in voltage unbalance in the power grid. While state-of-the-art EV models differ in their maximum DC charging power (50 – 270 kW [134]), the trend towards higher power is also apparent in this regard. [81]

Besides the EV model, the actual charging power depends on the supplying charging infrastructure. Thereby, one has to distinguish between public (non-discriminatory access for all users) and private (limited access) charging points [135]. Private charging points at home or work often support AC charging only. The installed charging power lies between 3.7 kVA – 22 kVA depending on the type of housing: Charging points with a maximum power of 11 kVA (in some cases 22 kVA) are primarily installed in single- or two-family houses. On the other hand, in multi-apartment residential buildings, most charging points provide a maximum power of 3.7 kVA (in some cases 11 kVA). [136] Public charging points can either provide AC, DC, or both. While AC charging is limited to 43 kVA [137], DC charging currently allows up to 350 kVA (increasing trend similar to EV models) per charging point [138].

5.2 Structure of the power system

The present-day power system is divided into the transmission- and the distribution system. The transmission system includes the extra-high voltage (380 and 220 kV) level, whereas the distribution system includes the MV (6 – 30 kV) and LV (< 1 kV) levels. The high voltage level (110 kV) can be assigned to the transmission or distribution system. [139] The Austrian power system (as well as the German and the Suisse one) is additionally classified into seven network levels: Network levels 1, 3, 5, and 7 represent the four voltage levels, levels 2, 4, and 6 represent the voltage transformation between them [140]. The latter is based on three-phase transformers located at the grid's substation (Figure 4). While AC charging stations are primarily connected to network levels 6 and 7, DC charging stations providing multiple charging points and high charging power can also be connected to the MV level, i.e., network-level 5. However, the presented thesis focuses exclusively on charging stations integrated into the LV level (network-level 7) or directly connected to MV/LV substations (network-level 6).

The topology of real-life LV grids differs in their structure and used equipment (lines and transformers). Both depend on the region the grid is located and its load density. LV grids in urban areas with high load density (> 30 MVA/km^2 [141]) are often structured based on multiple rings, in which feeders are connected via separation points (Figure 4b). Those rings are openly operated during normal grid conditions. Though, they can be closed to increase the supply reliability, e.g., in the event of a short circuit. Due to the high load density, grid customers in urban LV grids are primarily supplied by short feeders (< 300 m [142]). In contrast, suburban or rural LV grids with low load density (< 5 MVA/km^2 [141]) are usually built on a radial structure (Figure 4a) to supply grid customers via long feeders (up to 1,000 m [142]). [141, 143–145]

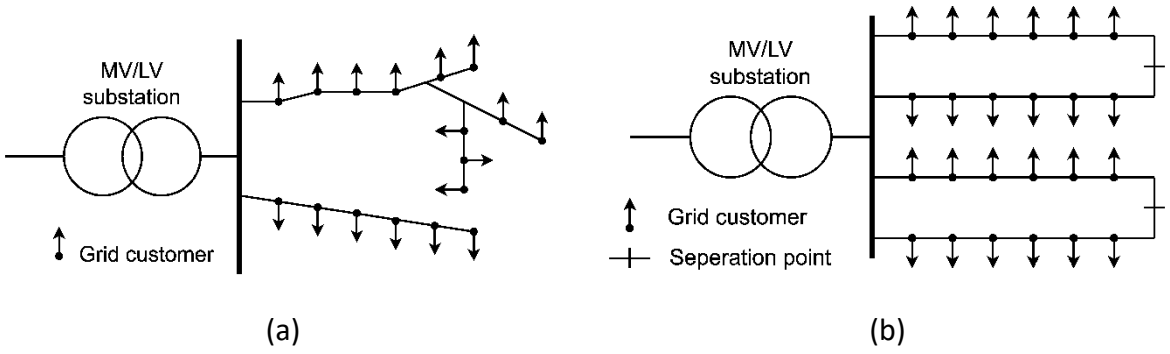

Figure 4: Grid topology of (a) a radial and (b) a ring network on the LV level (own illustration based on [141, 143])

Besides their structure, real-life LV grids vary regarding their equipment. Transformers integrated into the MV/LV substation typically have the following nominal capacities: 100 kVA, 250 kVA, 400 kVA, 630 kVA, 800 kVA, or 1000 kVA [142, 146]. However, MV/LV substations in urban areas with high load density are generally equipped with higher transformer capacity than those in suburban or rural areas with low load density.

From the MV/LV substation, the power is transmitted via overhead lines or cables with primarily aluminum conductors and a cross-sectional area between 50 – 240 mm^2 [141]. The electrical behavior of overhead lines and cables with short or medium length can be simulated using a π-equivalent circuit. The latter is characterized by a series resistance and a series inductance as well as a shunt capacitance and shunt conductance [147]. However, due to negligible capacitance and conductance of LV lines [141], their behavior can be simulated by considering the series resistance (R) and series inductance (X) exclusively (Figure 5a) [147, 148]. Although both overhead lines and cables share the same equivalent circuit, they differ in their specific (per km) impedance values (Table 2): Overhead lines on the LV level show higher specific resistance (R') and inductance (X') compared to LV cables. Furthermore, LV

cables (up to 10.8) have a higher ratio between resistance and inductance (R'/X') than overhead lines (up to 4.7). [141, 149]

Table 2: Specific resistance (R') and inductance (X') of LV overhead lines and cables (at ambient temperature) [141, 149]

Line type	R' (Ω/km)	X' (Ω/km)	R'/X' ratio
Overhead line	0.29 – 1.87	0.29 – 0.40	1.00 – 4.70
Cable	0.14 – 0.86	0.08	1.80 – 10.80

The impedance of grid lines, and thereby their length and type, influences the change in voltage along them. As illustrated in Figure 5b, the complex voltage difference ($\Delta\underline{U}$) between the sending- ($\underline{U}_1$) and the receiving-end voltage ($\underline{U}_2$) can be divided into a transverse (U_t) and a longitudinal voltage component (U_l). The former describes the phase angle between sending- and receiving-end voltages (ϑ). The longitudinal component specifies the difference between sending- and receiving ends' absolute voltage values ($\left|\underline{U}_1\right| - \left|\underline{U}_2\right|$) with sufficient accuracy. Thereby, it indicates the effective (or measurable) voltage change along the line. According to Eq. (5-1) [56, 149] and Figure 5b, the longitudinal voltage change equals the product of the line's transmitted active current (I_a) and its resistance (R), plus the product of the line's transmitted reactive current (I_r) and its inductance (X). [148]

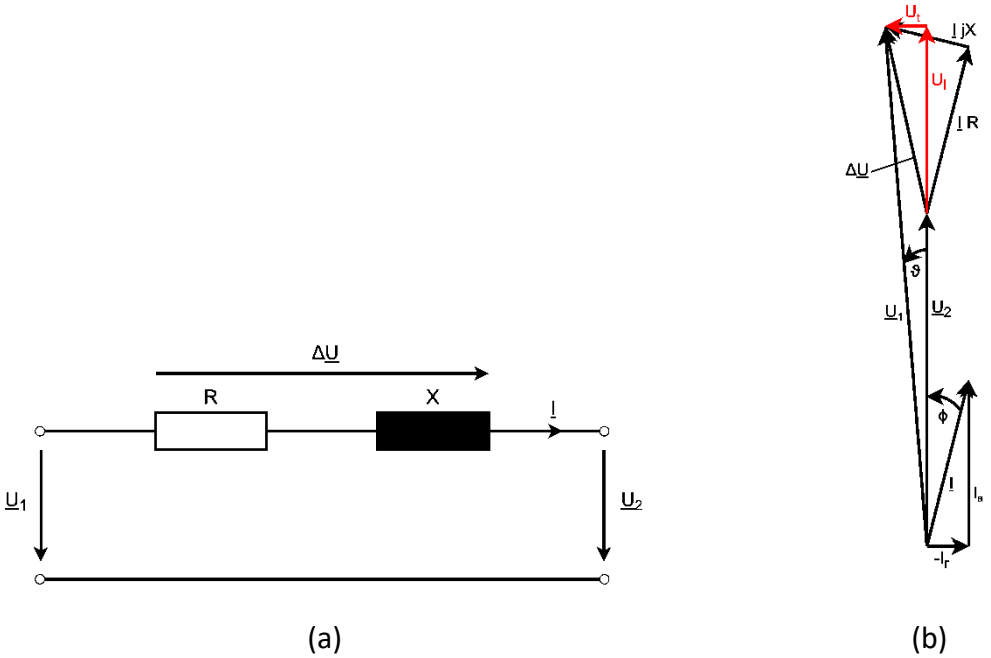

Figure 5: Simplified equivalent circuit of LV lines (a) and the respective phasor diagram supplying an ohmic/inductive customer (b) [56, 147]

Hence, in addition to the impedance, the voltage change along a line depends on the transmitted active (P) and reactive power (Q). However, considering LV lines with a high R‘/X‘-ratio (R‘ >> X‘), the effective voltage change is primarily caused by the active power transmitted. [149]

$$\left|\underline{U_1}\right| - \left|\underline{U_2}\right| \approx U_l = I_a \cdot R + I_r \cdot X = \frac{P}{3 \cdot U} \cdot R + \frac{Q}{3 \cdot U} \cdot X \qquad (5\text{-}1)$$

In order to calculate the voltage at a particular grid node, the voltage change of each line between the grid node and the power supply must be aggregated. Since LV grids have numerous grid nodes, modern-day planning relies on numerical load flow simulations to identify each nodes' voltages depending on the grid customers' active and reactive power (Chapter 5.3). However, a node's vulnerability regarding voltage violations can also be estimated without knowing active or reactive power flows by considering its short-circuit power ($S''_{s,node}$). According to Eq. (5-2), this parameter only depends on the nominal voltage ($U_{Nom.}$), the voltage factor (c), and the total impedance between the considered node and the power supply (Z_{node}) [56, 143].

$$S''_{s,node} = \frac{c \cdot U_{Nom.}^2}{Z_{node}} \qquad (5\text{-}2)$$

Thereby, a grid's voltage stability can be determined based on its most critical node, i.e., the one with the lowest short-circuit power (highest impedance): The higher the minimal short-circuit power in the LV grid, the higher the voltage stability [143]. Due to long feeders with primarily overhead lines, rural LV grids show a lower minimal short-circuit power (0.4 – 1.1 MVA [150]) than urban LV grids with short cables (1.2 – 3.1 MVA [150]). Hence, they are more sensitive to voltage violations. [151–153]

5.3 Load flow simulation

The modern-day planning, analysis, and operation of real-life power grids rely on numerical load flow simulations to determine their behavior in various scenarios. The objective of load flow simulations is to calculate active and reactive power flows, the grid nodes' voltages (absolute value and angle), and network losses depending on the load and generation in the power grid [147]. Thereby, power grids can be evaluated, e.g., in terms of congestions or the fulfillment of planning criteria (contingency or stability analysis), and optimized [154].

Besides the rarely used method based on Kirchhoff's voltage law, most load flow simulations rely on Kirchhoff's current law. Thereby, a grid with N nodes is analyzed using the linear equation system demonstrated in Eq. (5-3). While $\underline{U_i}$ represents the complex voltage of a

node i as output value, $\underline{I_i}$ represents the complex net current injected at node i as the load flow simulation's input value. Eq. (5-4) demonstrates the described equation system in matrix notation (matrices are illustrated in bold). [155, 156]

$$\begin{pmatrix} \underline{Y}_{11} & \underline{Y}_{12} & \cdots & \underline{Y}_{1i} & \cdots & \underline{Y}_{1N} \\ \underline{Y}_{21} & \underline{Y}_{22} & \cdots & \underline{Y}_{2i} & \cdots & \underline{Y}_{2N} \\ \vdots & \vdots & \ddots & \vdots & \ddots & \vdots \\ \underline{Y}_{i1} & \underline{Y}_{i2} & \cdots & \underline{Y}_{ii} & \cdots & \underline{Y}_{iN} \\ \vdots & \vdots & \ddots & \vdots & \ddots & \vdots \\ Y_{N1} & \underline{Y}_{N2} & \cdots & \underline{Y}_{Ni} & \cdots & \underline{Y}_{NN} \end{pmatrix} \cdot \begin{pmatrix} \underline{U_1} \\ \underline{U_2} \\ \vdots \\ \underline{U_i} \\ \vdots \\ \underline{U_N} \end{pmatrix} = \begin{pmatrix} \underline{I_1} \\ \underline{I_2} \\ \vdots \\ \underline{I_i} \\ \vdots \\ \underline{I_N} \end{pmatrix} \qquad (5\text{-}3)$$

$$\underline{\boldsymbol{Y}} \cdot \underline{\boldsymbol{U}} = \underline{\boldsymbol{I}} \qquad (5\text{-}4)$$

The parameter $\underline{\boldsymbol{Y}}$ represents the grid's node admittance matrix, including the admittances between each grid node. The elements in this matrix are calculated based on the equivalent circuit of transformers and lines between nodes. For example, $\underline{Y}_{12}$ defines the admittance of the line between nodes 1 and 2. If two nodes have no connection, the respective entry in the node admittance matrix is zero. The diagonal elements of the matrix (e.g., $\underline{Y}_{11}$) represent the negative self-admittance at a node (e.g., node 1) and serves exclusively as calculation value. [147, 157]

The method used to solve this equation system depends on the type of grid nodes and their load specification: If loads are defined as currents, the linear equation system (Eq. (5-3) is straightforward to solve. However, since the current injected at a node depends on its voltage, it is usually unknown. In fact, most grid nodes are parameterized by the following four parameters: Active- (P) and reactive power (Q), as well as the absolute value (U) and phase angle of their voltages (δ). While two of these parameters are specified by grid- or customer data, the remaining ones are unknown [56, 155]. Depending on the specified parameters, one generally differentiates between three types of nodes (Table 3): Each grid model requires at least one slack node to specify the reference voltage (U and δ) for all the other nodes and balance the grid's surplus and shortage of power. The slack node's active and reactive power (initially unknown) equals the sum of all supplied and generated powers, including grid losses.

Table 3: Most typical types of nodes including their specified and unknown parameters [156, 157]

Type of node	Specified input	Unknown output
PQ-node	P, Q	U, δ
PU-node	P, U	Q, δ
Slack node	U, δ	P, Q

Since active and reactive power is known for most consumers, they are connected to the so-called PQ-nodes. The PQ-nodes' absolute voltages and phases angles must be calculated using

load flow simulation. The active power and the absolute voltage are specified for each PU-node (e.g., based on generator data), whereas the reactive power and the phase angle are unknown. [156, 157]. The P- and Q-values defined at a grid node represent the aggregated power of all consumers and generators connected to it. Hence, both can either be positive or negative. In general, the following definitions are made [139]:

- P > 0: Node represents load and demands power from the grid
- P < 0: Node represents generator and feeds power into the grid
- Q > 0: Node demands inductive reactive power from the grid
- Q < 0: Node demands capacitive reactive power from the grid

Due to the parametrization of most grid nodes based on the injected power (instead of currents), the equation system in Eq. (5-4) must be converted accordingly. The three-phase complex apparent power injected at a node i ($\underline{S_i}$) can be expressed as the product of the node's complex voltage ($\underline{U_i}$) and the complex conjugated injected current ($\underline{I_i^*}$) multiplied by three (in a three-phase power system), illustrated in Eq. (5-5). This correlation can be expressed in matrix notation (bold) considering all grid nodes (Eq. (5-6). Expressing the injected complex conjugated currents ($\underline{\boldsymbol{I}}^*$) according to Eq. (5-4), reveals the non-linear correlation between the pre-defined active ($\boldsymbol{P}$) and reactive power ($\boldsymbol{Q}$) and the voltages ($\underline{\boldsymbol{U}}$) to determine. [158]

$$\underline{S_i} = P_i + jQ_i = 3 \cdot \underline{U_i} \cdot \underline{I_i^*} \qquad (5\text{-}5)$$

$$\underline{\boldsymbol{S}} = \boldsymbol{P} + j\boldsymbol{Q} = 3 \cdot diag\left(\underline{\boldsymbol{U}}\right) \cdot \underline{\boldsymbol{I}}^* = 3 \cdot diag\left(\underline{\boldsymbol{U}}\right) \cdot \underline{\boldsymbol{Y}}^* \cdot \underline{\boldsymbol{U}}^* \qquad (5\text{-}6)$$

Hence, the power-flow problem can be described as follows: The unknown output variables are to be determined in such a way that the predefined input values are set for each grid node (Table 3) [158]. Load flow simulations tackle this problem by iteratively determining all the nodes' voltages solving the described non-linear equation system. Furthermore, the calculated voltages serve as the basis for determining currents and power flows along elements (e.g., lines). In general, two iterative methods are applied to solve the non-linear equation system: The method of joints and the Newton-Raphson method [56, 155, 156]. However, since most load flow simulations rely on the latter [143], it is described in the following chapter.

5.3.1 Newton-Raphson method

The Newton-Raphson method (or Newton method) is based on the grid nodes' power equations, demonstrated in Eq. (5-6). The left side of the equation includes the power pre-defined by node data ($\boldsymbol{P} + j\boldsymbol{Q}$). The right side ($3 \cdot diag\left(\underline{\boldsymbol{U}}\right) \cdot \underline{\boldsymbol{Y}}^* \cdot \underline{\boldsymbol{U}}^*$) represents the power

transported via grid elements (e.g., lines). In the following, the diagonal matrix $diag(\underline{\boldsymbol{U}})$ is simple referred as $\underline{\boldsymbol{U}}$. In the first step of the Newton-Raphson method, the equation system is transformed to obtain a zero vector on the right side (Eq. (5-7). The terms $\Delta\boldsymbol{P}$ and $\Delta\boldsymbol{Q}$ represent the deviation between the power pre-defined by node data and the power transported via grid elements. The previously described power-flow problem now requests to determine these equation system's zeros. Therefore, the equation system is divided into a real- (Eq. (5-8) and imaginary part (Eq. (5-9). [156]

$$3 \cdot \underline{\boldsymbol{U}} \cdot \underline{\boldsymbol{Y}}^* \cdot \underline{\boldsymbol{u}}^* - (\boldsymbol{P} + j\boldsymbol{Q}) = \Delta\boldsymbol{P} + j\Delta\boldsymbol{Q} = \boldsymbol{0} + j\boldsymbol{0} \qquad (5\text{-}7)$$

$$Re\{3 \cdot \underline{\boldsymbol{U}} \cdot \underline{\boldsymbol{Y}}^* \cdot \underline{\boldsymbol{u}}^*\} - \boldsymbol{P} = \overline{\boldsymbol{P}} - \boldsymbol{P} = \Delta\boldsymbol{P} = \boldsymbol{0} \qquad (5\text{-}8)$$

$$Im\{3 \cdot \underline{\boldsymbol{U}} \cdot \underline{\boldsymbol{Y}}^* \cdot \underline{\boldsymbol{u}}^*\} - \boldsymbol{Q} = \overline{\boldsymbol{Q}} - \boldsymbol{Q} = \Delta\boldsymbol{Q} = \boldsymbol{0} \qquad (5\text{-}9)$$

In the next step, Eq. (5-8) and (5-9) are linearized for each iteration ν using the Taylor's series expansion, demonstrated in Eq. (5-10) and (5-11). The vector $\boldsymbol{x}$ includes all nodes' phase angles and voltages referred to the previous iteration's voltages. Finally, Eq. (5-10) and (5-11) are combined and transformed according to Eq. (5-12). [156]

$$\left(\frac{\partial\Delta\boldsymbol{P}}{\partial\boldsymbol{x}}\right)_{(\nu)} \Delta\boldsymbol{x}_{(\nu+1)} + \Delta\boldsymbol{P}_{(\nu)} = \boldsymbol{0} \qquad (5\text{-}10)$$

$$\left(\frac{\partial\Delta\boldsymbol{Q}}{\partial\boldsymbol{x}}\right)_{(\nu)} \Delta\boldsymbol{x}_{(\nu+1)} + \Delta\boldsymbol{Q}_{(\nu)} = \boldsymbol{0} \qquad (5\text{-}11)$$

$$\begin{bmatrix} \frac{\partial\Delta\boldsymbol{P}}{\partial\boldsymbol{x}} \\ \frac{\partial\Delta\boldsymbol{Q}}{\partial\boldsymbol{x}} \end{bmatrix}_{(\nu)} \Delta\boldsymbol{x}_{(\nu+1)} = \boldsymbol{J}_{(\nu)}\, \Delta\boldsymbol{x}_{(\nu+1)} = -\begin{bmatrix} \Delta\boldsymbol{P} \\ \Delta\boldsymbol{Q} \end{bmatrix}_{(\nu)} \qquad (5\text{-}12)$$

The coefficient matrix $\boldsymbol{J}$ is called the Jacobi matrix. It is built based on four sectional matrices, including the derivation of pre-defined parameters (active and reactive power) with respect to unknown parameters (voltages and phase angles). In contrast to the node admittance matrix, the Jacobi matrix depends on the particular operation point and must be calculated for each iteration. The reduced equation system (Eq. (5-12) is solved for each iteration until the deviation between the power pre-defined by node data and the power transported via grid elements falls below a defined limit. [158]

5.3.2 Variants of load flow simulations

While the procedure of iteratively calculating the grid's voltages and currents is always the same, three different variants of load flow simulations are primarily used in modern-day grid

planning: Time series-based simulations, (stochastic) Monte-Carlo simulations, and static deterministic simulations. Those variants differ in defining each grid node's active and reactive power.

Time series-based load flow simulations use time-resolved profiles of the grid's consumers and generators. These profiles define each grid node's power for each time step of a certain period (e.g., one year). Usually, time steps of 1, 5, 15, or 60 minutes are applied for load flow simulations [139]. While this variant allows the analysis of numerous load and generation cases, it requires detailed knowledge regarding grid customers' temporal behavior. Electrical loads of households, as well as commercial- and agricultural customers, can be modeled using standardized load profiles (e.g., [159]). Synthetic load profiles (e.g., [160]) of households and EVs allow even more realistic modeling of electrical loads. The generation by renewable energy sources can be modeled in detail based on location-specific temperature and weather data, e.g., provided by open-source data (e.g., [161]).

The Monte-Carlo simulation is a stochastic method to define the power at each grid node. Therefore, the probability of occurrence of different power values is determined based on statistical data and defined as probability density functions [56]. Load flow simulations are performed by iteratively drawing the power for each node based on these probability density functions and random numbers. Hence, the number of performed load flow simulations equals the number of analyzed iterations. Thereby, the probability of occurrence of thermal congestions and voltage violations can be identified. Like time series-based load flow simulations, this method requires detailed knowledge of grid customers' behavior. [139]

Static deterministic load flow simulations analyze worst-case load conditions and their impacts on the power grid. Therefore, two cases are investigated: The Load Case—representing the maximum load and minimum generation—and the Generation Case—representing the minimum load and maximum generation [62]. Thus, only two load flow simulations are performed to determine worst-case grid impacts. The power at each grid node is defined using coincidence factors for both cases. Considering a certain number of customers (NoC), their aggregated power ($P_{Aggregated}$) is calculated by multiplying the sum of all customers' maximum power ($P_{cust.}$) by the respective coincidence factor (Eq. (5-13) [63]. The coincidence factor considering a defined number of customers NoC represents the maximum of their aggregated electrical power divided by the sum of their individual maximum power (Eq. (5-14) [62].

$$P_{Aggregated}\,(NoC) = \sum_{i=1}^{NoC} \max_{t}(P_{cust.}(t)) * Coincidence\ factor\,(NoC) \qquad (5\text{-}13)$$

$$Coincidence\ factor\ (NoC) = \frac{\max_t(\sum_{i=1}^{NoC} P_{Cust.}(t))}{\sum_{i=1}^{NoC} \max_t(P_{Cust.}(t))} \quad (5\text{-}14)$$

The coincidence factor indicates the probability of temporal overlaps between grid customers' electrical consumption and generation. Hence, it decreases with an increasing number of considered customers (Figure 6). Furthermore, it depends on the considered customer class: Households show a rather stochastic load behavior, resulting in lower coincidence factors than electrical direct- or water heaters, characterized by similar behavior. However, the current state of research (Chapter 2.1.1) uses coincidence factors individually for each customer class and neglects the combination of several customers classes (e.g., households, EVs, and HPs).

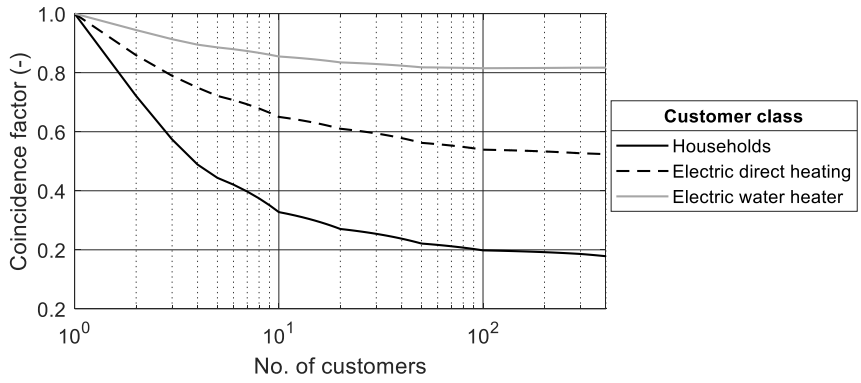

Figure 6: Coincidence factor of grid customers depending on their number and class (own illustration based on [63])

Table 4 provides a qualitative comparison of the previously described variants of load flow simulations. As already mentioned, time series-based or Monte-Carlo simulations require detailed knowledge regarding grid customers' temporal behavior for each grid node. As a result, they show a higher demand for modeling the grid nodes' power than static deterministic load flow simulations using coincidence factors. On the other hand, they provide information regarding the probability or the frequency of grid congestions, which is inhibited using the static deterministic approach. By performing time series-based load flow simulations, the duration of grid congestions can additionally be derived, which is crucial to evaluate grid-relieving measures (e.g., energy storage systems or demand-side measures).

Table 4: Qualitative comparison of different variants of load flow simulation (derived from [56, 62, 139])

	Time series-based	**Monte-Carlo**	**Static deterministic**
Demand for modeling nodes' power	+	+	++
Information to be gained	+++	++	+
Simulation effort	+	+	+++

However, since the static deterministic variant only requires two load flow simulations (one for the load- and generation case, respectively), they allow much faster computation than time series-based or Monte-Carlo simulations (Table 4) [60, 61]. As a result, they provide significant benefits for the large-scale simulation of numerous grid structures.

5.4 Grid-relieving measures preventing conventional grid reinforcements

The integration of future grid customers, such as EVs, PV modules, and electric HPs, will challenge the present-day power system. The conventional option to prevent future grid restrictions is the extension or reinforcement of existing grid structures, e.g., installing additional grid lines or exchanging the transformer at the substation. Besides classic grid reinforcements, grid-relieving measures might provide the required flexibility to integrate future e-mobility into the power system. The most important measures in this regard are explained in this chapter.

5.4.1 MV/LV transformers with on-load tap changer

Three-phase transformers convert the grid's nominal voltage between different voltage levels (Chapter 5.2). The transmission ratio is defined by the number of windings on the high- and LV sides. Usually, present-day MV/LV substations are equipped with conventional transformers, whose transmission ratio can only be adapted with zero potential and no connected loads. [158]

The integration of EVs or renewable energy sources into the LV level is often inhibited due to voltage violations. The EN 50160 [162] defines the admissible voltage range of ± 10 % of the nominal voltage. However, using conventional transformers with a fixed transmission ratio, this voltage range is specified for the MV and LV conjunctly. The exact distribution of the allowed voltage deviations between the high-voltage and LV levels is specified by each DSO individually. Considering the example in Figure 7, a maximal voltage deviation of 3 % (due to generation) and 5 % (due to consumers) are available on the LV level.

Transformers used at higher voltage levels are equipped with on-load tap changers. Thereby, they enable regulating the transmission ratio by adapting the transformer's effective windings during operation [163]. Implementing on-load tap changers into transformers between the MV and LV level allows the voltage control at the substation within a given control bandwidth (Figure 7). Thus, the nominal voltage at the MV/LV substation can be adapted depending on the particular grid condition, either maximum generation (voltage increase) or maximum load (voltage decrease). Based on this measure, the MV and LV levels are decoupled, which increases their allowed voltage range to ± 10%, respectively. As a result, the maximum voltage

deviation on the LV level is increased to 7 % (due to generation) and 9 % (due to consumers), considering the example in Figure 7. [38]

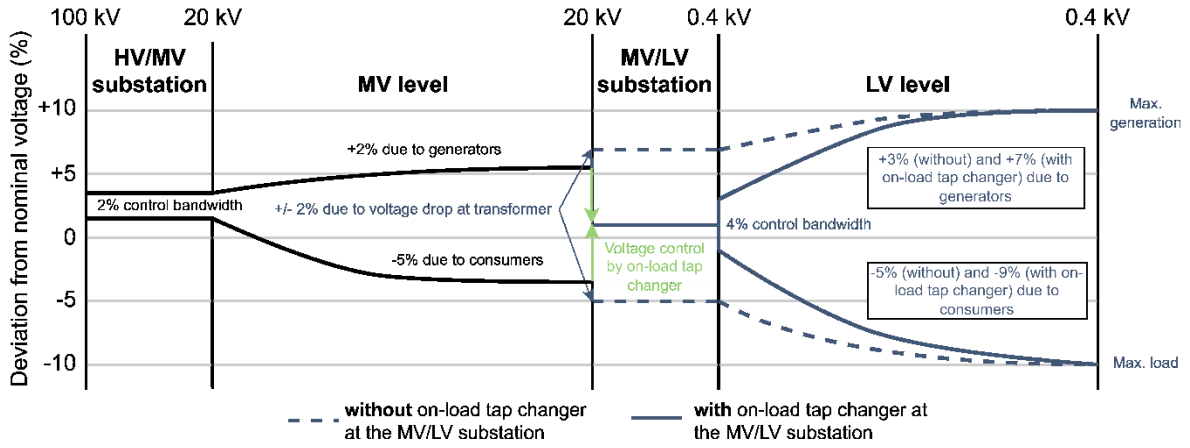

Figure 7: Exemplary distribution of the allowed voltage range (± 10 % of the nominal voltage) with and without an on-load tap changer at the MV/LV substation (own illustration based on [38])

The adaption of the MV/LV substation's voltage is automatically controlled based on the voltage measured in the local LV grid or centrally controlled by the DSO. All control strategies require the implementation of measurement equipment as well as information and communication technology into the power grid. [38] The application of such variable transformers has already been tested between the MV and LV levels to prevent voltage violations due to domestic PV modules or EVs [164]. Besides the MV/LV substation, the on-load voltage regulation can also be implemented in single feeders affected by critical voltages [165].

5.4.2 Voltage-controlled active- and reactive power regulation

The regulation of grid customers' active or reactive power represents another measure to mitigate potential grid restrictions. Voltage-controlled power regulation is effective, especially in LV grids sensitive to voltage violations, e.g., suburban or rural areas (Chapter 5.2). However, this measure requires the continuous detection of the local voltage at the grid customer's point of common coupling [76, 166]. Furthermore, grid customers (e.g., EV charging points) are equipped with fully automated active or reactive power regulation following a pre-defined characteristic (Figure 8) [73]. In most cases, the active power regulation of AC charging points relies on adapting the active current available for charging the EV [18]: If the voltage falls below a specific limit, the active current is limited (Figure 8a). Vice versa, the active power fed into the grid by generators (e.g., domestic PV modules) is limited if the voltage exceeds a defined voltage limit. Similarly, the fully automated regulation of grid customers' reactive power follows a pre-defined characteristic (Figure 8b): In case of a critical voltage increase (e.g., > 7 % of the nominal voltage), the ratio between inductive reactive power (Q) and the

nominal apparent power (S_{nom}) is increased. The reactive power demand changes to capacitive if the voltage falls below a specific limit (e.g., 92 %). [18]

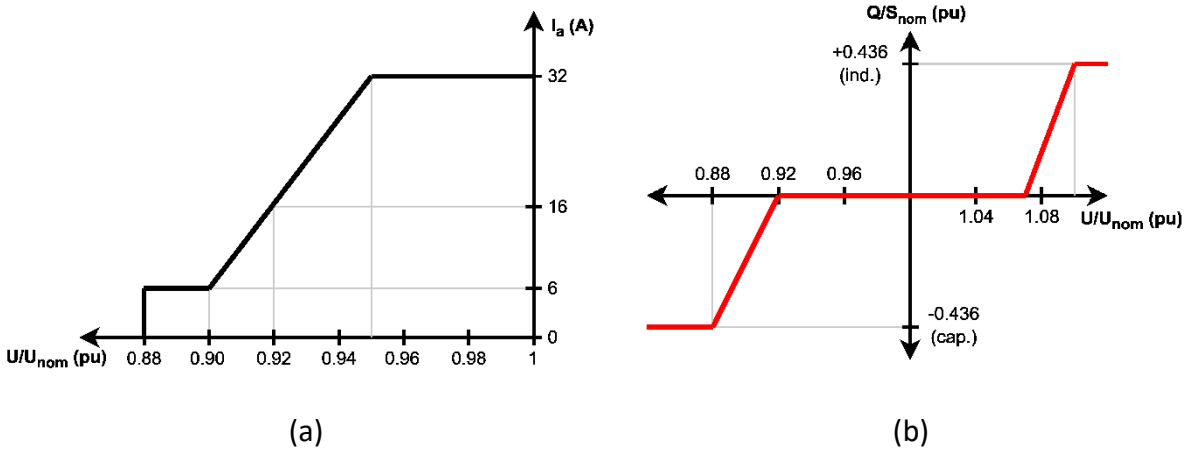

(a) (b)

Figure 8: Exemplary characteristic to regulate the power of EV charging points: (a) active current (I_a) and (b) the ratio between reactive power (Q) and nominal apparent power (S_{nom}) depending on the power grid's voltage (U) referred to the nominal voltage (U_{nom}) (own illustration based on [18])

Figure 9 illustrates how active and reactive power regulation affects the voltage deviation along a LV line based on the simplified equivalent circuit in Figure 5a (described in detail in Chapter 5.2). The regulation of grid customers' active and reactive power influences the complex current ($\underline{I}$) transmitted by the grid line. Consequently, it changes the complex ($\Delta\underline{U}$) and the effective voltage deviation (U_I) along the line, described in Eq. (5-1).

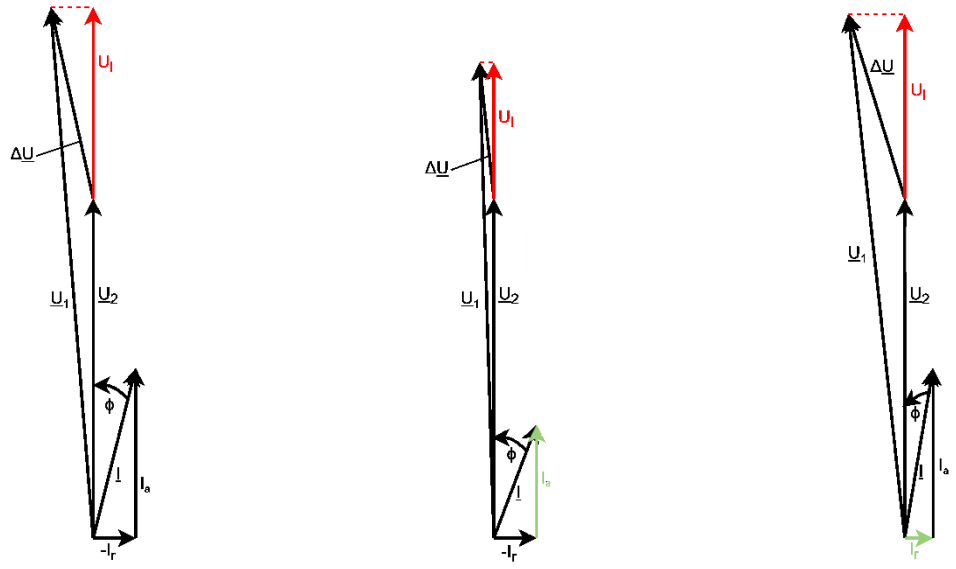

(a) (b) (c)

Figure 9: Phasor diagram of LV lines without power regulation (a), as well as with voltage-controlled active- (b) and reactive power regulation (c)

In this example, both active (I_a) and reactive currents (I_r) are adjusted to the same extent to decrease the effective voltage drop. However, as demonstrated in Table 2, LV lines are characterized by an R'/X' ratio of 1.0 – 10.8. As a result, the active power transmitted by the grid line has a more significant impact on the voltage deviation. Thus, active power regulation more decisively limits the effective voltage drop (Figure 9) on the LV level and is more suitable than reactive power regulation.

5.4.3 Decentralized energy storage systems (ESSs)

Implementing decentralized ESSs into the local power system is another measure to reduce grid congestions and prevent conventional grid reinforcements [167]. ESSs allow for a bidirectional power exchange with the power grid and can be applied as a consumer (charging of ESS) or generator (discharging of ESS). Hence, they might support the power grid in many forms, e.g., storing energy during high generation and supplying consumers during peak periods. [168] Implemented into the power grid, decentralized ESSs can mitigate EV-induced peak loads by discharging the stored energy to supply the charging of EVs (Figure 10). Thereby, EVs can be charged with high power, which without ESS would not comply with the capacity of the local power grid. ESS recharging with low power flattens the power grid's load curve and avoids critical grid conditions.

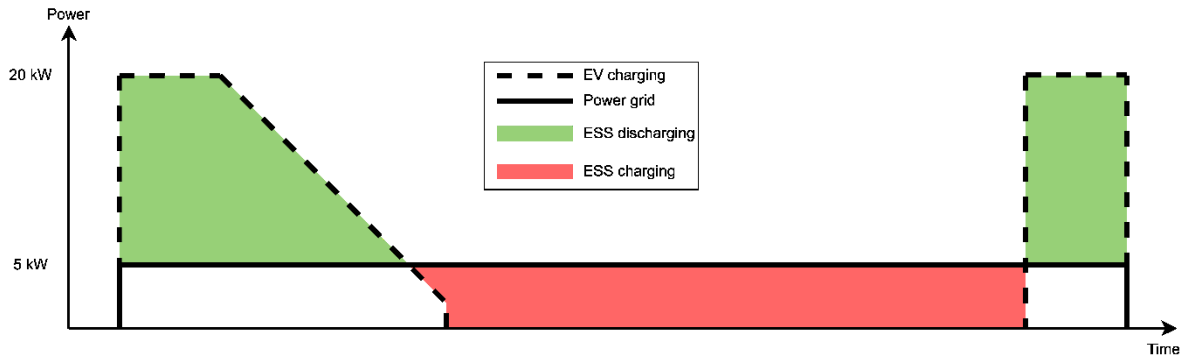

Figure 10: Mitigation of electric vehicle (EV) charging peak loads by the energy storage system (ESS)

In general, ESS technologies are classified into potential, kinetic, mechanical, thermal, and chemical ones [169]. However, to mitigate grid loads at the distribution level, especially battery- and flywheel ESSs, are applied and analyzed in the current state of research (Chapter 2.2). Compared to battery ESS, flywheels are characterized by low energy density [98, 170] and a high self-discharging rate due to standby energy losses [171]. However, when it comes to the support of high-power EV charging, they provide several advantages (compared to battery ESSs): High life cycle numbers [90, 98, 102, 170–176], high power density [98, 102, 170, 171, 173–176], short access time [98, 174], low maintenance effort [98, 174], high efficiency [90, 98, 171, 174], small environmental impact [98, 171–174] as well as the independency of power and energy content [171, 172].

5.4.4 Demand-side measures

While the previously mentioned measures are implemented at the supply side, i.e., the power grid, grid loads can successfully be regulated from the customer perspective. Thereby, demand-side measures describe any adaption of grid customers' load behavior [177]. In general, demand-side measures can be classified as dispatchable and non-dispatchable measures. The former refers to controlling the customer's electrical load by the system operator, which is today sometimes voluntarily granted by the grid customer in exchange for financial incentives. The latter, also called price-based measures, use dynamic electricity pricing rates to motivate the customer to adapt its load behavior. [178]

Like voltage-controlled power regulation (Chapter 5.4.2), demand-side measures can adapt the power supplied by or fed into the power grid. In addition, some measures allow controlling the time of electrical loads. Considering the charging of EVs, their charging can either be limited regarding the available power or temporarily rescheduled to times with low electricity prices or high grid capacity. Thereby, demand-side measures mitigate EV-induced peak loads in the power grid and flatten its load curve. [64]

Demand-side measures are not limited to the power supplied by the power grid to the EV. Since EVs' batteries have large energy capacities (Chapter 5.1), they can be discharged and fed power into the power grid. The so-called vehicle-to-grid technology allows the bidirectional power exchange between the EV and the power grid. [179] As a result, EVs can be operated as decentralized ESSs (Chapter 5.4.3). In addition to grid-relieving measures, the bidirectional operation of EVs enables other fields of applications, e.g., the provision of grid ancillary services or arbitrage activities [180, 181].

6 RESULTS

The following chapters present the results of the author's publications (Appendix A) to answer the proposed research questions (Chapter 3). Initially, the author's works in the field of identifying EV-induced grid restrictions are presented in Chapter 6.1., which is structured as follows: Chapter 6.1.1 presents novel coincidence factors (published in Paper 1), enabling the accurate consideration of temporal interdependencies between different customer classes (research question 1). Different approaches to apply these coincidence factors are examined in Chapter 6.1.2 to answer research question 2 (Paper 3). Furthermore, the correlation between the region of LV grids and their hosting capacity (research question 3) is identified in Chapter 6.1.3 (Paper 1). Chapter 6.1.4 answers research question 4 by examining different methods to quantify future grid reinforcement costs due to EVs, PV modules, and HPs (Paper 3). A fully automated large-scale grid simulation tool (published in Paper 3) is presented in Chapter 6.1.5, allowing the detailed simulation of several thousand grids (research question 5).

Chapter 6.2 summarizes the results in the field of evaluating grid-relieving measures and answers the respective research questions (6 - 8). Thereby, it differentiates between e-mobility use cases: On the one hand, Chapter 6.2.1 deals with measures supporting private EVs charged at home (published in CIRED 2019 and NEIS 2019). Chapter 6.2.2, on the other hand, discusses the implementation of decentralized ESSs to support the charging of remaining use cases (Paper 2 and IEWT 2021).

6.1 Identifying EV-induced grid restrictions using load flow simulations

6.1.1 Modeling novel coincidence factors considering temporal interdependencies between future grid customers

As described in Chapter 5.3, static deterministic load flow simulations use coincidence factors to estimate electrical loads at different locations in the power grid. However, real-life information concerning future grid customers' aggregated coincidence is missing due to currently low EV-, PV-, and HP-penetrations. On this account, novel coincidence factors are modeled in this work (Figure 11). Therefore, long-term (one year) time-series with high resolution (one minute) are modeled, considering existing (e.g., households, commercial and agricultural businesses) and future (EVs, PV modules, and HPs) customers. Thereby, the penetration of EVs, PV modules, and HPs is varied between 0 % (no future customers) and 100 % (all vehicles are electrified, and each house has a PV module and a HP). The coincidence factor of a defined number of customers is calculated using Eq. (5-14), described in

Chapter 5.3. The exact methodology applied is described in Paper 1 and 3. In contrast to the current state of research (Chapter 2), the novel coincidence factors modeled in this thesis consider various customer classes and their behavior conjunctly. As a result, they properly consider temporal interdependences between various customer classes and the accurate determination of grid conditions.

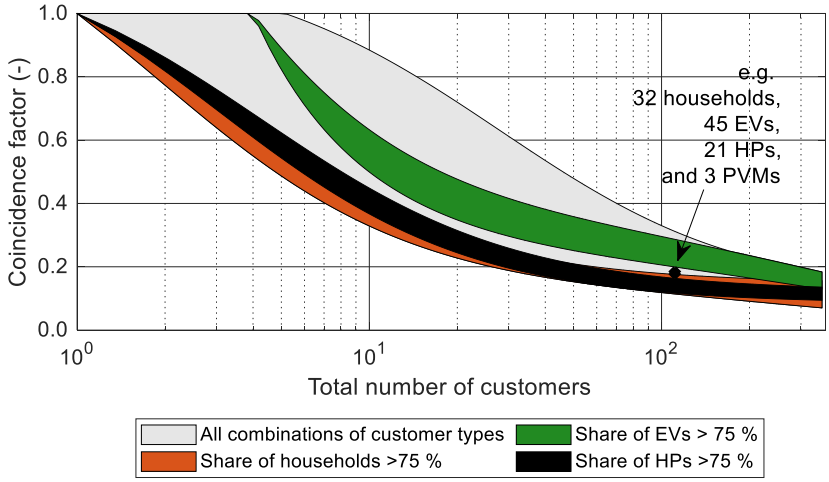

Figure 11: Novel coincidence factors regarding the temporal aggregation between households, electric vehicles (EVs), heat pumps (HPs), and photovoltaic (PV) modules [29]

Naturally, the coincidence factor decreases with an increasing number of customers (Chapter 5.3.2). Besides, it depends on the distribution of customer classes: Combinations with a high share of EVs (e.g., > 75 %) show a higher coincidence factor (based on the assumed uncontrolled charging primarily during evening hours) than combinations with a high share of households or HPs. For example, the aggregation of 32 households, 45 EVs, 21 HPs, and three PV modules results in a maximal coincidence of 0.18.

6.1.2 Analyzing different approaches to apply grid customers' coincidence factors

Identifying potential grid restrictions using static deterministic grid simulations relies on the appropriate application of coincidence factors. Therefore, it is crucial to determine the appropriate coincidence factor depending on the considered number of customers (Figure 11). In this thesis, different approaches to determine and apply grid customers' coincidence factors, according to the current research (Chapter 2), are examined and compared regarding their simulation results. At first, we qualitatively investigated the impact of the applied coincidence factor's value on the extent of grid restrictions (Paper 1). While the location of existing customer classes (households, commercial- and agricultural businesses) is provided by real-life grid data, future customer classes (EVs, PV modules, and HPs) are distributed uniformly in the grid depending on the analyzed penetration (0 – 100 %). Besides applying

coincidence factors for each customer class individually, novel coincidence factors combining various customer classes (Chapter 6.1.1) are analyzed. Static deterministic load flow simulations are performed using both approaches to validate their simulation results with those gained by time series-based simulations (Figure 12).

Applying coincidence factors individually for each customer class neglects their temporal interdependences of electrical loads. Consequently, aggregated loads are overestimated significantly compared to a detailed time series-based grid simulation. Furthermore, future grid restrictions, e.g., thermal congestions of lines and transformers and voltage violations, are misjudged (Figure 12). In fact, the potential error using individual coincidence factors increases with the number of considered customers and classes. Consequently, this grid planning approach, applied in several studies (Chapter 2.1.1) and used by several DSOs, is inadmissible for identifying future grid congestions unless adapted to comply with future grid customers. Therefore, the developed combined coincidence factors (Figure 11) take temporal interactions between all customer classes into account (Figure 12).

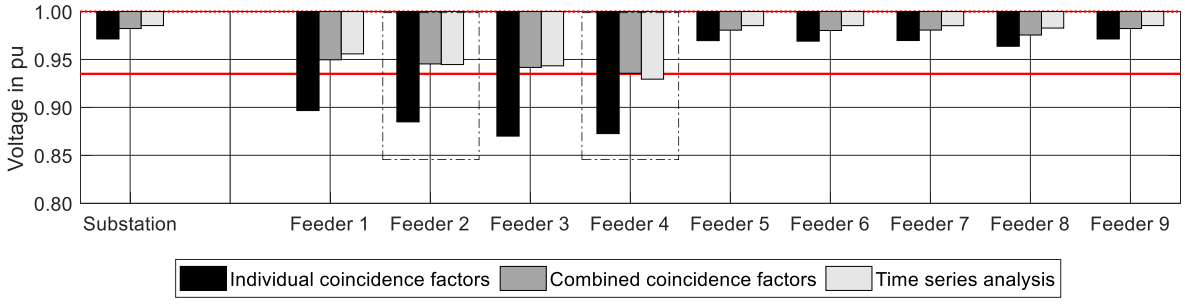

Figure 12: Comparison of voltage violations using static (individual and combined application of coincidence factors) and time series-based load approaches [29]

Hence, using these novel coincidence factors, static deterministic load flow simulations provide similar accuracy to time series-based ones while keeping the required computing time adequate. The latter aspect is crucial when simulating several thousand LV grids. As a result, most studies determining the total grid reinforcement costs in a large area with several thousand grids rely on this variant of load flow simulation (Chapter 5.3.2). Nevertheless, they use different approaches to apply grid customers' coincidence factors, have been examined in this work (Figure 13):

Due to geographical differences, real-life LV grids show considerable heterogeneity in the number and classes of customers (e.g., households, EVs, PV modules). Thus, when analyzing several thousand LV grids, applying one single coincidence factor (e.g., determined at the MV/LV substation) consistently to each grid might misjudge grid loads in some of them. As a result, the total demand for transformer- and line extensions might deviate considerably from

applying grid-specific coincidence factors. Hence, the appropriate coincidence factor of existing and future customers must be determined for each grid specifically to avoid that.

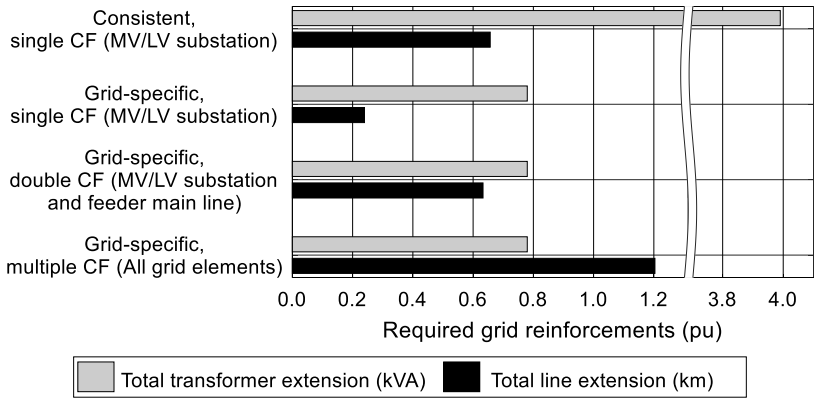

Figure 13: Comparison of required transformer- and line extensions indicated by various approaches to apply coincidence factors (CF) [108]

Furthermore, we analyzed the impact of how many coincidence factors (single, double, or multiple) are applied to each grid and based on which grid element they are determined (Paper 3). Therefore, three approaches to applying grid customers' coincidence factors are analyzed by simulating several thousand LV grids, respectively.

Single coincidence factors determined at the MV/LV substation (grid-specific) misjudge the coincidence factor at grid nodes with few customers connected. Consequently, the future demand for line extensions is underestimated compared to applying multiple coincidence factors depending on the analyzed grid element (Figure 13). Even considering double coincidence factors, determined at the MV/LV substation and feeder lines (connected to the LV bus bar), provides insufficient simulation accuracy. Hence, to estimate the future demand of grid reinforcements at the LV level accurately, multiple coincidence factors, determined for each grid element individually, must be determined and applied to grid customers.

6.1.3 Qualitative analysis of different grid regions' hosting capacity regarding EVs and HPs

The presented thesis identifies potential grid congestions on the LV level triggered by future e-mobility. In the first step, four real-life LV grids located in different regions (urban – city center, urban – outskirt, suburban, and rural) are analyzed using load flow simulations. Therefore, grid-specific (combined) coincidence factors are applied depending on the analyzed grid element (demonstrated in Chapters 6.1.1 and 6.1.2). Each grid's hosting capacity is determined based on voltage violations according to EN 50160 [162] and thermal congestions of transformers and lines. A qualitative comparison of the analyzed grid regions is made using the maximally integrable penetration of EVs (Figure 14). The investigated LV grids differ substantially regarding their hosting capacity: More than 80 % of vehicles can be

electrified in urban LV grids without any voltage violations or thermal congestions. In contrast, this study's suburban and rural grids face critical voltage violations at an EV penetration higher than 20 % and 10 % (Figure 14).

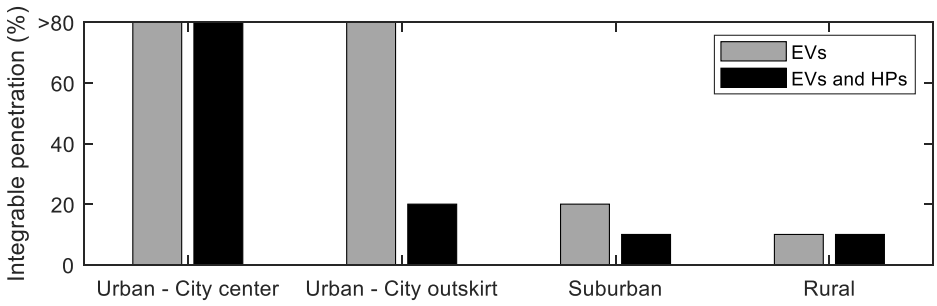

Figure 14: Maximally integrable penetration of electric vehicles (EVs) and heat pumps (HPs) depending on the grid region

Furthermore, potential synergies between EVs and HPs regarding their induced grid restrictions are demonstrated (Figure 14). Therefore, electric HPs are additionally integrated into the analyzed LV grids. Based on realistic time-resolved load profiles, a temporal aggregation of EVs' and HPs' electrical loads was demonstrated in many households, especially during the evening. This aspect affects the combined coincidence factor of EVs and HPs: Considering ten households with ten EVs and ten HPs (30 customers in total) leads to a combined coincidence factor of 0.52 (Figure 11). Due to temporal interdependences, the aggregated load in the power grid increases substantially if EVs and HPs must be supplied together, which decreases the maximum hosting capacity. A combined integration of EVs and HPs is especially critical in grid regions with many single- or two-family houses (Urban – City outskirt and suburban) equipped with both technologies (Figure 14). However, the investigation of only four LV grids, i.e., one grid per region, only allows a qualitative comparison of different regions. The simulation of several thousand LV grids might be necessary to allow more general conclusions.

6.1.4 Methods to quantify total grid reinforcement measures

While previous results include a qualitative comparison of four LV grids (Chapter 6.1.3), DSOs are urged to quantify grid reinforcement costs in a large area with several thousand grids. Therefore, future voltage violations and thermal congestions of transformers and lines are analyzed using load flow simulations. Then, necessary grid reinforcements (exchange or additional installation of transformers or lines) as countermeasures are determined, and respective costs are estimated. However, the current research uses two different methods (Chapter 2.1.2) to quantify grid reinforcement costs in a large area: Firstly, the simulation of selected representative grids and the scaling of their results to the whole area of investigation. Secondly, the simulation of all grids located in the area of investigation. Thus, four different

quantification methods are examined in the presented thesis to illustrate how many LV grids must be simulated to provide sufficient accuracy. Paper 3 provides a detailed description of the analyzed quantification methods.

In the first quantification method analyzed (QM 1), the results of three LV grids located in various grid regions (Urban – City center, suburban, and rural), demonstrated in Chapter 6.1.3 (Figure 14), are scaled to the whole area of investigation including 7,114 LV grids. However, as demonstrated in Chapters 5.2 and 6.1.3, power grids at the LV level show a high heterogeneity regarding topology and customers. In addition, present-day LV grids differ considerably even within the same grid region [182]. Consequently, grid reinforcement costs acquired by scaling grid regions' results deviate from those gained by simulating all LV grids (Figure 15).

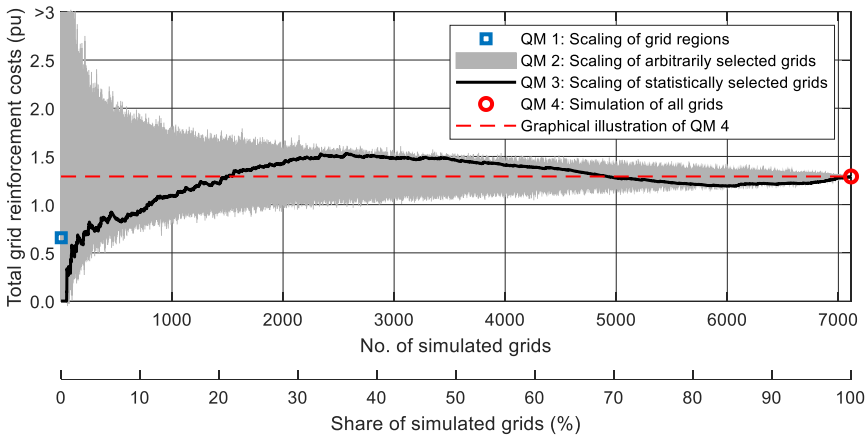

Figure 15: Grid reinforcement costs in the area of investigation (7,144 LV grids) identified using different quantification methods (QM) [108]

The scaling of representative LV grids' results depends on the selected grid structures and their number. If only a few grids are arbitrarily selected for simulation (QM 2), the determined grid reinforcement costs might be misjudged considerably. Even if LV grids are selected based on statistical data (using the root mean square deviation regarding the grids' transformer capacity, number of nodes, total line length, and number of customers) only slightly improves the acquired accuracy (QM 3). In fact, several thousand LV grids must be simulated to quantify total grid reinforcement needs with adequate accuracy (QM 4). For example, in the area investigated in this thesis (7,114 grids), more than 5,000 grids must be simulated to reach an accuracy of 95 %. These results demonstrate the need for automated large-scale grid simulation.

6.1.5 Fully automated large-scale grid simulation tool

Based on the insights and requirements presented in previous chapters, a fully automated large-scale grid simulation tool is developed in this thesis. It allows a detailed simulation of

several thousand grids, including evaluating potential grid reinforcement measures and resulting costs. Figure 16 illustrates the tool's scheme applied for each grid respectively:

In the first step, original grid data is converted from commercial grid simulation software (e.g., NEPLAN [183], PowerFactory [184]) into MATLAB [185] using tailor-made and automated interfaces. In the next step, future grid customers, e.g., EVs, PV modules, and HPs, are integrated into the grid model depending on the selected penetration (0 – 100 %) and spatial allocation algorithm (uniform or stochastic). Subsequently, required grid reinforcements due to thermal overloads or voltage violations are identified by performing static deterministic load flow simulations (Chapter 5.3). Therefore, each node's active and reactive power is determined, incorporating all previous insights regarding the grid customers' coincidence factor (Chapter 6.1.1) and its location of determination (6.1.2).

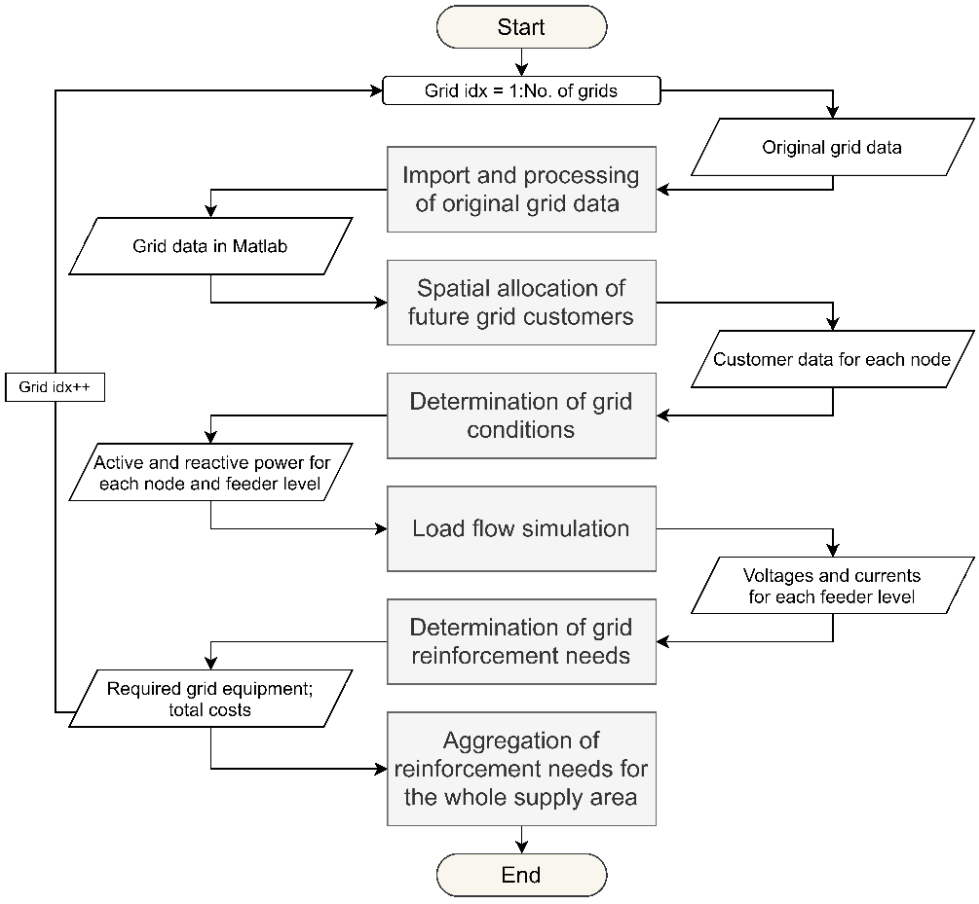

Figure 16: Scheme of the developed fully automated large-scale grid simulation tool [108]

Finally, the developed large-scale grid simulation tool provides the length of grid lines and transformers to be reinforced or additionally installed for each grid. Paper 3 (Appendix A) describes each of these steps in detail (Figure 16). The parallelization of the presented scheme using 32 CPUs (3 GHz, 128 GB RAM) allows simultaneously simulating several grid models. Thereby, the required computing time is decreased by 94 % (20.8 seconds per 1,000 grid nodes) compared to a sequential simulation.

6.2 Evaluating the potential of grid-relieving measures to mitigate EV-induced grid restrictions

6.2.1 Grid-relieving measures supporting private charging at home

Two studies performed in this thesis investigate different measures and their potential to reduce grid restrictions on the LV level caused by EVs charged at home. In the conference paper CIRED 2019 [111], we have first determined the impacts of domestic charging (with up to 22 kVA) on a suburban LV grid without any measures (Figure 17, red dashed line). Subsequently, the grid congestions we have identified are counteracted by implementing various voltage- and user-controlled grid-relieving measures:

The potential of variable distribution transformers between MV and LV levels (Chapter 5.4.1) strongly depends on the selected control strategy. The on-load tap changer adjustment based on local voltage control (based on the voltage measured at the MV/LV substation) prevents inadmissible voltages only slightly (Figure 17a, yellow line). In contrast, EV-induced voltage violations can successfully be avoided using a remote-controlled tap changer adjustment (based on the voltage measures at the end of critical feeders). The remote-controlled tap changer adjustment can be realized either at the MV/LV substation's transformer (green line) or by variable transformers installed in endangered feeders (grey line). Equipping e-mobility charging infrastructure with voltage-controlled phase-switches (connecting single-phase charging EVs to the grid phase with the highest voltage) provides the same relief in voltage violations (purple line). Furthermore, it successfully prevents voltage unbalance at the LV level if EVs are charged single-phased and distributed to the same phase.

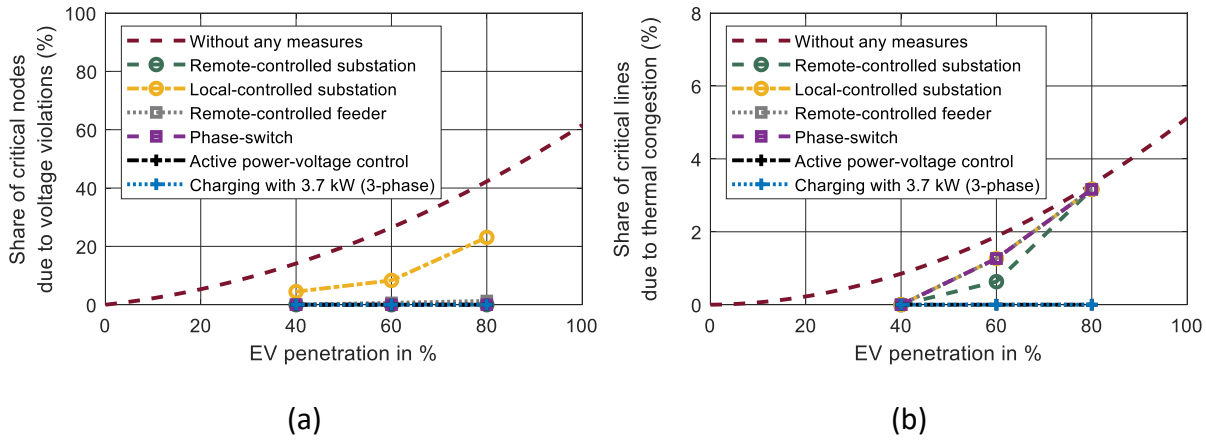

Figure 17: Share of (a) critical grid nodes (voltage violations) and (b) critical lines (thermal congestions) depending on the EV penetration and grid-relieving measures [111]

Despite preventing voltage violations, these measures miss protecting from thermal overloads in single grid lines due to domestic EV charging (Figure 17b). In fact, only two of the

investigated measures prevent voltage violations, critical voltage unbalance and thermal congestions: The implementation of voltage-controlled active power regulation at the charging infrastructure (black line), described in Chapter 5.4.2, and the limitation of available charging power to 3.7 kVA (blue line). The latter can be established without any loss in user comfort due to long parking periods during the night. Of course, this requires a transition from single- to three-phase EV charging or a uniform phase-distribution of single-phase charging EVs. With both measures, up to 80 % can be supplied by the investigated suburban LV grids without any voltage violations or thermal congestions. These results demonstrate that conventional grid reinforcement measures caused by domestic EV charging can be successfully counteracted by implementing grid-relieving measures into the LV level.

6.2.2 Implementation of decentralized ESSs to support high-power EV charging

In addition to voltage- and user-controlled measures, demonstrated in Chapter 6.2.1, the presented thesis analyzes the implementation of decentralized ESSs into charging infrastructure. Therefore, various e-mobility use cases charging with power higher than 11 kVA are addressed in two conference papers. NEIS 2019 [109] deals with public on-street AC charging of passenger EVs with 22 – 44 kVA. Complementarily, IEWT 2021 [110] determines required ESS specifications to supply highway fast-charging stations (DC charging with up to 350 kW), e-taxies, e-car sharing (both up to 100 kW), e-busses (up to 600 kW), and electric last-mile delivery vehicles (up to 350 kW).

In order to identify required ESS specifications for each e-mobility use case, time-resolved (one minute) charging load profiles (S_{EV}) are modeled based on real-life mobility data and EV specifics. As demonstrated in Eq. (6-1), each ESS's apparent power (S_{ESS}) is calculated for each time step t by subtracting the EV charging load and the respective grid element's initial load ($S_{Load,init}$) from its maximum thermal power ($S_{max,therm}$).

$$S_{ESS}(t) = S_{max,therm} - S_{Load,init}\ (t) - S_{EV}(t) \qquad (6\text{-}1)$$

$$Energy_{ESS}(t) = Energy_{ESS}(t-1) + \int_{t-1}^{t} P_{ESS} * dt \qquad (6\text{-}2)$$

$$required\ ESS\ discharging\ power = \frac{\min(S_{ESS}(t))}{\eta_{Discharging}} \qquad (6\text{-}3)$$

$$required\ ESS\ capacity = \min(Energy_{ESS}(t)) \qquad (6\text{-}4)$$

According to classic peak shaving, ESSs are discharged ($S_{ESS} < 0$) when EV charging loads exceed the available capacity of the grid. After discharging triggered by peak shaving needs, the supplied amount of energy is recharged ($S_{ESS} > 0$) into the ESS during off-peak periods, when the available grid capacity exceeds EV charging demands. The amount of energy stored in the ESS ($Energy_{ESS}$) is calculated in each time step t using Eq. (6-2). Finally, the required discharging power and energy capacity of each ESS is calculated based on Eq. (6-3) and (6-4). In this study, a discharging efficiency ($\eta_{Discharging}$) of 0.9 is used for ESSs.

This methodology reveals a broad range of required ESS specifications depending on the supplied EV use case and its charging characteristics (Figure 18): We found ESS capacities per charging point between 1 – 295 kWh, whereas an ESS discharging power between 6 – 356 kVA per charging point is necessary to provide sufficient grid support. E-mobility use cases integrated into the LV level (e.g., e-taxies, e-car charging) allow for even small ESS units (e.g., 5 kWh capacity and 100 kVA discharging power) to mitigate EV-induced peak loads. On the contrary, use cases charging with high power (> 100 kVA) require larger ESS units to prevent classic grid reinforcements. These results demonstrate that ESSs must be designed individually for each EV use case and application.

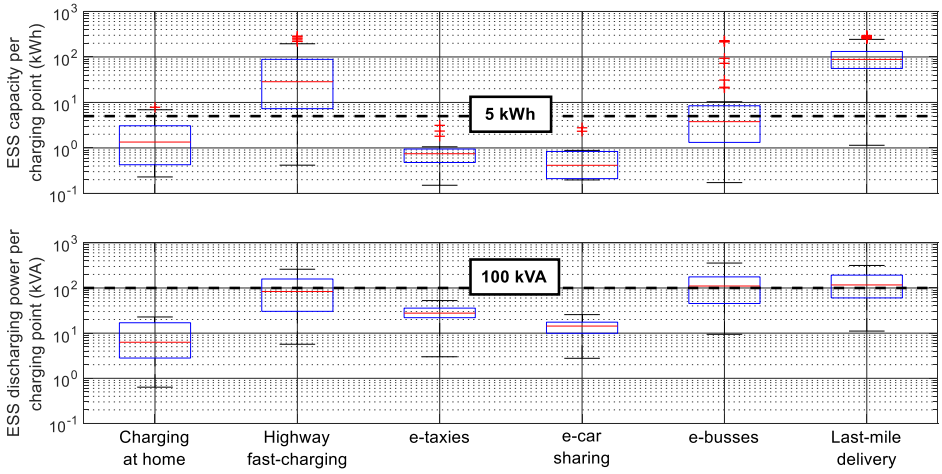

Figure 18: Specifications of energy storage systems (ESSs) required to prevent classic grid reinforcement measures depending on the supplied e-mobility use case [110]

In order to investigate the impact of the supplied EV application on the required ESS specifications, we have performed a comprehensive techno-economic analysis (Paper 2). Therefore, the correlations between EVs' mobility- and charging patterns, required ESS specifications, as well as technical- and economic aspects, are analyzed based on a sensibility analysis. Hence, the following parameters are altered while fixing the remaining ones to understand these correlations in detail: The covered distance per charging event, the available charging power per charging point, the number of installed charging points, and the installed grid capacity.

In our work, we focus primarily on flywheel ESSs, characterized by low energy- but high power density (Chapter 5.4.3). Thus, the required energy capacity of the ESS is selected as the first crucial indicator to evaluate its suitability. Since flywheels are also characterized by significant standby energy losses, their technical suitability is evaluated based on the ESS's energy efficiency as the second indicator. The total costs of operating the EV charging infrastructure, including grid connection, grid utilization, inverter, and flywheel, are selected as the third indicator.

Since flywheel ESSs allow for being discharged with very high power, three high-power charging EV use cases are selected for this analysis (see Table 1): Highway fast-charging of passenger vehicles (HFC), e-busses (EB), and electric last-mile delivery trucks (ELDT). By varying the previously mentioned parameters regarding EV charging, their influence on the required ESS capacity, the total annualized costs, and the ESS efficiency are identified for each use case. Figure 19 shows the correlation between the charging power of EVs and the total costs for operators of charging infrastructure (a) as well as the efficiency of flywheel ESS (b): Increasing the charging power of EVs increases the required ESS capacity and total costs. Simultaneously, it results in shorter charging periods, which increases the stand-by period of the flywheel. Due to higher stand-by losses, an increase in charging power decreases the efficiency of flywheel ESSs (Figure 19b). The correlations between each parameter and the analyzed indicators and their causes are described in Paper 2.

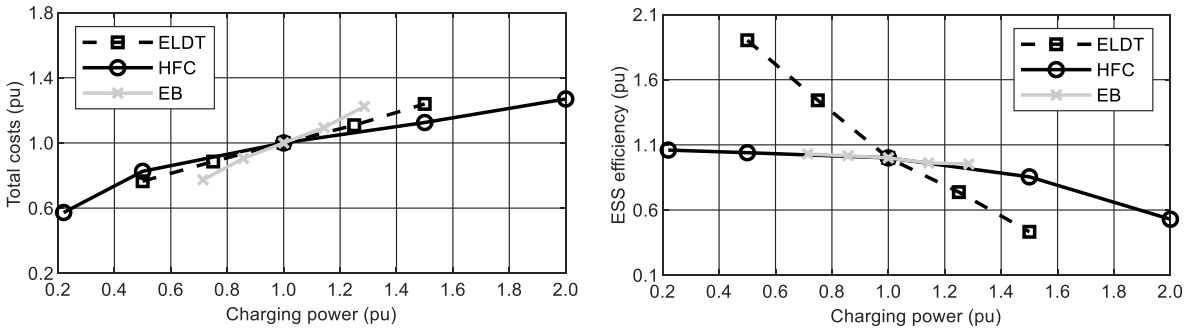

Figure 19: Impact of the EV charging power on (a) annualized total costs per charging point, and (b) ESS efficiency, regarding electric last-mile delivery trucks (ELDTs), highway fast-charging (HFC), and electric bus charging (EB) [107]

Based on these correlations, the economic (costs savings due to ESS) and technical suitability (ESS efficiency) are identified (Table 5). Short distances covered by EVs before recharging decrease the required ESS capacity, which allows higher cost savings when implementing ESSs. In contrast, they lead to shorter charging periods, which increases the stand-by period of ESSs and decreases their efficiency. Charging the EV with higher power leads to higher peak loads, which increases grid utilization charges. Consequently, the high-power charging of EVs allows

higher costs savings due to ESS. Vice versa, charging with higher power decreases the efficiency of ESS due to shorter charging periods (higher stand-by losses). Multiple charging points allow lower ESS costs per charging point than a single one.

Table 5: Correlations between EV charging parameters and the economic and technical suitability of (flywheel) ESSs

Parameter to be increased	Economical: Costs savings due to ESS	Technical: ESS efficiency
Covered distance per charging event	↓	↑
Charging power per charging point	↑	↓
Number of charging points	↑	↓

Hence, increasing the number of charging points improves the economic suitability of ESSs. In contrast, installing multiple charging points results in significant peak loads occurring only in a short period. However, the design of ESSs to cover these occasional short-term peak loads leads to low utilization and efficiency.

In summary, ESSs can provide costs benefits compared to classic grid reinforcements if multiple charging points supply low-distance EVs with high power. On this account, electric busses operated for urban transportation are the perfect use case for implementing ESSs. Stand-by energy losses (generally high due to short charging periods) are kept moderate due to the high frequency of bus stops and their recharging. Considering the supply of highway fast-charging and electrified last-mile delivery vehicles, ESSs enable minimal expenses only in the case of low-distance energy demands supplied with high charging power. However, the former criterion does not comply with the current mobility demand of these use cases. A significant decrease of specific ESS costs or a substantial rise in power-based grid utilization charges would definitely enhance the economic suitability of ESS, even for these two use cases.

The acquired conclusions regarding the economic suitability of flywheel ESSs can be applied to other ESS technologies, e.g., battery ESSs. In contrast, technical analysis of other ESS technologies would require another criterion (than stand-by energy losses applied in this study), e.g., the number of full cycles or lifetime.

7 DISCUSSION AND CONCLUSIONS

The implementation of future EV charging infrastructure must comply with the grid capacity of distribution networks. Potential bottlenecks in present-day distribution grids must be estimated realistically to plan the grid integration of e-mobility at an early stage. Consequently, DSOs are urged to identify potential grid reinforcement measures in their existing grids. However, the qualitative analysis of four LV grids (Chapter 6.1.3) demonstrates significant discrepancies between grid regions regarding their capacity to integrate EVs. While urban grids allow integrating numerous charging points, suburban and rural grids face inadmissible voltage deviations and/or transformer loads even at low EV penetrations. The hosting capacity of present-day LV grids also depends on the charging power of EVs: While charging with 11 kVA triggers significant grid restrictions even at low EV penetrations, three-phase charging with 3.7 kVA prevents any grid reinforcement measures.

The quantitative analysis of several thousand LV grids (Chapter 6.1.4) demonstrated that real-life distribution networks vary considerably in topology and customers even within the same grid region. The presented thesis examines this heterogeneity's impact on quantifying grid reinforcement costs for the first time: Several thousand LV grids must be simulated to evaluate the total need for grid reinforcement measures in a selected area with sufficient accuracy. In contrast, the simulation of only a few selected grids and their results' scaling might lead to erroneous results. Consequently, potential grid reinforcement needs and resulting costs due to future e-mobility might be misjudged significantly. **Hence, large-scale grid simulations become more and more crucial to help future grid planning.**

Nevertheless, the simulation of multiple grids requires significant computing resources and time. Static deterministic load flow simulation allows faster computation than time series-based or Monte-Carlo simulation (Chapter 5.3.2). In contrast, the latter two facilitate the consideration of temporal interdependences between grid customers' electrical loads. Static deterministic simulation methods applied in recent studies (Chapter 2.1.1) often neglect temporal intersections between grid customers, e.g., EVs, PV modules, or HPs. As a result, future grid conditions and resulting grid restrictions are misjudged substantially (Chapter 6.1.2). **As a countermeasure, grid customers' behavior and temporal interactions must be accurately considered in grid simulations.**

On the one hand, this includes the temporal intersection between different e-mobility use cases, e.g., charging at home or work. On the other, their temporal aggregation with other low carbon technologies (e.g., EVs, PV modules, or electric HPs) must also be considered. Novel coincidence factors developed in this study allow these considerations with adequate accuracy (Chapters 6.1.1 and 6.1.2).

Of course, the calculation of each customer's actual coincidence factor requires detailed knowledge concerning their actual behavior and characteristic. Considering EVs, both strongly depend on the particular use case. **As a result, modeling realistic charging profiles based on use case-specific mobility data is crucial for future grid planning processes to integrate e-mobility into the power system.** Furthermore, calculating each customer's actual coincidence factor increases the required computing time compared to more simplified load approaches. However, this level of detail is necessary to perform static load flow simulations with a sufficient level of accuracy.

In addition, the number of coincidence factors (single, double, or multiple) and the grid element based on which they are determined (e.g., the MV/LV substation) are crucial to perform accurate grid simulations. As analyzed in Chapter 6.1.2, simplified load approaches allow faster computation than more detailed ones. However, their misjudgment of grid customers' coincidence when evaluating remaining grid elements underestimates required grid reinforcement measures. **In conclusion, the coincidence factor applied to grid customers must be adapted according to the grid element to be analyzed. Hence, multiple coincidence factors per grid must be applied for load flow simulation to determine future grid loads accurately.**

In summary, the presented thesis demonstrates the following criteria to ensure accurate identification of future grid restrictions:

- Grid customer-combined coincidence factors, modeled based on realistic time series of existing and future grid customers, to include temporal interdependences (Chapter 6.1.1 and 6.1.2)
- Consideration of multiple coincidence factors depending on the grid element to be analyzed (Chapter 6.1.2)
- Large-scale grid simulation considering numerous grid structures (Chapter 6.1.3 and 6.1.4)

As demonstrated in Chapter 6.1, neglecting these aspects might misjudge future grid conditions and potential grid congestions. Consequently, the future power system might be designed inappropriately to integrate future grid customers. As part of the critical infrastructure, distribution networks must be designed to bear future power flows with sufficient certainty. Nevertheless, their oversizing should be avoided due to cost- and time-intensive grid planning and construction processes. **Hence, classic deterministic load approaches are inadmissible for identifying future grid congestions unless adapted to comply with future grid customers.**

All the presented criteria are considered when developing a fully automated large-scale grid simulation tool (Chapter 6.1.5). As a result, the developed grid simulation tool allows accurate quantification of grid reinforcement measures and costs triggered by future EVs, PV modules, and HPs. Therefore, novel coincidence factors are modeled, validated, and presented in this work (Chapter 6.1.1). By applying these combined coincidence factors, future grid loads induced by EVs, PV modules, or HPs, can be estimated correctly and applied for grid planning (6.1.2). Thereby, the benefits of static (fast computation) and time series-based grid simulations (considering temporal interdependences of customers accurately) can successfully be combined. **Tools and methods presented in this thesis allow us to overcome the highlighted shortcomings in the field of grid simulation. Thereby, it helps plan the integration of future customers, EVs in particular, more adequately.**

At this stage, the presented grid simulation tool only includes classic grid reinforcement measures, e.g., exchange of transformers, installation of additional grid lines. However, as demonstrated in Chapter 6.2, the analyzed grid-relieving measures can successfully prevent those measures. Hence, besides accurate grid simulation, future grid planning processes must include several flexibility options, e.g., ESSs, demand-side measures, and local grid reinforcements. Their selection, though, depends on the particular e-mobility use case. In particular, it depends on the use case's charging characteristics and the voltage level to be integrated. On the LV level, voltage violations induced by future EVs charging at home can successfully be prevented by installing a variable transformer at the MV/LV substation or critical feeders of present-day grids (Chapter 6.2.1). These measures could substantially increase the capacity to integrate future EVs, especially in suburban and rural areas, with primarily voltage violations as the most limiting factor (Chapter 6.1.3).

Nevertheless, variable transformers have no impact on thermal congestions of lines or transformers and are not applicable in urban areas. **Regardless of the considered grid region, a decrease of available charging power represents the most effective measure to mitigate grid congestions**. If charged, e.g., with 3.7 kVA, numerous EVs can be supplied by present-day distribution networks, avoiding voltage violations and thermal overloads (Chapter 6.2.1). In contrast, the increase of charging power (e.g., 11 kVA) increases the number of grid congestions and the demand for flexibility options.

As demonstrated in Chapter 5.4, there are two ways to limit the available power of EV charging: Grid-controlled (voltage- or current-controlled) or user-controlled. The former requires adequate information and communication technology to detect voltages or currents in the grid and adapt the charging power accordingly. Considering the latter, each EV user can freely decide about the power available at its charging point. Of course, to reduce the available charging power, adequate business models providing attractive incentives to the user must

be implemented. Adequate network tariffs, allowing the temporal switch between low- and high-power charging, could provide the required flexibility to the power grid. Besides the required amount of energy, the costs of charging the EVs would then depend on the selected charging power: If EV users choose to charge with low power (e.g., 3.7 kVA), charging costs can be reduced. Still, they would have the possibility to increase the available charging power if needed (e.g., to 11 kVA), of course, with higher charging costs. Analyzing real-life mobility data of the use case "Charging at home" illustrates that most users' mobility needs mainly comply with low-power charging (Figure 20). While 40 % of EVs do not require increased charging power during one year, only 8 % require high-power charging (> 3.7 kVA) more than 20 times a year. **Hence, implementing power-based charging tariffs can avoid expensive and time-consuming grid reinforcement measures while fulfilling the user's mobility needs.**

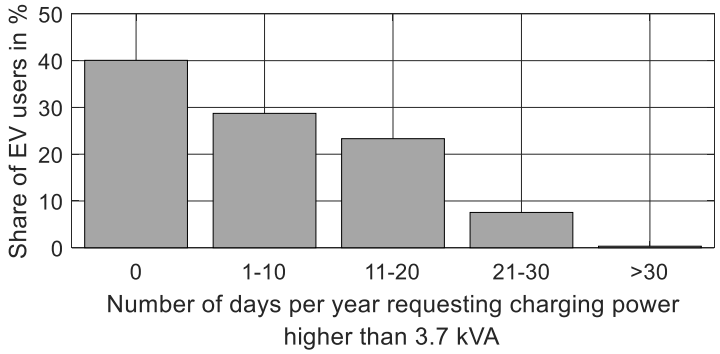

Figure 20: Annual frequency of high-power charging (> 3.7 kVA) required to fulfill EV users' mobility needs (Use case: Charging at home)

Of course, the limitation of charging power increases the required time of charging. While power-based charging tariffs do not lead to a loss in user comfort for private EV users, many e-mobility use cases (e.g., e-taxies, e-busses, highway fast-charging of passenger vehicles, and electric last-mile delivery vehicles) are characterized by strict schedules. **Since these use cases request high charging power to fulfill these schedules, they inhibit many demand-side measures, e.g., the temporal limitation of charging power.** High-power charging use cases challenge present-day distribution networks in particular due to considerable peak loads (Chapter 2). Although, charging peak loads occur only for short periods, in most cases, only a few minutes per year (Paper 2). Decentralized ESSs can successfully cover these short-term EV-induced peak loads by discharging the stored energy amount. The recharging of ESSs with low power during off-peak periods flattens the power grid's load curve and prevents classic grid reinforcements.

In fact, even small ESS units with a capacity of 5 kWh and 100 kVA can provide substantial grid support, supplying e-taxies or e-car sharing vehicles (Chapter 6.2.2). However, high-power charging EV use cases provide the most appropriate application of decentralized ESSs: Charging points of e-busses, highway fast chargers, and electric last-mile delivery vehicles are

mostly integrated into the MV level via specially installed transformers. ESSs can cover short-term peak loads and reduce the required transformer capacity (Chapter 6.2.2). Thereby, costs of grid connection and -utilization can be reduced considerably. For e-bus charging points, ESSs even allow substantial cost benefits compared to an exclusive supply by the local power grid (Chapter 6.2.2). Moreover, the local supply of e-bus charging represents the technically optimum application of flywheel ESSs. Due to its constant charging behavior and high EV charging power, flywheel ESSs can be operated with the highest efficiency, i.e., lowest standby energy losses from all the analyzed use cases (Chapter 6.2.2).

The characteristic of the charging demand of electric last-mile delivery vehicles or highway fast-charging EVs inhibits in most cases an economical implementation of ESSs. Unless the following framework conditions change: Firstly, ESSs would benefit from increased power-based system utilization charges in the upcoming years. Thereby, peak load shaving of short-term EV charging loads becomes more crucial and increases the economic suitability of ESSs. Several DSOs already demanded such tariffs to accomplish the integration of future grid customers [23]. Secondly, the total costs of ESSs must be reduced to compete with classic grid reinforcement measures economically. However, from a technical standpoint, flywheel ESSs are not suitable to supply electric last-mile delivery vehicles and highway fast-charging EVs (Chapter 6.2.2). Their charging behavior, characterized by long off-peak periods, results in significant standby energy losses using this ESS technology. Thus, besides economic aspects, technical criteria must be considered in grid planning processes, especially since energy savings are on the political agenda (e.g., [3]). Of course, ESS's standby energy losses during charging processes can be avoided by using other ESS technologies (e.g., battery ESS) to supply these use cases. Nevertheless, the results presented in Chapter 6.2.2 demonstrates that considering ESSs in future grid planning processes is crucial, especially concerning high-power charging EV use cases with short-term peak loads. Therefore, both economic and technical aspects must be taken into account.

Although this work focuses primarily on flywheel ESSs, its design methods and findings can also be applied to other ESS technologies, e.g., battery ESS or supercapacitors. Furthermore, the detected demand of flexibility, in this work provided by user- or voltage-controlled measures (Chapter 6.2.1) or ESSs (Chapter 6.2.2), can be provided by any form of flexibility option. In fact, the presented results clearly show that several grid-relieving measures can prevent classic grid reinforcement measures triggered by EV charging. Although, the individual selection of the optimum measure must undoubtedly comply with the supplied EV use case and its charging characteristics. **Consequently, from demand-side measures over ESSs to classic grid reinforcements, various solutions must be part of the future power system.** Only this way, future e-mobility use cases are integrated most efficiently.

The accurate identification of EV-induced grid restrictions (Chapter 6.1) and the adequate evaluation of countermeasures (Chapter 6.2) require detailed knowledge of grid customers' electrical loads. Concerning EVs, this knowledge can be acquired by real-life mobility data. Furthermore, EV classes (e.g., passenger vehicles, trucks) and models (e.g., Tesla Model S, BMW i3) differ significantly regarding the following aspects (Chapter 5.1): Charging process (possible charging power, number of phases, charge curve, power factor), battery capacity, specific energy demand. **Both real-life mobility data and EV specifics must also be included when modeling realistic charging profiles of EVs**. Hence, future grid planning would benefit from an extensive database containing users' mobility patterns and vehicle charging specifics. Of course, in an anonymous form fulfilling all data protection issues.

8 OUTLOOK

Although the presented thesis answers the highlighted research questions (Chapter 3), it still shows room for improvements and future research. Initially, a fully automated large-scale grid simulation tool developed and published in this work uses static (or steady-state) deterministic load flow simulations. While those allow significantly faster computation than time series-based simulations, they inhibit considering time-related aspects. For example, the duration of grid congestions or voltage violations according to the EN 50160 (evaluation based on 10-minute mean values) [162] are excluded. Furthermore, adequate implementation of ESSs or demand-side measures relies on a time-resolved comparison of grid conditions (e.g., voltages) and the flexibility potential (e.g., available energy stored in the ESS or given mobility needs). Therefore, future work should focus on the presented grid simulation tool's extension to allow time-resolved load flow simulations. Of course, the required computing time must still be reasonable. On this account, further studies should also analyze the trade-off between time resolution (e.g., 1 minute vs. 15 minutes) and simulation accuracy concerning the investigation of future grid customers.

Besides, this work analyzes the potential of various measures to integrate EVs in a grid-friendly way separately. Thus, it neglects a combined implementation of multiple flexibility options and its grid-relieving potential. However, the integration of future e-mobility will rely on the optimum cooperation of multiple options. This cooperation will depend on the particular e-mobility use case and the local distribution network. For example, if some EV users in LV grids refuse demand-side measures, individual power regulation or local grid reinforcement measures might additionally be required.

Furthermore, schedules of high-power charging e-mobility use cases (e.g., e-busses) might be modified to reduce the required ESS capacity required to mitigate peak loads. Future research should optimize the cooperation of multiple grid-relieving measures regarding different EV use cases. Of course, the actual application of flexibility options will strongly or entirely depend on their economic suitability. Therefore, future work should compare multiple flexibility options' economic efficiency (including grid reinforcement measures) to guide future grid planners.

Finally, the presented thesis focuses in particular on decentralized flywheels as an energy storage technology. While the findings of the presented thesis can validly be applied to other ESS technologies, each of them has its benefits and shortcomings. On this account, the suitability of various ESS technologies to supply different EV use cases would be interesting. Also, in this regard, the current state of research would benefit from comparing ESS technologies' total costs of ownership.

9 REFERENCES

[1] WORLD METEOROLOGICAL ORGANIZATION: *State of the Global Climate 2020*. 2021

[2] EUROPEAN ENVIRONMENT AGENCY: *National emissions reported to the UNFCCC and to the EU Greenhouse Gas Monitoring Mechanism*. URL https://www.eea.europa.eu/data-and-maps/daviz/share-of-transport-ghg-emissions-2#tab-googlechartid_chart_11 – Überprüfungsdatum 2020-07-24

[3] EUROPEAN COMMISION: *Communication from the Commission to the European Parliament, the European Council, the Council, the European Economic and Social Committee and the Committee of the Regions* (idF v. COM(2019) 640 final) (2019-12-11) – Überprüfungsdatum 2019-05-14

[4] EUROPEAN PARLIAMENT: *MEPs approve new CO2 emissions limits for trucks*. URL https://www.europarl.europa.eu/news/en/press-room/20190412IPR39009/meps-approve-new-co2-emissions-limits-for-trucks – Überprüfungsdatum 2020-07-24

[5] EUROPEAN PARLIAMENT: *Parliament backs new CO2 emissions limits for cars and vans*. URL https://www.europarl.europa.eu/news/en/press-room/20190321IPR32112/parliament-backs-new-co2-emissions-limits-for-cars-and-vans – Überprüfungsdatum 2020-07-24

[6] UNITED NATIONS: *Environment programme*. URL https://www.unep.org/explore-topics/transport/what-we-do/electric-mobility/why-does-electric-mobility-matter#_msocom_1 – Überprüfungsdatum 2021-07-29

[7] XUE, Chenlei ; ZHOU, Huaguo ; WU, Qunqi ; WU, Xueying ; XU, Xingbo: *Impact of Incentive Policies and Other Socio-Economic Factors on Electric Vehicle Market Share: A Panel Data Analysis from the 20 Countries*. In: *Sustainability* 13 (2021), Nr. 5, S. 2928

[8] EUROPEAN COURT OF AUDITORS (Hrsg.): *Infrastructure for charging electric vehicles* : *More charging stations but uneven deployment makes travel across the EU complicated*. May, 2021

[9] NEUBAUER, Jeremy ; WOOD, Eric: *The impact of range anxiety and home, workplace, and public charging infrastructure on simulated battery electric vehicle lifetime utility*. In: *Journal of Power Sources* 257 (2014), S. 12–20

[10] KLOESS, Maximilian ; MÜLLER, Andreas: *Simulating the impact of policy, energy prices and technological progress on the passenger car fleet in Austria—A model based analysis 2010–2050*. In: *Energy Policy* 39 (2011), Nr. 9, S. 5045–5062

[11] STATISTICS AUSTRIA: *Stock of motor vehicles*

[12] UMWELTBUNDESAMT GMBH (Hrsg.): *Elektromobilität in Österreich* : *Szenario 2020 und 2050*. REP-0257. 2010

[13] EBERHARD, T. ; STEGER-VONMETZ, C.: *Elektro-Autos zuhause laden* : *Bedarf an und Maßnahmen für Heimladestationen in Wohnanlagen*. 2019

[14] AJANOVIC, Amela ; SIEBENHOFER, Marina ; HAAS, Reinhard: *Electric Mobility in Cities: The Case of Vienna*. In: *Energies* 14 (2021), Nr. 1, S. 217

[15] SOMMER, Mark ; KRATENA, Kurt ; MEYER, Ina ; KIRCHNER, Matthias: *Energy Scenarios 2030-2050* : *Energy-economic Impacts from Reaping Energy Efficiency Potentials in Industry and Households*. URL www.wifo.ac.at – Überprüfungsdatum 23 Ausgust, 2021

[16] *Electric vehicles and the energy sector* : *Impacts on Europe's future emissions*. [Luxembourg] : [Publications Office], 2016 (EEA briefing)

[17] LIU, Ryan ; DOW, Luther ; LIU, Edwin: A survey of PEV impacts on electric utilities. In: *ISGT 2011* : IEEE, 2011 - 2011, S. 1–8

[18] EP ELEKTROMOBILITÄT DES AK VERTEILERNETZE: *Aktuelle und zukünftige Anforderungen an Ladeeinrichtungen für Elektrofahrzeuge* : *Leitfaden*. 22.08.2018

[19] OESTERREICHS ENERGIE: *E-Mobilitätstage: 14 Prozent mehr Strom für 100 Prozent E-Mobilität in Österreich*. URL https://oesterreichsenergie.at/aktuelles/presseinformationen/detailseite/default-ff4c437761. – Aktualisierungsdatum: 2021-11-25 – Überprüfungsdatum 2021-11-25

[20] OESTERREICHS ENERGIE: *Abschlussbericht des EP EMN Ladeinfrastruktur des AK Verteilernetze*. 2016

[21] VERBAND DER ELEKTROTECHNIK ELEKTRONIK INFORMATIONSTECHNIK E.V.: *Netzintegration Elektromobilität* : *Leitfaden für eine flächendeckende Verbreitung von E-Fahrzeugen*

[22] AGORA VERKEHRSWENDE ; AGORA ENERGIEWENDE ; REGULATORY ASSISTANCE PROJECT (RAP): *Verteilnetzausbau für die Energiewende – Elektromobilität im Fokus*. 2019

[23] ASSOCIATION OF AUSTRIAN ELECTRICITY COMPANIES: *Netzberechnungen Österreich - Einfluss der Entwicklungen von Elektromobilität und Photovoltaik auf das österreichische Stromnetz*. URL www.oesterreichsenergie.at/die-welt-des-stroms/stromnetze/studie-netzberechnungen-oesterreich.html. – Aktualisierungsdatum: January 2021

[24] SHAHNIA, Farhad ; GHOSH, Arindam ; LEDWICH, Gerard ; ZARE, Firuz: *Predicting Voltage Unbalance Impacts of Plug-in Electric Vehicles Penetration in Residential Low-voltage Distribution Networks*. In: *Electric Power Components and Systems* 41 (2013), Nr. 16, S. 1594–1616

[25] SHAFIEE, Soroush ; FOTUHI-FIRUZABAD, Mahmud ; RASTEGAR, Mohammad: *Investigating the Impacts of Plug-in Hybrid Electric Vehicles on Power Distribution Systems*. In: *IEEE Transactions on Smart Grid* 4 (2013), Nr. 3, S. 1351–1360

[26] STEEN, David ; LE TUAN, Anh ; CARLSON, Ola ; BERTLING, Lina: *Assessment of Electric Vehicle Charging Scenarios Based on Demographical Data*. In: *IEEE Transactions on Smart Grid* 3 (2012), Nr. 3, S. 1457–1468

[27] DUBEY, Anamika ; SANTOSO, Surya: *Electric Vehicle Charging on Residential Distribution Systems: Impacts and Mitigations*. In: *IEEE Access* 3 (2015), S. 1871–1893

[28] NAVARRO-ESPINOSA, Alejandro ; OCHOA, Luis F.: *Probabilistic Impact Assessment of Low Carbon Technologies in LV Distribution Systems*. In: *IEEE Transactions on Power Systems* 31 (2016), Nr. 3, S. 2192–2203

[29] THORMANN, Bernd ; KIENBERGER, Thomas: *Evaluation of Grid Capacities for Integrating Future E-Mobility and Heat Pumps into Low-Voltage Grids*. In: *Energies* 13 (2020), Nr. 19, S. 5083

[30] HARDMAN, Scott ; JENN, Alan ; TAL, Gil ; AXSEN, Jonn ; BEARD, George ; DAINA, Nicolo ; FIGENBAUM, Erik ; JAKOBSSON, Niklas ; JOCHEM, Patrick ; KINNEAR, Neale ; PLÖTZ, Patrick ; PONTES, Jose ; REFA, Nazir ; SPREI, Frances ; TURRENTINE, Tom ; WITKAMP, Bert: *A review of consumer preferences of and interactions with electric vehicle charging infrastructure*. In: *Transportation Research Part D: Transport and Environment* 62 (2018), S. 508–523

[31] BARESCH, Martin ; MOSER, Simon: *Allocation of e-car charging: Assessing the utilization of charging infrastructures by location*. In: *Transportation Research Part A: Policy and Practice* 124 (2019), S. 388–395

[32] GNANN, Till ; PLÖTZ, Patrick ; WIETSCHEL, Martin: How to address the chicken-egg-problem of electric vehicles? Introducing an interaction market diffusion model for EVs and charging infrastructure. In: *Proceedings of the ECEEE Summer Study 2015*.

[33] LIU, Jian: *Electric vehicle charging infrastructure assignment and power grid impacts assessment in Beijing*. In: *Energy Policy* 51 (2012), S. 544–557

[34] NATIONALE PLATTFORM ELEKTROMOBILITÄT: *Zweiter Bericht der Nationalen Plattform Elektromobilität*

[35] KLEY, Fabian: *Ladeinfrastruktur für Elektrofahrzeuge* : *Entwicklung und Bewertung einer Ausbaustrategie auf Basis des Fahrverhaltens*. Zugl.: Karlsruhe, KIT, Diss., 2011. Stuttgart : Fraunhofer Verl., 2011 (ISI-Schriftenreihe "Innovationspotenziale")

[36] NEWMAN, Daniel ; WELLS, Peter ; DONOVAN, Ceri ; NIEUWENHUIS, Paul ; DAVIES, Huw: *Urban, sub-urban or rural: where is the best place for electric vehicles?* In: *International Journal of Automotive Technology and Management* 14 (2014), 3/4, S. 306

[37] SINHA, Rakesh ; BAK-JENSEN, Birgitte ; PILLAI, Jayakrishnan Radhakrishna: *Operational flexibility of electrified transport and thermal units in distribution grid*. In: *International Journal of Electrical Power & Energy Systems* 121 (2020), S. 106029

[38] BÜCHNER, J. ; KATZFEY, J. ; FLÖRCKEN, O. ; MOSER, A. ; SCHUSTER, H. ; DIERKES, S. ; ET AL.: *Moderne Verteilnetze fuer Deutschland. Verteilernetzstudie*. 2014

[39] *Electric buses: where are we?* In: *IES SYNERGY* (2021-03-04)

[40] SCHUSTER, Markus ; STEINACHER, Irene ; LINK, Christoph: *Marktübersicht* : *Elektro- und Wasserstoffbusse*. January 2021

[41] OTS.AT: *Wiener Stadtwerke starten eines der weltweit größten E-Taxi Projekte*. URL https://www.ots.at/presseaussendung/OTS_20150521_OTS0057/wiener-stadtwerke-starten-eines-der-weltweit-groessten-e-taxi-projekte-bild. – Aktualisierungsdatum: 2021-08-25 – Überprüfungsdatum 2021-08-25

[42] OTS.AT: *Premiere für österreichweites E-Car-Sharing*. URL https://www.ots.at/presseaussendung/OTS_20210701_OTS0179/premiere-fuer-oesterreichweites-e-car-sharing-bild. – Aktualisierungsdatum: 2021-08-25 – Überprüfungsdatum 2021-08-25

[43] EUROPEAN ENVIRONMENT AGENCY (Hrsg.): *The first and last mile — the key to sustainable urban transport* : *Transport and environment report 2019*. 2019

[44] STATISTA: *Österreichische Post AG - Elektro-Fahrzeuge ohne Tochterunternehmen 2020*. – Aktualisierungsdatum: 2021-08-25 – Überprüfungsdatum 2021-08-25

[45] THORMANN, Bernd ; PURGSTALLER, Wilfried ; KIENBERGER, Thomas: *Evaluating the potential of future e-mobility use cases for providing grid ancillary services*. In: *Proceedings to CIRED conference 2021* (2021)

[46] CERIO MENDAZA, Iker Diaz de ; BAK-JENSEN, Birgitte ; CHEN, Zhe ; JENSEN, Allan: Stochastic impact assessment of the heating and transportation systems electrification on LV grids. In: *IEEE PES Innovative Smart Grid Technologies Conference Europe (ISGT-Europe), 2014 : 12 - 15 Oct. 2014, Istanbul*. Piscataway, NJ : IEEE, 2014, S. 1–6

[47] HÜLSMANN ET AL.: Electric Vehicle and Heat Pump Hosting Capacity Assessment for a German 25,000-noded Distribution Network. In: *Proceedings of the 3rd E-Mobility Power System Integration Symposium 2019*.

[48] SHAO, N. ; YOU, S. ; SEGERBERG, H.: Integration of 100% heat pumps and electric vehicles in the low voltage distribution network: A Danish case story. : In Proceedings of 3rd International Conference on Microgeneration and Related Technologies 2013. In:

[49] LI, Y. ; CROSSLEY, P. A.: Monte Carlo study on impact of electric vehicles and heat pumps on LV feeder voltages. In: *12th IET International Conference on Developments in Power System Protection (DPSP 2014)* : *March 31 2014-April 3 2014*. Piscataway, NJ : IEEE, 2014, 12.13-12.13

[50] BACCINO, F. ; MASSUCCO, S. ; SILVESTRO, F. ; GRILLO, S.: Management strategy for unbalanced LV distribution network with electric vehicles, heat pumps and domestic photovoltaic penetration. In: *2014 IEEE PES general meeting* : *Conference & exposition ; 27-31 July 2014, National Harbor, MD*. Piscataway, NJ : IEEE, 2014, S. 1–5

[51] BIRK, Sascha ; BROSIG, Christian ; WAFFENSCHMIDT, Eberhard ; SCHNEIDERS, Thorsten: Influence of Sector Coupling in Future Inner City Low Voltage Grids. In: *2018 7th International Energy and Sustainability Conference (IESC)* : *17-18 May 2018*. Piscataway, NJ : IEEE, 2018, S. 1–8

[52] KATHAN, J. ; SCHWALBE, R. ; BRUNNER, H. ; KOLLMANN, A. ; TALJAN, G. ; NEUMANN, K. ; ET AL.: *leafs - Integration of Loads and Electric Storage Systems into advanced Flexibility Schemes for LV Networks*. Vienna, September 2019

[53] GUPTA, Ruchi ; PENA-BELLO, Alejandro ; STREICHER, Kai Nino ; RODUNER, Cattia ; FARHAT, Yamshid ; THÖNI, David ; ET AL.: *Spatial analysis of distribution grid capacity and costs to enable massive deployment of PV, electric mobility and electric heating*. In: *Applied Energy* 287 (2021), S. 116504

[54] AGRICOLA, A. ; HÖFLICH, B. ; RICHARD, P. ; VÖLKER, J. ; REHTANZ, C. ; GREVE, M. ; ET AL.: *dena-Verteilnetzstudie. Ausbau- und Innovationsbedarf der Stromverteilnetze in Deutschland bis 2030. Edited by Energiesysteme und Energiedienstleistungen*. Berlin, Germany, 2012

[55] VU, Trung: *A Stochastic Methodology to Determine Reinforcement Cost of Power Distribution Grid for Integrating Increasing Share of Renewable Energies and Electric Vehicles*, S. 1–5

[56] SCHWAB, Adolf J.: *Elektroenergiesysteme*. Berlin, Heidelberg : Springer Berlin Heidelberg, 2012

[57] HARTVIGSSON, Elias ; ODENBERGER, Mikael ; CHEN, Peiyuan ; NYHOLM, Emil: *Estimating national and local low-voltage grid capacity for residential solar photovoltaic in Sweden, UK and Germany*. In: *Renewable Energy* 171 (2021), S. 915–926

[58] FLINN, J. ; WEBBER, C. ; TONG, N. ; COX, R.: *Customer Distributed energy resources grid integration study* : *Residential Zero Net Energy Building Integration Cost Analysis*

[59] LEMMENS, Joris ; MACHARIS, Bruno ; GYS, Roy ; VONKEN, Dieter; My University (Mitarb.): *Data-driven asset management with the NGIN analytics platform: Assessing EV and PV impact on the Flemish LV grid*. 2019

[60] ROTHROCK, Ling ; NARAYANAN, S.: *Human-in-the-Loop Simulations*. London : Springer London, 2011

[61] M. WAHL ; L. HEIN ; A. MOSER: Fast Power Flow Calculation Method for Grid Expansion Planning. In: *2019 21st European Conference on Power Electronics and Applications (EPE '19 ECCE Europe)*, 2019, P.1-P.7

[62] WILLIS, H. Lee: *Power distribution planning reference book*. 2. ed., rev. and expanded., 2004 (Power engineering)

[63] OESTERREICHS ENERGIE (Hrsg.); OVE ÖSTERREICHISCHER VERBAND FÜR ELEKTROTECHNIK (Hrsg.): *TAEV 2012* : *Technical connection conditions for connection to public supply networks with operating voltages up to 1000 Volt*. (in German: Technische Anschlussbedingungen für den Anschluss an öffentliche Versorgungsnetze mit Betriebsspannungen bis 1000 Volt

[64] SHAO, Shengnan ; PIPATTANASOMPORN, Manisa ; RAHMAN, Saifur: *Demand Response as a Load Shaping Tool in an Intelligent Grid With Electric Vehicles*. In: *IEEE Transactions on Smart Grid* 2 (2011), Nr. 4, S. 624–631

[65] FADDEL, Samy ; MOHAMMED, Osama A.: *Automated Distributed Electric Vehicle Controller for Residential Demand Side Management*. In: *IEEE Transactions on Industry Applications* 55 (2019), Nr. 1, S. 16–25

[66] BRINKEL, N.B.G. ; SCHRAM, W. L. ; ALSKAIF, T. A. ; LAMPROPOULOS, I. ; VAN SARK, W.G.J.H.M.: *Should we reinforce the grid? Cost and emission optimization of electric vehicle charging under different transformer limits*. In: *Applied Energy* 276 (2020), S. 115285

[67] RICHARDSON, Peter ; FLYNN, Damian ; KEANE, Andrew: *Local Versus Centralized Charging Strategies for Electric Vehicles in Low Voltage Distribution Systems*. In: *IEEE Transactions on Smart Grid* 3 (2012), Nr. 2, S. 1020–1028

[68] CLEMENT-NYNS, K. ; HAESEN, E. ; DRIESEN, J.: *The Impact of Charging Plug-In Hybrid Electric Vehicles on a Residential Distribution Grid*. In: *IEEE Transactions on Power Systems* 25 (2010), Nr. 1, S. 371–380

[69] García-Villalobos, J. ; Zamora, I. ; Knezović, K. ; Marinelli, M.: *Multi-objective optimization control of plug-in electric vehicles in low voltage distribution networks*. In: *Applied Energy* 180 (2016), S. 155–168

[70] Goli, P. ; Shireen, W.: *PV powered smart charging station for PHEVs*. In: *Renewable Energy* 66 (2014), S. 280–287

[71] Liu, Nian ; Zou, Fuqiang ; Wang, Lingfeng ; Wang, Cheng ; Chen, Zhineng ; Chen, Qifang: *Online energy management of PV-assisted charging station under time-of-use pricing*. In: *Electric Power Systems Research* 137 (2016), S. 76–85

[72] Leemput, N. ; van Roy, J. ; Geth, F. ; Tant, P. ; Claessens, B. ; Driesen, J.: Comparative analysis of coordination strategies for electric vehicles. In: *2011 2nd IEEE PES International Conference and Exhibition on Innovative Smart Grid Technologies* : IEEE, 122011, S. 1–8

[73] Zecchino, Antonio ; Marinelli, Mattia: *Analytical assessment of voltage support via reactive power from new electric vehicles supply equipment in radial distribution grids with voltage-dependent loads*. In: *International Journal of Electrical Power & Energy Systems* 97 (2018), S. 17–27. URL https://www.sciencedirect.com/science/article/pii/S0142061517308979

[74] Knezović, Katarina ; Marinelli, Mattia: *Phase-wise enhanced voltage support from electric vehicles in a Danish low-voltage distribution grid*. In: *Electric Power Systems Research* 140 (2016), S. 274–283

[75] Geth, Frederik ; Leemput, Niels ; van Roy, Juan ; Buscher, Jeroen ; Ponnette, Raf ; Driesen, Johan: Voltage droop charging of electric vehicles in a residential distribution feeder. In: *2012 3rd IEEE PES innovative smart grid technologies Europe (ISGT Europe 2012)* : *International conference and exhibition] ; Berlin, Germany, 14 - 17 October 2012*. Piscataway, NJ : IEEE, 2012, S. 1–8

[76] Ireshika, Muhandiram Arachchige Subodha Tharangi ; Lliuyacc-Blas, Ruben ; Kepplinger, Peter: *Voltage-Based Droop Control of Electric Vehicles in Distribution Grids under Different Charging Power Levels*. In: *Energies* 14 (2021), Nr. 13, S. 3905

[77] Al-Awami, Ali T. ; Sortomme, Eric ; Asim Akhtar, Ghous Muhammad ; Faddel, Samy: *A Voltage-Based Controller for an Electric-Vehicle Charger*. In: *IEEE Transactions on Vehicular Technology* 65 (2016), Nr. 6, S. 4185–4196

[78] Leemput, Niels ; Geth, Frederik ; van Roy, Juan ; Büscher, Jeroen ; Driesen, Johan: *Reactive power support in residential LV distribution grids through electric vehicle charging*. In: *Sustainable Energy, Grids and Networks* 3 (2015), S. 24–35

[79] MANBACHI, Moein ; FARHANGI, Hassan ; PALIZBAN, Ali ; ARZANPOUR, Siamak: *A novel Volt-VAR Optimization engine for smart distribution networks utilizing Vehicle to Grid dispatch*. In: *International Journal of Electrical Power & Energy Systems* 74 (2016), S. 238–251. URL https://www.sciencedirect.com/science/article/pii/S0142061515003166

[80] MORVAJ, Boran ; KNEZOVIĆ, Katarina ; EVINS, Ralph ; MARINELLI, Mattia: *Integrating multi-domain distributed energy systems with electric vehicle PQ flexibility: Optimal design and operation scheduling for sustainable low-voltage distribution grids*. In: *Sustainable Energy, Grids and Networks* 8 (2016), S. 51–61

[81] LEEMPUT, Niels ; GETH, Frederik ; VAN ROY, Juan ; DELNOOZ, Annelies ; BUSCHER, Jeroen ; DRIESEN, Johan: *Impact of Electric Vehicle On-Board Single-Phase Charging Strategies on a Flemish Residential Grid*. In: *IEEE Transactions on Smart Grid* 5 (2014), Nr. 4, S. 1815–1822

[82] YONG, Jia Ying ; RAMACHANDARAMURTHY, Vigna K. ; TAN, Kang Miao ; MITHULANANTHAN, N.: *Bi-directional electric vehicle fast charging station with novel reactive power compensation for voltage regulation*. In: *International Journal of Electrical Power & Energy Systems* 64 (2015), S. 300–310

[83] KRASSELT, Peter ; SURIYAH, Michael R. ; LEIBFRIED, Thomas: *Reactive power support for optimal grid integration of fast-charging infrastructure in German low-voltage networks*. In: *CIRED 2015 conference procedings* (2015)

[84] FRANCO, John Fredy ; PROCOPIOU, Andreas T. ; QUIRÓS-TORTÓS, Jairo ; OCHOA, Luis F.: *Advanced control of OLTC-enabled LV networks with PV systems and EVs*. In: *IET Generation, Transmission & Distribution* 13 (2019), Nr. 14, S. 2967–2975

[85] HUANG, Shaojun ; PILLAI, Jayakrishnan R. ; LISERRE, Marco ; BAK-JENSEN, Birgitte: Improving photovoltaic and electric vehicle penetration in distribution grids with smart transformer. In: *4th IEEE/PES innovative smart grid technologies Europe (ISGT Europe), 2013* : *Conference] ; 6 - 9 Oct. 2013, Lyngby [near] Copenhagen, Denmark*. Piscataway, NJ : IEEE, 2013, S. 1–5

[86] NAVARRO-ESPINOSA, Alejandro: *Deliverable 4.1 "Assessment of Potential LV network solutions"*. 2014

[87] XIE, Qiangqiang ; SHENTU, Xiangrong ; WU, Xusheng ; DING, Yi ; HUA, Yongzhu ; CUI, Jiadong: *Coordinated Voltage Regulation by On-Load Tap Changer Operation and Demand Response Based on Voltage Ranking Search Algorithm*. In: *Energies* 12 (2019), Nr. 10, S. 1902

[88] GRABER, G. ; GALDI, V. ; CALDERARO, V. ; MANCARELLA, P.: A stochastic approach to size EV charging stations with support of second life battery storage systems. In: *2017 IEEE Manchester PowerTech* : *18-22 June 2017*. Piscataway, NJ : IEEE, 2017, S. 1–6

[89] DAI, Qiongjie ; LIU, Jicheng ; WEI, Qiushuang: *Optimal Photovoltaic/Battery Energy Storage/Electric Vehicle Charging Station Design Based on Multi-Agent Particle Swarm Optimization Algorithm*. In: *Sustainability* 11 (2019), Nr. 7, S. 1973

[90] NEGARESTANI, Soodeh ; FOTUHI-FIRUZABAD, Mahmud ; RASTEGAR, Mohammad ; RAJABI-GHAHNAVIEH, Abbas: *Optimal Sizing of Storage System in a Fast Charging Station for Plug-in Hybrid Electric Vehicles*. In: *IEEE Transactions on Transportation Electrification* 2 (2016), Nr. 4, S. 443–453

[91] SALAPIC, Vjekoslav ; GRZANIC, Mirna ; CAPUDER, Tomislav: Optimal sizing of battery storage units integrated into fast charging EV stations. In: *2018 IEEE International Energy Conference (ENERGYCON)* : *3-7 June 2018*. Piscataway, NJ : IEEE, 2018, S. 1–6

[92] DOMÍNGUEZ-NAVARRO, J. A. ; DUFO-LÓPEZ, R. ; YUSTA-LOYO, J. M. ; ARTAL-SEVIL, J. S. ; BERNAL-AGUSTÍN, J. L.: *Design of an electric vehicle fast-charging station with integration of renewable energy and storage systems*. In: *International Journal of Electrical Power & Energy Systems* 105 (2019), S. 46–58

[93] HUSSAIN ; BUI ; BAEK ; KIM: *Stationary Energy Storage System for Fast EV Charging Stations: Simultaneous Sizing of Battery and Converter*. Energies, 12(23), 4516 (2019)

[94] CHANDRA MOULI, G. R. ; BAUER, P. ; ZEMAN, M.: *System design for a solar powered electric vehicle charging station for workplaces*. In: *Applied Energy* 168 (2016), S. 434–443

[95] DING, Huajie ; HU, Zechun ; SONG, Yonghua: *Value of the energy storage system in an electric bus fast charging station*. In: *Applied Energy* 157 (2015), S. 630–639

[96] BAI, Sanzhong ; YU, Du ; LUKIC, Srdjan: Optimum design of an EV/PHEV charging station with DC bus and storage system. In: *Proceedings of the IEEE Energy Conversion Congress and Expo (ECCE), Atlanta, Georgia, 2010*, pp. 1178–1184

[97] BAYRAM, I. Safak ; MICHAILIDIS, George ; DEVETSIKIOTIS, Michael ; BHATTACHARYA, Subhashish ; CHAKRABORTTY, Aranya ; GRANELLI, Fabrizio: Local energy storage sizing in plug-in hybrid electric vehicle charging stations under blocking probability constraints. In: *IEEE International Conference on Smart Grid Communications (SmartGridComm 2011)* : *17 - 20 Oct. 2011, Brussels, Belgium*. Piscataway, NJ : IEEE, 2011, S. 78–83

[98] JOOS, G. ; FREIGE, M. de ; DUBOIS, M.: Design and simulation of a fast charging station for PHEV/EV batteries. In: *Electrical Power and Energy Conference (EPEC) 2010* :

Sustainable energy for an intelligent grid : August 25-27, 2010, Halifax, NS, Canada. [Piscataway, N.J.] : IEEE, 2010, S. 1–5

[99] MARJAN GJELAJ ; NATALY BAÑOL ARIAS ; CHRESTEN TRAEHOLT ; SEYEDMOSTAFA HASHEMI: *Multifunctional applications of batteries within fast-charging stations based on EV demand-prediction of the users' behaviour*. In: *The Journal of Engineering* 2019 (9280), Nr. 18, S. 4869–4873

[100] PIROMJIT, Pittayut ; TAYJASANANT, Thavatchai: Peak-demand management for improving undervoltages in distribution systems with electric vehicle connection by stationary battery. In: *2017 IEEE Transportation Electrification Conference and Expo, Asia-Pacific (ITEC Asia-Pacific)* : *7-10 Aug. 2017*. Piscataway, NJ : IEEE, 2017, S. 1–6

[101] HELD, Lukas ; KRAMER, Hannah ; ZIMMERLIN, Martin ; SURIYAH, Michael R. ; LEIBFRIED, Thomas ; RATAJCZAK, Levin ; LOSSAU, Selma ; KONERMANN, Martin: Dimensioning of battery storage as temporary equipment during grid reinforcement caused by electric vehicles. In: *2018 53rd International Universities Power Engineering Conference (UPEC)* : *4th-7th September 2018, Glasgow, United Kingdom : proceedings*. Piscataway, NJ : IEEE, 2018, S. 1–6

[102] DRAGICEVIC, Tomislav ; SUCIC, Stjepan ; VASQUEZ, Juan C. ; GUERRERO, Josep M.: *Flywheel-Based Distributed Bus Signalling Strategy for the Public Fast Charging Station*. In: *IEEE Transactions on Smart Grid* 5 (2014), Nr. 6, S. 2825–2835

[103] LIU, Yang ; TANG, Yuejin ; SHI, Jing ; SHI, Xiaohan ; DENG, Jiaxi ; GONG, Kang: *Application of Small-Sized SMES in an EV Charging Station With DC Bus and PV System*. In: *IEEE Transactions on Applied Superconductivity* 25 (2015), Nr. 3, S. 1–6

[104] T. S. BRYDEN ; G. HILTON ; B. DIMITROV ; C. PONCE DE LEÓN ; A. CRUDEN: *Rating a Stationary Energy Storage System Within a Fast Electric Vehicle Charging Station Considering User Waiting Times*. In: *IEEE Transactions on Transportation Electrification* 5 (2019), Nr. 4, S. 879–889

[105] LIGEN, Yorick ; VRUBEL, Heron ; GIRAULT, Hubert: *Local Energy Storage and Stochastic Modeling for Ultrafast Charging Stations*. Energies, 12(10), 1986 (2019)

[106] YAN, Yian ; WANG, Huang ; JIANG, Jiuchun ; ZHANG, Weige ; BAO, Yan ; HUANG, Mei: *Research on Configuration Methods of Battery Energy Storage System for Pure Electric Bus Fast Charging Station*. In: *Energies* 12 (2019), Nr. 3, S. 558

[107] THORMANN, Bernd ; PUCHBAUER, Philipp ; KIENBERGER, Thomas: *Analyzing the suitability of flywheel energy storage systems for supplying high-power charging e-mobility use cases*. In: *Journal of Energy Storage* 39 (2021), S. 102615

[108] THORMANN, Bernd ; KIENBERGER, Thomas: *Estimation of Grid Reinforcement Costs Triggered by Future Grid Customers: Influence of the Quantification Method (Scaling vs. Large-Scale Simulation) and Coincidence Factors (Single vs. Multiple Application)*. In: *Energies* (2022), 15, 1383

[109] THORMANN, Bernd ; KIENBERGER, Thomas: *Grid-friendly Integration of Future Public Charging Infrastructure by Flywheel Energy Storage Systems (FESS)*. In: *Proceedings to the Conference on Sustainable Energy Supply and Energy Storage Systems (NEIS)* (2019)

[110] THORMANN, Bernd ; BRAUNSTEIN, René ; KIENBERGER, Thomas: *FlyGrid – Integration of Flywheel Energy Storage Systems into EV Fast Charging Infrastructure*. In: *Proceedings to the 12th International Energy Economics Conference (IEWT)* (2021). URL https://iewt2021.eeg.tuwien.ac.at/ – Überprüfungsdatum 14 September, 2021

[111] THORMANN, Bernd ; BRAUNSTEIN, René ; WISIAK, Johannes ; STREMPFL, Franz ; KIENBERGER, Thomas: Evaluation of grid relieving measures for integrating electric vehicles in a suburban low-voltage grid. In: *CIRED Conference Proceedings 2019*.

[112] KAMPKER, Achim ; VALLÉE, Dirk ; SCHNETTLER, Armin: *Elektromobilität* : *Grundlagen einer Zukunftstechnologie*. Berlin, Heidelberg : Springer Vieweg, 2013

[113] KARLE, Anton: *Elektromobilität* : *Grundlagen und Praxis*. München : Carl Hanser Verlag, 2015

[114] HOFMANN, Peter: *Hybridfahrzeuge* : *Ein alternatives Antriebssystem für die Zukunft*. 2. Aufl. Wien, Heidelberg : Springer, 2014

[115] DOPPELBAUER, Martin: *Grundlagen der Elektromobilität* : *Technik, Praxis, Energie und Umwelt*. Wiesbaden, Heidelberg : Springer Vieweg, 2020 (Lehrbuch)

[116] &AMP, M. TruckA.N. ; SE, Bus: *MAN Lion's City E | MAN AT*. URL https://www.man.eu/at/de/bus/der-man-lion_s-city/elektroantrieb/man-lion_s-city-e.html. – Aktualisierungsdatum: 2021-10-14 – Überprüfungsdatum 2021-10-14

[117] DAIMLER: *Mercedes-Benz Trucks läutet neue Ära ein: Weltpremiere des eActros am 30. Juni | Daimler*. URL https://www.daimler.com/produkte/lkw/mercedes-benz/eactros.html. – Aktualisierungsdatum: 2021-10-14 – Überprüfungsdatum 2021-10-14

[118] NISSAN: *Der neue NISSAN e-NV200 EVALIA–Elektro familienauto 7-Sitzer | NISSAN*. URL https://www.nissan.at/fahrzeuge/neuwagen/e-nv200-evalia.html. – Aktualisierungsdatum: 2021-10-14 – Überprüfungsdatum 2021-10-14

[119] TESLA: *Model 3 | Tesla*. URL https://www.tesla.com/model3. – Aktualisierungsdatum: 2021-10-14 – Überprüfungsdatum 2021-10-14

[120] *BMW i3 : Technische Daten*. URL http://www.bmw.at/de/neufahrzeuge/bmw-i/i3/2016/technische-daten.html – Überprüfungsdatum 2017-06-26

[121] ALLGEMEINER DEUTSCHER AUTOMOBIL CLUB: *Eco-Test*. URL https://www.adac.de/infotestrat/tests/eco-test

[122] *Reichweite und Aufladen | Renault KANGOO E-Tech | Batterie*. URL https://www.renault.de/elektromodelle/kangoo-ze/batterie-und-laden.html. – Aktualisierungsdatum: 2021-10-15 – Überprüfungsdatum 2021-10-15

[123] *Der neue ABT e-Transporter 6.1 | Volkswagen Nutzfahrzeuge*. URL https://www.volkswagen-nutzfahrzeuge.de/de/elektromobilitaet/modelle/abt-e-transporter-6-1.html. – Aktualisierungsdatum: 2021-10-12 – Überprüfungsdatum 2021-10-15

[124] *eVito Kastenwagen | Ausstattung & Zubehör | Mercedes-Benz*. URL https://www.mercedes-benz.at/vans/de/vito/e-vito-panel-van/equipment. – Aktualisierungsdatum: 2021-10-14 – Überprüfungsdatum 2021-10-15

[125] *Der neue E-Ducato | Elektrotransporter | Fiat Professional*. URL https://www.fiatprofessional.com/at/e-ducato/modellauswahl. – Aktualisierungsdatum: 2021-12-14 – Überprüfungsdatum 2021-12-15

[126] GAO, Zhiming ; LIN, Zhenhong ; LACLAIR, Tim J. ; LIU, Changzheng ; LI, Jan-Mou ; BIRKY, Alicia K. ; WARD, Jacob: *Battery capacity and recharging needs for electric buses in city transit service*. In: *Energy* 122 (2017), S. 588–600

[127] *Volvo FH Electric*. URL https://www.volvotrucks.com/en-en/trucks/trucks/volvo-fh/volvo-fh-electric.html. – Aktualisierungsdatum: 2021-10-13 – Überprüfungsdatum 2021-10-15

[128] BYD USA: *Class 6 Truck - BYD USA*. URL https://en.byd.com/truck/class-6-truck/. – Aktualisierungsdatum: 2021-10-15 – Überprüfungsdatum 2021-10-15

[129] SCHULZ, Alexandra: *Batterieelektrische Fahrzeuge im gewerblichen Flottenbetrieb*. Dissertation. 2015

[130] KUNITH, Alexander W.: *Elektrifizierung des urbanen öffentlichen Busverkehrs*. Springer Fachmedien Wiesbaden, 2017. URL http://dx.doi.org/10.1007/978-3-658-19347-8

[131] GAO, Zhiming ; LIN, Zhenhong ; FRANZESE, Oscar: *Energy Consumption and Cost Savings of Truck Electrification for Heavy-Duty Vehicle Applications*. In: *Transportation Research Record: Journal of the Transportation Research Board* 2628 (2017), Nr. 1, S. 99–109

[132] EARL, Thomas ; MATHIEU, Lucien ; CORNELIS, Stef ; KENNY, Samuel ; CALVO AMBEL, Carlos ; NIX, James: *Analysis of long haul battery electric trucks in EU* : *Marketplace and technology, economic, environmental, and policy perspectives*. In: *Proceedings to the 8th Commercial Vehicle Workshop* (2018). URL https://www.transportenvironment.org/discover/analysis-long-haul-battery-electric-trucks-eu/ – Überprüfungsdatum 15 October, 2021

[133] AUSTRIAN MOBILE POWER (Hrsg.): *Factsheet #12* : *Übersicht Netzanschluss & Ladedauer*, 2019

[134] EV SAFE CHARGE: *DC Fast Charging Explained - EV Safe Charge*. URL https://evsafecharge.com/dc-fast-charging-explained/. – Aktualisierungsdatum: 2021-01-19 – Überprüfungsdatum 2021-12-15

[135] THE EUROPEAN PARLIAMENT AND THE COUNCIL OF THE EUROPEAN UNION: *Directive 2014/94/EU of the European Parliament and of the Council of 22 October 2014 on the deployment of alternative fuels infrastructure Text with EEA relevance* (in Kraft getr. am 22. 10. 2014) (2014-10-22)

[136] *Expert interview with employees of the charging station manufacturer SMATRICS GmbH & Co KG and ABL SURSUM Bayerische Elektrozubehör GmbH & Co. KG*. Interview mit . 07/2017

[137] FOLEY, A. M. ; WINNING, I. J. ; O GALLACHOIR, B. P.: State-of-the-art in electric vehicle charging infrastructure. In: *IEEE Vehicle Power and Propulsion Conference (VPPC), 2010* : *1-3 Sept. 2010, Lille, France*. Piscataway, NJ : IEEE, 2010, S. 1–6

[138] IONITY EU: *IONITY EU*. URL https://ionity.eu/de. – Aktualisierungsdatum: 2021-10-15 – Überprüfungsdatum 2021-10-15

[139] WERTH, Torsten: *Netzberechnung mit Erzeugungsprofilen*. Wiesbaden : Springer Fachmedien Wiesbaden, 2016

[140] AUSTRIAN NATIONAL COUNCIL: *Bundesgesetz, mit dem die Organisation auf dem Gebiet der Elektrizitätswirtschaft neu geregelt wird* (in Kraft getr. am 2010) (2010). URL https://www.ris.bka.gv.at/GeltendeFassung.wxe?Abfrage=Bundesnormen&Gesetzesnummer=20007045 – Überprüfungsdatum January 2021

[141] HEUCK, Klaus ; DETTMANN, Klaus-Dieter ; SCHULZ, Detlef: *Elektrische Energieversorgung*. Wiesbaden : Springer Fachmedien Wiesbaden, 2013

[142] SCHEFFLER, J.: *Bestimmung der maximal zulässigen Netzanschlussleistung photovoltaischen Energiewandlungsanlagen in Wohnsiedlungsgebieten*. Düsseldorf, 2004

[143] CRASTAN, Valentin: *Elektrische Energieversorgung 1*. Berlin, Heidelberg : Springer Berlin Heidelberg, 2012

[144] KERBER, Georg: *Aufnahmefähigkeit von Niederspannungsverteilnetzen für die Einspeisung aus Photovoltaikkleinanlagen*. Zugl.: München, Techn. Univ., Diss., 2011. Uelvesbüll : Der Andere Verl., 2011

[145] STRUNZ, K. ; FLETCHER, R. H. ; CAMPBELL, R. ; GAO, F.: *Developing benchmark models for low-voltage distribution feeders* (2009), S. 1–3

[146] LINDNER, M. ; AIGNER, C. ; GÖDDE, M.: Aktuelle Musternetze zur Untersuchung von Spannungsproblemen in der Niederspannung. In: *Procedings to the 14th Symposium, 2016*.

[147] GRAINGER, John J. ; STEVENSON, William D.: *Power system analysis*. Internat. ed. New York : McGraw-Hill, 1994 (McGraw-Hill series in electrical and computer engineering Power and energy)

[148] FLOSDORFF, René ; HILGARTH, Günther: *Elektrische Energieverteilung*. 7., überarb. Aufl. Stuttgart : Teubner, 2000 (Leitfaden der Elektrotechnik)

[149] UNIV.PROF. DR. HERWIG RENNER: *Spannungsqualität und Versorgungssicherheit*. Technische Universitaet Graz, Institut für Elektrische Anlagen,

[150] REIMANN, Thorsten ; HECKMANN, Wolfram: Blinding-Effekte im Niederspannungsnetz : Berücksichtigung im Schutzkonzept bei dezentraler Erzeugung. In: *Tagung Zukünftige Stromnetze für Erneuerbare Energien*.

[151] CLOTEAUX, B.: *Limits in Modeling Power Grid Topology*. In: *2013 IEEE 2nd Network Science Workshop (NSW)* (2013) – Überprüfungsdatum 2021-03-21

[152] SCHEFFLER, Jörg: *Verteilnetze auf dem Weg zum Flächenkraftwerk* (2016)

[153] LEVI, V. ; STRBAC, G. ; ALLAN, R.: *Assessment of performance-driven investment strategies of distribution systems using reference networks*. In: *IEE Proceedings - Generation, Transmission and Distribution* 152 (2005), Nr. 1, S. 1

[154] CRASTAN, Valentin ; WESTERMANN, Dirk: *Elektrische Energieversorgung 3*. Berlin, Heidelberg : Springer Berlin Heidelberg, 2012

[155] SCHÄFER, Karl Friedrich: *Netzberechnung*. Wiesbaden : Springer Fachmedien Wiesbaden, 2020

[156] OEDING, Dietrich ; OSWALD, Bernd Rüdiger: *Elektrische Kraftwerke und Netze*. Berlin, Heidelberg : Springer Berlin Heidelberg, 2011

[157] OSWALD, Bernd R.: *Berechnung von Drehstromnetzen*. Wiesbaden : Springer Fachmedien Wiesbaden, 2013

[158] HOSEMANN, Gerhard (Hrsg.): *Elektrische Energietechnik* : *Netze*. Berlin, Heidelberg, s.l. : Springer Berlin Heidelberg, 2001 (Klassiker der Technik)

[159] E-CONTROL: *Sonstige Marktregeln Strom: Kapitel 6 - Zählwerte, Datenformate und standardisierte Lastprofile*

[160] PFLUGRADT, N.: *Modellierung von Wasser- und Energieverbräuchen in Haushalten*. Technischen Universität Chemnitz. Dissertation. 2016

[161] *Renewables.ninja*. URL https://www.renewables.ninja/. – Aktualisierungsdatum: 2021-12-29 – Überprüfungsdatum 2021-12-29

[162] ISO EN 50160. 2011. *Voltage characteristics of electricity supplied by public electricity networks*

[163] MARENBACH, Richard ; NELLES, Dieter ; TUTTAS, Christian: *Elektrische Energietechnik*. Wiesbaden : Springer Fachmedien Wiesbaden, 2013

[164] BRUNNER, Helfried ; SCHWALBE, Roman ; PRÜGGLER, Wolfgang ; ABART, Andreas ; RADAUER, Markus: *DG DemoNet – Smart LV Grid* : *Control concepts for active low voltage network operation with a high share of distributed energy resources*. Final report. 2015

[165] CZESCHKA, Dominik: *Spannungshaltung in Niederspannungsnetzen: Strangregler versus Batteriespeicher*. Technical University of Vienna. Diplomarbeit. 2017

[166] E-CONTROL: *Technische und organisatorische Regeln für Betreiber und Benutzer von Netzen* : *TOR Erzeuger: Anschluss und Parallelbetrieb von Stromerzeugungsanlagen des Typs A und Kleinsterzeugungsanlagen*. URL www.e-control.at/

[167] SCHULZ, Detlef: *Nachhaltige Energieversorgung und Integration von Speichern* : *Tagungsband zur NEIS 2015*. Wiesbaden : Springer Vieweg, 2015

[168] SCHMIEGEL, Armin U.: *Energiespeicher für die Energiewende* : *Auslegung und Betrieb von Speichersystemen ; mit 130 Bildern, 29 Tabellen und 38 Übungsaufgaben*. München : Hanser, 2019 (Hanser eLibrary)

[169] KOMARNICKI, Przemyslaw ; LOMBARDI, Pio ; STYCZYNSKI, Zbigniew A.: *Elektrische Energiespeichersysteme*. Berlin, Heidelberg : Springer Berlin Heidelberg, 2021

[170] JUNSEOK SONG, A. TOLIYAT, D. TURTLE AND A. KWASINSKI: A rapid charging station with an ultracapacitor energy storage system for plug-in electrical vehicles. In: *2010 International Conference on Electrical Machines and Systems, Incheon*, pp. 2003-2007.

[171] AMIRYAR, Mustafa ; PULLEN, Keith: *A Review of Flywheel Energy Storage System Technologies and Their Applications*. In: *Applied Sciences* 7 (2017), Nr. 3, S. 286

[172] BUCHROITHNER, Armin ; WEGLEITER, Hannes ; SCHWEIGHOFER, Bernhard: Flywheel Energy Storage Systems Compared to Competing Technologies for Grid Load Mitigation in EV Fast-Charging Applications. In: *2018 IEEE 27th International Symposium on Industrial Electronics (ISIE)* : *Proceedings : Cairns Convention Centre, Cairns, Australia, 13 - 15 June, 2018 / sponsored by the Institute of Electrical and Electronics Engineers (IEEE), IEEE Industrial Electronics Society (IES)*. Piscataway, NJ : IEEE, 2018, S. 508–514

[173] GABBAR, H. A. ; OTHMAN, A. M.: Flywheel-Based Fast Charging Station – FFCS for Electric Vehicles and Public Transportation. In: *IOP Conference Series: Earth and Environmental Science, Volume 83, 2nd International Conference on Green Energy Technology (ICGET 2017) 18–20 July 2017, Rome, Italy*.

[174] FAHAD, Abul Hasan ; GABBAR, Hossam A.: Wireless Flywheel-Based Fast Charging Station (WFFCS). In: *2018 IEEE International Conference on Renewable Energy and Power Engineering (REPE 2018)* : *November 24-26, 2018, Toronto, Canada*. Piscataway, NJ : IEEE Press, 2018, S. 1–6

[175] VAZQUEZ, Sergio ; LUKIC, Srdjan M. ; GALVAN, Eduardo ; FRANQUELO, Leopoldo G. ; CARRASCO, Juan M.: *Energy Storage Systems for Transport and Grid Applications*. In: *IEEE Transactions on Industrial Electronics* 57 (2010), Nr. 12, S. 3881–3895

[176] SUN, Bo ; DRAGICEVIC, Tomislav ; FREIJEDO, Francisco D. ; VASQUEZ, Juan C. ; GUERRERO, Josep M.: *A Control Algorithm for Electric Vehicle Fast Charging Stations Equipped With Flywheel Energy Storage Systems*. In: *IEEE Transactions on Power Electronics* 31 (2016), Nr. 9, S. 6674–6685

[177] HU, Zhaoguang ; HAN, Xinyang ; WEN, Quan: *Integrated resource strategic planning and power demand-side management*. Beijing, Berlin, Heidelberg : China Electric Power Press; Springer, 2013 (Power systems)

[178] SHARIATZADEH, Farshid ; MANDAL, Paras ; SRIVASTAVA, Anurag K.: *Demand response for sustainable energy systems: A review, application and implementation strategy*. In: *Renewable and Sustainable Energy Reviews* 45 (2015), S. 343–350

[179] YILMAZ, Murat ; KREIN, Philip T.: *Review of the Impact of Vehicle-to-Grid Technologies on Distribution Systems and Utility Interfaces*. In: *IEEE Transactions on Power Electronics* 28 (2013), Nr. 12, S. 5673–5689

[180] TURTON, Hal ; MOURA, Filipe: *Vehicle-to-grid systems for sustainable development* : *An integrated energy analysis*. In: *Technological Forecasting and Social Change* 75 (2008), Nr. 8, S. 1091–1108

[181] SCHULLER, Alexander ; RIEGER, Fabian: *Assessing the Economic Potential of Electric Vehicles to Provide Ancillary Services: The Case of Germany*. In: *Zeitschrift für Energiewirtschaft* 37 (2013), Nr. 3, S. 177–194

[182] KADAM, Serdar: *Defintion and Validation of Reference Feeders for Low-Voltage Networks*. PhD Thesis. URL https://repositum.tuwien.at/handle/20.500.12708/7709. – Aktualisierungsdatum: 2018 – Überprüfungsdatum 2021-08-18

[183] NEPLAN AG: *NEPLAN*. 8700 Küsnacht - Zürich Switzerland. URL http://www.neplan.ch/ – Überprüfungsdatum 2017-09-05

[184] DIGSILENT: *PowerFactory*. URL www.digsilent.de/de/powerfactory.html – Überprüfungsdatum 7 September, 2021

[185] THE MATHWORKS INC.: *MATLAB*. USA. URL https://www.mathworks.com – Überprüfungsdatum 0509.2017

10 APPENDIX A: PEER-REVIEWED PUBLICATIONS AND RELEVANT CONFERENCE PROCEEDINGS

Paper 1 (Status: Accepted): Evaluation of Grid Capacities for Integrating Future E-Mobility and Heat Pumps into Low-Voltage Grids

Thormann, B.; Kienberger, T., In: Energies 2020, 13, 5083. doi.org/10.3390/en13195083

Conceptualization, B.T. and T.K.; Data curation, B.T.; Formal analysis, B.T. and T.K.; Funding acquisition, T.K.; Investigation, B.T. and T.K.; Methodology, B.T. and T.K.; Project administration, T.K.; Resources, B.T. and T.K.; Software, B.T.; Supervision, T.K.; Validation, B.T. and T.K.; Visualization, B.T.; Writing—original draft, B.T.; Writing—review and editing, T.K.

Paper 2 (Status: Accepted): Analyzing the suitability of flywheel energy storage systems for supplying high-power charging e-mobility use cases

Thormann, B.; Puchbauer, P.; Kienberger, T., In: Journal of Energy Storage 2021, 39, 102615, doi:10.1016/j.est.2021.102615.

Conceptualization, B.T. and T.K.; Data curation, B.T.; Funding acquisition, T.K.; Methodology, B.T., P.P.; Project administration, T.K.; Software, B.T. and P.P.; Supervision, T.K.; Validation, B.T. and T.K.; Visualization, B.T.; Writing—original draft, B.T.; Writing—review and editing, T.K.

Paper 3 (Status: Accepted): Estimation of Grid Reinforcement Costs Triggered by Future Grid Customers: Influence of the Quantification Method (Scaling vs. Large-Scale Simulation) and Coincidence Factors (Single vs. Multiple Application)

Thormann, B.; Kienberger, T., In Energies 2022, In: Energies 2022, 15, 1383, doi: 10.3390/en15041383

Conceptualization, B.T. and T.K.; Data curation, B.T.; Formal analysis, B.T.; Funding acquisition, T.K.; Investigation, B.T.; Methodology, B.T. and T.K.; Project administration, T.K.; Resources, B.T. and T.K.; Software, B.T.; Supervision, T.K.; Validation, B.T. and T.K.; Visualization, B.T.; Writ-ing—original draft, B.T.; Writing—review & editing, T.K.

CIRED 2019 (Status: Accepted): Evaluation of Grid Relieving Measures for Integrating Electric Vehicles in a Suburban Low-Voltage Grid

Thormann, B., Braunstein, R., Wisiak, J., Strempfl, F. & Kienberger, T., In: CIRED 2019 conference proceedings, June 2019, Madrid, Spain

Conceptualization, B.T. and T.K.; Data curation, B.T. and R.B.; Funding acquisition, T.K.; Methodology, B.T. and T.K.; Project administration, T.K.; Software, B.T.; Supervision, T.K. and

R.B.; Validation, B.T. and T.K.; Visualization, B.T.; Writing—original draft, B.T.; Writing—review and editing, T.K.

NEIS 2019 (Status: Accepted): Grid-friendly Integration of Future Public Charging Infrastructure by Flywheel Energy Storage Systems (FESS)

> *Thormann, B. & Kienberger, T., In: NEIS 2019 Conference proceedings, September 2019, Hamburg, Germany*

Conceptualization, B.T. and T.K.; Data curation, B.T.; Funding acquisition, T.K.; Methodology, B.T. and T.K.; Project administration, T.K.; Software, B.T.; Supervision, T.K.; Validation, B.T. and T.K.; Visualization, B.T.; Writing—original draft, B.T.; Writing—review and editing, T.K.

IEWT 2021: (Status: Accepted): FlyGrid – Integration of Energy Storage Systems into EV Fast Charging Infrastructure

> *Thormann, B., Braunstein, R., Kienberger, T., , In: 12th International Energy Economic conference proceedings (IEWT), September 2021, Vienna, Austria*

Conceptualization, B.T. and T.K.; Data curation, B.T. and R.B.; Funding acquisition, T.K.; Methodology, B.T. and T.K.; Project administration, T.K.; Software, B.T.; Supervision, T.K. and R.B.; Validation, B.T. and T.K.; Visualization, B.T.; Writing—original draft, B.T.; Writing—review and editing, T.K.

10.1 Paper 1

Evaluation of Grid Capacities for Integrating Future E-Mobility and Heat Pumps into Low-Voltage Grids

energies

MDPI

Article

Evaluation of Grid Capacities for Integrating Future E-Mobility and Heat Pumps into Low-Voltage Grids

Bernd Thormann * and Thomas Kienberger

Chair of Energy Network Technology, Department of Environmental and Energy Process Engineering, Montanuniversitaet Leoben, A-8700 Leoben, Austria; thomas.kienberger@unileoben.ac.at

* Correspondence: bernd.thormann@unileoben.ac.at; Tel.: +43-3842-402-5409

Received: 13 August 2020; Accepted: 25 September 2020; Published: 29 September 2020

Abstract: While an area-wide implementation of electric vehicles (EVs) and electric heat pumps (HPs) will contribute to a decarbonization of the energy system, they represent new challenges for existing low-voltage (LV) power grids. Hence, this study investigates potential grid congestions on the basis of three contrasting load approaches applied to four different grid regions. Within the three load approaches, temporal characteristics of various grid customer classes (EVs, HPs, households etc.) are derived from highly resolved realistic load profiles. In accordance with classic grid planning, firstly a static load approach is analyzed by applying the modeled coincidence for each consumer class individually. Secondly, this static approach is modified by including combined coincidence factors, taking temporal consumer class interactions into account. Finally, both static load approaches are compared with detailed annual time series analyses by means of load flow simulations using real-life LV grid data. The evaluation of inadmissible voltage characteristics and thermal congestions identifies future grid extension needs depending on the considered grid region. In addition, the variation of the applied load approach highlights the need to consider consumer-specific temporal behavior. In fact, by neglecting temporal interactions between conventional and future grid customers, the classic grid planning approach overestimates future grid extension needs. To counteract an oversizing of future grid structures, this paper presents a combined consideration of EVs' and HPs' coincidence as well as resulting grid consequences on the LV level.

Keywords: low-voltage level; electric vehicle; heat pump; load approach; grid region

1. Introduction

In 2019, the European Commission announced its vision to achieve the EU's climate neutrality by 2050 [1]. Considering the energy-related end user greenhouse gas (GHG) emissions in the European Union [2], the transportation and residential sectors represent crucial fields of action. Thus, on the one hand, this vision is further concretized by the European Green Deal [3], which includes, inter alia, a 90% reduction in traffic-related GHG emissions by 2050 as one cornerstone to reach this ambitious goal. Thereby, the EU intends to accelerate the shift to sustainable mobility by an area-wide implementation of one million (2019: 0.14 Mio.) public charging stations by 2025 [3]. In accordance with Norway's leading role with respect to electric vehicle (EV) numbers [4], this measure will likely result in an increasing number of battery EVs in the EU. On the other hand, the European Commission's vision is supposed to be realized by increasing the residential sector's energy efficiency [3], e.g., by an area-wide implementation of electric heat pumps (HPs) [5,6]. In fact, a large-scale transition to electric HPs could decrease the European residential sector's GHG emissions by up to 30%, assuming a market share of 100% [7]. Besides positive aspects regarding the decarbonization of the traffic and residential sectors, these future technologies will confront the existing power system with new challenges [6]. Since most charging processes take place at home [8,9] and electrical HPs

will be installed primarily in residential areas, these challenges will especially affect the low-voltage (LV) level. However, due to today's relatively low penetration of EVs and electric HPs, these potential consequences for existing distribution grids are hard to identify by the use of actual measurements. Despite the early stage of EV- and HP-penetration, future challenges for distribution system operators (DSOs) have to be analyzed now in order to develop appropriate adaption strategies.

1.1. State of Research

Numerous studies analyze potential impacts of future EVs on the LV level with regards to voltage characteristics [10–15], thermal overload of grid lines [15,16], distribution substation (DS) transformer utilizations [12,15,17] as well as the effects on load curves of existing grid customers [11,12,18–22]. Analogously, the implementation of electric HPs and its consequences for existing (LV) grids are investigated by several publications [6,22–26]. Navarro-Espinosa et al. (2016) [27] assess the impacts of, inter alia, EVs and HPs on numerous LV feeders individually based on a Monte Carlo simulation using time series, but their study lacks a combined evaluation of potential synergies. In contrast, the following studies deal with possible grid extension needs induced by an aggregation of these technologies and are therefore described in detail.

Mendaza et al. (2014) [28] use a static Monte Carlo simulation, in order to investigate the capability of a rural LV grid to integrate future EV- and HP-loads. Therefore, the authors vary EVs and HPs spatially in numerous iterations depending on various penetrations, but applying consumer class-specific peak loads exclusively. Hülsmann et al. (2019) [29] analyze the capacity of a German 25,000-noded network to integrate these future grid customers conjunctly considering numerous penetration levels. Based on maximum individual coincidence factors for EVs and HPs, static Monte Carlo simulations are performed. On the other hand, Shao et al. (2013) [30] apply time series with a resolution of one hour in order to examine the integration of a 100% penetration of EVs and HPs into one Danish urban LV grid. Li et al. (2014) [31] analyze EV- and HP-induced voltage deviations and voltage imbalance in one LV feeder based on daily load profiles with a time resolution of one minute, considering several penetration levels. Similarly, Baccino et al. (2014) [32] determine possible grid congestions in one LV grid in order to test the presented demand response algorithms. On this account, they apply daily load profiles considering a certain number of integrated EVs and HPs (one penetration level exclusively). Birk et al. (2018) [33] determine critical voltage characteristics and thermal congestions caused by a penetration of EVs and HPs of 60% in a section of an urban LV grid located in the city center by applying 15-min resolved time series. Finally, Sinha et al. (2020) [34] test the operation flexibility of EVs and HPs combined, implemented into one LV grid. Therefore, one penetration level of these technologies is simulated as the reference scenario, using highly resolved load profiles and a steady-state time series analysis.

In summary, future grid congestions triggered by a combined integration of e-mobility and the electrification of the space heating sector are examined using two different simulation approaches: On the one hand, a static simulation approach considering one time step, mostly in the form of a stochastic Monte Carlo simulation [28,29]. On the other hand, the majority of studies [30–34] apply time series analyses based on time-resolved load profiles. Besides static (stochastic) Monte Carlo simulations, classic power grid planning performed by DSOs is based on an analytical static load approach [35,36] because of its simple and fast application. While Monte Carlo simulations model a variety of grid conditions stochastically based on their probability of occurrence [35], analytical static simulations apply worst-case load conditions. Therefore, the aggregated peak load of a number of grid customers is calculated by multiplying the number of customers by the respective coincidence factor and the average individual peak load [35]. The coincidence factor thereby takes temporal characteristics and resulting load aggregations of numerous grid customers of one consumer class (households, EVs etc.) into account. Both static approaches attempt to consider temporal aggregations for each consumer class individually by the application of individual coincidence factors, whereby temporal interactions between various consumer classes are neglected (e.g., [28,29,35]). Nevertheless, while a stochastic Monte Carlo simulation must be performed for a certain number of iterations [37], any analytical static modeling approach simulating one time step offers advantages in terms of the

calculation effort compared to detailed time series analyses [38]. This becomes more important when it comes to the large-scale simulation of numerous grid structures.

Besides the consideration of temporal consumer class interactions, recent studies differ in terms of the analyzed grid region: While the majority fail to define the analyzed grid region (e.g., [29,31,32,34]), urban [30,33] and rural [28] LV grids are investigated in a few studies. However, these studies exclude the fact that real-life housing types (family houses, multi-apartment residential buildings etc.) depend on the considered grid region, which is crucial for evaluating grid impacts especially in urban areas.

1.2. Open Research Questions and Structure of This Paper

The previous section presents the state-of-the-art research in the field of grid simulations analyzing future impacts of EVs and HPs. Thereby, the unanswered research questions with respect to the temporal (1) and spatial (2) components are as follows:

1. What impact does the applied load approach have on the estimation of future grid extension needs on the LV level? Is it necessary to take realistic temporal interactions between conventional grid customers, EVs and HPs into account? How can fast static grid simulation meet with a detailed consideration of these consumer class interactions? Does the classic grid planning approach comply with an increase in various grid customer classes, and is it applicable for future grid planning?
2. What impact does the considered grid region have on the determination of grid congestions, applying consistent simulation approaches as well as real-life grid topologies and housing types?

To answer these research questions, this paper identifies potential impacts on the LV level triggered by projected numbers of EVs and HPs based on co-simulations. Therefore, four LV grid structures in various regions are modeled in detail (Section 2.1) using real-life grid data. The method for modeling time-resolved load profiles considering conventional grid customers (Section 2.2.1), future EV charging (Section 2.2.2) as well as future electric HPs (Section 2.2.3) using the software MATLAB [39] is described in this paper. Both grid and consumer load modeling are based on real grid and consumer data, provided in an anonymous form and in compliance with data protection regulations by the Austrian DSO Energienetze Steiermark GmbH [40]. Based on modeled time series, the coincidence of various consumer classes (Section 2.3) is determined depending on the considered number of consumers. To analyze the effects of temporal load aggregations of several grid customers, two static load approaches (applying coincidence factors) as well as a time series-based load approach (Section 2.4) are investigated in the form of load flow simulations using the software NEPLAN [41]. These simulation methods are applied consistently for all LV grids, providing a uniform comparison of various grid regions (Section 3), which are discussed in detail (Section 4).

2. Methodology

2.1. Grid Topologies and Modeling

This analysis deals with the comparison of methods for the determination of potential grid extension needs in various grid regions caused by private charging of EVs and HP loads. Therefore, four real-life LV grids are selected for grid simulations and classified in accordance with the Degree of Urbanization (DEGURBA) defined by the European Commission [42] as urban (densely populated), suburban (intermediate density) and rural (thinly populated). However, we analyze the urban area based on two LV grids, one located in the city center and one located in the city outskirts (Table 1). The selected LV grids are each characterized by a DS (Figure 1), transforming the medium voltage (MV) of 20 kV to a nominal voltage of 400 V (phase-to-phase) via a three-phase transformer (vector group Dyn5). With a classic radial grid structure typical for the LV level [43], this substation supplies a number of feeders and points of common coupling (PCCs) via cables or overhead lines. However, the suburban and urban grids are equipped with several grid separation points, enabling

the creation of a partial ring network structure in case of failure. The selected LV grids show significant differences (Table 1) in terms of nominal transformer power at the DS, number of feeders, number of PCCs, degree of cabling, admissible building density, total line length and the share of family houses (FHs).

Table 1. Grid configurations depending on the grid region.

	Urban (City Center)	Urban (City Outskirts)	Suburban	Rural
Nom. transformer power [kVA]	2 × 630	630	250	100
No. of feeders	14	12	9	3
No. of PCCs	21	80	87	18
Degree of cabling [%]	100	100	91	57
Admissible building density	0.6–1.2	0.3–0.8	0.2–0.4	0.2–0.3
Total line length [km]	2.17	6.13	5.64	2.31
Share of family houses [%]	0	87.5	100	100

The latter is especially significant for the possibility of investigating private parking at home or the installation of electric HPs. While FHs are predominant in the suburban and rural area, the urban grid located in the city center is characterized by multi-apartment residential buildings (MARBs) exclusively, which show limited possibility for private parking and inhibit the installation of HPs. For the implementation of load flow simulations, the mentioned grid configurations (e.g., Figure 1) are modeled in detail using the software NEPLAN [41]. For this purpose, real-life line- and transformer-specifications as well as real-life PCC-allocations of present grid customers are applied. As a result, potential grid consequences (e.g., voltage deviations and thermal overload) are identified with a high level of detail. In each of the four grid models, the higher voltage side of the DS is connected to a slack node (Figure 1), providing constant voltage. Consequently, voltage deviations in the MV level are excluded, which is taken into account when contrasting node voltages with standardized voltage limits (e.g., Section 2.4.2).

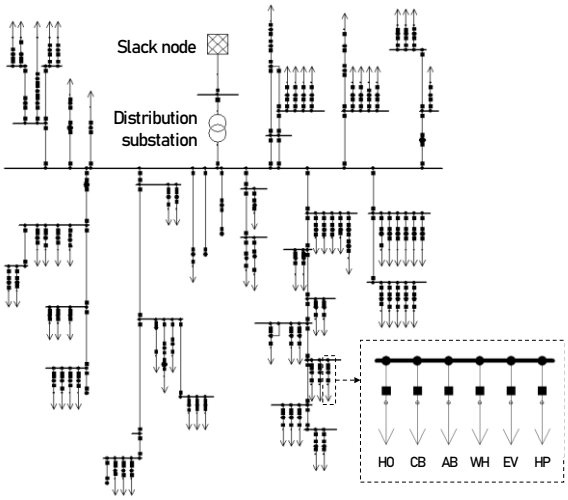

Figure 1. Grid model of an urban low-voltage grid located in the city outskirts.

To model future grid customers, each PCC is equipped with six load modules, representing conventional consumer loads—present household (HO) loads, commercial businesses (CBs), agricultural businesses (ABs), electrical water heaters (WHs)—future EV charging loads (EV) as well as future electric HP demands (HP). All of these load modules are provided with either static load values or annual time series with a time resolution of one minute in order to perform long-term load flow simulations.

2.2. Modeling of Grid Loads as Time Series

2.2.1. Conventional Consumer Loads

Spatially and time-resolved loads of conventional grid customers are modeled separately depending on their consumer class. Therefore, consumers are classified in accordance with Austrian Grid Codes [44] into HOs as well as CBs, ABs and WHs (Table 2). In the first step, time series of CB-, AB- and WH-loads are modeled by means of standardized load profiles pursuant to [45], which further classifies them into seven CB types, three AB types and six WH types.

Table 2. Number of persons (estimated) and number of conventional grid customers depending on consumer type and grid region.

	Urban (City Center)	**Urban (City Outskirts)**	**Suburban**	**Rural**
Estimated number of persons	509	346	231	50
Households (HOs)	331	170	88	18
Commercial businesses (CBs)	76	31	22	1
Agricultural businesses (ABs)	0	1	10	4
Electrical water heaters (WHs)	298	85	19	2

These load profiles provide annual phase-balanced active power time series for numerous consumer classes unified for an annual energy consumption of 1000 kWh. Finally, the scale of these unified load profiles by the real consumer's annual energy demand provides consumer class-dependent active and reactive power loads (a power factor of 0.98 lagging is assumed). Besides these standardized load profiles, HO load profiles are modeled with the behavior-based load profile generator by Pflugradt [46]. Thereby, this tool provides pre-defined HO structures, which differ in terms of the number, age and behavior of residents. For each of the grid's HOs, one of these pre-defined HO structures and its according active load profile is selected randomly based on the number of persons. While the number of persons of pre-defined HO structures is provided by the applied load profile generator, this information is not available within the DSO's data. Therefore, the number of persons is estimated for each of the LV grids' HOs by the real-time annual energy consumption and an average energy demand of 2050 kWh per person [47]. This results in an aggregated number of 509 (urban—city center), 346 (urban—city outskirts), 231 (suburban) and 50 (rural) persons (Table 2). After selecting the appropriate pre-defined HO (active power) profile based on the estimated number of persons, reactive power characteristics are taken into account depending on households' underlying devices and their power factor [48,49]. All the modeled time series cover one year with a time resolution of one minute, taking seasonal as well as daily load deviations into account. Finally, all types of conventional consumer loads (CB-, AB- and WH-loads as well as HO-loads) are aggregated for each PCC (e.g., Figure 2), distributed symmetrically to all the grid phases and calibrated with real data acquired by long-term measurements (described in detail in Appendix A.1). The load profile calibration using measured data enables an (almost) exact load simulation on the DS level considering conventional grid customers exclusively (neither EV nor HP). Nevertheless, since measured transformer loads at the DS level include grid losses during operation, this calibration results in a slight overestimation of conventional consumer loads. As a result, the maximum thermal utilization of the LV grids' transformers determined by grid simulations in the form of time series analyses exceeds the measured one by 0.57% (urban: city center), 0.55% (urban: city outskirts), 0.64% (suburban) and 2.02% (rural). Still, the performed load profile calibration allows for an accurate consideration of existing grid customers, required for a detailed analysis of the LV grids' capacity for integrating additional consumer loads, such as EVs or HPs.

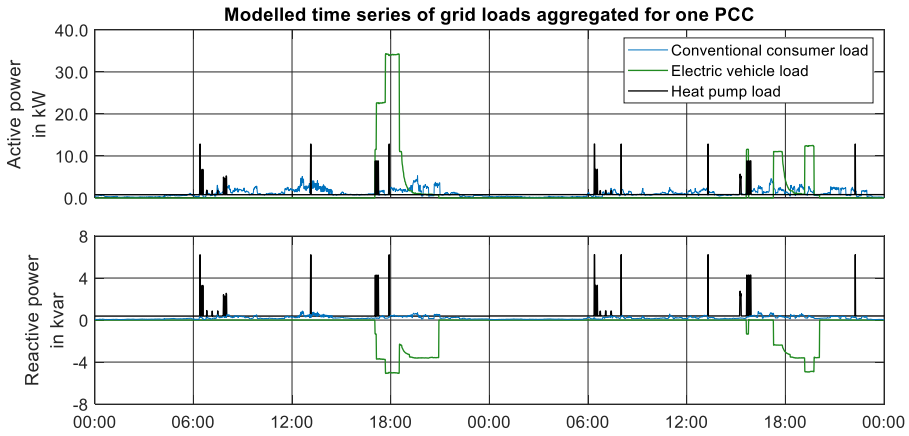

Figure 2. Modeled time series aggregated for one point of common coupling (PCC) supplying conventional consumers (three households), three electric vehicles charged at home as well as one heat pump.

2.2.2. Electric Vehicle Charging Loads

In addition to conventional grid customers, this study deals with potential grid impacts caused, inter alia, by the future supply of EVs, charged at private charging points. The European Directive 2014/94/EU of the European Parliament and of the Council of October 22nd 2014 on the deployment of alternative fuels infrastructure [50] defines public charging infrastructure for EVs as non-discriminatory access for all users within the European Union. However, due to a missing definition of private charging, all charging possibilities may be defined as private charging points, which violates non-discriminatory access, e.g., by several kinds of authorization, usage or payment. Hence, two of these private charging EV user groups are taken into account in this study:

- Charging at home: This user group deals with EVs charged at domestic charging points
- Charging at work: EVs of this user group are charged at the enterprise parking area

Analogously to the methods applied in previous studies [12,51,52], an uncontrolled, stochastic charging behavior is taken into account for both of them. To model this stochastic charging behavior, the following aspects must be considered individually for each user group: the spatial distribution of charging points, individual mobility patterns (time of charging and covered distance), EV model specifics (battery capacity, specific energy consumption, charging efficiency and charging power). A detailed description of the stochastic determination of these characteristics is presented in Appendixes A.2–A.4 as well as in the authors' recent publications [53–55]. Before modeling time series of EV charging loads, the actual charging power must be defined for each connection between an EV and its charging point. Therefore, the available installed power of private charging infrastructure depending on the grid area must be taken into account: Private parking or rather charging possibilities depend significantly on the housing type, which is differentiated into FHs and MARBs. In Austria (and a few other countries), the vast majority of HOs are integrated into the LV level based on a three-phase connection [36], tolerating a maximum installed charging power of 11 kVA. Nevertheless, most of the charging points in MARBs are equipped with reduced charging power [56]. Hence, charging points at FHs and at work are in this study considered to be equipped with 11 kVA available power, whereas charging points at MARBs are considered to provide only limited power of 3.7 kVA per charging point. Since all of the considered EV models enable charging with 11 kVA (Appendix A.4), the actual available charging power depends solely on whether it is charged at a FH, a MARB or at work. As a result, EVs are charged with 11 kVA in the rural (100% of charging processes), the suburban (100%) and the urban LV grid located in the city outskirts (61.3%). In contrast, 100% (city center) and 38.7% (city outskirts) of charging processes are supplied with 3.7 kVA by the urban LV grids (Figure 3). Assuming a uniform phase-allocation at MARBs, low-power

charging with 3.7 kVA (usually in the form of single-phase charging) is considered as phase-balanced three-phase charging.

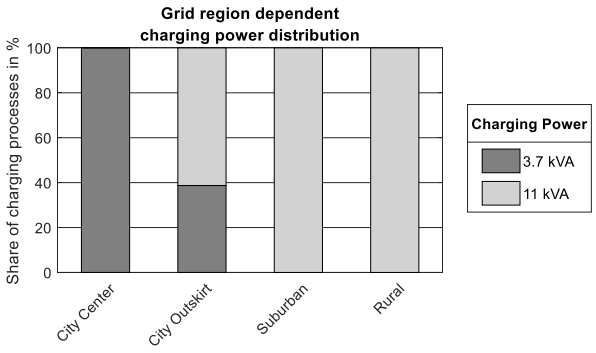

Figure 3. Share of available charging power depending on the grid region.

Finally, after determining the spatial distribution of private charging points (where are EVs charged?), user group-specific mobility patterns, state-of-the-art EV model specifics (when and for how long are they charged?) and the available charging power (with which power?), annual time series of EV charging loads with a time resolution of one minute are modeled for each EV. Therefore, measured charging data available for all the listed EV models (Table A5), including phase-imbalanced active and reactive power profiles, are applied. Depending on the selected EV model (Appendix A.4), the measured charging data are scaled according to the defined charging power, while maintaining original (measured) power factors. For each charging event, these scaled charging curves are adapted pursuant to the required amount of energy and added to the EV-specific annual load profile according to the time of charging. After modeling EV charging load profiles (one year) for all EVs, active and reactive power profiles are aggregated for each PCC (e.g., Figure 2), in accordance with the EVs' spatial allocation depending on the considered EV-penetration.

2.2.3. Electric Heat Pump Loads

Analogous to the modeling of time-resolved EV charging loads, potential grid impacts triggered by electric HPs depend on a spatial (where?) and a temporal (when?) component. For dealing with the former, the same approach as for determining the spatial distribution of private EV charging points (Appendix A.2) is applied. Therefore, the maximum number of HPs (HP-penetration of 100%) within each LV grid is initially detected based on the respective housing type (FH or MARB). Since only FHs allow the installation of future HPs, the maximum number of potential HPs equals the number of FHs supplied by the according LV grid: 0 (urban—city center), 60 (urban—city outskirts), 70 (suburban) and 15 (rural). Similar to the analysis of future EV numbers, this study analyzes potential impacts induced by future HP-penetrations (0%, 5%, 10%, 20%, 30%, 50% and 80%). However, for defining which FH is virtually equipped with a HP considering a certain HP-penetration, a uniform HP-share is applied to each of the LV grid's feeders.

For modeling the temporal component on the other hand, time-resolved HP load profiles, pre-defined for numerous house structures (e.g., single-family house hosting 1–2 persons, house with a solar thermal system, 300 L storage tank and gas heating etc.) are acquired also by Pflugradt [46]. Furthermore, these HP load profiles are uniformly scaled according to an average domestic space heating demand of 14316 kWh/a/household and an average domestic warm water demand of 2995 kWh/a/household [57,58] assuming a coefficient of performance of 3.0. Reactive power profiles are derived by applying a constant power factor of 0.9 (lagging) [23,24,26]. Finally, considering a certain HP-penetration, the individual HP-loads of FHs are aggregated for the supplying PCC (e.g., Figure 2) in accordance with the spatial determination, defined in the previous step. The modeled HP load profiles show HP-typical characteristics according to Brendan et al. (2014) [23], e.g., increased starting current/power due to the compressor motor as well as a certain base load during operation. If an FH

is virtually equipped with a HP, the previously modeled electric water heating loads (WH) as well as loads for electrical space heating are neglected.

2.3. Modeling the Coincidence of Current and Future Grid Loads

The coincidence of grid customers' electrical loads represents a crucial aspect for grid operators regarding the planning and operation of power grids. This "is a measure of the simultaneity of peak demands of a group of N customers" [35] and describes temporal aggregations of numerous electric loads: Considering a certain number of grid customers, a high coincidence equals a high probability for a power demand at the same time. Equation (1) [35] describes this correlation in the form of the coincidence factor (*CF*) considering a certain number of customers (*NoC*). It is defined by the ratio between the maximum of the aggregated load, $\max(\sum_{i=1}^{NoC} P_i(t))$, and the aggregated maxima of individual loads, $\sum_{i=1}^{NoC} \max(P_i(t))$.

$$CF\ \ (NoC) = \frac{\max(\sum_{i=1}^{NoC} P_i(t))}{\sum_{i=1}^{NoC} \max(P_i(t))} \quad (1)$$

Due to currently low EV- and HP-penetrations, real information with respect to the coincidence of numerous charging EVs and HPs is missing. On account of this, the presented analysis provides the coincidence of existing and future grid customers based on long-term time series with a resolution of one minute, necessary for deriving the exact coincidence of grid customers [35]. Therefore, the modeled load profiles of households (HOs), commercial businesses (CBs), agricultural businesses (ABs), electrical water heaters (WHs), electric vehicles (EVs) and electrical heat pumps (HPs) are applied for each grid respectively. Since this study investigates potential grid impacts within a time period of one year, the maximum coincidence is stochastically modeled for this period and each *NoC*. Assuming an *NoC* of ten units for example, ten daily load profiles of the according consumer class are randomly selected, aggregated and divided by the aggregated maxima of these selected load profiles for each day of the year, according to Equation (1). Finally, the year's maximum *CF* (maximum of 365 daily values) is detected for each *NoC* and each consumer class, demonstrated in Figure 4a for the suburban LV grid.

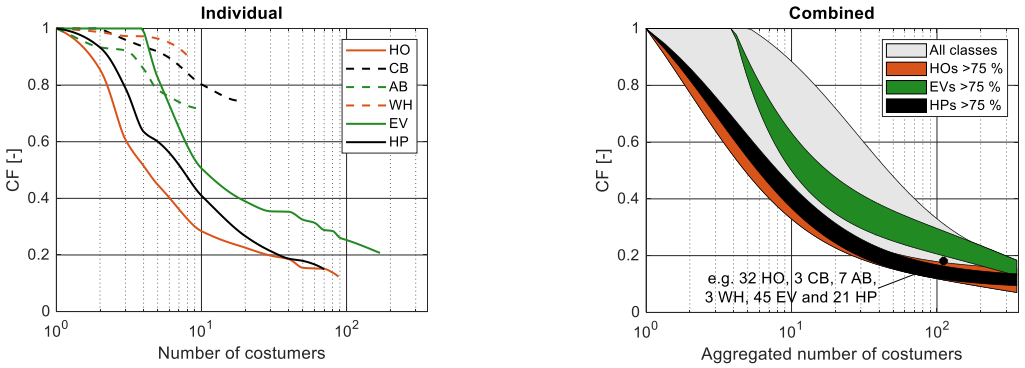

(**a**) (**b**)

Figure 4. Coincidence factor (*CF*) of various consumer classes modeled individually (**a**) and in a combined way (**b**) including *CF*-areas predominated (>75%) by households (HOs), electric vehicles (EVs) or heat pumps (HPs).

In addition to varying consumer classes, two different approaches for dealing with the coincidence between these are investigated by this study: the *CF*-modeling for each consumer class individually (Figure 4a) as well as the *CF*-consideration of various consumer classes combined (Figure 4b). The former determines the coincidence of each consumer class on its own, neglecting the temporal correlation with other consumer classes (e.g., as applied in [29] using a Monte Carlo simulation). In contrast, the latter takes temporal interactions between various consumer classes into account by aggregating all kinds of electrical loads supplied by the power grid. Based on numerous

possible customer class compositions, the combined coincidence at a certain aggregated *NoC* varies within the modeled and illustrated bandwidth (Figure 4b). In addition, Figure 4b highlights *CF*-areas defined by a predominant proportion (>75%) of HOs, EVs or HPs in relation to the total aggregated *NoC*. As already demonstrated by an individual *CF*-consideration (Figure 4a), EVs are characterized by increased simultaneity compared to HOs and HPs. Consequently, the analysis of grid customers representing EVs primarily requires a higher *CF* compared to customer groups with a predominant share of HOs or HPs, especially at a low aggregated *NoC*. Based on the assumed uncontrolled charging primarily during evening hours (Appendix A.3), a *CF* of (almost) one is determined even at a number of four vehicles (Figure 4a), considering EV charging with 3.7–11 kVA and both EV user groups. Regardless of consumer class and modeling approach, the probability of a simultaneous grid demand and thereby the *CF* decreases with an increasing number of customers [35] starting from one. The application of standardized load profiles for modeling CBs, ABs and electric WHs (Section 2.2.1) results in high coincidence compared to other consumer classes. In fact, a more accurate modeling of their coincidence would require more individual load profiles, e.g., measured during real-life operation.

2.4. Grid Simulations Using Load Flow Calculations

2.4.1. Load Approaches Analyzing Temporal Interactions between Various Consumer Classes

In this study, we analyze two static simulation approaches based on the modeled coincidence (Figure 4) in combination with the aggregated peak power of modeled load profiles. On the one hand, we investigate a static individual aggregation (SIA) of several consumer classes in accordance with classic grid planning [35], using the consumer class-individual coincidence factors. Hence, the electrical grid customers' aggregated load P in this approach is calculated by accumulating the mathematical product of the maximum power of each consumer class $P_{max,class}$ and the according individual coincidence factor $CF_{ind,class}$ for all the considered consumer classes (Table 3).

Table 3. Comparison of various load approaches applied for grid simulation.

Load Approach	No. of Time Steps	Power Determination
Static individual aggregation (SIA)	1	$P = \sum_{class=1}^{No.of\ \ classes} (P_{max,class} \cdot CF_{ind,class})$
Static combined aggregation (SCA)	1	$P = \left(\sum_{class=1}^{No.of\ \ classes} P_{max,class} \right) \cdot CF_{comb,No.of\ \ classes}$
Time series analysis (TSA)	525,600	$P = \max \left(\sum_{class=1}^{No.of\ \ classes} P_{class}(t) \right)$

On the other hand, a static combined aggregation (SCA) of various consumer classes is examined within a second approach: The electrical grid customers' aggregated load P results from the aggregation of the maximum power of each consumer class $P_{max,class}$ multiplied by a consumer class-combined coincidence factor $CF_{comb,No.of\ \ classes}$. The latter is selected from the modeled *CF*-bandwidth (Figure 4b) depending on the number of HOs, CBs, ABs, WHs, EVs and HPs. The maximum power of each consumer class $P_{max,class}$ is defined by the maximum of the aggregated load profile, including a certain number of consumers of a certain consumer class (e.g., ten households).

Despite similarities between these two static simulation approaches (SIA and SCA), they differ significantly with regards to the consideration of temporal overlaps between considered electrical consumer classes. This difference is demonstrated by a simple load determination, considering 32 HOs (with a peak load of 2 kVA each), three CBs (3 kVA each), seven ABs (2 kVA), three electric WHs (5 kVA), 45 EVs (11 kVA) and 21 electrical HPs (10 kVA), resulting in an aggregated peak load of 807

kVA. The SIA applying individual coincidence factors of 0.195, 0.96, 0.756, 0.973, 0.339 and 0.262 (Figure 4a) results in an aggregated peak load of 269.1 kVA. In contrast, a combined consideration of grid customers' coincidence (SCA) of 0.181 (highlighted in Figure 4b) results in an aggregated peak load of 146.1 kVA (−46%). In addition to these static load approaches, a real-life simulation approach on the basis of modeled annual time series with a time resolution of one minute is applied. Using this time series analysis (TSA), the electrical grid customers' aggregated load P is identified by the maximum of aggregated load profiles including all consumer classes (Table 3). While the TSA enables the implementation of time-resolved reactive power profiles (Section 2.2), constant power factors (PF) are applied in order to determine the reactive power demand in the SIA- and SCA-approach. Therefore, an average PF of 0.955 (lagging) is estimated considering existing grid loads based on long-term measurements at the DS (Figure A1) and applied for consumer classes HO, CB, AB and WH. Similarly, the reactive power demand of EVs is determined by measured charging data (applied for modeling time series of EV charging loads) including 15 varying EV models. These measured charging data demonstrate, that for most EV models, the power factor strongly differs between constant-current-phase (average PF of 0.995, leading) and constant-voltage-phase (0.280, leading) during the charging process. Consequently, an annual average PF including all the modeled time series of EV charging is detected (0.971, leading) and applied for the SIA- and SCA-approach. Due to missing measurement data regarding electrical HPs, a PF of 0.9 (lagging) [23,24,26] is assessed, analogous to the modeled time series (Section 2.2.3). For a combined aggregation of various consumer classes in the SCA-approach, an average PF weighted by individual numbers of consumer classes is applied in a simplified manner (e.g., the combined consideration of two HOs, two EVs and one HP results in a PF of 0.993, lagging).

2.4.2. Evaluation of Grid Reinforcement Needs

To examine the future need for grid extensions in various LV grids, induced by EVs and/or HPs, the mentioned load approaches are analyzed by determining grid loads at certain grid locations (Figure 5) including the DS and each feeder separately. Therefore, both static load approaches require the number of grid customers (for identifying the according *CF*) and the aggregated peak load of each consumer class, depending on the considered point of load determination. The aggregated load calculated at these locations is distributed to all involved PCCs (points of load application in Figure 5) according to their contribution to the feeders' or distribution substation's peak load. In the TSA-approach, time series are modeled for each of the involved grid customers and aggregated for each time step in accordance with the point of load application. To evaluate inadmissible voltage characteristics caused by future EV- and HP-numbers, voltage deviations are detected at the distribution substation's LV side (DS1; Figure 5) as well as at the farthest grid node in each feeder (e.g., F1; Figure 5). Furthermore, detected voltage deviations are examined regarding the compliance with EN 50,160 [59], which defines an admissible voltage range of ± 0.1 per unit (pu) compared to the nominal voltage. In fact, this permitted voltage range is shared by the MV and LV levels conjunctly. However, pursuant to the voltage range partitioning presented in [60], a voltage range of only [−0.065 pu; +0.045 pu] is available on the LV level.

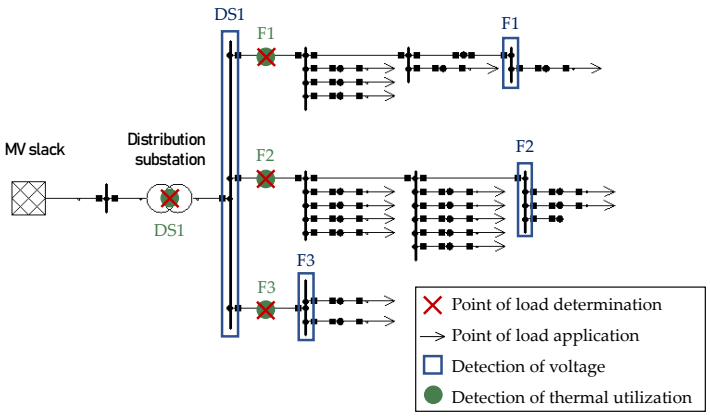

Figure 5. Grid locations of load determination, load application, voltage detection and the detection of thermal overload.

As a result, this admissible voltage range is taken into account to evaluate the number of critical grid nodes with respect to inadmissible voltage deviations. Besides voltage characteristics, potential needs for grid reinforcement measures are additionally derived based on the thermal utilization of feeders (e.g., F1; Figure 5) and the thermal utilization of the distribution substation's transformer (DS1).

3. Results

This study deals with potential grid impacts caused by future grid customers by analyzing three varying load approaches and four different grid regions. Therefore, the results of performed grid simulations in the form of load flow calculations are classified accordingly: Firstly, deviating results in terms of voltage characteristics and thermal overload considering the analyzed load approaches are presented (Section 3.1). Secondly, this study provides an estimation of future grid expansion needs depending on the grid region, the applied load approach and the considered EV- and HP-penetration (Section 3.2).

3.1. Comparison of Various Load Approaches

To demonstrate the influence of the applied load approach, voltage deviations (Figure 6) and thermal utilizations (Figure 7) are contrasted considering the LV grids' distribution substation (DS1) and feeders (F1, F2 etc.). Due to the fact that it has the highest number of EVs and HPs, the load approach comparison is demonstrated using the suburban LV grid's simulation results. Therefore, three degrees of existing and future grid customers are investigated taking various EV- and HP-penetration levels into account: conventional consumers only (CC), conventional consumers in combination with EVs (CC and EV) as well as conventional consumers in combination with EVs and HPs (CC, EV and HP). The evaluated voltage deviations in the suburban LV grid (Figure 6) considering these different degrees of consumer classes differ significantly with the applied load approach. The SIA-approach results in minimal voltages (feeder F4) of 0.955 pu (CC), 0.933 pu (CC and EV) and 0.915 pu (CC, EV and HP), exceeding the defined voltage limit of 0.935 pu even at an EV-penetration of 5%. Additionally, a voltage decrease of 0.017 pu (CC), 0.018 pu (CC and EV) and 0.022 pu (CC, EV and HP) is detected at the LV side of the distribution substation (DS1). As a result, one (CC and EV) or rather three feeders (CC, EV and HP) face inadmissible voltage reductions caused by charging EVs or rather EVs in combination with HPs.

In contrast, the SCA- and TSA-approaches show rather similar impacts on voltage deviations, all complying with the admissible voltage range: While conventional consumers only (CC) causes a minimal voltage (F4) of 0.964 pu (SCA) and 0.968 pu (TSA), these values decrease to 0.961 pu (SCA) and 0.954 pu (TSA) supplying 5% EVs or rather to 0.951 pu (SCA) and 0.948 pu (TSA) supplying 5% EVs and HPs (Figure 6). Using the SCA-approach, the following voltages are detected at DS1: 0.989 pu (CC), 0.988 pu (CC and EV) and 0.988 pu (CC, EV and HP).

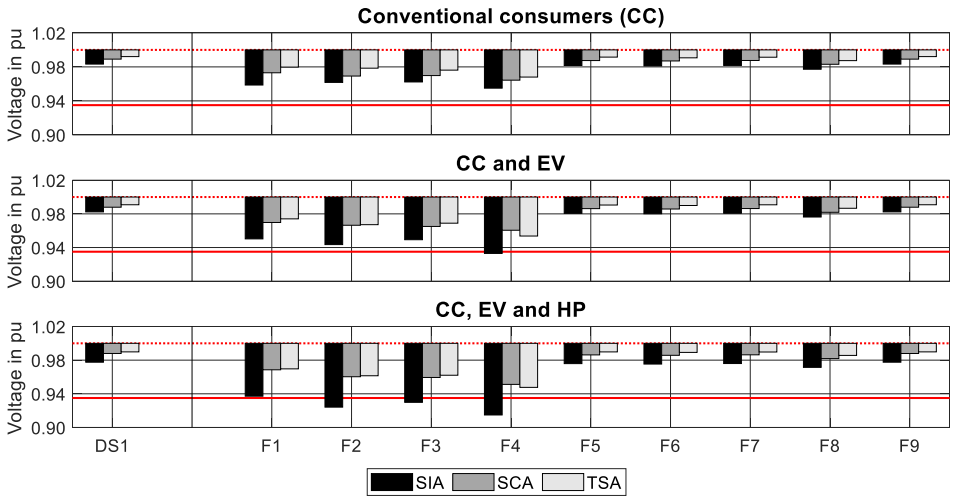

Figure 6. Comparison of various load approaches regarding voltage deviations at the distribution substation (DS1) as well as at feeders (F1–F9) considering an EV- and HP-penetration of 5% supplied by the suburban LV grid.

Otherwise, voltages of 0.992 pu, 0.991 pu and 0.990 pu are triggered at DS1 by these grid loads applying the TSA load approach. In addition to CC-, EV- and HP-caused voltage deviations, we discover a maximal thermal utilization in the LV grid's most critical feeder (F4) of 40.4% (CC), 61.3% (CC and EV) and 73.0% (CC, EV and HP) presuming the SIA-approach. The SCA load approach on the other hand results in a thermal load of 36.3%, 38.2% and 50.4%. Finally, a maximal thermal utilization of 29.4%, 38.2% and 41.4% is determined based on the TSA-approach (Figure 7).

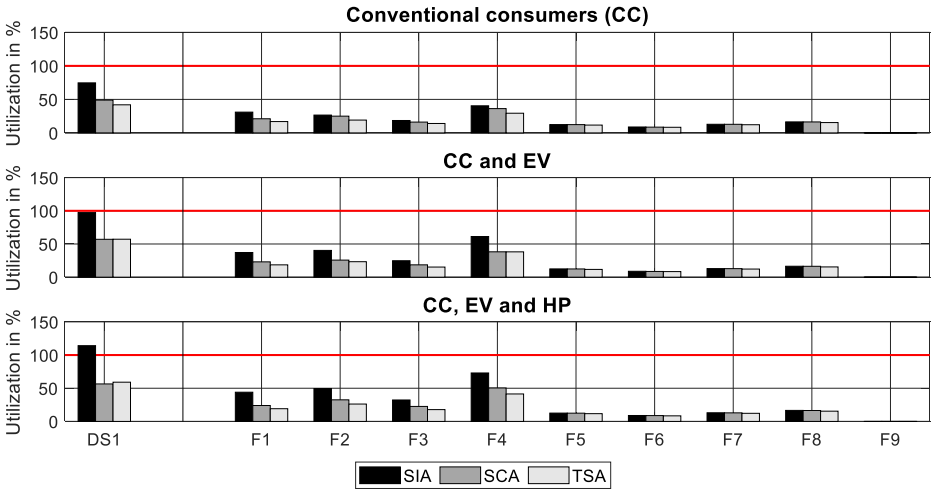

Figure 7. Comparison of various load approaches regarding the thermal utilization of the distribution substation's transformer (DS1) as well as feeders (F1–F9) considering an EV- and HP-penetration of 5% supplied by the suburban LV grid.

Analogously, the evaluation of the suburban LV grid's transformer (DS1) illustrates a similar trend: 74.7% (CC), 97.3% (CC and EV) and 114.1% (CC, EV and HP) are detected using the SIA-approach; 48.9%, 56.5% and 57.1% using the SCA-approach; and 41.9% (CC), 57.2% (CC and EV) and 59.1% (CC, EV and HP) using the TSA-approach. Besides differences regarding the most critical grid locations—e.g., feeder F4 (voltage) and the transformer at the DS (thermal overload)—we analyze the correlation between load approach-induced deviations and the number of additional grid customers in the grid. Therefore, we determine the normalized root mean square deviation (NRMSD) between the static load approaches (SIA and SCA) and the time series analysis (TSA) as a function of numerous EV- and HP-penetration levels: Equations (2) and (3) show the NRMSD's exact calculation regarding

voltage V deviations (referring to an admissible voltage range of 6.5 pu) and thermal utilization U deviations (referring to a maximal thermal load of 100%) including all feeders.

$$NRMSD_{Voltage} = \frac{\sqrt{\frac{1}{No.of\ \ feeders} \cdot \sum_{i=1}^{No.of\ \ feeders} (V_{TSA} - V_{SIA\ \ or\ \ SCA})^2}}{Admissible\ \ voltage\ \ range\ \ of\ \ 6.5\ \ pu} \quad (2)$$

$$NRMSD_{Utilization} = \frac{\sqrt{\frac{1}{No.of\ \ feeders} \cdot \sum_{i=1}^{No.of\ \ feeders} (U_{TSA} - U_{SIA\ \ or\ \ SCA})^2}}{Admissible\ \ maximal\ \ thermal\ \ load\ \ of\ \ 100\%} \quad (3)$$

Figure 8 demonstrates load approach-induced NRMSDs compared to the TSA for the suburban LV grid depending on the considered EV- and HP-penetration. The NRMSD analysis for the urban LV grid in the city center (Figure A5), the urban grid in the city outskirts (Figure A6) as well as the rural LV grid (Figure A7) is demonstrated in Appendix A.5. It points out that the static load approaches differ when it comes to the grid simulation of numerous different grid customer classes and penetration levels: Considering the supply of conventional consumers (CC)—HOs, CBs, ABs and electrical WHs—only (EV- and HP-penetration of 0%), the estimation using the SIA-approach deviates by 19.64% (voltage) and 12.12% (utilization) from the according thresholds (6.5 pu and 100%) compared to the time series analysis (Figure 8). In contrast, the application of the SCA load approach results in an NRMSD of 7.93% and 3.93%.

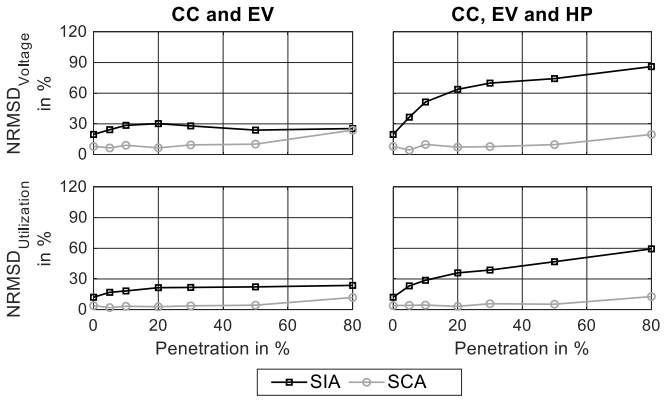

Figure 8. Load approach-induced normalized root mean square deviations (NRMSDs) compared to the TSA in terms of voltage characteristics and thermal utilization considering the suburban LV grid.

Both voltage- and utilization-NRMSD show very similar trajectories as a function of increasing EV- and HP-penetrations. Nevertheless, they differ significantly depending on the applied load approach. On the one hand, the SCA- and TSA-approaches provide very similar results rather independent of the EV- and HP-penetration (Figure 8): The determined $NRMSD_{Voltage}$ fluctuates between 4.62% (5% EV- and HP-penetration) and 24.62% (80% EV-penetration), and the $NRMSD_{Utilization}$ fluctuates between 1.98% (5% EV-penetration) and 12.77% (80% EV- and HP-penetration). On the other hand, the NRMSD between the SIA- and the TSA-approach increases decisively when considering an additional customer class: While the simulation of conventional grid customers in combination with future EVs (CC and EV) results in maximal $NRMSD_{Voltage}$ and $NRMSD_{Utilization}$ of 30.77% (20% EV-penetration) and 23.72% (80%), these values increase to 86.15% and 59.44% (both at 80% EV- and HP-penetration) when including additional HPs (CC, EV and HP).

3.2. Comparison of Different Grid Regions

In addition to the load approach analysis, we analyze future grid extension needs in four different grid regions. Therefore, the share of critical feeders with respect to inadmissible voltage characteristics (dropping below 0.935 pu) and thermal overloads (exceeding 100%) is determined for each LV grid and each load approach (Figures 9 and 10), considering CC and EVs (a) as well as CC,

EVs and HPs (b). The evaluation of inadmissible voltage deviations shows a clear influence of the considered grid region in particular. The urban LV grid located in the city center shows no impacts on voltage characteristics, neither with regard to the applied load approach nor with regard to the degree of grid customer classes (Figure 9). The urban grid located in the city outskirts faces critical voltage decreases starting with 10% (SIA), 80% (SCA) and 30% (TSA) EV- and HP-penetration. Still, the supply of conventional consumers in combination with EVs (without HPs) can be provided even for high EV numbers (Figure 9b), applying the SCA or TSA. Using the SIA, this provision is limited to an EV-penetration of 10% in 8.3% (one) of all feeders. Initial voltage problems also occur even at low penetration levels in at least one of the suburban grid's feeders: 5% (SIA) and 30% (SCA and TSA) penetration supplying CC and EV and 5% (SIA), 30% (SCA) and 20% (TSA) integrating additional HP-loads (Figure 9). Similarly, the rural LV grid is strongly affected by future EV- and HP-numbers with respect to critical voltage deviations. While only 10% (SIA and TSA) and 20% (SCA) of EVs can be supplied, the integration of additional HPs is restricted to 10% (SCA and TSA) or even impeded completely (SIA).

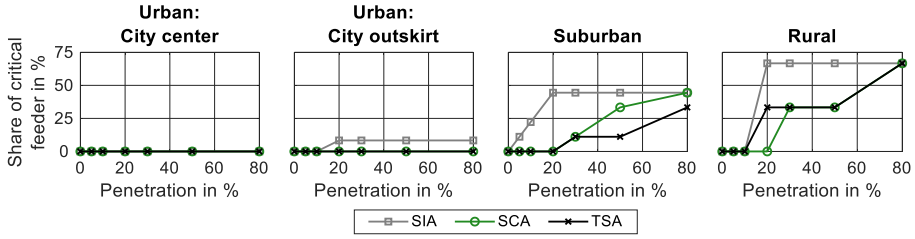

(**a**)

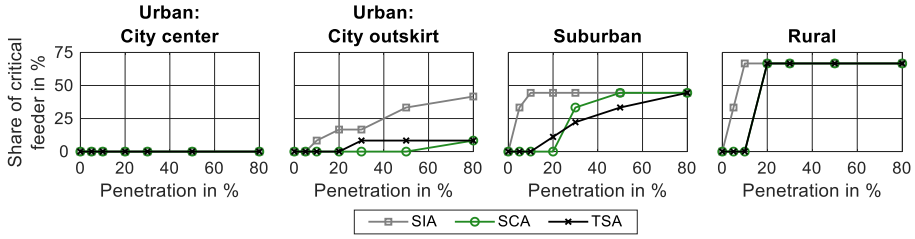

(**b**)

Figure 9. Share of critical feeders in terms of inadmissible voltage deviations caused by CC and EV (**a**) as well as CC, EV and HP (**b**) considering various load approaches, grid regions and penetration levels.

Furthermore, the SIA-approach determines thermal overloads caused by CC and EVs in at least one feeder in the urban grid located in the city outskirts (80% EV-penetration) and the suburban one (50%). The supply of CC, EVs and HPs on the other hand triggers grid line overloads at 30% (outskirts), 20% (suburban) and 80% (rural) EV- and HP-penetration (Figure 10). Using the SCA- or TSA-approach, thermal problems only occur in one feeder in the suburban LV grid at 80% (CC and EV) and 50% (CC, EV and HP) penetration.

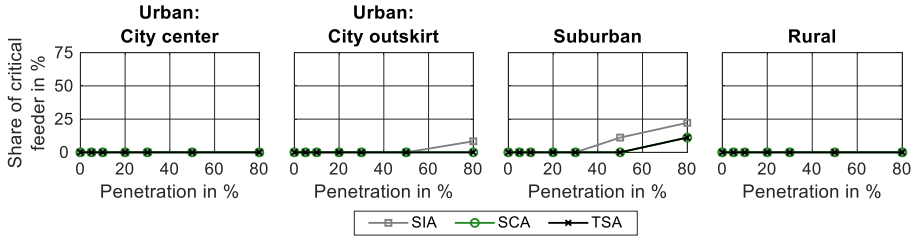

(**a**)

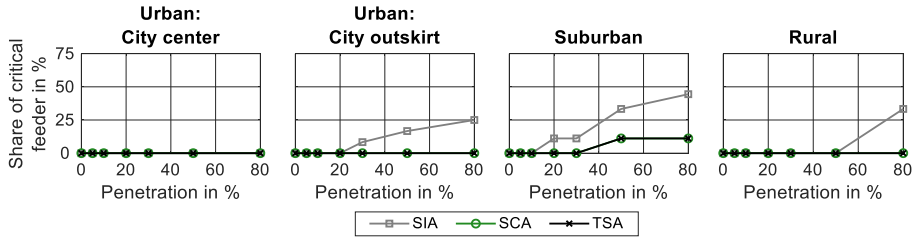

(**b**)

Figure 10. Share of critical feeders in terms of thermal overloads caused by CC and EV (**a**) as well as CC, EV and HP (**b**) considering various load approaches, grid regions and penetration levels.

In addition to critical voltage characteristics and thermal overloads, we investigate the maximal thermal utilization of the LV grids' DS depending on the supplied grid customers (Figure 11): CC and EV (a) or CC, EV and HP (b). The urban (city center) grid's transformer shows a maximal thermal load of 75.8% (SIA), 46.1% (SCA) and 28.2% (TSA) supplying CC and EV and thereby the compliance with its nominal transformer capacity (Table 1). Since the investigated urban grid structure impedes the installation of HPs, no additional loads are added in the CC, EV and HP scenario.

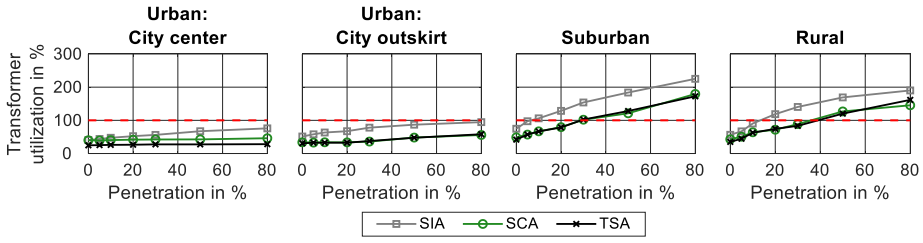

(**a**)

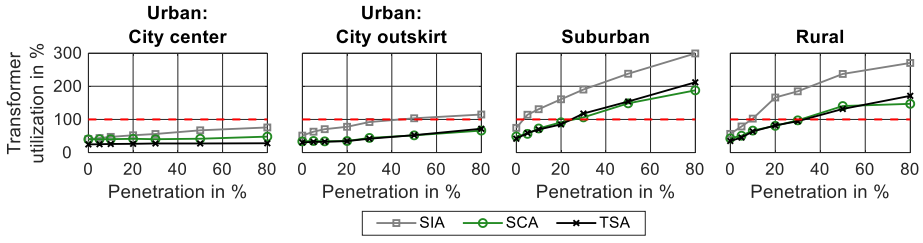

(**b**)

Figure 11. Maximal thermal utilization of the distribution substation's transformer caused by CC and EV (**a**) as well as CC, EV and HP (**b**) considering various load approaches, grid regions and penetration levels.

The urban grid located in the city outskirts faces grid restrictions (only) when applying the static individual load aggregation (SIA) and considering CC, EV and HP. In fact, the supply of these EV- and HP-numbers results in a maximal transformer load of 114.80% (SIA), 66.44% (SCA) and 71.91% (TSA). Without integrated HPs, the maximal transformer load decreases to 94.6% (SIA), 55.8% (SCA) and 58.1% (TSA). In the suburban LV grid on the other hand, the congestion of the transformer's capacity depends strongly on the applied load approach: While the SIA-approach results in a maximal thermal utilization of 106.0% (CC and EV) and 130.8% (CC, EV and HP) powering a penetration of 10%, the SCA- (66.5% and 72.8%) and TSA-approach (66.8% and 69.7%) estimate this scenario differently (Figure 11). An integration of numerous EVs (80% penetration) creates a maximal thermal utilization of 225.1% (SIA), 179.5% (SCA) and 172.4% (TSA) in the suburban grid's DS,

whereas the installation of additional electric HPs increases this load to 298.9%, 187.7% and 211.9%. Despite lower nominal capacity (Table 1), the rural grid's transformer shows quite similar results in this respect (Figure 11): Initial thermal restrictions are triggered by 20% (CC and EV) and 10% (CC, EV and HP) applying the static individual load aggregation (SIA). Using the static combined load approach (SCA), these EV- and HP-numbers induce a maximal thermal utilization of 71.7% and 80.7%. Furthermore, the performed time series analyses (TSAs) indicate utilizations of 74.3% (CC and EV) and 82.0% (CC, EV and HP) compared to the nominal transformer power.

4. Discussion

By means of static (SIA and SCA) and time series-based (TSA) load flow calculations, we analyze the impacts of the following factors on the identification of future grid extension needs on the LV level:

- The consideration of temporal load aggregations of various grid consumer classes in the form of three load approaches;
- The investigated grid region, including realistic housing types, affecting the available charging power and HP-numbers.

The analyzed load approaches—static individual aggregation (SIA), static combined aggregation (SCA) and time series analysis (TSA)—vary in terms of the consideration of temporal interactions between numerous consumer classes: While the SIA-approach assumes a temporal aggregation of all consumer classes' peaks, the other two take consumer class-specific peak periods into account, either by "combined" coincidence factors (SCA) or stochastically modeled time series (TSA). On both the DS-transformer level as well as the feeder level, grid analyses based on the static load aggregation applying an individual coincidence (SIA) result in an overestimation of aggregated maximal loads, compared to the SCA- and TSA-approach. Neglecting temporal consumer class interactions, peak loads of all consumer classes are summed up, resulting in increased voltage decreases (Figure 6) and thermal utilizations (Figure 7). As a result, even the simulation of existing grid customers only (0% penetration) in the form of HOs, CBs, ABs and WHs reveals much higher transformer load (e.g., 74.7% in the suburban grid) compared to that measured during real-life operation (42.0%). This high degree of deviation between modeled and measured loads, even when evaluating present-day grid conditions, highlights the need to calibrate modeled grid customer loads with real-life data (Appendix A.1). The TSA benefits from this calibration and thereby allows for an exact consideration of current consumer loads. On this account, the TSA provides this study's "true" results as a benchmark for static load approaches.

Besides conventional consumer loads, deviations between the SIA and the TSA become more considerable with an increasing number of supplying grid customer classes and with increasing EV- and/or HP-penetrations. In fact, the more grid customers are taken into account for grid simulations, the more temporal peak load aggregations between EVs, HPs and conventional consumers (CC) are assumed by the SIA-approach. While deviations compared to the TSA-approach slightly increase (thermal utilization) or even decrease (voltage) with raising EV-numbers (CC and EV), the inclusion of an additional consumer class varying in terms of temporal load characteristics, e.g., in the form of electric HPs (CC, EV and HP), enhances this effect (Figure 8). Considering EV charging with 3.7 kVA and 11 kVA in combination with electrical HPs, the presented SIA-approach differs by up to 86.15% (voltage) and 59.44% (thermal loads) with reference to the defined thresholds and compared to a grid simulation based on time series. Consequently, these load approach deviations result in a significantly higher extent of calculated grid reinforcement needs: Except for the urban LV grid located in the city center, all grid regions face initial inadmissible voltage deviations as well as thermal overload at much lower EV- and HP-penetrations and thereby at a much earlier stage.

The load aggregation applying a "combined" coincidence factor (SCA) on the other hand corresponds more precisely to detailed long-term TSAs (Figure 8). Due to a missing load profile calibration, deviations compared to the TSA cannot be prevented completely in the reference scenario (excluding EVs and HPs), although they are decreased significantly compared to the ones between

the SIA and TSA. More importantly, deviations compared to the TSA show reduced dependence on the number of varying grid customer classes (demonstrated by two cases: CC and EV as well as CC, EV and HP) in contrast to the SIA-approach. Despite a low NRMSD including all grid components, increasing penetration levels reveal substantial differences between the SCA and TSA in single feeders. Due to the missing calibration of conventional consumer loads, the SCA-approach results in slightly higher grid loads compared to the TSA considering CC only. As a result, the majority of feeders follow this trend when considering additional EV- and HP-numbers: Supplying an EV- and HP-penetration of 20% (Figure 12a) and 50% (Figure 12b), the SCA identifies slightly higher voltage drops in most feeders relative to the TSA-approach. Considering for example a penetration of 50%, the TSA reveals inadmissible voltage characteristics in one (CC and EV) or three feeders (CC, EV and HP) respectively, whereas the SCA-approach detects these in three or four feeders (Figure 9) respectively. However, the SCA-approach reveals slightly decreased grid loads and, thereby, lower voltage deviations in feeder F2 and F4 (Figure 12) compared to the TSA. This finding is based on the stochastic nature applied for modeling consumer load profiles and their coincidence.

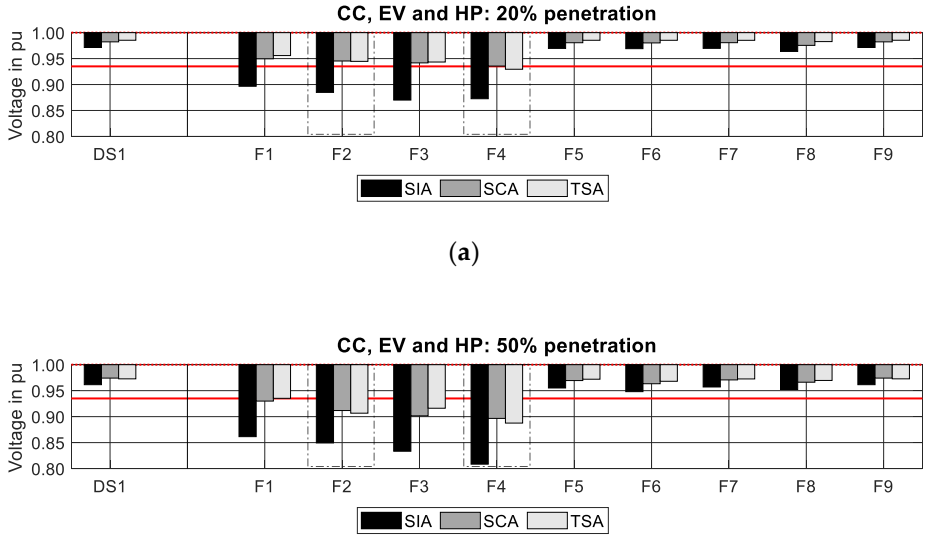

Figure 12. Comparison of various load approaches regarding voltage deviations at the distribution substation (DS1) as well as at feeders (F1–F9) considering an EV- and HP-penetration of 20% (**a**) and 50% (**b**) supplied by the suburban LV grid.

As described in Section 2.3., the latter is modeled by selecting individual load profiles randomly (according to the number of supplied consumers) from a pool of all the modeled time series and by aggregating them for each iteration (365) representing each day of the year. According to probability theory's urn problem, the number of possible combinations when drawing r individual load profiles from a pool of n load profiles is calculated by the binominal coefficient $\binom{n}{r}$ [61]. Since the SCA-approach uses a combined consideration of grid customers' coincidence, theoretically the number of possible load profile combinations of each grid customer class (HO, CBs etc.) must be multiplied. Therefore, to determine all possible load profile combinations in feeder F2 supplying 32 HOs (out of 231), three CBs (88), seven ABs (22), three WHs (10), eleven EVs (160) and five HPs (70), a number of $1.46 \cdot 10^{75}$ combinations must be considered. Hence, the maximum coincidence may be underestimated in single feeders based on a limited number of 365 iterations applied for this study. As a result, the SCA- (zero feeder) and TSA-approach (one feeder) reveal a different share of inadmissible voltage characteristics in the suburban LV grid considering an EV- and HP-penetration of 20%, demonstrated in Figures 9b and 12a. This stochastic nature also affects the SIA-approach and its accuracy when determining the maximum coincidence of individual consumer classes.

Furthermore, with an increasing EV- and HP-penetration, the number of grid consumers (and classes) rises, which enhances this stochastic effect. Based on the disproportional impact of large deviations on the NRMSD, it is very sensitive to outliers [62]. As a result, this stochastic nature influences the NRMSD in both static load approaches, especially at higher penetration levels: While the SCA's slight underestimation of grid loads in single feeders compared to the TSA results in increasing NRMSDs, the SIA's overestimation of grid loads is reduced, which triggers a decrease in the NRMSD (Figure 8). Apart from the suburban region, the urban (city outskirts) and rural LV grids are both affected by this issue, causing an underestimation of aggregated grid loads and, thereby, voltage problems in single feeders by the SIA compared to the TSA-approach. In order to solve this problem, yet avoiding having to run all possible combinations, the number of iterations could be increased until certain criteria are fulfilled, e.g., the standard error of the mean is below a defined limit [37], completely decoupled from the number of analyzed grid customers. However, even with 365 iterations the described effect only leads to minor differences. In general, deviations between static and time series simulations in terms of voltage estimations can result from a uniform spatial distribution of static loads to the feeder's (or substation's) grid nodes [35]. In this study, this aspect is counteracted by spatially allocating the calculated aggregated static load according to the PCC's contribution to the aggregated feeder (or substation) load (Section 2.4.1). Nevertheless, small deviations between the analyzed load approaches will remain, even with high numbers of iterations, due to this effect.

Besides an investigation into various load approaches, the presented results allow an estimation of grid extension needs induced by future EVs and HPs considering four different grid regions. In fact, the analyzed urban LV grid in the city center shows little impacts, based on the assumed charging power of 3.7 kVA (three-phase) available at MARBs and their lack of potential for installing electric HPs. This insight correlates with the findings of Birk et al. (2018) [33], in which, inter alia, the impact of EV charging with 3 kW on a city center LV grid is found to be nonexistent. Furthermore, even the urban LV grid located in the city outskirts faces little impacts regarding inadmissible voltage deviations (the TSA-approach identifies critical voltage only in one feeder starting at an EV- and HP-penetration of 30%) and thermal overload (neither grid lines nor transformer) applying the SCA- or TSA-approach. On the contrary, EV charging with 11 kVA in combination with the supply of electric HPs in the suburban and rural regions triggers inadmissible voltage deviations and/or transformer loads at the DS even at low EV- and HP-penetrations. For example, a penetration of 20% EVs and HPs combined already results in thermal congestions in suburban and rural DS transformers, while preventing thermal overload in grid lines—both similarities to Hülsmann et al. (2019) [29]. In addition, these penetration levels cause inadmissible voltage deviations in the suburban and rural LV grid, comparable with the findings of Mendaza et al. (2014) [28]. Apart from region-specific grid structures (e.g., degree of cabling, number of PCCs etc.), these results demonstrate the significance of considering realistic housing types (e.g., available charging power and possibility of installing HPs) for evaluating future grid extension needs on the LV level. Furthermore, they clarify that EV charging with a reduced power of 3.7 kVA (neglecting HPs) enables a grid-friendly integration of numerous vehicles, presuming a balanced phase-allocation. Otherwise, further simulations dealing with imbalanced grid conditions caused by an area-wide implementation of single-phase charging EVs must be performed. Of course, potential incentives for EV users aimed at low-power charging (e.g., tariff-based charging) must be addressed in addition. Moreover, a variation of available state-of-the-art charging power and its impacts on existing power grids are crucial for detailed grid planning.

Besides the abovementioned limitations due to a time period of one year and the need to investigate additional EV charging characteristics, further studies should focus on the simulation of a higher number of LV grids per region, enabling a more general comparison of different grid regions and their capacity for integrating future grid customers. Furthermore, in this study only certain grid lines and bus bars are examined in terms of voltage characteristics and thermal overload, assuming a uniform spatial distribution of EV- and HP-penetrations. Still, based on local aggregations of EV charging loads or HP-loads, certain feeders may require grid reinforcements at an earlier stage. On the other hand, voltage evaluation in accordance with the EN 50,160 [59] is based on the calculation of ten-minute means, from which 95% must comply with defined limits in each week. Compared to

this study, which assesses inadmissible voltage characteristics according to their minimum during one year considering a time resolution of one minute, this would provide more room for EV- and/or HP-induced voltage deviations. However, the authors will address the highlighted aspects by means of further research projects and will publish new findings in this field.

5. Conclusions

The performed grid simulations clarify the range of potential grid restrictions induced by future EVs and electric HPs, depending on two aspects: the applied load approach and the considered grid region. The former's variation demonstrates the need to include consumer-specific temporal behavior and thereby load aggregations along with other grid customers. Since the analyzed classic grid planning approach (SIA) is based on consumer class individual coincidence factors, it overestimates future grid extension needs, assuming the temporal aggregation of all consumer classes' peak loads. In fact, this issue becomes more important with an increasing number of varying consumer classes (households, EVs, HPs etc.). Consequently, this classic grid planning approach is inadmissible for identifying future grid congestions, unless it is adapted to comply with future grid customers. Therefore, this paper presents the modeling of applicable coincidence factors based on highly resolved time series using a combined load aggregation of conventional grid customers, EVs and electric HPs. Applying the modeled combined coincidence factors (SCA), temporal load aggregations of various consumer classes are estimated in a realistic way, allowing their application in future grid planning. Nevertheless, slight deviations remain compared to detailed time series analyses (TSAs) using calibrated consumer loads. This finding highlights the need to integrate measured consumer data into future grid planning procedures.

As for the second aspect, this paper demonstrates significant differences in terms of the considered grid region, applying real-life grid structures and realistic housing types. While urban LV grids (located in the city center and in the city outskirts) show increased capacity for integrating future grid customers, suburban and rural grids face inadmissible voltage deviations and/or transformer loads even at low EV- and HP-penetrations. Consequently, when it comes to the evaluation of grid extension needs induced by future grid customers, various grid regions must be evaluated individually including real-life grid structures and housing types. Furthermore, this work points out that EV charging with 11 kVA triggers future grid extension requirements even at low EV numbers, whereas the reduction of charging power enables a grid-friendly integration of numerous EVs.

Author Contributions: Conceptualization, B.T. and T.K.; Data curation, B.T.; Formal analysis, B.T. and T.K.; Funding acquisition, T.K.; Investigation, B.T. and T.K.; Methodology, B.T. and T.K.; Project administration, T.K.; Resources, B.T. and T.K.; Software, B.T.; Supervision, T.K.; Validation, B.T. and T.K.; Visualization, B.T.; Writing—original draft, B.T.; Writing—review and editing, T.K. All authors have read and agreed to the published version of the manuscript.

Funding: This research was funded by the Austrian Federal Ministry of Transport, Innovation and Technology via the FFG program "Energie der Zukunft", grant number 854637, and by the "Klima- und Energiefonds" via the FFG program "Leuchttürme eMobilität", grant number 865447.

Acknowledgments: The authors would like to acknowledge the provision of real-life grid structures and consumer data in an anonymous form and in compliance with data protection regulations by Energienetze Steiermark GmbH. They also give special thanks and appreciation to Energie Steiermark Technik GmbH for the performance of long-term measurements and the provision of measured data.

Conflicts of Interest: The authors declare no conflicts of interest.

Appendix

Appendix A.1. Calibration of Modeled Time Series Representing Conventional Consumer Loads

The time-resolved calibration of conventional consumer loads uses measured active ($P_{DS,measurement}$) and reactive power profiles ($Q_{DS,measurement}$) from each distribution substation (DS). Figure A1 demonstrates these time series with a time resolution of one minute.

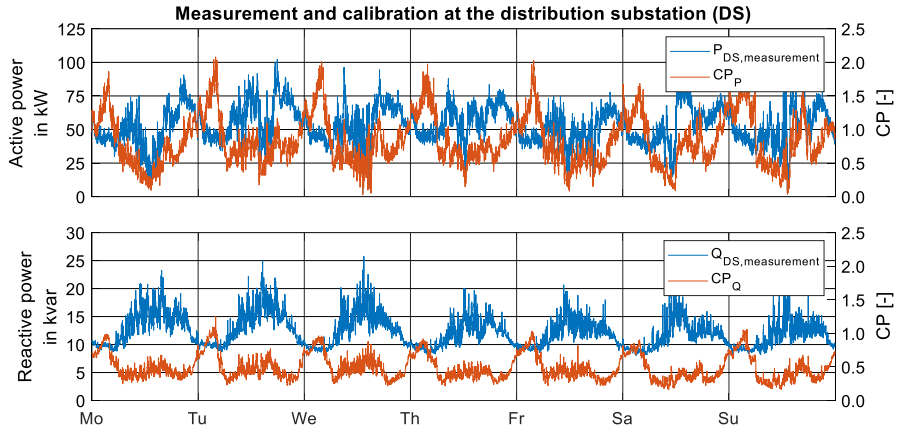

Figure A1. Measured load profiles and calibration parameter (CP), including active and reactive power, considering the suburban LV grid's distribution substation (DS).

The correlation between measured and modeled active and reactive power time series is determined on the DS level by a time-resolved calibration parameter $CP(t)$ calculated with Equations (A1) and (A2).

$$CP_P(t) = \frac{P_{DS,measurement}(t)}{\sum_{PCC=1}^{No.ofPCC} P_{PCC,modelled}(t)} \quad \text{(A1)}$$

$$CP_Q(t) = \frac{Q_{DS,measurement}(t)}{\sum_{PCC=1}^{No.ofPCC} Q_{PCC,modelled}(t)} \quad \text{(A2)}$$

The calibration of modeled conventional consumer load profiles with real measured data demonstrates the need to use real-time load profiles: On the one hand, modeled HO- and CB-loads are decreased ($CF < 1$) in most of the time steps during the day. One the other hand, this calibration increases modeled electrical WH-loads significantly during the night ($CF > 1$), which is based on the usage of standardized, averaged load profiles considering this consumer class. Finally, these time-resolved calibration parameters are applied to adapt modeled conventional consumer load profiles to each time step t and each *PCC* according to Equations (A3) and (A4).

$$P_{PCC}(t) = P_{PCC,modelled}(t) \cdot CP_P(t) \quad \text{(A3)}$$

$$Q_{PCC}(t) = Q_{PCC,modelled}(t) \cdot CP_Q(\mathrm{t}) \quad \text{(A4)}$$

Appendix A.2. Modeling the Spatial Distribution of EV Charging Points

To model the spatial distribution of privately charged EVs individually for each LV grid, we initially determine the total number of vehicles (corresponding to an EV-penetration of 100%) for each *PCC* and both user groups. The LV grids' total number of vehicles charging at home is determined according to Equation (A5) based on the estimated number of persons per household (Table 2) in combination with a grid region-dependent degree of mobility (DoM) [63]. The DoM represents the correlation between the number of passenger vehicles and the number of persons (Table A1).

$$No.of\ \ vehicles\ \ charging\ \ at\ \ home_{PCC} = \ \ No.of\ \ persons_{PCC} \cdot DoM + No.of\ \ AB_{PCC} \quad \text{(A5)}$$

In Equation (A5), we additionally assume one vehicle per agricultural business (AB) taking domestic EV charging at farms into account. Furthermore, the number of vehicles charging at work is estimated for each PCC on the basis of available parking possibilities (one EV per parking lot) at commercial businesses (CBs), identified by the use of Geographic Information System (GIS) data [64]. However, since CBs in the considered LV grids are small- and medium-sized enterprises exclusively, these parking possibilities and thereby the total number of employees charging at work are rather low (Table A1) compared to domestic charging at home. For example, despite the existence of CBs in the rural grid and the urban grid located in the city center, they show no possibility of installing potential charging points at work.

Table A1. Degree of mobility (DoM) and number of vehicles depending on the grid region.

	Urban (City Center)	Urban (City Outskirts)	Suburban	Rural
Degree of mobility (DoM) [%]. [63]	47.7	47.7	61.6	61.6
No. of vehicles charging at home	243	152	153	34
No. of vehicles charging at work	0	5	17	0

To analyze potential grid impacts induced by future EV-numbers, we simulate several EV-penetration rates (0%, 5%, 10%, 20%, 30%, 50% and 80%), which represent the share of EVs in relation to the total number of passenger vehicles. Of course, the EV-penetration may differ spatially within a certain LV grid or a certain feeder depending on demographic, (age, gender etc.), sociological (income, level of education etc.) and psychological aspects (motives, attitudes etc.) [20]. Therefore, after determining the total number of vehicles and defining the considered EV-penetration rate, it has to be decided which of the LV grid's passenger vehicles are electrified and require a supply by the local power grid. However, to enable a feeder-specific analysis of potential grid restrictions, in this study the selected EV-penetration rate is applied to each feeder uniformly. In other words, the number of EVs supplied by a certain grid feeder equals its number of vehicles multiplied by the EV-penetration rate.

Furthermore, these EVs are distributed to the feeder's PCCs in accordance with their total number of vehicles: Starting with the PCC at the end of each feeder, EVs are "added" one by one to PCCs closer to the DS until the feeder's number of supplying EVs is reached. If all vehicles allocated to a certain PCC are electrified, this PCC is skipped for further EV-allocations. The selected allocation method results in a slightly higher EV density at the end of the feeder, providing rather critical analyses of future EV-induced grid impacts.

Appendix A.3. Modeling Realistic Mobility Patterns of Passenger Vehicles

Independent of the spatial component, a time-resolved modeling of EV charging loads requires detailed knowledge about user group-specific mobility patterns, including the time of charging and the driven mileage. Since this study deals with uncontrolled charging of numerous EV users (without any temporal coordination of EV charging or price-triggered charging etc.), the following assumptions are made: While domestically charged EVs are connected to the power grid for recharging after their final trip of the day, EVs are charged at work during morning periods after their arrival at the parking lot. For modeling these uncontrolled charging characteristics, the hour-resolved probability density of the time of arrival at home and at work (Figure A2) is acquired by real-life traffic analysis [53–55,65]. The histograms of the time of arrival demonstrate clear peak periods between 14:00 and 18:00 (at home) and between 6:00 and 10:00 (at work). Considering uncontrolled EV charging, the majority of vehicles are connected to the grid during these periods of the day. Furthermore, the cumulative distribution function (CDF) of the time of arrival is approximated for both user groups by using a linear interpolation between hourly resolved sample points (Figure A4).

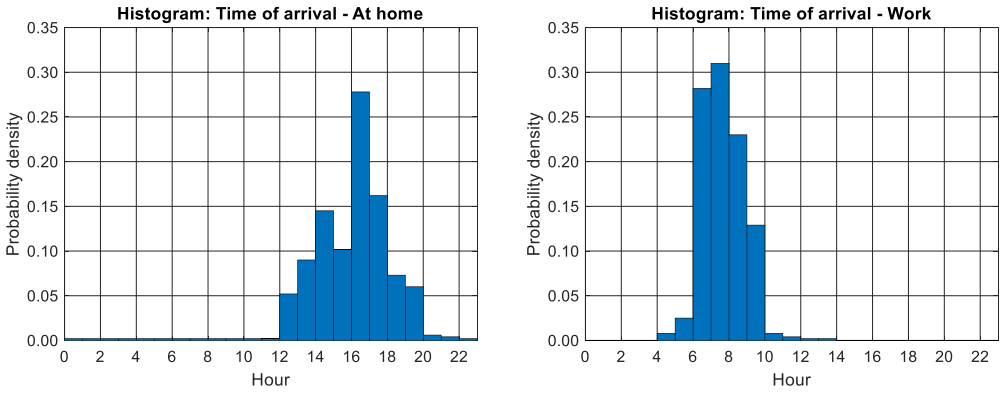

(**a**) (**b**)

Figure A2. Probability density of the time of arrival at home (**a**) and at work (**b**) [65].

In addition to the time of charging, the modeling of EV charging load profiles requires the determination of traveled distances for each day of the year. Considering EVs charged at home, we apply statistical data concerning the mobility indicator, the number of trips per day and the share of trips covered by motorized individual transport (MIT) in the form of standard normal distributions, acquired by traffic surveys [66], considering various regions, seasons and weekdays (Table A2).

Table A2. Mean (μ) and standard deviation (σ) of the standard normal distribution considering the mobility indicator, the number of trips per day as well as the share of trips covered by motorized individual transport (MIT) depending on season, weekday and grid region (urban–suburban–rural) [66].

	Mobility Indicator [%]	Number of Trips per Day	Share of Trips Covered by MIT
μ: summer workday	85.1–83.0–80.0	3.58–3.44–3.32	34.9–54.8–57.7
μ: summer Saturday	81.8–77.3–72.7	3.39–3.35–3.37	33.8–48.4–53.6
μ: summer Sunday	73.5–61.0–66.1	3.02–2.89–2.88	32.2–41.6–43.9
μ: transition workday	86.1–83.0–84.5	3.47–3.39–3.25	41.5–50.7–55.5
μ: transition Saturday	82.7–77.3–76.8	3.29–3.30–3.30	40.2–44.8–51.8
μ: transition Sunday	74.4–61.0–69.8	2.93–2.85–2.82	38.3–38.5–42.2
μ: winter workday	80.6–81.7–82.5	3.41–3.38–3.43	36.6–44.0–55.9
μ: winter Saturday	77.4–76.1–75.0	3.23–3.29–3.48	35.5–38.9–51.9
μ: winter Sunday	69.7–60.0–68.1	2.88–2.84–2.97	33.8–33.4–42.5
σ: summer	35.6–37.6–40.0	1.77–1.80–1.68	47.7–49.8–49.4
σ: transition	34.6–37.6–36.1	1.63–1.79–1.69	49.3–50.0–49.7
σ: winter	39.5–38.6–38.0	1.68–1.63–1.91	48.2–49.6–49.7

The mobility indicator is defined as the share of mobile persons out of the total number of persons and is applied to define whether a vehicle leaves its charging point at home for a trip on a certain day. While EVs charged at home may perform several trips per day, a mobility indicator of 100% and a constant number of trips per day covered by MIT of one is assumed for each workday considering EVs charging at work. Still, despite the annual modeling of mobility patterns, potential periods of the year with no EV charging (holidays, sick leave, vehicle service etc.) are neglected. In addition, the traffic surveys used [66] provide user group-specific statistical data with regards to the covered distance per trip homewards and to work depending on the grid region and weekday (Table A3).

Table A3. Share of trips in % according to the covered distance depending on the EV user group, weekday and grid region (urban–suburban–rural) [66].

Covered Distance	Homeward—Weekday	Homeward—Saturday	Homeward—Sunday	To work—Weekday
<0.5 km	0.9–2.3–1.9	2–1.6–2.4	1.1–2.7–1.7	3.3–3.6–6
0.5–1.0 km	4.4–4.6–5.5	2.3–7.5–5.9	2.5–5.1–4.7	5.3–4–6.2
1.0–2.5 km	13–13.8–11.4	11.3–12.4–17.6	8.6–12.5–13.9	11.7–11.7–8.6
2.5–5.0 km	27.7–20.3–20.4	28.2–24.4–19.6	23.8–20.1–19.4	29.3–13.6–14.9
5.0–10 km	24.8–21.1–19.5	22.7–19.7–16.2	21.9–15.4–20.1	25.9–20.1–15.4
10–20 km	16.2–18.9–19.6	20.8–16.9–18.1	22.4–18.8–22.2	15.8–22–19.9
20–50 km	9–14.4–16.1	6.8–12.5–15.1	12.3–13.6–11.7	6.4–20.8–22
>50 km	4–4.6–5.6	5.9–5–5.1	7.4–11.8–6.3	2.3–4.2–7

Evidently, the probability density of covered distances per trip indicates very similar distributions regarding homeward trips and trips to work. The majority of trips (e.g., 95.4% homewards and 95.8% to work on a workday in a suburban region) are characterized by distances of less than 50 km, which can easily be supplied by state-of-the-art EV models (Table A5). The applied data with regards to the time of arrival and the covered distance show high similarity to those presented by Lojowska et al. (2012) [51]. Furthermore, we apply these statistical data in order to approximate the CDF of covered distances by log-normal distributions for each weekday and each user group (Table A4). Assuming no trips to work on Saturdays and Sundays, only workdays are relevant for this user group.

Table A4. Mean (μ) and standard deviation (σ) of the log-normal distribution of covered distances per trip derived from statistical data (Table A3) [66], depending on the EV user group, weekday and grid region (urban–suburban–rural).

	Homeward—Weekday	Homeward—Saturday	Homeward—Sunday	To work—Weekday
μ	1.86–1.96–2.05	1.94–1.88–1.90	2.17–2.13–2.02	1.67–2.1–2.07
σ	1.14–1.27–1.31	1.19–1.29–1.37	1.21–1.47–1.31	1.13–1.32–1.50

Based on the prepared statistical mobility data, annual driving performances are individually modeled for each EV of both user groups (Figure A3) by a probabilistic predictive approach according to [19,53–55,67]. Therefore, we initially examine for each day of the year the occurrence of a trip (home)—by applying a random number (1. RN) and the CDF (1) of the mobility indicator of MIT—as well as whether it is a workday or not (work). If so, the time of arrival at home after the final trip of the day or the time of arrival at the workplace's parking lot is determined by applying additional random numbers (2. RN and 6. RN) and the prepared mobility data in the form of CDFs (2 and 6), demonstrated in Figure A4. In the next step, the number of trips—3. RN and (3)—and the share of trips covered by MIT—4. RN and (4)—are defined and applied to calculate the number of trips covered by MIT. Considering EV charging at work, the number of trips covered by MIT equals one on workdays and zero on Saturdays and Sundays. Finally, the covered distance is determined for each MIT-trip by using 5. RN and 7. RN as well as (5) and (7). Since this study deals with grid impacts caused by private charging at home and at work, public (re-)charging during the day is neglected. As a result, the complete electric energy demand is supplied exclusively by private charging points at home or at work, depending on the considered user group.

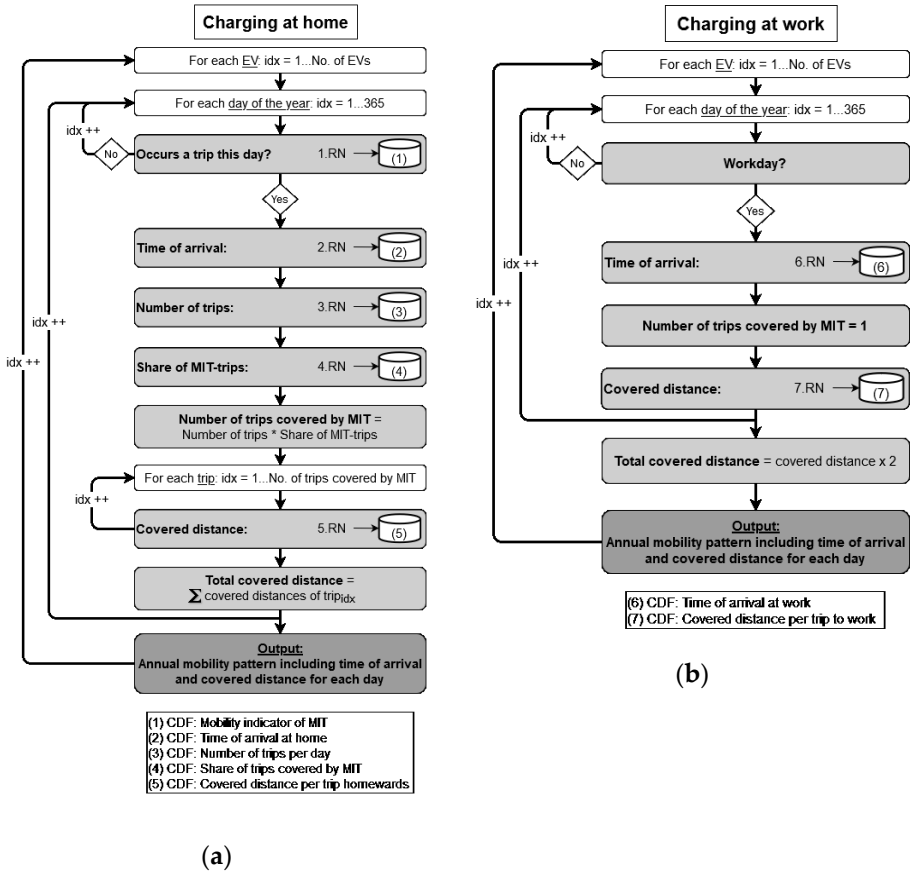

Figure A3. Probabilistic modeling of mobility patterns: charging at home (**a**) and charging at work (**b**).

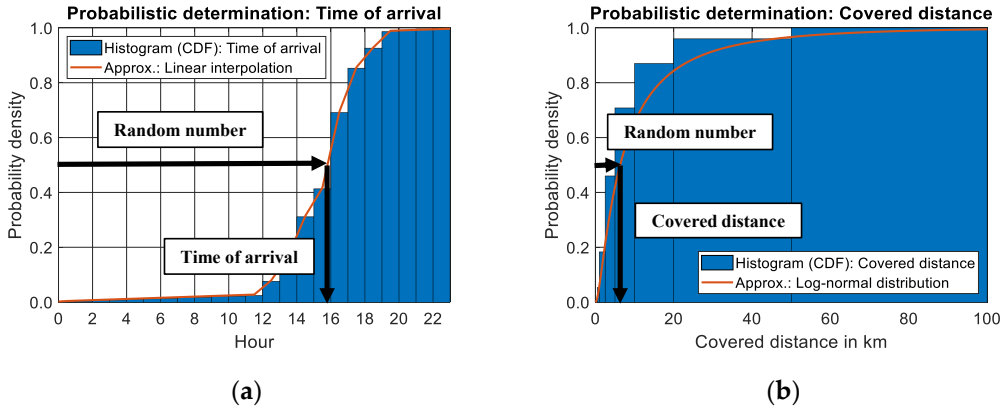

Figure A4. Probabilistic determination of time of arrival (**a**) and covered distance (**b**) based on real mobility data.

Therefore, the daily trips' covered distances are aggregated to identify the total distance each EV has covered on this day. Assuming charging at work solely, the stochastically determined work-trip's distance is multiplied by two, taking round trips (work–home–work) into account. In the end, this probabilistic approach provides the time of charging as well as the covered distance of each EV for both user groups, for each day of the year.

Appendix A.4. EV Model Specifics

Besides realistic mobility patterns, the time-resolved modeling of EV loads requires the consideration of several EV model specifics. Since both EV user groups (charging at home and charging at work) deal with passenger vehicles, numerous commercial EV models are taken into account. Therefore, Germany's 15 most registered EV models are picked for this study, based on the number of registrations in the year of 2019 [68]. Finally, state-of-the-art EV model specifics (Table A5) are acquired for each of them: the frequency of occurrence [68], battery capacity, specific energy consumption and charging efficiency [69].

Table A5. Specifics of EV models applied for modeling EV charging loads.

EV Model	Frequency (%) [68]	Battery Capacity (kWh) [69]	Specific Energy Consumption (kWh/km) [69]	Charging Efficiency (-) [1] [69]
1	19.0	41	0.203	0.828
2	16.8	75	0.209	0.838
3	15.0	27.2	0.184	0.708
4	8.6	34.9	0.173	1.000
5	7.3	17.6	0.183	1.000
6	6.4	95	0.237	1.000
7	6.3	64	0.195	0.866
8	4.5	40	0.221	1.000
9	4.1	17.6	0.183	1.000
10	3.2	28	0.147	0.906
11	2.9	27	0.191	1.000
12	1.6	90	0.276	0.893
13	1.5	90	0.240	1.000
14	1.3	18.7	0.177	1.000
15	1.3	40	0.281	0.853

[1] In the case of an efficiency of 1.0, charging losses are included in the energy consumption.

Since the listed specific energy consumption was measured at an ambient temperature of 20 °C [69], the impact of ambient temperature is estimated for all EV models equally considering summer (mean temperature of 18.8 °C [70], increase of 1.6%), transition (mean temperature of 10.5 °C [70], increase of 13.1%) and winter periods (mean temperature of 2.7 °C [70], increase of 28.3%) based on Tober (2016) [71]. Besides individual EV specifics, measured EV charging profiles of all the listed EV models including phase-imbalanced active and reactive power are applied to model annual charging profiles. These real-life charging curves enable the consideration of realistic charging characteristics, e.g., the EV-model-specific transition from constant-current-phase to constant-voltage-phase. Analogous to the probabilistic determination of mobility patterns (Figure A4), the individual vehicle model (including vehicle specifics) is selected for each EV by applying the EV models' frequency of occurrence (Table A5) in the form of the CDF (approximated by linear interpolation) in combination with random numbers. Based on the determined specific energy consumption and charging efficiency of a certain EV model in combination with the predefined daily covered distance, the energy demand supplied by the grid is calculated and limited to the battery capacity eventually. Considering state-of-the-art EV models and the trend towards increasing charging power (even at private charging points at home or at work), charging with 11 kVA is technically feasible for each of the selected EV models. Nevertheless, the actual available charging power might be limited by restricted power installed at the interconnected charging point at home or at work.

Appendix A.5. Supplementary Results: Deviations between Static and Time Series-Based Load Approaches

In addition to load approach deviations in the suburban LV grid demonstrated in Section 3.1, Figures A5–A7 show the remaining analyzed grid regions.

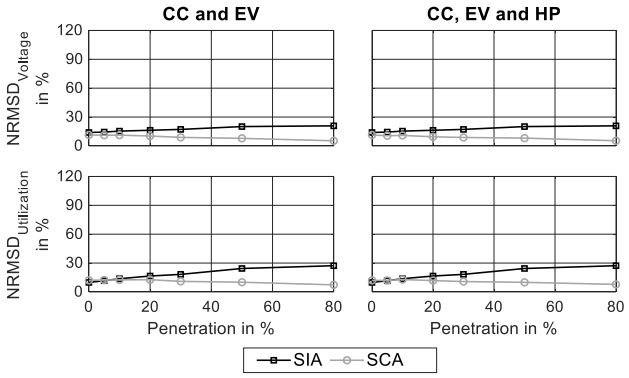

Figure A5. Load approach-induced normalized root mean square deviations (NRMSDs) compared to the TSA in terms of voltage characteristics and thermal utilization considering the urban LV grid located in the city center.

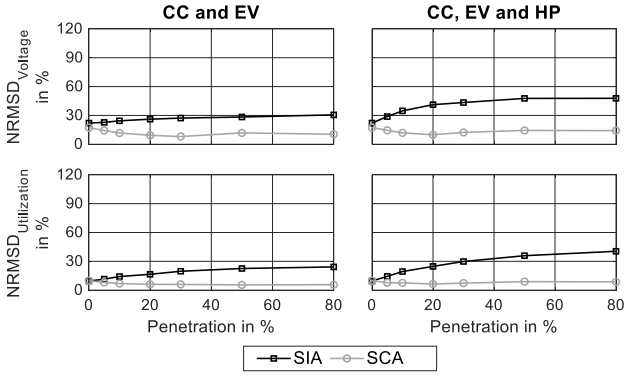

Figure A6. Load approach-induced normalized root mean square deviations (NRMSDs) compared to the TSA in terms of voltage characteristics and thermal utilization considering the urban LV grid located in the city outskirts.

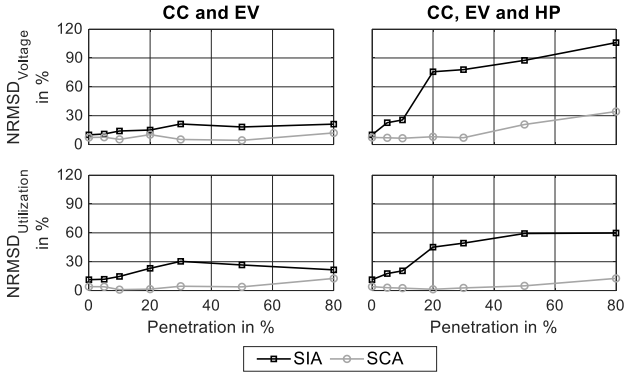

Figure A7. Load approach-induced normalized root mean square deviations (NRMSDs) compared to the TSA in terms of voltage characteristics and thermal utilization considering the rural LV grid.

References

1. European Commission. A Clean Planet for all—A European strategic long-term vision for a prosperous, modern, competitive and climate neutral economy. In *Communication from the Commission to the European Parliament;* The European Council, the European Economic and Social Committee, the Committee of the Regions and the European Investment Bank; European Commission: Brussels, Belgium, 2019.
2. Environment Agency Austria. Greenhouse Gases—Traffic Sector. Available online: https://www.umweltbundesamt.at/umweltsituation/verkehr/auswirkungen_verkehr/verk_treibhausgase/ (accessed on 31 January 2020).

3. European Commission. *Communication from the Commission to the European Parliament*; The European Council, the Council, the European Economic and Social Committee and the Committee of the Regions, the European Green Deal; European Commission: Brussels, Belgium, 2019.
4. Figenbaum, E.; Assum, T.; Kolbenstvedt, M. Electromobility in Norway: Experiences and Opportunities. *Res. Transp. Econ.* **2015**, *50*, 29–38, doi:10.1016/j.retrec.2015.06.004.
5. *Directive 2010/31/EU of the European Parliament and of the Council of 19 May 2010 on the energy performance of buildings*; Directive; European Parliament and the Council of the European Union: Strasbourg, France, 2010; 3, 124–146.
6. Protopapadaki, C.; Saelens, D. Heat pump and PV impact on residential low-voltage distribution grids as a function of building and district properties. *Appl. Energy* **2017**, *192*, 268–281, doi:10.1016/j.apenergy.2016.11.103.
7. Bayer, P.; Saner, D.; Bolay, S.; Rybach, L.; Blum, P. Greenhouse gas emission savings of ground source heat pump systems in Europe: A review. *Renew. Sustain. Energy Rev.* **2012**, *16*, 1256–1267, doi:10.1016/j.rser.2011.09.027.
8. Liu, J. Electric vehicle charging infrastructure assignment and power grid impacts assessment in Beijing. *Energy Policy* **2012**, *51*, 544–557, doi:10.1016/j.enpol.2012.08.074.
9. Baresch, M.; Moser, S. Allocation of e-car charging: Assessing the utilization of charging infrastructures by location. *Transp. Res. Part A Policy Pract.* **2019**, *124*, 388–395, doi:10.1016/j.tra.2019.04.009.
10. Shahnia, F.; Ghosh, A.; Ledwich, G.; Zare, F. Predicting Voltage Unbalance Impacts of Plug-in Electric Vehicles Penetration in Residential Low-voltage Distribution Networks. *Electr. Power Compon. Syst.* **2013**, *41*, 1594–1616, doi:10.1080/15325008.2013.834004.
11. Shafiee, S.; Fotuhi-Firuzabad, M.; Rastegar, M. Investigating the Impacts of Plug-in Hybrid Electric Vehicles on Power Distribution Systems. *IEEE Trans. Smart Grid* **2013**, *4*, 1351–1360, doi:10.1109/TSG.2013.2251483.
12. Steen, D.; Le Tuan, A.; Carlson, O.; Bertling, L. Assessment of Electric Vehicle Charging Scenarios Based on Demographical Data. *IEEE Trans. Smart Grid* **2012**, *3*, 1457–1468, doi:10.1109/TSG.2012.2195687.
13. Dubey, A.; Santoso, S. Electric Vehicle Charging on Residential Distribution Systems: Impacts and Mitigations. *IEEE Access* **2015**, *3*, 1871–1893, doi:10.1109/ACCESS.2015.2476996.
14. Bollen, M.H.J.; Rönnberg, S.K. Hosting Capacity of the Power Grid for Renewable Electricity Production and New Large Consumption Equipment. *Energies* **2017**, *10*, 1325, doi:10.3390/en10091325.
15. Clement-Nyns, K.; Haesen, E.; Driesen, J. The Impact of Charging Plug-In Hybrid Electric Vehicles on a Residential Distribution Grid. *IEEE Trans. Power Syst.* **2010**, *25*, 371–380, doi:10.1109/TPWRS.2009.2036481.
16. Wang, Y.; Infield, D. Markov Chain Monte Carlo simulation of electric vehicle use for network integration studies. *Int. J. Electr. Power Energy Syst.* **2018**, *99*, 85–94, doi:10.1016/j.ijepes.2018.01.008.
17. Sexauer, J.M.; McBee, K.D.; Bloch, K.A. Applications of probability model to analyze the effects of electric vehicle chargers on distribution transformers. *IEEE Trans. Power Syst.* **2013**, *28*, 847–854, doi:10.1109/TPWRS.2012.2210287.
18. Rahman, S.; Shrestha, G.B. An investigation into the impact of electric vehicle load on the electric utility distribution system. *IEEE Trans. Power Deliv.* **1993**, *8*, 591–597, doi:10.1109/61.216865.
19. Qian, K.; Zhou, C.; Allan, M.; Yuan, Y. Modeling of Load Demand Due to EV Battery Charging in Distribution Systems. *IEEE Trans. Power Syst.* **2011**, *26*, 802–810, doi:10.1109/TPWRS.2010.2057456.
20. Fischer, D.; Harbrecht, A.; Surmann, A.; McKenna, R. Electric vehicles' impacts on residential electric local profiles—A stochastic modelling approach considering socio-economic, behavioural and spatial factors. *Appl. Energy* **2019**, 233-234, 644–658, doi:10.1016/j.apenergy.2018.10.010.
21. Dyke, K.J.; Schofield, N.; Barnes, M. The Impact of Transport Electrification on Electrical Networks. *IEEE Trans. Ind. Electron.* **2010**, *57*, 3917–3926, doi:10.1109/TIE.2010.2040563.
22. Fischer, D.; Scherer, J.; Flunk, A.; Kreifels, N.; Byskov-Lindberg, K.; Wille-Haussmann, B. Impact of HP, CHP, PV and EVs on households electric load profiles. In Proceedings of the PowerTech, IEEE Eindhoven, IEEE Eindhoven PowerTech, Eindhoven, Netherlands, 29 June–2 July 2015; pp. 1–6, ISBN 978-1-4799-7693-5.
23. Fox, B.; Morrow, J.D.; Akmal, M.; Littler, T. Impact of heat pump load on distribution networks. *IET Gener. Transm. Distrib.* **2014**, *8*, 2065–2073, doi:10.1049/iet-gtd.2014.0056.
24. Heffernan, W.J.B.; Watson, N.R.; Buehler, R.; Watson, J.D. Harmonic performance of heat-pumps. *J. Eng.* **2013**, *2013*, 31–44, doi:10.1049/joe.2013.0012.

25. Navarro-Espinosa, A.; Mancarella, P. Probabilistic modeling and assessment of the impact of electric heat pumps on low voltage distribution networks. *Appl. Energy* **2014**, *127*, 249–266, doi:10.1016/j.apenergy.2014.04.026.
26. Kusch, W.; Stadler, I.; Bhandari, R. Heat pumps in low voltage distribution grids by energy storage In *Proceedings of the 2015 International Energy and Sustainability Conference (IESC), Farmingdale, NY, USA, 12–13 November 2015*; Conference I.E.A.S., Ed.; IEEE: Piscataway, NJ, USA, 2015; pp 1–6, ISBN 978-1-4673-9770-4.
27. Navarro-Espinosa, A.; Ochoa, L.F. Probabilistic Impact Assessment of Low Carbon Technologies in LV Distribution Systems. *IEEE Trans. Power Syst*. **2016**, *31*, 2192–2203, doi:10.1109/TPWRS.2015.2448663.
28. Cerio Mendaza, I.D. Bak-Jensen, B.; Chen, Z.; Jensen, A. Stochastic impact assessment of the heating and transportation systems electrification on LV grids. In *Proceedings of the IEEE PES Innovative Smart Grid Technologies Conference Europe (ISGT-Europe), Istanbul, Turkey, 12—15 October 2014*; IEEE: Piscataway, NJ, USA, 2014; pp. 1–6, ISBN 978-1-4799-7720-8.
29. Hülsmann, L.; Schlößer, T.; Tröster, E.; Koch, M.; Ohl, U. Electric Vehicle and Heat Pump Hosting Capacity Assessment for a German 25,000-noded Distribution Network. Presented at Proceedings of the 3rd E-Mobility Power System Integration Symposium, Dublin, Ireland, 14 October 2019; EMOB19-276.
30. Shao, N.; You, S.; Segerberg, H. Integration of 100% heat pumps and electric vehicles in the low voltage distribution network: A Danish case story. In Proceedings of the 3rd International Conference on Microgeneration and Related Technologies, 15-17 April 2013.
31. Li, Y.; Crossley, P.A. Monte Carlo study on impact of electric vehicles and heat pumps on LV feeder voltages. In *Proceedings of the 12th IET International Conference on Developments in Power System Protection (DPSP 2014), Copenhagen, Denmark, 31 March–3 April 2014*; IEEE: Piscataway, NJ, USA, 2014; ISBN 978-1-84919-834-9.
32. Baccino, F.; Massucco, S.; Silvestro, F.; Grillo, S. Management strategy for unbalanced LV distribution network with electric vehicles, heat pumps and domestic photovoltaic penetration. In *Proceedings of the 2014 IEEE PES General Meeting, Conference & Exposition, National Harbor, MD, USA, 27–31 July 2014*; IEEE Power & Energy Society: Piscataway, NJ, USA, 2014; pp. 1–5, ISBN 978-1-4799-6415-4.
33. Birk, S.; Brosig, C.; Waffenschmidt, E.; Schneiders, T. Influence of Sector Coupling in Future Inner City Low Voltage Grids. In *Proceedings of the 2018 7th International Energy and Sustainability Conference (IESC), Cologne, Germany,17–18 May 2018*; IEEE: Piscataway, NJ, USA 2018; pp 1–8, ISBN 978-1-5386-5497-2.
34. Sinha, R.; Bak-Jensen, B.; Pillai, J.R. Operational flexibility of electrified transport and thermal units in distribution grid. *Int. J. Electr. Power Energy Syst.* **2020**, *121*, 106029, doi:10.1016/j.ijepes.2020.106029.
35. Willis, H.L. *Power Distribution Planning Reference Book*; 2nd ed.; CRC press: Boca Raton, FL, USA, 2004, ISBN 0824748751.
36. TAEV. *Technical Connection Conditions for Connection to Public Supply Networks with Operating Voltages up to 1000 Volt*; In German: Technische Anschlussbedingungen für den Anschluss an öffentliche Versorgungsnetze mit Betriebsspannungen bis 1000 Volt; Oesterreichs Energie; OVE Österreichischer Verband für Elektrotechnik, Eds.; TAEV: Viena, Austria, 2012.
37. Rothrock, L.; Narayanan, S. *Human-in-the-Loop Simulations*; Springer London: London, UK, 2011, ISBN 978-0-85729-882-9.
38. Wahl, M.; Hein, L.; Moser, A. Fast Power Flow Calculation Method for Grid Expansion Planning. In Proceedings of the 21st European Conference on Power Electronics and Applications (EPE '19 ECCE Europe), Genova, Italy, 3–5 September 2019; pp. 1–7.
39. The MathWorks Inc. MATLAB; Natick, MA, USA. Version: R2018b, 2018.
40. Energienetze Steiermark GmbH. Available online: https://www.e-netze.at (accessed on 30 July 2020).
41. NEPLAN AG (8700 Küsnacht, Switzerland). NEPLAN – Power System Analysis. 2019
42. European Commision. Degree of Urbanisation (DEGURBA)—Local Administrative Units. Available online: https://ec.europa.eu/eurostat/ramon/miscellaneous/index.cfm?TargetUrl=DSP_DEGURBA (accessed on June 2020).
43. Schwab, A.J. *Elektroenergiesysteme*; Springer: Berlin/Heidelberg, Germany 2012, ISBN 978-3-642-21957-3.
44. Sonstige Marktregeln Strom: Kapitel 6—Zählwerte, Datenformate und standardisierte Lastprofile; Version 3.7; E-Control: Vienna, Austria, 2020 (last revision). Available online: https://www.e-control.at/documents/1785851/1811582/20150716-SoMa-6-V3-6.pdf/39973f05-a048-425a-957c-46342f0659fa?t=1512133351998 (accessed on 24 September 2020)

45. Meier, H. Repräsentative VDEW—Lastprofil. Available online: https://www.bdew.de/media/documents/1999_Repraesentative-VDEW-Lastprofile.pdf (accessed on 23 July 2020).
46. Pflugradt, N. Online Load Profile Generator. Available online: https://www.loadprofilegenerator.de (accessed on June 2019).
47. Bittermann, W.; Gollner, M.; Angabe, K. *Modelling of Power Consumption in Private Households in Austria According to Type of Usage*; Statistics Austria: Viena, Austria, 2011.
48. Richardson, I. Integrated High-resolution Modelling of Domestic Electricity Demand and Low Voltage Electricity Distribution Networks. Doctoral Thesis, Loughborough University, Loughborough, UK, 2010.
49. Jörg Scheffler. Bestimmung der maximal zulässigen Netzanschlussleistung photovoltaischen Energiewandlungsanlagen in Wohnsiedlungsgebieten. Dissertation, Technische Universität Chemnitz, Chemnitz, Germany, June 2002.
50. *Directive 2014/94/EU of the European Parliament and of the Council of 22 October 2014 on the deployment of alternative fuels infrastructure*; Directive; European Parliament and the Council of the European Union: Strasbourg, France, 2014. Availabe online: https://eur-lex.europa.eu/legal-content/en/ALL/?uri=CELEX%3A32014L0094 (accessed on September 2020).
51. Lojowska, A.; Kurowicka, D.; Papaefthymiou, G.; Van der Sluis, L. Stochastic Modeling of Power Demand Due to EVs Using Copula. *IEEE Trans. Power Syst*. **2012**, *27*, 1960–1968, doi:10.1109/TPWRS.2012.2192139.
52. Hartmann, N.; Özdemir, E.D. Impact of different utilization scenarios of electric vehicles on the German grid in 2030. *J. Power Sources* **2011**, *196*, 2311–2318, doi:10.1016/j.jpowsour.2010.09.117.
53. Thormann, B.; Kienberger, T. *Comparison of Electromobility-Impacts on the Low-Voltage Level in Different Grid Regions*. In Proceedings of the 2nd E-Mobility Power System Integration Symposium, Stockholm, Sweden, 15 October 2018
54. Thormann, B.; Braunstein, R.; Wisiak, J.; Strempfl, F.; Kienberger, T. Evaluation of Grid Relieving Measures for Integrating Electric Vehicles in a Suburban Low-Voltage Grid. In Proceedings of the Grid, CIRED Conference Proceedings, Madrid, Spain, 3–6 June 2019.
55. Thormann, B.; Kienberger, T. Grid-friendly Integration of Future Public Charging Infrastructure by Flywheel Energy Storage Systems (FESS). In Proceedings of the NEIS 2019–Conference on Sustainable Energy Supply and Energy Storage Systems, Hamburg, Germany, 19–20 September 2019
56. SMATRICS GmbH, Co KG and ABL SURSUM Bayerische Elektrozubehör GmbH & Co. KG. Expert interview with employees of the charging station manufacturer. 2017.
57. STATISTICS AUSTRIA. Private households in 2017 classified according to household type and federal state. Available online: http://www.statistik.at/web_en/statistics/PeopleSociety/population/population_censuses_register_based_census_register_based_labour_market_statistics/households/index.html (accessed on May 2020).
58. STATISTICS AUSTRIA. Overall consumption of all fuels by purposes in 2017/18. Available online: http://www.statistik.at/web_en/statistics/EnergyEnvironmentInnovationMobility/energy_environment/energy/energy_consumption_of_households/036844.html (accessed on May 2020).
59. OVE Österreichischer Verband Elektrotechnik, Austrian Standards Institute (Vienna, Austria). Voltage characteristics of electricity supplied by public electricity networks (EN 50160). 2011.
60. Büchner, J.; Katzfey, J.; Flörcken, O.; Moser, A.; Schuster, H.; Dierkes, S.; van Leeuwen, T.; Verheggen, L.; Uslar, M.; van Amelsvoort, M.; Modern distribution grids for Germany, Final report. Federal Ministry for Economic Affairs and Energy, Germany (in German: Moderne Verteilernetze für Deutschland, Abschlussbericht), 2014.
61. Johnson, N.L.; Kotz, S. Urn models and their application. In *An Approach to Modern Discrete Probability Theory*; Wiley: New York, NY, USA, 1977; ISBN 0471446300.
62. Pontius, R.G.; Thontteh, O.; Chen, H. Components of information for multiple resolution comparison between maps that share a real variable. *Environ. Ecol. Stat.* **2008**, *15*, 111–142, doi:10.1007/s10651-007-0043-y.
63. STATISTICS AUSTRIA. Stock of Motor Vehicles. 2019. Available online: www.statistik.at (accessed on 13 May 2019).
64. Federal Province of Styria. Online Geographic Information System (GIS) Data. Available online: www.landesentwicklung.steiermark.at/ (accessed on 10 December 2019).

65. Verkehrplus GmbH. *Mobility Data Provided Within the Scope of the Move2Grid Project Funded by the Autrian Reasearch Promotion Agency FFG*; Verkehrplus GmbH: Graz, Austria, 2017.
66. Österreich unterwegs 2013/2014 – Ergebnisbericht zur österreichweiten Mobilitätserhebung; Final report; Austrian Federal Ministry of Transport, Innovation and Technology: Vienna, 2016.
67. Ul-Haq, A.; Cecati, C.; El-Saadany, E. Probabilistic modeling of electric vehicle charging pattern in a residential distribution network. *Electr. Power Syst. Res.* **2018**, *157*, 126–133, doi:10.1016/j.epsr.2017.12.005.
68. Kraftfahrt-Bundesamt Deutschland. Number of Registered Vehicles Classified According to Brand and Model Between January and July 2019. Available online: https://www.kba.de/EN/Statistik_en/Fahrzeuge_en/fahrzeuge_node_en.html (accessed on December 2019).
69. Allgemeiner Deutscher Automobil Club. Eco-Test. Available online: https://www.adac.de/infotestrat/tests/eco-test (accessed on October 2019).
70. 70. World Meteorological Organization. Mean Daily Temperature Provided for each Month by "World Weather Information Service". Available online: http://www.wwis.dwd.de (accessed on May 2019).
71. Tober, W. *Experience Report Electromobility and Internal Combustion Engine—Analysis of Electrified Drive Concepts of Passenger Vehicles*; In German: Praxisbericht Elektromobilität undVerbrennungsmotor—Analyse elektrifizierter Pkw-Antriebskonzepte; Springer Vieweg: Wiesbaden, Germany, 2016; ISBN 9783658136017.

10.2 Paper 2

Analyzing the suitability of flywheel energy storage systems for supplying high-power charging e-mobility use cases

Journal of Energy Storage 39 (2021) 102615

Contents lists available at ScienceDirect

Journal of Energy Storage

journal homepage: www.elsevier.com/locate/est

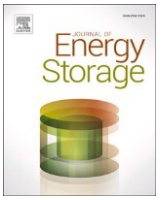

Analyzing the suitability of flywheel energy storage systems for supplying high-power charging e-mobility use cases

Bernd Thormann *, Philipp Puchbauer *, Thomas Kienberger

Montanuniversitaet Leoben, Chair of Energy Network Technologies, Franz-Josef-Strasse 18, 8700 Leoben, Austria

ARTICLE INFO

Keywords:
Electric vehicle
Use cases
Flywheel energy storage system
Economic optima
Technical optima

ABSTRACT

The trend towards increasing the charging power of future e-mobility will challenge existing distribution power systems and raise grid utilization- and connection costs. Flywheel energy storage systems (FESSs) may reduce future power grid charges by providing peak shaving services, though, are characterized by significant standby energy losses. On this account, this study evaluates the economic- and technical suitability of FESSs for supplying three high-power charging electric vehicle use cases. Therefore, we initially investigate the impact of individual charging patterns on the required FESS capacity, the annualized costs, and the FESS efficiency. Based on these correlations, the economic and technical optima of FESS applications are identified for each use case: The supply of electric buses enables a cost-efficient operation at the technical optima of FESSs. In contrast, the economic suitability of FESSs considering electric last-mile delivery trucks or highway fast-charging is restricted to low recharging energy demands and high charging power of electric vehicles. Furthermore, a cost-efficient operation of FESSs at the technical optima requires either a reduction of flywheel costs or an increase of power-based grid utilization charges in the upcoming years.

1. Introduction

Since more than a fourth of greenhouse gas emissions in the European Union are caused by the transport sector, the EU's targeted carbon-neutrality till 2050 will depend significantly on traffic-related emission savings [1]. These traffic-related emissions are, besides shipping and aviation, primarily caused by road transport, including passenger cars (43.5%), heavy-duty trucks and busses (18.8%), and light-duty trucks (8.5%) [2]. Consequently, the European Parliament approved new CO_2-emission targets in 2019 [3,4], which should be complied, among other things, by enhanced electrification of the traffic sector in the upcoming years [1]. Nevertheless, while forced electrification of various vehicle classes will clearly contribute to the transport sector's decarbonization, it will face the existing power system with unknown energy- and especially power demand. Aside from private charging of passenger vehicles at home or work [5–9], numerous studies demonstrate that future grid loads are triggered by electric vehicles (EVs) urging for high-power charging: electric busses (EBs) [10–12], highway fast-charging (HFC) of passenger vehicles [13,14] or electric last-mile delivery trucks (ELDTs) [5]. In combination with the energy system's ongoing electrification, these new, increased power demands will limit local grid capacities. Since classic grid reinforcement measures often entail significant investment costs and lengthy approval processes [15], the future integration of additional EV charging points (CPs) could be inhibited. As a countermeasure, flexibility options on the customer side allow for a decrease of installed grid capacity and should be considered in future grid connection processes. Therefore, implementing these flexibility tools must comply with the respective EV use case and its user behavior. Demand-side measures [16–21], for example, interfere with EV customer charging behavior [22] and are rather unsuitable for EV use cases with a strict schedule [11]. Similarly, grid support provided by bidirectional charging via vehicle-to-grid technology depends significantly on the EV parking time, which inhibits its provision by EV use cases with short idle times (e.g. EBs, HFC, ELDT, etc.) [23]. Energy storage systems (ESSs), on the other hand, contribute to increased flexibility in the power system [11,24], while allowing uncontrolled EV charging without interventions in daily life. Besides developing suitable operation- and control strategies [22,25–32], the integration of ESSs

Abbreviations: EV, Electric vehicle; EB, Electric bus; HFC, Highway fast-charging; ELDT, Electric last-mile delivery truck; CP, Charging point; ESS, Energy storage system; FESS, Flywheel energy storage system; BESS, Battery energy storage system; GRF, Grid relief factor.

* Corresponding authors.
E-mail address: bernd.thormann@unileoben.ac.at (B. Thormann).

https://doi.org/10.1016/j.est.2021.102615
Received 30 March 2021; Received in revised form 14 April 2021; Accepted 15 April 2021
Available online 1 May 2021

into future planning processes certainly requires detailed knowledge about required ESS specifications regarding various high-power charging EV use cases.

1.1. State of research

Numerous studies deal with the design of ESS-specifications required for smoothing EV-induced peak loads according to classic peak shaving measures. However, these works differ substantially in terms of the applied design criteria and are therefore classified as followed.

1.1.1. FESS design based on predefined grid capacity

The majority of works [23,33–36] use predefined grid capacity for designing appropriate ESSs: Ligen et al. (2019) [23], for instance, examine varying ESS-specifications to limit potential grid reinforcement needs at an EV ultra-fast-charging station. Therefore, they iteratively increase the ESS capacity (starting with 100 kWh) until a month of operation can be supplied safely, assuring compliance with the available grid capacity. Bai et al. (2010) [33] design an ESS for supplying a public fast-charging station in a simplified way: Based on stochastically modeled charging profiles of ten passenger EVs, the average power is defined as the available grid capacity, whereas exceeding power peaks are supplied by an ESS. Based on that, they determine ESS specifications necessary for complying with the available grid capacity. Joos et al. (2010) [34] analyze a combined integration of a flywheel energy storage system (FESS) and a supercapacitor into a public fast-charging station, though, excluding realistic EV charging behavior. Gjelaj et al. (2019) [35] propose the design of a battery energy storage system (BESS) for integrating public DC fast-charging points into the low-voltage level. Therefore, EV charging demands are stochastically modeled based on real-life mobility data and applied for ESS-design. Bryden et al. (2019) [36] demonstrate a method to identify the ESS's optimum capacity to support a fast-charging station. Therefore, the authors initially indicate the required number of fast-charging points at a specific location depending on EV users' acceptable average waiting time.

1.1.2. FESS design based on the prevention of voltage violations

Required ESS-specifications are also determined based on local grid restrictions in the form of voltage violations [37,38]: Piromjit et al. (2017) [37] identify appropriate sizes of ESSs to prevent inadmissible voltage deviations within the medium-voltage IEEE 34-Node test feeder. For that purpose, time-resolved residential load profiles and domestic EV charging loads are aggregated and, in addition to lithium-ion BESSs, integrated into power grid simulations. Similarly, Held et al. (2018) [38] use an optimal power flow algorithm to determine BESS specifications required to avoid inadmissible voltage deviations and thermal congestions in a suburban low-voltage grid.

1.1.3. FESS design based on economic aspects

Besides the design of ESSs based on local grid restrictions, some other authors [11,12,23,39] focus on economic aspects: Ligen et al. (2019) [23] apply the previously described method (Section 1.1.1) on a specific case study in Switzerland to examine potential cost benefits of ESSs. Ding et al. (2015) [11], for instance, investigate cost minimization (including investment and charging costs combined) of one existing EB charging station by a stationary ESS. Therefore, they design lithium-ion BESSs using a mixed-integer linear programming model. However, the minimization problem addressed in this study includes the limitation of electricity purchase, among other things, by the possibility of price arbitrage. This aspect may deviate results compared to an ESS design exclusively based on the available grid- or transformer capacity. Similarly, Yan et al. (2019) [12] examine three BESS configuration methods to support high-power EB charging. Hence, optimum ESS capacities are calculated based on a multi-objective cost model, including operation- and investment costs. Bayram et al. (2011) [39] examine numerous variations of the installed grid- and ESS-capacity, to find the best combination—in terms of quality of service and profit—for implementing public fast-charging stations.

1.2. Open research topics

As demonstrated in Section 1.1, state-of-the-art research covers the design of ESSs based on local grid restrictions and economic aspects. Though, when it comes to the determination of optimum ESS-designs for supplying high-power charging EVs, the presented studies lack an evaluation based on technical aspects. However, the inclusion of technical criteria, like standby losses or the efficiency of ESSs, into the design approach is crucial, especially since energy-saving measures are on the political agenda.

Furthermore, the majority of state-of-the-art research [23,33–36,39] focuses on implementing ESSs into public charging stations. In contrast, only a few studies cover domestic charging at home [37,38], EB charging [11,12], or they even miss to define the considered use case [29,30]. However, besides public charging of passenger EVs and EB charging, none of these studies cover the supply of ELDTs by integrated ESSs. Moreover, most studies highlighted in the previous section are limited to investigating only one EV use case, one charging power, and a fixed number of available CPs, respectively. Hence, the correlation between mobility behavior, available charging power, and installed number of CPs on the one side, and the suitability of ESS applications on the other, is missing in state-of-the-art research. Due to the mentioned open research topics, the following main contributions are provided by this study:

(1) Firstly, this work analyzes the impact of varying charging characteristics on the required ESS capacity as well as on economic and technical criteria. Therefore, mobility patterns, available charging power, and the installed number of CPs are varied for three different EV use cases.
(2) Secondly, this study presents a comparison between economic- and technical optima of ESS applications. While economic optima represent minimized investment- and operation costs, technical optima include applications with maximum ESS efficiency. Based on that, it demonstrates which ESS applications are applicable in present-day conditions and which require future changes regarding the economic framework.

Besides the considered EV use case and the applied design criteria, state-of-the-art research deviates as well in terms of the analyzed ESS technology. While some studies consider ESS in general [33,36,39] or FESSs [22,29,34,40], the majority of recent studies focuses on BESS in general [23,35,38] or lithium-based BESS [11,12,26–28,31,37] in particular. When it comes to the short-term supply of high-power EV charging, FESSs certainly show several advantages compared to BESSs: High life cycle numbers [29,34,40–42], high power density [29,34,41,42], short access time [34,41], low maintenance effort [34,41], small environmental impact [34,40–42] as well as the independency of power and energy content [40,42]. On this account, we selected the FESS as the appropriate energy storage technology to support future EV charging within this work.

1.3. Structure of this work

This work starts with the modeling of time-resolved EV charging profiles, considering three different EV use cases: ELDTs (Section 2.1.1), HFC (Section 2.1.2) and EBs (Section 2.1.3). Based on these charging load profiles, required FESS specifications are determined depending on the available power provided by the power grid (Section 2.2). Furthermore, numerous FESS applications are evaluated based on economic and technical criteria (Section 2.3). The performed sensibility analysis (Section 3.1) indicates correlations between varying input variables on the one side, and the required FESS-capacity as well as economic- and

technical criteria on the other. These correlations are finally used to identify optimum FESS applications (Section 3.2) depending on the individual EV use case and its particular charging demand. Finally, this study investigates the discrepancy between economic- and technical optima based on a techno-economic analysis (Section 3.3).

2. Material and methods

2.1. Modeling of time-resolved ev charging loads considering varying input variables

The evaluation of suitable FESS applications bases on detailed, time-resolved modeling of EV charging loads. To investigate the impact of mobility behavior and charging characteristics on economic- and technical criteria, we vary the following input variables (Table 1) for modeling EV charging loads of each use case: While the number of CPs is varied from two to eight for each considered use case, five different distances per charging event are selected for each use case individually, either based on mobility patterns (ELDTs and EBs) [43,44] or state-of-the-art EV battery capacities (HFC) [45]. Besides, we alter the available charging power per CP between 100 – 300 kVA (ELDT) [43], 22 – 200 kVA (HFC) [45], and 250 – 450 kVA (EBs) [10–12] based on state-of-the-art charging technology.

One EV charging load profile is modeled for each combination of covered distance, number of CPs, and charging power (resulting in 175 profiles per use case), covering a period of one year with a time resolution of one minute (Fig. 1). Therefore, realistic temporal charging patterns are derived from real-life mobility data. In our work, only uncontrolled charging is assumed for each use case. As a result, each charging event's start time equals the time of arrival at the CP. In addition to mobility data, EV model specifics—specific energy demand, charging efficiency, and charging power factor—depending on the considered use case are taken into account (Table 2). Both charging patterns, as well as EV specifics, are described in detail in Sections 2.1.1. – 2.1.3. Based on these aspects, time-resolved active- and reactive power are modeled for each charging event and each EV. Finally, each EV's annual time series are aggregated depending on the respective number of CPs.

Based on the aggregated EV charging profiles, we derive the temporal occupancy of CPs for each use case (Fig. 1). The occupancy of CPs at a specific time step equals the aggregated charging power at this specific time step divided by the aggregated installed charging power (the number of CPs multiplied by the charging power per CP). As a result, the occupancy of CPs represents the share of simultaneously charging vehicles. Fig. 1 illustrates the annual duration curves considering the occupancy of eight CPs. They illustrate the maximum occupancy and the period of maximum occupancy throughout one year. In this particular case, covered distances of 60 km (ELDT), 150 km (HFC), and 6 km (EB) are recharged with a charging power of 200 kVA, 150 kVA, and 350 kVA per CP.

However, regardless of the EV use case, the temporal occupancy of CPs, and thereby the number of simultaneously charging vehicles, depends on the following charging characteristics: Both the maximum CP-occupancy (defining the aggregated peak load) as well as the number of hours with maximum occupancy, increase with a raising distance before recharging, due to an increased duration of charging. On the contrary, both decrease with raising charging power (due to a decreased duration of charging events) and with a growing number of CPs (c.f. Thormann et al. (2020) [52]).

Table 1
Variation of mobility- and charging parameters considering electric last-mile delivery trucks (ELDT), highway fast-charging (HFC), and electric busses (EBs).

Input variable to be varied	ELDT	HFC	EB
Covered distance per charging event (km)	20:20:100	50:50:250	2:2:10
Available charging power per charging point (kVA)	100:50:300	22, 50:50:200	250:50:450
Number of installed charging points (-)	2:1:8		

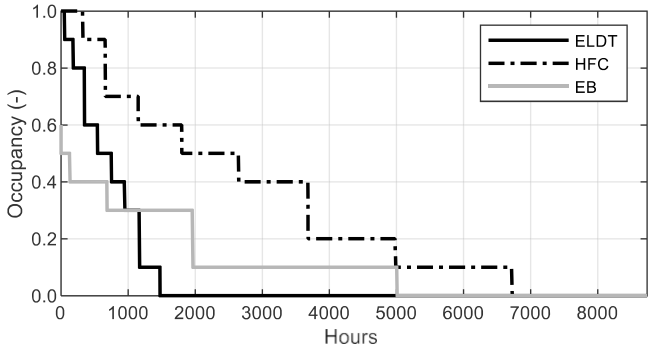

Fig. 1. Annual duration curves considering the temporal occupancy of eight charging points (CP) supplying electric last-mile delivery trucks (ELDTs) charging, highway fast-charging (HFC), and electric busses (EBs).

Table 2
EV model specifics considering electric last-mile delivery trucks (ELDTs), highway fast-charging (HFC), and electric bus (EB) charging [43,46–51].

Parameter	ELDTs	HFC	EBs
Specific energy demand (kWh/km): Summer	2.000	0.150 – 0.290	1.860
Specific energy demand (kWh/km): Transition	2.090	0.170 – 0.320	1.240
Specific energy demand (kWh/km): Winter	2.130	0.190 – 0.360	2.480
Charging efficiency	0.930	0.710 – 1.000	0.920
Charging power factor	0.950	0.280 – 0.996	0.990

2.1.1. Modeling of ELDT charging loads

Temporal mobility patterns of ELDTs are derived by a real-life schedule, covering a total daily distance between 200 – 240 km, provided by last-mile delivery providers [43]. To vary the covered distance per charging event (Table 1) while assuring the overall mobility need of ELDTs, we adapt the initial schedule in terms of the following indicators: Covered distance per trip (or charging event), number of trips per day as well as the period available for loading and unloading at the distribution hub (Table 3). All the listed routes include several trips per day on weekdays and Saturdays, whereas Sundays are excluded from last-mile delivery services. Each route's mean trip durations are determined by assuming an average speed of 13.9 km/h (including driving, loading, and unloading) [43].

Based on that, each trip's actual duration is stochastically determined by applying a normal distribution (standard deviation of 5%) in combination with random numbers. Assuming a starting time of 04:00 in the morning for each route, the arrival time (or rather the start of charging) after the first trip of the day is then determined by adding the start time to the trip's actual duration. After arriving at the distribution hub, ELDTs stay there for a defined period (Table 3), in which they are

Table 3
Last-mile delivery routes' schedules applied for modeling realistic charging patterns of ELDTs.

Route	Covered distance per trip (km)	Mean trip duration (hours)	No. of trips per day	Period of (un-) loading at the hub (hours)
1	20	1.4	10	0.5
2[1]	40	2.9	5	1.0
3	60	4.3	4	1.5
4	80	5.8	3	2.0
5	100	7.2	2	2.5

[1] Ori inal last-mile delivery route [43].

(un-)loaded and recharged for their next trip. The original period of one hour [43] is adapted according to each route's demands, though assuring complete recharging in this period. Based on these assumptions, the time of arrival of every following trip and each vehicle is determined by adding this trip's actual duration and the route-specific period of loading at the hub to the previous trip's arrival time. In this study, the delay of delivery schedules caused by ELDTs waiting for an available CP is prevented by assuming one CP per vehicle. Hence, the number of available CPs equals the number of ELDTs at a particular distribution hub. In the next step, the required amount of recharged energy is calculated for each charging event, using a specific energy demand between 2.00 – 2.13 kWh/km [46] (Table 2) and the respective distance per charging event. Finally, the end of charging is defined by the calculated energy demand to be recharged, the respective charging power (Table 1), and the vehicle-specific charging efficiency and charging power factor (Table 2). Since, for the approach discussed here (one ELDT per CP), CPs are completely occupied (1.0) only 54 h per year (Fig. 1), the implementation of FESSs could decrease the required grid capacity by covering short-term load peaks. However, most of the time (7285 h), no ELDT is recharged at the distribution hub.

2.1.2. Modeling of HFC loads

Besides EV charging at home, the implementation of fast-charging points at highways will be a crucial step towards e-mobility, enabling long-distance traveling. For modeling the time-resolved recharging demands at a specific HFC station, we use present-day traffic data [53], providing the number of passenger vehicles passing the selected highway station at each hour (Fig. 2): While morning and evening hours are characterized by increased traffic volume, only a few vehicles (357) are counted between 00:00 – 04:00. The number of passing passenger EVs is finally derived for each hour by assuming an EV penetration of 5%. Knowing the number of EVs passing the highway station at each hour, their exact time of passing is determined stochastically, assuming a uniform distribution within each hour (c.f. Xie et al. (2018) [54]). Furthermore, the vehicles' state of charge (SOC) is randomly determined between 0.1 and 0.9 based on a normal distribution (c.f. Rios et al. (2014) [55]). Therefore, a standard deviation of 0.25 and a mean value of 0.625 (from 05:00 to 09:59 on weekdays) or instead 0.5 (rest of the week) is estimated. This temporal variation of the SOC distribution also takes vehicles, which are completely charged before the first trip of the day, during weekday morning hours, into account (c.f. Bae et al. (2019) [56]).

After that, we categorize all passing EVs into four different groups according to their SOC to ascertain the number of EVs with recharging needs. Each group is defined by individual recharging actions (Table 4): While EVs with a SOC higher than 0.20 (Group 1) do not enter the highway station at all, EVs with a SOC between 0.20 and 0.15 [54] (Group 2) recharge only if at least one CP is available. Recharging actions of vehicles in group 3 depend on whether the minimal waiting time is lower than 6 min (c.f. [36]). EVs with a SOC of 0.10 or lower enter the highway station independent of the availability of CPs or waiting time and recharge their vehicle. Analogous to use case ELDT, the number of installed CPs is varied between two and eight (Table 1).

Table 4
Classification of passenger EVs according to their state of charge (SOC) and definition of respective recharging actions.

Group	SOC range	Action
1	SOC > 0.20	No charging
2	0.20 ≥ SOC > 0.15	Charging, if at least one CP is available
3	0.15 ≥ SOC > 0.10	Charging, if the minimum waiting time is lower than 6 min
4	SOC ≤ 0.10	Charging

After picking out EVs entering the highway station (time of passing equals the time of arrival), this method eventually requires the postponing of charging events: If no CP is available (Group 3 and 4) at the time of arrival, the beginning of charging is postponed until at least one CP is available. On the contrary, in case of available CPs, the EV's arrival time represents the start of charging, assuming uncontrolled charging behavior. This simplified queuing model uses a "first come, first served" principle (c.f. Bryden et al. (2019) [36]). Each charging events' duration and, thereby, end time depends on the respective covered distance and charging power (Table 1), as well as the vehicles' specific energy demand, charging efficiency, and charging power factor (Table 2). Considering passenger EVs, the latter three are stochastically derived using present-day registration numbers of EV models. The methodology for modeling charging load profiles of passenger vehicles using real-life measured charging data of present-day EV models is described in Thormann et al. (2020) [52]. The annual occupancy duration curve of an HFC station (Fig. 1) demonstrates an increased occupancy of CPs compared to ELDTs and EBs: While no charging power is demanded during 2035 h a year, the installed CPs are completely occupied for recharging during 326 h a year.

2.1.3. Modeling of EB charging loads

The modeling of EB charging profiles is also based on real-life traffic patterns, provided by the open data platform of Vienna [44], in the form of General Transit Feed Specification data. These annual traffic data include inter alia, departure time, arrival time, and each trip's distance considering several terminal stations and numerous bus lines (101) operated by Wiener Linien GmbH [57]. On weekdays, the first trip of the day starts at 04:40 in the morning, whereas the final trip ends at 01:02 in the morning the following day. Considering these urban bus routes, most covered trips (59.4%) between terminal stations are between 2 – 6 km (Fig. 3). To investigate the impacts of the covered distance per charging event and the available charging power, we apply the same present-day temporal mobility patterns (i.e., time of arrival and period of parking

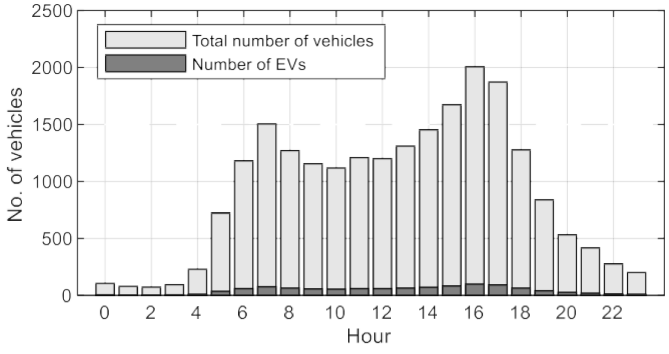

Fig. 2. Number of passenger vehicles and electric passenger vehicles (EVs) passing the selected highway station at each hour.

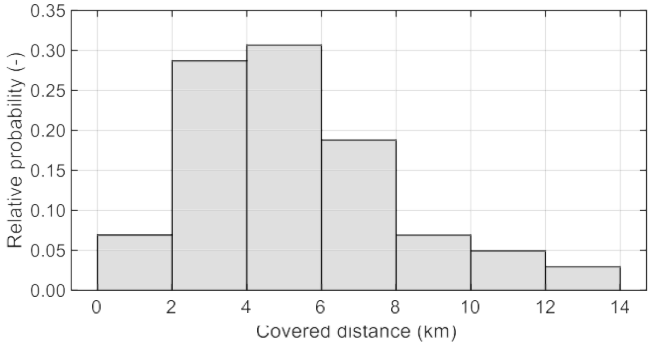

Fig. 3. Distribution of distances (terminal-to-terminal) covered by urban bus routes [44].

according to schedule) throughout their variation. Therefore, we initially select eight bus routes, which allow recharging of EB charging needs in compliance with present-day schedules for each of the selected distances and charging powers (Table 1).

In this study, we assume one CP per bus route installed at the terminal station, each providing the respective charging power (250 – 450 kVA). Besides, EBs are recharged exclusively at the terminal station after each trip (c.f. Rogge et al. (2015) [10]). Consequently, we derive the start of each charging event from the time of arrival at the terminal station. Analogous to the other use cases, each charging events' duration is calculated using the respective covered distance and available charging power (Table 1) as well as the specific energy demand [47,48], charging efficiency [49–51], and the charging power factor (Table 2). The annual occupancy duration curve (Fig. 1) of the selected terminal station with eight CPs demonstrates that up to five EBs (maximum occupancy of 0.63) are charged simultaneously for only 0.4 h a year. In contrast, EBs are disconnected from the charging infrastructure for 3760 h a year.

2.2. Determination of required FESS-specifications

In this study, high-performance FESSs are integrated into fast-charging stations as follows (Fig. 4): Distribution system (AC/DC), CPs (DC/DC or DC/AC), and FESS (DC/AC) are connected to a DC voltage link via the respective inverter (c.f. Dragicevic et al. (2014) [29] and Yan et al. [12]). EV charging demands are either supplied by the distribution system, by the FESS (in case of available energy capacity), or both.

Notwithstanding the above, both AC and DC power can be provided by the CP, depending on the supplying EV use case and EV charging power. [40,58] Based on the previously modeled time-resolved EV charging profiles, we determine FESS-specifications required for peak shaving services and, thereby, the decrease of installed grid capacity. However, since this study deals with several EV applications, the required grid capacity depends on the considered EV use case, charging power per CP, and the number of CPs.

To evaluate the correlation between grid capacity and FESS design independent of these aspects, we initially implement the "grid relief factor" (GRF). The GRF defines the share of EV charging peak load, covered by the integrated FESS—e.g., a GRF of 0.1 indicates that the FESS covers 10% of EVs' aggregated peak load, whereas the power grid supplies lower EV loads. Both the GRF and the maximum EV charging load (S_{EV}) further define the required grid capacity ($S_{Grid,cap}$), according to Eq. (1).

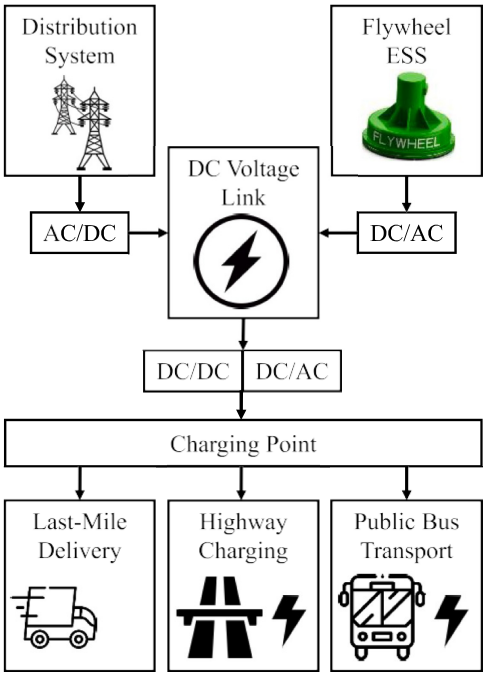

Fig. 4. Integration of flywheel energy storage system (ESS) into charging infrastructure supplying varying EV use cases.

$$S_{Grid,cap} = \max(S_{EV}) \tag{1}$$

Based on the calculated grid capacity, the periods of charging and discharging the FESS are identified: As demonstrated in Eq. (2), FESSs are discharged when EV charging loads $S_{EV}(t)$ exceed the grid capacity ($S_{FESS}(t) > 0$) and recharged during off-peak periods ($S_{FESS}(t) < 0$). For both charging and discharging of the FESS, power losses in the electric machine- ($\eta_{E\ Machine}$) and in the inverter ($\eta_{Inverter}$) are considered (Table 5). In the first step of FESS-design, we use Eq. (3) to identify the requested discharging power $FESS_{dischargingPower}$, which equals the maximum FESS power.Since we assume equal power available for charging and discharging, the maximum charging power $FESS_{chargingPower}$ equals the designed discharging power of the FESS. Furthermore, FESS-charging ($S_{FESS}(t) < 0$) is limited to the determined maximum charging power, demonstrated in Eq. (4). To identify the required storage capacity, active charging and discharging power is calculated by multiplying apparent power $S_{FESS}(t)$ by power factors $PF_{charging}$ or $PF_{discharging}$ (Table 5), according to Eq. (5). While the discharging power factor of the FESS equals the power factor of the EV charging load (PF_{EV}), a power factor of 1.0 is applied for recharging the FESS. Based on that, the amount of energy stored in the FESS $Energy_{FESS}(t)$ is determined at each time step based on Eq. (6). To ensure that FESSs only recharge the amount of energy they have discharged during previous operation, the stored energy $Energy_{FESS}(t)$ is limited to [0, ∞]. The necessary storage capacity of the FESS is finally defined by Eq. (7) as the maximum amount of stored energy considering one year.

$$S_{FESS}(t) = \begin{cases} t: S_{EV}(t) \geq S_{Grid,cap}, & \dfrac{S_{EV}(t) - S_{Grid,cap}}{\eta_{E\ Machine} \cdot \eta_{Inverter}} \\ t: S_{EV}(t) < S_{Grid,cap}, & (S_{EV}(t) - S_{Grid,cap}) \cdot \eta_{E\ Machine} \cdot \eta_{Inverter} \end{cases} \tag{2}$$

$$FESS_{dischargingPower} = \max(S_{FESS}(t)) = FESS_{chargingPower} \tag{3}$$

$$S_{FESS}(t) = \{t: S_{FESS}(t) < FESS_{chargingPower}, \quad FESS_{chargingPower} \tag{4}$$

$$P_r(t) = \begin{cases} t: S_{FESS}(t) \geq 0, & S_{FESS}(t) \cdot PF_{Discharging} \\ t: S_{FESS}(t) < 0, & S_{FESS}(t) \cdot PF_{Charging} \end{cases} \tag{5}$$

$$Energy_{FESS}(t) = Energy_{FESS}(t-1) + \int_{t-1}^{t} P_{FESS} \cdot dt \tag{6}$$

$$FESS_{Capacity} = \max(Energy_{FESS}(t)) \tag{7}$$

Table 5
Parameters of the flywheel energy storage system (FESS) [42,58,59].

FESS parameter		Value
Efficiency of the electric machine	$\eta_{E\ Machine}$	0.93
Efficiency of the inverter	$\eta_{Inverter}$	0.95
Charging power factor	$PF_{Charging}$	1.00
Discharging power factor	$PF_{Discharging}$	PF_{EV}
Minimum bearing losses per kWh capacity (SOC = 0%)	$P_{BL,min}$	3.0 W
Maximum bearing losses per kWh capacity (SOC = 100%)	$P_{BL,max}$	12.0 W
Minimum flow losses of per kWh capacity (SOC = 0%)	$P_{FL,min}$	0.0 W
Maximum flow losses of per kWh capacity (SOC = 100%)	$P_{FL,max}$	14.0 W
Weight compensation per kWh capacity	P_{WC}	15.0 W
Vacuum pump per kWh capacity	P_{VP}	7.3 W
Cooling system per kWh capacity	P_{CS}	24.7 W

The resulting active power supplied by the distribution grid $P_{Grid}(t)$ is finally determined with Eq. (8), including power losses and additional power demand of the FESS ($P_{FESS,Losses}$). The latter is calculated with Eq. (9), considering the following components: Bearing- (Eq. (10)) and flow losses of the flywheel (Eq. (11)) depend on the flywheel's SOC (Table 5), based on an assumed linear characteristic between 0% and 100%.

$$P_{Grid}(t) = P_{EV}(t) \quad P_{FESS}(t) + P_{FESS,Losses}(t) \tag{8}$$

$$P_{FESS,Losses}(t) = (P_{BL}(t) + P_{FL}(t) + P_{WC} + P_{VP} + P_{CS}) \cdot FESS_{Capacity} \tag{9}$$

$$P_{BL}(t) = P_{BL,min} + \frac{P_{BL,max} \quad P_{BL,min}}{(100\ \% \quad 0\ \%)} \cdot SOC_{FESS}(t) \tag{10}$$

$$P_{FL}(t) = P_{FL\,min} + \frac{P_{FL,max} \quad P_{FL,min}}{(100\ \% \quad 0\ \%)} \cdot SOC_{FESS}(t) \tag{11}$$

In this study, we assume a linear correlation between the flywheel's useable SOC and its speed: For a SOC of 100%, the flywheel runs at a speed of 30,000 rpm. However, a minimum speed of 10,000 rpm allows no further discharging (SOC = 0%) of the FESS [59]. On the other hand, we apply a constant power demand due to the flywheel's magnetic weight compensation, the vacuum pump, and the cooling system. All the applied power loss components of the FESS are described in detail by Haidl (2021) [59]. Specific values of all components (per kWh FESS capacity) are listed in Table 5. Though, their actual power demand depends on the respective flywheel size. Therefore, we scale all power loss components by the determined FESS capacity, demonstrated in Eq. (9). Since the analyzed e-mobility use cases are clearly characterized by off-peak periods (Section 2.1)—on Sundays (ELDT), between 00:00 – 04:00 (HFC) or between 01:02 – 04:40 (EB)—with no or low recharging needs, the FESSs is turned off ($P_{FESS,Losses} = 0$) during these periods to prevent unnecessary power losses. This work deals with a power-based approach for designing required FESS specifications with a time resolution of one minute. However, the impact of FESSs on power quality is not addressed and is reserved for future works.

2.3. Evaluating the suitability of FESS-applications

2.3.1. Economic criteria

The economic evaluation of suitable FESS applications bases on annualized total costs per CP, including all cost components from Eq. (12): Grid connection costs, grid utilization costs, flywheel costs, and inverter costs. Eq. (13) – (18) describe the calculation of all relevant cost components, whereas all applied parameters and their values are listed in Table 6 and Table 7. According to Eq. (14), grid utilization costs are further divided into an energy-based component, a power-based component, and additional flat rate charges (*AFR*). However, the costs of charging stations are excluded in this investigation.

Table 6
Cost parameters regarding the connection and utilization of the power grid [11,12,61–63].

Parameter		Value
Specific purchase and installation costs of the transformer (€/kVA)	c_T	610
System provision charge (€/kW)	SPC	133.8
Discount rate (%)	i	3
Transformer lifetime (years)	T_T	40
Annual transformer maintenance costs as the share of purchase and installation costs (%)	$x_{T,Maintenance}$	1
Electricity price (€/kWh)	EP(t)	0.11 – 0.12
System utilization charge (€/kW)	SUC	41.04
Additional power-based cost component (€/kW)	*PBC*	10.96
Additional energy-based cost component (€/kWh)	*EBC*	0.0441
Annual flat rate (€)	AFR	961.1

Table 7
Cost parameters regarding the flywheel energy storage system, including flywheel and inverter [12,40,64,65].

Parameter		Value
Specific purchase and installation costs of the flywheel (€/kWh)	c_F	2500
Flywheel lifetime (years/cycles)	T_F	30/ 3e5
Annual flywheel maintenance costs as the share of purchase and installation costs (%)	$x_{F,Maintenance}$	5
Specific purchase and installation costs of the inverter (€/kVA)	c_I	340
Inverter lifetime (years)	T_I	30
Annual inverter maintenance costs as the share of purchase and installation costs (%)	$x_{T,Maintenance}$	5

$$Annualized\ costs\ per\ CP = \frac{C_{Grid,Connection} + C_{Grid,Utilization} + C_{Flywheel} + C_{Inverter}}{No.\ of\ CPs} \tag{12}$$

$$C_{Grid,Connection} = S_{Grid,cap} \cdot \left[c_T + SPC \right] \cdot \frac{i \cdot (1+i)^{T_T}}{(1+i)^{T_T} \quad 1} + c_T \cdot x_{T,Maintenance} \tag{13}$$

$$C_{Grid,Utilization} = C_{Grid,Utilization,Energy} + C_{Grid,Utilization,Power} + AFR \tag{14}$$

$$C_{Grid,Utilization,Energy} = \left(\sum E_{Grid}(t) \cdot EP(t) \right) + \left(\sum E_{Grid}(t) \right) \cdot EBC \tag{15}$$

$$C_{Grid,Utilization,Power} = S_{Grid,cap} \cdot (SUC + PBC) \tag{16}$$

$$C_{Flywheel} = FESS_{Capacity} \cdot c_F \cdot \left(\frac{i \cdot (1+i)^{T_F}}{(1+i)^{T_F} \quad 1} + x_{F,Maintenance} \right) \tag{17}$$

$$C_{Inverter} = FESS_{dischargingPower} \cdot c_I \cdot \left(\frac{i \cdot (1+i)^{T_I}}{(1+i)^{T_I} \quad 1} + x_{I,Maintenance} \right) \tag{18}$$

This study assumes grid connection of the charging infrastructure at the distribution level, particularly at ENTSO-e network-level six [60]. Consequently, all relevant cost parameters related to the power grid connection and utilization (Table 6) are acquired for this network level from the Austrian energy market regulator E-Control [61]. These cost parameters include system provision charges (*SPC*), system utility charges (*SUC*), general power-based components (*PBC*; green electricity support payments), general energy-based components (*EBC*; electricity levy, green electricity support payments, charges for system losses, charges for system services, metering charges, etc.) and additional flat rate charges (*AFR*: flat-rate renewable charge and green electricity support payments). In addition, we use a time-resolved (15 min) energy price $EP(t)$, provided by Energy Exchange Austria [62].

One-time costs (material- and installation costs as well as system provision charges [61]) are annualized by using a lifetime-based annuity factor (c.f. Schroeder et al. (2012) [66] and Yan et al. (2019) [12]), which depends on the discount rate i and the equipment's lifetime T_T (transformer), T_F (flywheel) and T_I (inverter). While transformers and inverters are taken into account based on a specific temporal lifetime of certain years, flywheels must be replaced either after 30 years of operation or 3e5 full cycles, depending which occurs first. Furthermore, their annual maintenance costs are taken into account by $x_{T,Maintenance}$, $x_{F,Maintenance}$ and $x_{I,Maintenance}$ as the share of total purchase- and installation costs (Table 7). The latter are determined with specific material- and installation costs c_T, c_F, and c_I and the equipment's respective design specifics $S_{Grid,cap}$, $FESS_{Capacity}$ and $FESS_{dischargingPower}$ (Section 2.2).

2.3.2. Technical criteria

Besides economic criteria, this study evaluates numerous FESS ap-

plications also from a technical standpoint. Considering short-term peak load shaving, high self-discharging rates of FESSs represent the most challenging drawback compared to other ESS technologies [42]. On this account, this work examines the technical suitability of a FESS based on its efficiency (η_{FESS}) during operation—illustrated in Eq. (19).

$$\eta_{FESS} = \frac{E_{Discharging}}{E_{Charging} + E_{FESS,Losses}} = \frac{\int_{t=1a} P_{Discharging}(t) \cdot dt}{\int_{t=1a} \left(P_{Charging}(t) + P_{FESS,Losses}(t) \right) \cdot dt} \quad (19)$$

Therefore, the annual amount of discharged energy ($E_{Discharging}$) is divided by the sum of the annual amount of charged energy ($E_{Charging}$) and annual energy losses ($E_{FESS,Losses}$). All energy amounts are calculated by the integral of the respective time-resolved power component (Fig. 5) over one year. Thus, the efficiency of FESSs includes several loss components demonstrated in Section 2.2. Besides power losses during discharging and charging, FESSs are characterized by significant standby losses during periods without charging or recharging: According to Eq. (9), a FESS with a capacity of 8 kWh causes standby power losses of 0.58 kW at a SOC of 100% (Fig. 5). Considering a standby period of, e.g., two hours, an energy amount of 1.16 kWh must be provided by the power grid to compensate FESS losses.

Consequently, the efficiency of FESSs is primarily affected by standby energy losses during operation. These, on the other hand, depend on the frequency of operation (i.e., how often FESSs are required for peak load shaving) and the duration of charging and recharging periods (i.e., how long they are operated). Both of them further correlate with the respective EV charging patterns as well as the available grid capacity.

2.3.3. Sensibility analysis: Identifying the impact of different input variables on the suitability of FESSs

In this study, we evaluate the suitability of FESSs for covering short-term EV charging peak loads based on economic- (Section 2.3.1) as well as technical criteria (Section 2.3.2). Both further depend on the required FESS specifications. Since FESSs are characterized by low energy densities [34,67], this study focuses primarily on the required FESS capacity (Section 2.2) as the most crucial FESS specification. Considering the supply of EV charging, the required FESS capacity, and economic- and technical criteria, depend on the supplied EV use case, individual EV charging patterns, and the charging infrastructure. To understand these correlations in detail, we initially perform a sensibility analysis. Therefore, we alter the covered distance per charging event, the available charging power per CP, the number of installed CPs (according to Table 1) as well as the GRF (between 0.0 and 0.6), respectively, while fixing the others to use case-specific reference values (Table 8).

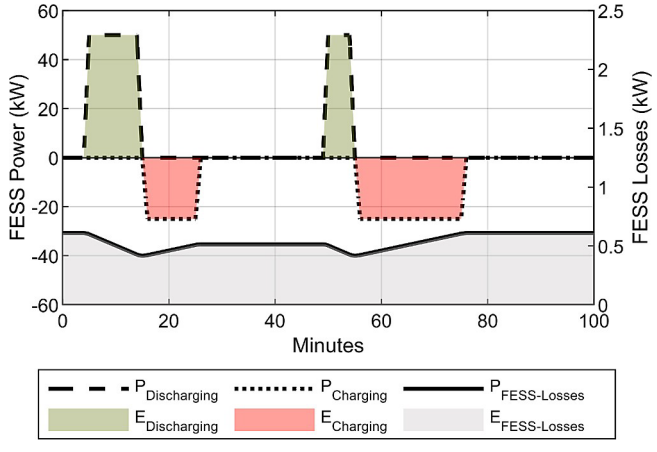

Fig. 5. Illustration of discharging, charging, and losses of a FESS (8 kWh capacity).

Table 8
Reference values of input variables applied for sensibility analysis.

Input variable	ELDT	HFC	EB
Covered distance per charging event (km)	60	150	6
Available charging power per charging point (kVA)	200	100	350
Installed number of charging points (-)	5	5	5
Grid relief factor (-)	0.1	0.1	0.1

For each variation of input variables, the required FESS capacity (Eq. (7)), annualized costs per CP (Eq. (12)), as well as the efficiency of the FESS (Eq. (19)) is determined. Thereby, this sensibility analysis provides crucial information, how different charging demands and varying supply infrastructures affect the economic and technical suitability of FESSs.

2.3.4. Determination of economically- and technically optimum FESS-applications

While we alter both charging demands (covered distance and available charging power) and supply infrastructure (installed number of CPs and GRF) arbitrarily in the sensibility analysis, these two groups differ in terms of their definition: Concerning the analyzed use cases, the former group of input variables is often predetermined by strict mobility needs. The covered distance per charging event depends on individual daily routes' characteristics (ELDT and EB) or user patterns (HFC). The available charging power must allow a fast onward journey and correlates with schedules (ELDT and EB) or the acceptable break period (HFC). In contrast, the number of installed CPs, and the GRF, are in most cases, freely selectable by charging infrastructure owners. On this account, we apply the correlations illustrated by the sensibility analysis (Section 2.3.3) to identify the optimal supply infrastructure for each EV use case and each of its charging demands. Therefore, we use mixed-integer nonlinear programming to optimize the number of installed CPs (integers between 2 – 8) as well as the installed GRF (float number between 0.00 – 1.00), based on economic- (Eq. (20)) and technical objective functions (Eq. (21)).

$$Min(Annualized\ costs\ per\ CP) \quad (20)$$

$$Max(\eta_{FESS}) \quad (21)$$

While identifying economic optima bases on minimizing annualized costs per CP (Section 2.3.1), we maximize the efficiency during operation (Section 2.3.2) to identify technically optimum FESS applications.

3. Results and discussion

3.1. Impact of different input variables on the suitability of FESSs

3.1.1. Reference results

The performed sensibility analysis demonstrates correlations between different input variables (covered distance, charging power, number of CPs, and GRF) and selected output variables (FESS capacity, annualizes costs per CP, and FESS efficiency). To illustrate these correlations uniformly and independently of the EV use case, all the varied input variables are referred to the respective reference values (Table 8) and demonstrated as per unit (p.u.) values. For example, a covered distance of ELDTs of 80 km equals 1.33 p.u. (reference value of 60 km). Similarly, the sensibility analysis' output variables are referred to the respective reference results (Table 9), calculated by applying the described methodology and the reference input variables in Table 8. In addition to the sensibility analysis' output variables, Table 9 lists all relevant cost components and annual standby energy losses. These reference results already demonstrate substantial differences between the analyzed EV use cases: The supply of EB charging causes the highest costs per CP due to increased energy- and power-based grid utilization costs. However, this use case requires the lowest FESS capacity, which

Table 9
Reference values of output variables, calculated by the performed sensibility analysis.

Output variable	ELDT	HFC	EB
FESS capacity (kWh)	68.1	58.3	5.9
Total annualized costs per CP (k€)	34.0	34.5	46.6
Annualized grid connection costs (k€)	29.0	14.5	30.4
Annualized grid utilization costs: Energy-based (k€)	72.5	117.4	147.4
Annualized grid utilization costs: Power-based (k€)	46.8	23.4	49.1
Annualized flywheel costs (k€)	17.2	14.7	1.5
Annualized inverter costs (k€)	3.4	1.7	3.6
FESS efficiency (-)	0.22	0.38	0.66
Annual standby energy losses (MWh)	35.9	26.3	3.2

further results in the lowest flywheel costs of all considered use cases. In contrast, the supply of ELDTs or HFC requires higher storage (or FESS) capacities, which raises flywheel costs significantly.

Furthermore, reference results demonstrate the correlation between FESS efficiency and EV use case: Due to a high frequency of charging and low FESS capacity, the supply of EBs results in relatively low standby energy losses compared to ELDTs or HFC. As a result, FESSs are operated more efficiently. While these results relate to one particular reference case only (Table 8), the following sections demonstrate the correlation between different input variables on the one side and the required FESS capacity, annualized costs, and FESS efficiency on the other.

3.1.2. Impact of the covered distance per charging event

Varying EVs' covered distance per charging event (while fixing the remaining input variables) affects the required FESS capacity significantly (Fig. 6a). The higher the distance covered before recharging, the higher the required energy demand at the charging station. Assuming a constant GRF (as in this sensibility analysis), the amount of energy required by the FESS raises similarly: If the distance is increased from 0.34 p.u. to 1.00 p.u., integrated FESSs must increase their capacity by 0.68 p.u. (ELDT: 43 kWh), 0.87 p.u. (HFC: 51 kWh) and 0.33 p.u. (EB: 2 kWh) to provide peak load shaving (according to the reference values in Table 8). Furthermore, a covered distance of 1.67 p.u. requires a capacity of 1.47 p.u., 3.15 p.u. and 1.33 p.u. (Fig. 6a). Due to the broadest spectrum of analyzed distances (50 – 250 km), use case HFC shows the highest impact on the FESS capacity, especially at distances higher than 1 p.u. (150 km).

As a result of higher FESS capacities, an increasing distance per charging event also raises the flywheel's (energy-dependent) costs. Additionally, it increases energy-based grid utilization costs caused by higher energy demands from the power grid (Section 2.3.1). Both aspects contribute to raising total annualized costs per CP when extending the covered distance per charging event—with or without FESS (Fig. 6b): An extension from 0.34 p.u. to 1.00 p.u. increases the annualized costs by 0.12 p.u., 0.50 p.u. and 0.29 p.u., whereas a further extension to 1.67 p.u. results in an increase by 0.04 p.u. (ELDT), 0.50 p.u. (HFC) and 0.10 p.u. (EB).

Besides FESS capacity and costs, the covered distance affects the FESS's efficiency (Fig. 6c). Assuming constant charging power, the duration of EV charging increases with raising distances (or rather energy demand). Consequently, the FESS is charged and discharged for a more extended period, which decreases its standby energy losses, and increases its efficiency. Extending the distance of use case HFC (while fixing the remaining variables according to Table 8) from 0.34 p.u. to 1.67p.u. raises the FESS's efficiency from 0.41 p.u. to 1.02 p.u. The extension of the covered distance allows a 1.5-times higher efficiency (from 0.71 p.u. to 1.04 p.u.) when supplying EBs (Fig. 6c). Since we maintain the daily route's total distance as the overall mobility need of ELDTs (Section 2.1.1), the variation of covered distances per charging event entails a deviating number of routes per day (Table 3). Naturally, fewer routes per day result in fewer charging events and higher standby energy losses. As a result, the FESS efficiency decreases with raising covered distance considering ELDTs in this analysis (Fig. 6c).

3.1.3. Impact of EV charging power per CP

The EV charging power per CP, available at the charging station, influences the required FESS capacity in two ways: Firstly, an increasing EV charging power requires higher discharging power of the FESS, assuming a constant GRF (applied for the sensibility analysis). Since we equate FESS's discharging- and charging power, this enables faster recharging of the FESS. Faster recharging of the FESS increases the

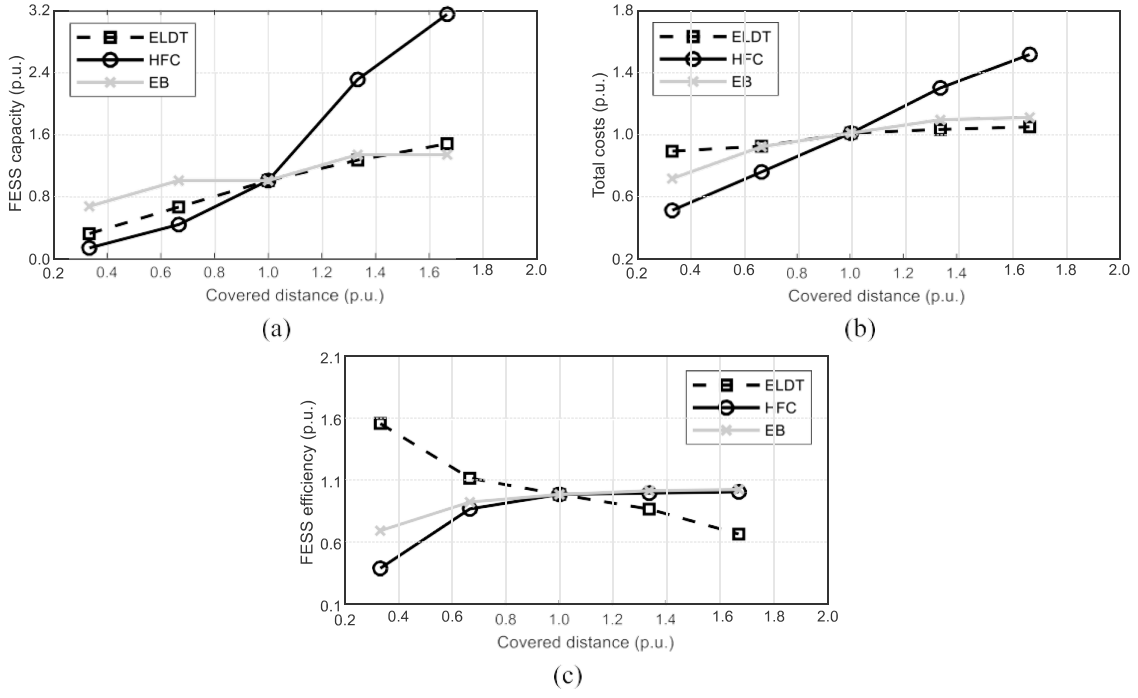

Fig. 6. Impact of the covered distance on **(a)** the required FESS capacity, **(b)** annualized total costs per CP, and **(c)** FESS efficiency, regarding electric last-mile delivery trucks (ELDTs), highway fast-charging (HFC), and electric bus charging (EB).

available energy stored in the FESS at the next EV charging event and reduces the need for larger FESS capacity. This limitation by low recharging power of FESSs becomes more crucial the lower the available EV charging power, illustrated by use case HFC (Fig. 7a). Secondly, an increasing EV charging power reduces the duration of the maximum occupancy of CPs due to shorter charging periods. While we detect this effect in the range of several minutes considering ELDT and HFC, the period of the maximum occupancy of EBs is reduced in the range of seconds due to a higher power level. However, since we model EB charging load profiles with a time resolution of one minute, this effect is limited: Except for charging with 250 kVA (four minutes), each charging power (300 – 450 kVA) results in a maximum occupancy of CPs of three minutes in average. Though, the supply with increasing power during an (almost) constant period requires higher energy demands. As a result, the required FESS capacity decreases (Fig. 7a) from charging with 250 kVA (0.95 p.u.) to 300 kVA (0.85 p.u.) due to shorter peak shaving periods (three instead of four minutes). Though, it raises to 1.29 p.u., if the charging power is increased to 1.29 p.u. (450 kVA) due to constant peak shaving periods (three minutes). While the modeling of EV charging loads with a time resolution of one minute provides sufficient accuracy for use cases ELDT and HFC, EB charging with power higher than 350 kVA may require a finer temporal resolution. Indeed, the two described characteristics trigger decreasing capacity needs with increasing charging power considering the other use cases: ELDT-charging with 0.50 p.u. instead of 1.50 p.u. reduces the required FESS capacity from 1.04 p.u. to 0.90 p.u. Similarly, HFC with higher power results in lower FESS energy demands—from 1.92 p.u. with a power of 0.22 p.u. to 0.60 p.u. with a power of 2.00 p.u. (Fig. 7a).

Despite decreasing FESS capacity and flywheel costs, the increase of available charging power raises annualized investment and operation costs per CP (Fig. 7b). In fact, they correlate with the available charging power in a (rather) linear way, based on the power-based component of grid utilization costs (Section 2.3.1) and (negligible) power-based inverter costs. If ELDTs are charged with 0.50 p.u. and 1.50 p.u. instead of 1.00 p.u. annualized costs per CP deviate by −0.25 p.u. and +0.24 p.u. (Fig. 7b). An increase of HFC power from 0.22 p.u. to 1.00 p.u. (and further to 2.00 p.u.) triggers a rise of costs by 0.43 p.u. (0.27 p.u.). When varying the available charging power per CP of EBs between 0.71 – 1.28 p.u., annualized costs fluctuate between 0.77 – 1.22 p.u. On the other hand, the energy-based cost component shows a negligible impact regarding the available charging power. While the extension of EVs' distances prolongs the duration of FESS-operation (Section 3.1.2), EV charging with increased power has quite the opposite effects: The higher the EV charging power, the shorter EV charging processes and the shorter periods of FESS-operation. Consequently, standby losses of FESSs increase with raising EV charging power, which decreases the efficiency of the FESS (Fig. 7c): Raising the available charging power per CP from 0.50 p.u. to 1.50 p.u.—while fixing the remaining input variables according to Table 8—reduces the FESS efficiency of use case ELDT from 1.90 p.u. (0.42) to 0.43 p.u. (0.10). Varying the charging power from 0.22 p.u. to 2.00 p.u. (HFC) or from 0.71 p.u. to 1.28 p.u. (EB), triggers a reduction of efficiency by 0.53 p.u. (HFC) or 0.08 p.u. (EB).

3.1.4. Impact of the number of CPs

As the third input variable, we alter the number of installed CPs while fixing the remaining input variables to examine its impact on the FESS capacity and economic- and technical criteria. In general, the more CPs are installed at the charging station, the more EVs must be supplied by the FESS. Hence, the required FESS capacity increases with an increasing number of CPs (Fig. 8a): When fixing all the remaining input variables, a growth of CPs from 0.40 p.u. (two CPs) to 1.60 p.u. (eight CPs) raises the required FESS capacity by 0.96 p.u. (ELDT) and 0.67 p.u. (EB). However, we detect the following characteristic analyzing use case HFC, already described in Section 3.1.3.: The FESS-supply of a few CPs (e.g., two) requires only low discharging power, compared to the supply of numerous CPs (e.g., eight). Due to the same discharging and charging power of the FESS, assumed in this study (Section 2.2), a low number of CPs limits the FESS's recharging.

Thereby, it requires a higher storage capacity to supply the upcoming EV charging event. In the sensibility analysis, the supply of two CPs (0.4 p.u.) requires a FESS capacity of 108 kWh, whereas the supply of eight CPs (1.6 p.u.) requires only 44 kWh. While the total FESS capacity (supplying all CPs) increases (or even decreases considering use case HFC), the FESS capacity per CP decreases with a growing number of CPs.

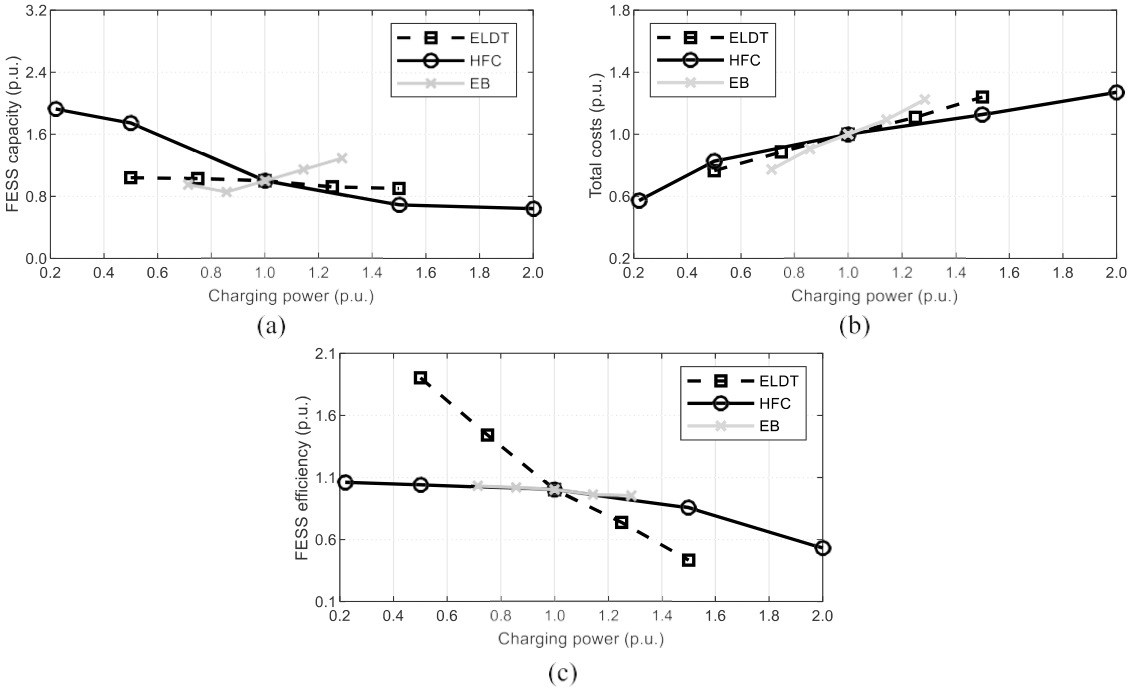

Fig. 7. Impact of the charging power on **(a)** the required FESS capacity, **(b)** annualized total costs per CP, and **(c)** FESS efficiency, regarding electric last-mile delivery trucks (ELDTs), highway fast-charging (HFC), and electric bus charging (EB).

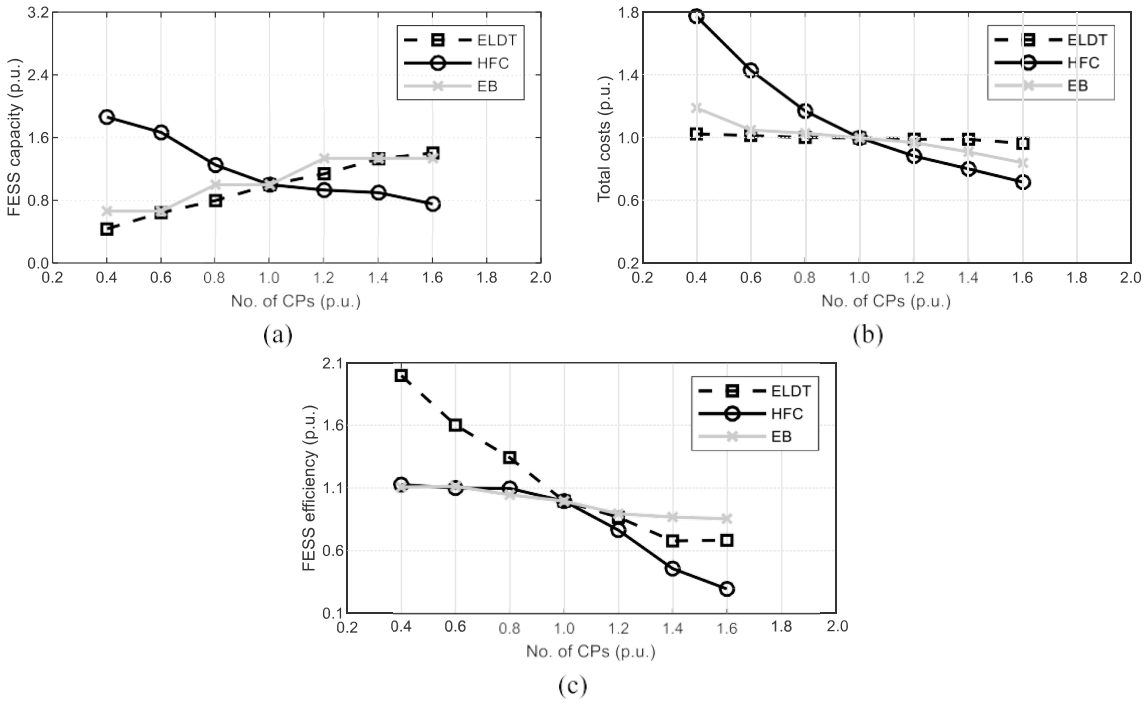

Fig. 8. Impact of the number of charging points on **(a)** the required FESS capacity, **(b)** annualized total costs per CP, and **(c)** FESS efficiency, regarding electric last-mile delivery trucks (ELDTs), highway fast-charging (HFC), and electric bus charging (EB).

This aspect results in lower flywheel costs per CP. As described in Section 2.1, the maximum occupancy of CPs, and thereby the number of simultaneously charging EVs decreases the more CPs are installed. Hence, power-based cost components per CP also decrease with the number of CPs, whereas the energy-based cost component per CP shows little deviation. Based on these characteristics, total annualized costs per CP decrease if the number of CPs is increased from two (0.4 p.u.) to eight (1.6 p.u.): From 1.03 p.u. to 0.97 p.u. for use case ELDT; from 1.8 p.u. to 0.72 p.u. for use case HFC; from 1.19 p.u. to 0.84 p.u. for use case EB (Fig. 8b). Besides the level of the maximum occupancy of CPs, the number of available CPs also affects the number of hours with maximum occupancy: The more CPs are installed, the shorter the period of maximum CP-occupancy (and the maximum number of simultaneously charging EVs) and the shorter the occurrence of the aggregated EV charging peak load. Assuming a constant GRF (and other input variables) in this sensibility analysis, this results in shorter periods of FESS-

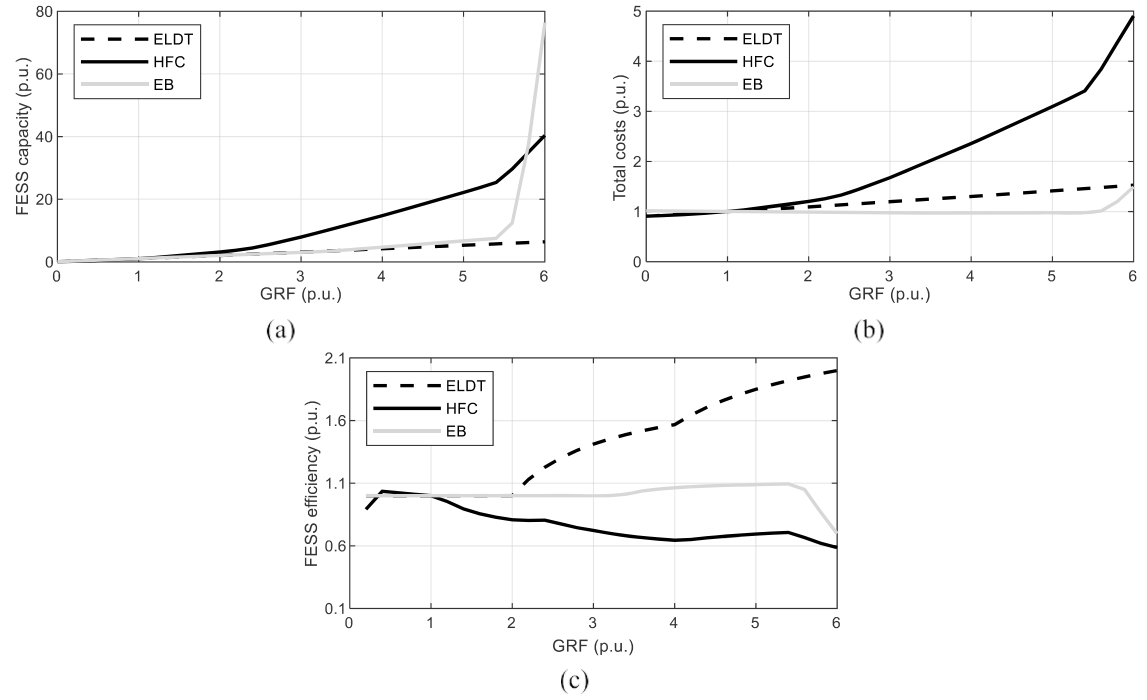

Fig. 9. Impact of the grid relief factor (GRF) on **(a)** the required FESS capacity, **(b)** annualized total costs per CP, and **(c)** FESS efficiency, regarding electric last-mile delivery trucks (ELDTs), highway fast-charging (HFC), and electric bus charging (EB).

operation, which further induces higher standby losses. Consequently, the efficiency of the FESS during operation (Fig. 8c) is reduced by 1.31 p.u. (ELDT), 0.83 p.u. (HFC) and 0.25 p.u. (EB), when the number of CPs is extended from two (0.4 p.u.) to eight (1.6 p.u.) while remaining input variables remain constant (Table 8).

3.1.5. Impact of the grid relief factor

Finally, the variation of the GRF between 0.0 – 0.6 (0.0 – 6.0 p.u.) illustrates its consequences for the suitability of FESSs regarding different use cases. A GRF of 0.0 equals a complete supply by the local power grid and excludes any FESS. Implementing a GRF of, e.g., 0.1 (1.00 p.u.), on the other hand, requires a FESS discharging (and charging) power of 10% of the EV charging peak load. Additionally, it requires a FESS capacity of 1.00 p.u., which corresponds to the reference capacities listed in Table 9. The higher the GRF, the higher the share of EVs' peak load covered by the FESS, and the higher the required FESS capacity (Fig. 9a): If the GRF is increased, e.g., from 0.1 (1.0 p.u.) to 0.6 (6 p.u.) while fixing the other input variables, a 6.4- (ELDT), 40- (HFC) and 76-times higher FESS capacity is required (Fig. 9a).

While this effect is rather linear considering the supply of ELDTs and EB (until a GRF of 5.4 p.u.), the capacity requirement of HFC raises rather quadratically with the GRF. As a result of higher FESS capacity, total annualized costs per CP of use cases ELDT and HFC grow analogously if other input variables remain constant (Fig. 9b): Starting at a GRF of 0.0 p.u. (without FESS) with minimal costs of 0.91 p.u., a GRF of 4.0 p.u. causes 1.43- (ELDT) and 2.64-times higher annualized costs. In other words, in this analysis, minimal costs of use cases ELDT and HFC are achieved with an exclusive grid supply, without FESS (GRF of 0.0). In contrast, use case EB is characterized by high power-based grid costs yet requires minimal FESS capacity than the other use cases (Table 9). Thus, power-based grid costs can be reduced substantially by implementing a FESS with low capacity and comparatively low costs. In the reference case, according to Table 8, the supply of EBs requires a GRF of 0.54 (5.4 p.u.) to provide maximal cost benefits (Fig. 9b). Simultaneously in this sensibility analysis, this particular GRF of 5.4 p.u. allows minimal standby losses and the highest efficiency of the FESS when supplying EBs (Fig. 9c). As demonstrated in Table 5 and Fig. 5, the FESS's power losses depend on its average SOC during operation. Considering the supply of EB, a GRF lower than 0.54 p.u. results in a lower amount of discharged energy from the FESS, which results in a higher average SOC. On the other hand, a GRF higher than 0.54 requires a significantly higher FESS capacity (Fig. 9a), thus, also increases the average SOC. Both phenomena are also detected when supplying use cases ELDT and HFC: Since the required FESS capacity of ELDTs only slightly raises with the GRF (Fig. 9a), the lowest average SOC and the highest efficiency of the FESS is achieved at a GRF of 0.60 (6.0 p.u.)—the maximum GRF in this sensibility analysis. In contrast, the supply of HFC with increasing GRFs requires substantially higher FESS capacities, which increases the average SOC and standby losses of the FESS. Thereby, the maximum efficiency of use case HFC in this sensibility analysis is enabled at a GRF of 0.04 (0.4 p.u.).

Of course, the optimal GRFs demonstrated in this section represent only one particular case, characterized by reference values listed in Table 8. Moreover, the spectrum of analyzed GRFs analyzed only varies between 0.0 and 0.6, which neglects FESS applications with a GRF higher than that.

3.2. Economic- and technical optima of FESS-applications depending on EVs' charging demand

In the performed sensibility analysis (Section 3.1.), we vary only one input variable respectively while fixing the remaining ones to the reference values in Table 8. Although, the identification of optimum FESS applications requires the simultaneous variation of all input variables. On this account, we additionally perform a mathematical optimization to provide the optimum GRF (Section 3.2.1 and 3.2.2) for several charging demands (covered distance, charging power, and number of CPs). While economic optima represent minimized total annualized costs per CP, technical optima represent the application with the highest FESS efficiency. As demonstrated in Section 3.1.4, the previously performed sensibility analysis reveals a substantial discrepancy between economic- (Fig. 8b) and technical optima (Fig. 8c) in terms of their ideal number of CPs. Annualized costs per CP are minimized at a high number of CPs. Accordingly, the mathematical optimization process identifies economic optima for each use case at the maximum number of CPs (eight). In contrast, the maximization of the FESS's efficiency requires a low number of CPs. Hence, the results of technical optima include a minimum number of CPs (two).

3.2.1. Optimum grid relief factor (GRF) based on economic criteria

In general, the economic suitability of FESS applications depends on the relation between cost savings due to a reduced grid capacity required on the one hand and FESS costs on the other. The higher the aggregated EV charging peak load and the lower the required FESS capacity, the higher the economically optimum GRF. In other words, the higher the EV peak load per kWh FESS capacity, the higher the economically optimum share covered by the FESS. Both EV peak load and FESS capacity strongly correlate with the e-mobility charging demand, namely, the covered distance per charging event and the available charging power per CP. As demonstrated in Section 3.1.2, an increasing distance of EVs raises the required FESS capacity (Fig. 6a). The maximum occupancy of CPs and the maximum EV peak load also increase with raising distances, though negligible compared to the growing capacity need. On the other hand, charging with a higher power increases the maximum EV peak load while decreasing (or slightly increasing considering EBs) the required FESS capacity (Fig. 7a). Based on these correlations, the economically optimum GRF decreases with extending distances of EVs and increases with raising charging power (Fig. 10): For most charging demands of ELDTs (Fig. 10a) and HFC (Fig. 10b), economic optima require a GRF of 0.0. (supply exclusively by the grid without any FESS). Nevertheless, when supplying low-distance trips of ELDTs (up to 20 km) with a charging power of 250 or instead 300 kVA, the most cost-efficient application includes a GRF of 0.12 or rather 0.25 (Fig. 10a) and the according FESS with a capacity of 36 kWh or instead 75 kWh. Cost-efficient recharging of short distances of use case HFC with high charging power urges for the following GRFs (and the respective FESS energy capacities): 0.57 (54 kWh) when recharging after 50 km with a charging power of 100 kVA; 0.01 – 0.62 (2.5 – 62 kWh) when recharging after 50 – 100 km with 150 kVA; 0.01 – 0.71 (3 – 88 kWh) when recharging after 50 – 200 km with 200 kVA (Fig. 10b).

In contrast to the supply of ELDTs and HFC, all the analyzed charging demands of EBs enable an economical implementation of FESSs (Fig. 10c). The most cost-efficient supply of short-distance (2 km) EB charging demands is enabled with a GRF between 0.58 (with a charging power of 250 kVA) and 0.73 (450 kVA), which requires a FESS capacity of 30 kWh and 41 kWh. Bus routes with a distance of 10 km, on the other hand, request a GRF of 0.40 (FESS: 28 kWh) and 0.45 (76 kWh) if recharged with the same power, respectively. In summary, the supply of EB charging provides the most promising application of FESSs from an economic standpoint. Since the implementation of EB charging infrastructure requires the highest costs per CP and per year (Table 9), peak load shaving by an integrated FESS allows the most saving potential: If, for instance, EBs are charged with 450 kVA, an exclusive grid supply costs between 34,910 € (2 km distance) and 61,600 € (10 km) per CP. Compared to that, the integration of a FESS with a power of 45% (2 km distance) – 73% (10 km) of the EV peak load reduces annualized costs per CP by 7 – 16%. These price ranges correlate with the findings of recent studies, analyzing one particular number of CPs and one particular charging power of EBs: Ding et al. (2015) [11] determine cost savings between 9.0 – 22.9%, depending on the ESS technology, when supplying six CPs with a charging power of 450 kVA each. Similarly, Yan et al. (2019) [12] identify cost benefits between 11.7 – 15.8%,

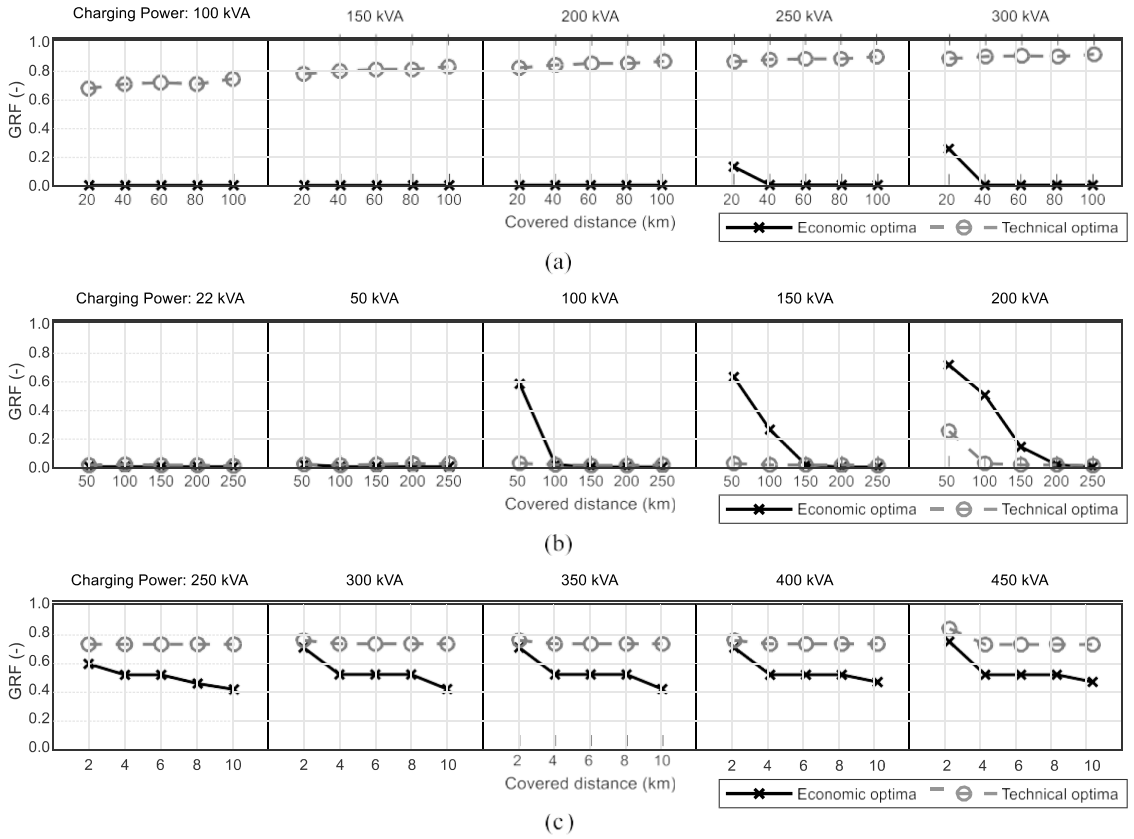

Fig. 10. Economically and technically optimum grid relief factors (GRF) regarding the supply of varying charging demands of **(a)** electric last-mile delivery trucks, **(b)** highway fast-charging, and **(c)** electric busses.

depending on the applied ESS configuration, when supplying eight CPs with 450 kVA each.

In comparison, the integration of FESSs into ELDT- (recharging after a distance of 20 km with 300 kVA) and HFC charging infrastructure (recharging after a distance of 50 km with 200 kVA) allows maximum cost reduction of 4.3% and 15.6%. This measure requires a FESS capacity of 172 kWh and 88 kWh. Nevertheless, regarding these two use cases, the assurance of economic benefits by FESSs requires minimal recharging energy demands in combination with high EV charging power.

3.2.2. *Optimum grid relief factor based on technical criteria*

As demonstrated in Sections 3.1.2 and 3.1.3, standby losses and the efficiency of the FESS strongly correlate with the covered distance per charging event (Fig. 6c) and the available charging power (Fig. 7c): Due to lower standby losses, the FESS efficiency increases with raising distance per charging event (except use case ELDT, described in Section 3.1.2). The increase of charging power per CP, on the other hand, triggers a reduction of the FESS's efficiency. Consequently, the technically optimum GRF slightly decreases with increasing covered distance (except use case ELDT) and decreasing charging power (Fig. 10b,c): The majority of HFC charging demands request a GRF lower than 0.05 to maximize FESS efficiency. Based on that, they require only little FESS capacities between 1 – 20 kWh. Although, the supply of HFC with low-distance energy demand (50 km) and 200 kVA reaches its technical optima at a GRF of 0.25 (Fig. 10b), which increases the required FESS capacity to 40 kWh.

Considering the supply of EBs, technically optimum GRFs show little impact regarding the covered distance or the charging power: 0.71 if EBs are charged with 250 kVA or between 0.71 and 0.82 if charged with 450 kVA. Thereby, the integrated FESS must provide an energy capacity of 22 kWh (250 kVA) or between 25 – 39 kWh (450 kVA). Similar to other use cases, technically optimum GRFs of use case ELDT increase with raising charging power (Fig. 10a): From an average (including all distances) of 0.71 with 100 kVA charging power to an average of 0.90 (300 kVA). This increase of charging power only slightly affects the required average FESS capacity, which raises from 214 kWh (100 kVA) to 276 kWh (300 kVA) on average. Nevertheless, as described in Section 3.1.2, the FESS's efficiency decreases with extending distances per charging event (Fig. 6c) due to the applied modeling approach. As a result, a higher distance requires a higher GRF to maximize the FESS efficiency (Fig. 10a). Recharging after a distance of 20 km with 200 kVA, for example, requires a GRF of 0.82, whereas recharging after a distance of 100 km requires a GRF of 0.86. These GRFs require a FESS capacity of 88 kWh and 435 kWh to cover ELDTs' peak loads.

3.3. *Techno-economic analysis*

As demonstrated in the previous sections, optimum FESS applications differ in terms of economic- and technical criteria: Regardless of the considered EV use case, the ideal number of installed CPs must be either low (technical) or high (economic) to reach the respective optima. On the contrary, the deviation between economically and technically optimum GRFs depends crucially on the analyzed use case: While the supply of ELDTs shows significant divergences (Fig. 10a), use cases HFC (Fig. 10b) and EBs (Fig 10c) allow quite similar GRFs. Hence, the following questions appear in terms of technically optimum FESS applications: Can technical optima be realized in a cost-efficient way, i.e., providing cost benefits compared to an exclusive grid supply without FESS? If not, which adaptions regarding grid charges or FESS costs are necessary? To answer these questions, we select the two cost parameters, most likely to be changed in the upcoming years: Firstly, specific purchase costs of flywheels (Table 7), which may be reduced due to industrial series production [40]. Secondly, many distribution system

operators already recommend an increase of power-based grid utilization charges (Table 6) to accomplish the integration of future grid customers [68]. By transforming Eqs. (12) – (18), we calculate maximally allowed flywheel costs and minimally required system utilization charges (SUC), respectively, providing the same annualized costs as an exclusive grid supply (GRF of 0.0). Fig. 11 demonstrates specific flywheel costs (per kWh) and SUC for each use case depending on the covered distance and the available charging power (according to Fig. 10). The comparison between calculated costs and reference costs illustrates the need for change: Maximally allowed flywheel costs of EBs (Fig. 11a) exceed costs of 2500 €/kWh in 2020 (assumed in this study), which indicates that technical optima can already be realized in an economic sense. Simultaneously, the cost-efficient supply of EBs at technical optima requires a SUC lower than the present-day SUC of
41.04 €/kW (Fig. 11b), signifying no need for cost adaption neither. In contrast, the economic integration of technically optimum FESSs into ELDT charging infrastructure requires the following changes: Either a reduction of specific flywheel costs (e.g., to 53 – 1657 €/kWh when charging with "High" power), an increase of SUC (to 56 – 240 €/kW), or both. Although we stochastically model vehicle-specific schedule deviations, we assume the same route characteristics for each ELDT (Section 2.1.1). As a result, the modeled aggregated ELDT charging profiles are characterized by a high coincidence of charging during peak periods. While this assumed mobility behavior represents the best case in terms of economic criteria (due to high EV peak load), it represents the worst case in terms of technical ones. The temporal sequencing of vehicles' schedules could decrease standby energy losses of the FESS and increase its efficiency. While the impact of controlled charging on the ESS-design has already been analyzed for EBs (e.g., Ding et al. (2015) [11]), future research should include this possibility when analyzing the supply of ELDTs by ESSs.

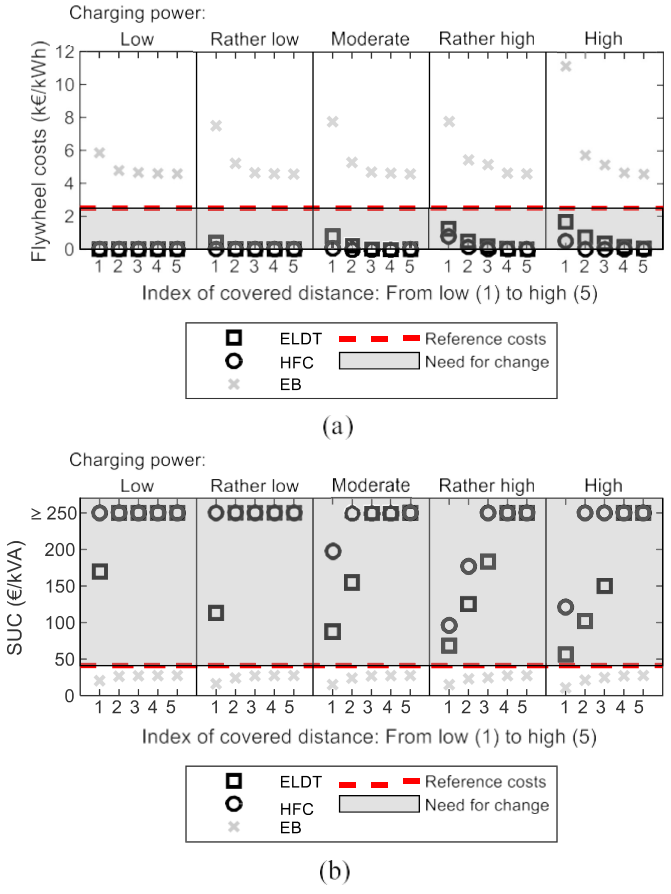

Fig. 11. (**a**) Maximally allowed specific flywheel costs and (**b**) minimally required system utility charges (SUC), required to enable cost parity between exclusive grid supply and technical optima of FESSs supplying electric last-mile delivery trucks (ELDT), highway fast-charging (HFC) of electric passenger vehicles or electric bus (EB) charging.

Considering use case HFC, the operation of FESSs at technical optima allows economic benefits in the case of the following conditions: A reduction of flywheel costs (lower than 771 €/kWh) or an increase of SUC (higher than 96 €/kW) compared to 2020 (Fig. 11). Nevertheless, this requires low-distance energy demands in combination with high charging power. Long-distance recharging of EVs (e.g., 250 km) with low charging power (e.g., 22 kVA) inhibits a cost-efficient FESS-operation at technical optima. This study focuses on the identification of economic and technical optima of FESS applications and their comparison. However, possible compromises in FESS design between these optima are not part of this work. Thus, the authors' future work will focus on possible design approaches combining economic and technical aspects. Future studies will also provide a guideline for configuring FESSs for supplying future EV charging based on several practical examples.

4. Conclusions

The suitability of FESSs for covering EV charging peak loads depends strongly on the supplied EV use case and its particular charging demand (covered distance, charging power, and the number of charging points). Though, this study identifies substantial differences between the economic- and technical suitability of FESSs. The economic suitability of FESSs is evaluated based on annualized investment- and operation costs and increases with

- decreasing distances of EVs covered before recharging (due to decreasing flywheel capacities and -costs),
- raising charging power per CP (due to increasing grid utilization charges),
- and a growing number of CPs (due to decreasing flywheel costs per CP).

Consequently, several analyzed charging demands of EBs allow the integration of a FESS to minimize investment and operation costs. In fact, even low storage capacities enable significant cost benefits compared to an exclusive grid supply (without FESS). On the contrary, most charging demands of use cases ELDT and HFC inhibit an economical implementation of FESSs. Though, low-distance energy demands of these use cases supplied with high charging power allow FESSs to achieve minimal expenses.

The technical suitability of FESSs for covering short-term EV peak loads is evaluated based on its efficiency during operation. The latter crucially correlates with the amount of standby energy losses of the FESS, which decreases with

- increasing distances of EVs,
- decreasing charging power per CP,
- and a decreasing number of CPs.

Due to the demonstrated discrepancies, economically and technically optimum FESS applications (characterized by the optimum number of CPs and the optimum grid relief factor) differ significantly. On this account, this study additionally investigates which FESS applications allow a cost-efficient implementation of FESSs at technical optima: Considering use cases ELDT and HFC, a cost-efficient FESS-operation at technical optima requires either a reduction of flywheel costs or an increase of power-based grid utilization charges. On the contrary, the supply of EBs by FESSs allows both the maximization of FESS efficiency and the reduction of investment and operation costs.

Declaration of Competing Interest

The authors declare that they have no known competing financial interests or personal relationships that could have appeared to influence the work reported in this paper.

Acknowledgments

Funding: This work is part of the project "FlyGrid" (www.flygrid.tugraz.at), funded by the Austrian "Klima- und Energiefonds" via the Austrian Research Promotion Agency (FFG) program "Leuchttürme eMobilität" (grant number 865447).

Paper: **Analyzing the Suitability of Flywheel Energy Storage Systems for Supplying High-power Charging E-mobility Use Cases**

Authors: Bernd Thormann, Philipp Puchbauer and Thomas Kienberger

Bernd Thormann: Conceptualization, Methodology, Software, Validation, Data Curation, Writing- Original draft preparation and Visualization

Philipp Puchbauer: Methodology and Software

Thomas Kienberger: Conceptualization, Validation, Writing-Reviewing and Editing, Supervision, Project administration and Funding acquisition

All authors contributed to the manuscript and have given approval to the final version of the manuscript.

Supplementary materials

Supplementary material associated with this article can be found, in the online version, at doi:10.1016/j.est.2021.102615.

References

[1] Communication from the Commission to the European Parliament, the European Council, the Council, the European Economic and Social Committee and the Committee of the Regions: The European Green Deal, 2019.
[2] European Environment Agency: National emissions reported to the UNFCCC and to the EU Greenhouse Gas Monitoring Mechanism, www.eea.europa.eu/data-and-maps/daviz/share-of-transport-ghg-emissions-2#tab-googlechartid_chart_11, accessed on 24 July 2020.
[3] European Parliament: Parliament backs new CO2 emissions limits for cars and vans, www.europarl.europa.eu/news/en/press-room/20190321IPR32112/parliament-backs-new-co2-emissions-limits-for-cars-and-vans, accessed on 24 July 2020.
[4] European Parliament: MEPs approve new CO2 emissions limits for trucks, www.europarl.europa.eu/news/en/press-room/20190412IPR39009/meps-approve-new-co2-emissions-limits-for-trucks, accessed on 24 July 2020.
[5] Y. Mu, J. Wu, N. Jenkins, H. Jia, C. Wang, A Spatial–Temporal model for grid impact analysis of plug-in electric vehicles, Appl. Energy 114 (2014) 456–465, https://doi.org/10.1016/j.apenergy.2013.10.006.
[6] A. Dubey, S. Santoso, Electric Vehicle Charging on Residential Distribution Systems: impacts and Mitigations, In IEEE Access 3 (2015) 1871–1893, https://doi.org/10.1109/ACCESS.2015.2476996.
[7] H.R. Galiveeti, A.K. Goswami, N.B. Dev Choudhury, Impact of plug-in electric vehicles and distributed generation on reliability of distribution systems, Eng. Sci. Technol. Int. J. 21 (2018) 50–59, https://doi.org/10.1016/j.jestch.2018.01.005.
[8] D. Fischer, A. Harbrecht, A. Surmann, R. McKenna, Electric vehicles' impacts on residential electric local profiles – A stochastic modelling approach considering socio-economic, behavioural and spatial factors, Appl. Energy 233-234 (2019) 644–658, https://doi.org/10.1016/j.apenergy.2018.10.010.
[9] K. Clement-Nyns, E. Haesen, J. Driesen, The impact of charging plug-in hybrid electric vehicles on a residential distribution grid, In IEEE Trans. Power Syst. 25 (2010) 371–380, https://doi.org/10.1109/TPWRS.2009.2036481.
[10] M. Rogge, S. Wollny, D. Sauer, Fast charging battery buses for the electrification of urban public transport—a feasibility study focusing on charging infrastructure and energy storage requirements, In Energies 8 (2015) 4587–4606, https://doi.org/10.3390/en8054587.
[11] H. Ding, Z. Hu, Y. Song, Value of the energy storage system in an electric bus fast charging station, Appl. Energy 157 (2015) 630–639, https://doi.org/10.1016/j.apenergy.2015.01.058.
[12] Yan, et al., Research on configuration methods of battery energy storage system for pure electric bus fast charging station, In ***Energies*** 12 (2019) 558, https://doi.org/10.3390/en12030558.
[13] H. Zhang, S.J. Moura, Z. Hu, Y. Song, PEV fast-charging station siting and sizing on coupled transportation and power networks, In IEEE Trans. Smart Grid 9 (2018) 2595–2605, https://doi.org/10.1109/TSG.2016.2614939.
[14] P. Jochem, E. Szimba, M. Reuter-Oppermann, How many fast-charging stations do we need along European highways? Transp. Res. Part D: Transp. Environ. 73 (2019) 120–129, https://doi.org/10.1016/j.trd.2019.06.005.
[15] R. Sinha, B. Bak-Jensen, J.R. Pillai, Operational flexibility of electrified transport and thermal units in distribution grid, Int. J. Electrical Power Energy Syst. 121 (2020), 106029, https://doi.org/10.1016/j.ijepes.2020.106029.
[16] S. Shao, M. Pipattanasomporn, S. Rahman, Demand Response as a Load Shaping Tool in an Intelligent Grid With Electric Vehicles, In IEEE Trans. Smart Grid (2) (2011) 624–631, https://doi.org/10.1109/TSG.2011.2164583.
[17] P. Finn, C. Fitzpatrick, D. Connolly, Demand side management of electric car charging: benefits for consumer and grid, In Energy 42 (2012) 358–363, https://doi.org/10.1016/j.energy.2012.03.042.
[18] P. Mesarić, S. Krajcar, Home demand side management integrated with electric vehicles and renewable energy sources, In Energy Build. 108 (2015) 1–9, https://doi.org/10.1016/j.enbuild.2015.09.001.
[19] Liu, et al., Online energy management of PV-assisted charging station under time-of-use pricing, In Electric Power Syst. Res. 137 (2016) 76–85, https://doi.org/10.1016/j.epsr.2016.04.002.
[20] Goli, P.; Shireen, W.: PV powered smart charging station for PHEVs, In Renewable Energy, 2014, 66, pp. 280–287, doi:10.1016/j.renene.2013.11.066.
[21] B. Thormann, R. Braunstein, J. Wisiak, F. Strempfl, T. Kienberger, Evaluation of grid relieving measures for integrating electric vehicles in a suburban low-voltage grid, in: CIRED Conference Proceedings, 2019, https://doi.org/10.34890/398.
[22] T. Dragicevic, S. Bo, E. Schaltz, J.M. Guerrero, Flexible local load controller for fast electric vehicle charging station supplemented with flywheel energy storage system, in: Proceedings of the IEEE Electric vehicle conference, Florence, Italy, 2014, pp. 1–6, https://doi.org/10.1109/IEVC.2014.7056133.
[23] Y. Ligen, H. Vrubel, H. Girault, Local Energy Storage and Stochastic Modeling for Ultrafast Charging Stations, In Energies 12 (10) (2019) 1986, https://doi.org/10.3390/EN12101986.
[24] A. Hussain, V.-.H. Bui, J.-.W. Baek, H.-.M. Kim, Stationary Energy Storage System for Fast EV Charging Stations: optimality Analysis and Results Validation, In Energies 13 (2020) 230, https://doi.org/10.3390/en13010230.
[25] Ryu, et al., An Innovative Operation Strategy of ESS for Capacity Expansion of Renewable Energy and Customer Load with Electric Vehicle Chargers in Low Voltage Distribution Systems, In ***Energies*** 12 (2019) 4668, https://doi.org/10.3390/en12244668.
[26] Held, et al., Operation of Battery Storage as a Temporary Equipment During Grid Reinforcement Caused by Electric Vehicles, In Electronics (2020) 888, https://doi.org/10.3390/electronics9060888, 9.
[27] Makohin, et al., Use of lithium iron phosphate energy storage system for EV charging station demand side management, in: Proceedings of the 8th IEEE International Symposium on Power Electronics for Distributed Generation Systems, Florianopolis, Brazil, 2017, https://doi.org/10.1109/PEDG.2017.7972528.
[28] L. Richard, M. Petit, Fast charging station with battery storage system for EV: grid services and battery degradation, in: IEEE International Energy Conference (ENERGYCON), Limasol, 2018, https://doi.org/10.1109/ENERGYCON.2018.8398744.
[29] T. Dragicevic, S. Sucic, J.C. Vasquez, J.M. Guerrero, Flywheel-Based Distributed Bus Signalling Strategy for the Public Fast Charging Station, In IEEE Trans. Smart Grid 5 (2014) 2825–2835, https://doi.org/10.1109/TSG.2014.2325963.
[30] Liu, et al., Application of Small-Sized SMES in an EV Charging Station With DC Bus and PV System, In IEEE Trans. Appl. Supercond. 25 (2015) 1–6, https://doi.org/10.1109/TASC.2014.2374174.
[31] H. Zhao, A. Burke, Evaluation of a PV Powered EV Charging Station and Its Buffer Battery, In ***JEPE*** (2016) 10, https://doi.org/10.17265/1934-8975/2016.02.007.
[32] L. Novoa, J. Brouwer, Dynamics of an integrated solar photovoltaic and battery storage nanogrid for electric vehicle charging, J. Power Sources 399 (2018) 166–178, https://doi.org/10.1016/j.jpowsour.2018.07.092.
[33] S. Bai, D. Yu, S. Lukic, Optimum design of an EV/PHEV charging station with DC bus and storage system, in: Proceedings of the IEEE Energy Conversion Congress and Expo (ECCE), Atlanta, Georgia, 2010, pp. 1178–1184, https://doi.org/10.1109/ECCE.2010.5617834.
[34] G. Joos, M. Freige, M. de; Dubois, Design and simulation of a fast charging station for PHEV/EV batteries, in: Electrical Power and Energy Conference (EPEC), Halifax, NS, Canada, 2010, pp. 1–5, https://doi.org/10.1109/EPEC.2010.5697250.
[35] M. Gjelaj, N.B. Arias, C. Træholt, S. Hashemi Toghroljerdi, Multifunctional applications of batteries within fast-charging stations based on EV demand-prediction of the users' behavior, J. Eng. (2019) 4869–4873, https://doi.org/10.1049/joe.2018.9280.
[36] Bryden, et al., Rating a Stationary Energy Storage System Within a Fast Electric Vehicle Charging Station Considering User Waiting Times, IEEE Trans. Transp. Electrification 5 (2019) 879–889, https://doi.org/10.1109/TTE.2019.2910401.
[37] P. Piromjit, T. Tayjasanant, Peak-demand management for improving undervoltages in distribution systems with electric vehicle connection by stationary battery, in: 2017 IEEE Transportation Electrification Conference and Expo, Harbin, China, 2017, https://doi.org/10.1109/ITEC-AP.2017.8081033.
[38] Held, et al., Dimensioning of battery storage as temporary equipment during grid reinforcement caused by electric vehicles, in: Proceedings of the 53rd International Universities Power Engineering Conference (UPEC), Glasgow, United Kingdom, 2018, https://doi.org/10.1109/UPEC.2018.8542035.
[39] Bayram, et al., Local energy storage sizing in plug-in hybrid electric vehicle charging stations under blocking probability constraints, in: IEEE International Conference on Smart Grid Communications (SmartGridComm 2011), Brussels, Belgium, 2011, https://doi.org/10.1109/SmartGridComm.2011.6102396.

[40] A. Buchroithner, H. Wegleiter, B. Schweighofer, Flywheel Energy Storage Systems Compared to Competing Technologies for Grid Load Mitigation in EV Fast-Charging Applications, in: Proceedings of the IEEE 27th International Symposium on Industrial Electronics (ISIE), Cairns, Australia, 2018, https://doi.org/10.1109/ISIE.2018.8433740.
[41] A.H. Fahad, H.A. Gabbar, Wireless Flywheel-Based Fast Charging Station (WFFCS), in: Proceedings of the 2018 IEEE International Conference on Renewable Energy and Power Engineering (REPE 2018), Toronto, Canada, 2018, https://doi.org/10.1109/REPE.2018.8657482.
[42] M. Amiryar, K. Pullen, A review of flywheel energy storage system technologies and their applications, Appl. Sci. 7 (2017) 286, https://doi.org/10.3390/app7030286.
[43] Bilateral information exchange with leaders of electric mobility flagship projects "LEEFF" and "MEGAWATT", funded by the Climate and Energy Fund, 2019, www.klimafonds.gv.at/mobilitaetswende/projekte/leuchttuerme-der-elektromobilitaet, assessed in June 2020.
[44] City of Vienna: Bus schedule data provided by Wiener Linien, 2020. www.data.gv.at, assessed in September 2020.
[45] Allgemeiner Deutscher Automobil Club: Eco-Test, www.adac.de/infotestrat/tests/eco-test, accessed in October 2019.
[46] A. Schulz, PhD-Thesis, 2015, https://doi.org/10.14279/depositonce-4515.
[47] Gao, et al., Battery capacity and recharging needs for electric buses in city transit service, In Energy 122 (2017) 588–600, https://doi.org/10.1016/j.energy.2017.01.101.
[48] A.W. Kunith, Elektrifizierung Des Urbanen öffentlichen Busverkehrs, Springer Fachmedien Wiesbaden, 2017, https://doi.org/10.1007/978-3-658-19347-8.
[49] QCBUS: Charge Station for Busses: Technical specification, www.electricmobility.efacec.com, accessed in June 2020.
[50] Siemens: Charge your future – with the Siemens eBus charging infrastructure, www.siemens.com/mobility, accessed in June 2020.
[51] Heliox Automotive B.V.: 300kW Opportunity Charger: technical specifications, www.heliox-energy.com, accessed in June 2020.
[52] B. Thormann, T. Kienberger, Evaluation of Grid Capacities for Integrating Future E-Mobility and Heat Pumps into Low-Voltage Grids, In Energies 13 (2020) 5083, https://doi.org/10.3390/en13195083.
[53] Autobahnen- und Schnellstraßen-Finanzierungs-Aktiengesellschaft: Location-based traffic count data, 2019, www.asfinag.at.
[54] R. Xie, W. Wei, M.E. Khodayar, J. Wang, S. Mei, Planning Fully Renewable Powered Charging Stations on Highways: a Data-Driven Robust Optimization Approach, In IEEE Trans. Transp. Electrific. 4 (2018) 817–830, https://doi.org/10.1109/TTE.2018.2849222.
[55] Rios, et al., Load demand profile for a large charging station of a fleet of all-electric plug-in buses, J. Eng. (2014) 379–387, https://doi.org/10.1049/joe.2014.0152.
[56] S. Bae, A. Kwasinski, Spatial and Temporal Model of Electric Vehicle Charging Demand, In IEEE Trans. Smart Grid 3 (2012) 394–403, https://doi.org/10.1109/TSG.2011.2159278.
[57] Official website of Wiener Linien GmbH, www.wienerlinien.at, accessed on 1 February 2021.
[58] Offcial Site of the FlyGrid project, www.tugraz.at/en/projekte/flygrid/home, accessed on 28 July 2020.
[59] P. Haidl, PhD Thesis, (pending publication - under review), Technische Universitaet Graz, 2021.
[60] Austrian National Council: Federal Act Providing New Rules for the Organisation of the Electricity Sector (Electricity Act 2010 – ElWOG 2010), Vienna, 2010, www.ris.bka.gv.at/GeltendeFassung.wxe?Abfrage=Bundesnormen&Gesetzesnummer=20007045, assessed on 19 March 2021.
[61] Official website of the Austrian energy market regulator (E-Control), www.e-control.at, assessed on 19 March 2021.
[62] Official website of the Energy Exchange Austria (EXAA), www.exaa.at, assessed on 19 March 2021.
[63] N. Brinkel, W.L. Schram, T.A. AlSkaif, I. Lampropoulos, W. van Sark, Should we reinforce the grid? Cost and emission optimization of electric vehicle charging under different transformer limits, In Appl. Energy 276 (2020), 115285, https://doi.org/10.1016/j.apenergy.2020.115285.
[64] International Renewable Energy Agency: Electricity storage and renewables: Costs and markets to 2030, 2017, www.irena.org/publications/2017/Oct/Electricity-storage-and-renewables-costs-and-markets, accessed in December 2020.
[65] M.A. Ramli, A. Hiendro, S. Twaha, Economic analysis of PV/diesel hybrid system with flywheel energy storage, In Renew. Energy 78 (2015) 398–405, https://doi.org/10.1016/j.renene.2015.01.026.
[66] A. Schroeder, T. Traber, The economics of fast charging infrastructure for electric vehicles, In Energy Policy 43 (2012) 136–144, https://doi.org/10.1016/j.enpol.2011.12.041.
[67] Junseok Song, A. Toliyat, D. Turtle, A. Kwasinski, A rapid charging station with an ultracapacitor energy storage system for plug-in electrical vehicles, in: Proceedings of the 2010 International Conference on Electrical Machines and Systems, Incheon, 2010. Electronic ISBN: 978-89-86510-11-9.
[68] Association of Austrian Electricity Companies (Oesterreichs Energie): netzberechnungen Österreich - Einfluss der Entwicklungen von Elektromobilität und Photovoltaik auf das österreichische Stromnetz. www.oesterreichsenergie.at/die-welt-des-stroms/stromnetze/studie-netzberechnungen-oesterreich.html, assessed on 19 March 2021.

10.3 Paper 3

Estimation of Grid Reinforcement Costs Triggered by Future Grid Customers: Influence of the Quantification Method (Scaling vs. Large-Scale Simulation) and Coincidence Factors (Single vs. Multiple Application)

energies

MDPI

Article

Estimation of Grid Reinforcement Costs Triggered by Future Grid Customers: Influence of the Quantification Method (Scaling vs. Large-Scale Simulation) and Coincidence Factors (Single vs. Multiple Application)

Bernd Thormann * and Thomas Kienberger

Chair of Energy Network Technologies, Montanuniversitaet Leoben, 8700 Leoben, Austria; thomas.kienberger@unileoben.ac.at

* Correspondence: bernd.thormannn@stud.unileoben.ac.at; Tel.: +43-3842-402-5409

Abstract: The integration of future grid customers, e.g., electric vehicles, heat pumps, or photovoltaic modules, will challenge existing low-voltage power grids in the upcoming years. Hence, distribution system operators must quantify future grid reinforcement measures and resulting costs early. On this account, this work initially evaluates different methods to quantify future grid reinforcement needs, applied by the current state of research. Thereby, it indicates the significance of large-scale grid simulations, i.e., simulating several thousand low-voltage grids, to quantify grid reinforcements accurately. Otherwise, a selected area's total grid reinforcement costs might be misjudged significantly. Due to its fast application, deterministic grid simulations based on coincidence factors are most commonly used in the current state of research to simulate several thousand grids. Hence, in the second step, recent studies' approaches to applying grid customers' coincidence factors are evaluated: While simplified approaches allow fast simulation of numerous grids, they underestimate potential grid congestion and grid reinforcement costs. Therefore, a fully automated large-scale grid simulation tool is developed in this work to allow the simulation of multiple grids applying grid customers' coincidence factors appropriately. As a drawback, the applied deterministic framework only allows an estimation of future grid reinforcement costs. Detailed determination of each grid's grid reinforcement costs requires time-resolved grid simulations.

Keywords: distribution power networks; grid reinforcement; grid simulation; electric vehicle; photovoltaic; heat pump

Citation: Thormann, B.; Kienberger, T. Estimation of Grid Reinforcement Costs Triggered by Future Grid Customers: Influence of the Quantification Method (Scaling vs. Large-Scale Simulation) and Coincidence Factors (Single vs. Multiple Application). *Energies* **2022**, *15*, 1383. https://doi.org/10.3390/en15041383

Academic Editors: Abu-Siada Ahmed and Mahdi Khosravy

Received: 15 December 2021
Accepted: 11 February 2022
Published: 14 February 2022

1. Introduction

Carbon-neutrality has been declared a priority objective on both the European [1] and national level (e.g., in Austria [2]) to mitigate global warming in the upcoming years. This ambitious objective shall be fulfilled, among other things, by the enhancement of renewable energy sources and a transition towards climate-neutral mobility with a high share of battery electric vehicles (EVs) [1]. In addition, the residential sector's energy efficiency shall be increased, e.g., by implementing residential electric heat pumps (HPs) [1,3]. While these transitions will reduce the traffic, energy, and residential sector's carbon footprint, they require integrating numerous new grid customers into the existing power system. The majority (in number) of EVs, photovoltaic modules (PVMs), and electric HPs will be connected to the low-voltage (LV) level [4,5].

As a result, these trends will unquestionably challenge existing LV grids in the following years [6–8]. However, future power system structures are planned and designed several decades in advance [9]. Hence, distribution system operators (DSOs) pursue quantifying future grid reinforcement measures (and resulting costs) in their service area at an early stage [9–11]. Besides statistical approaches (e.g., [12]), modern-day grid planning

relies on numerical load flow simulations to identify potential grid reinforcement measures caused by voltage violations or thermal congestions [13]. Therefore, future grid customers' loads must be modeled realistically using real-life information (e.g., type, installed power, and energy demand of grid customers). Grid customers' loads are then implemented into grid models, modeled based on real-life grid topologies and data (e.g., line length and cross-section area) [14].

However, a DSO's service area often includes several thousand LV grids. The simulation of several thousand grids requires a significant amount of data and computing resources [15]. For DSOs, both are not always available to the required extent. Consequently, quantifying future grid reinforcement needs in a DSO's service area, including the applied approach to model grid customers' loads, must comply with given data- and computing criteria. Nevertheless, since grid reinforcements cause significant investment costs for the public sector, the accuracy of grid simulations must not suffer. On this account, this work evaluates different methods to quantify future grid reinforcement costs, applied in the current state of research (Section 2). Furthermore, recent studies' approaches to model grid customers' loads are examined regarding accuracy and computing time.

2. State of Research

While several studies analyze the impacts of EVs, PVMs, and HPs on individual LV grids (e.g., [16–18]), the presented work focuses on quantifying future grid reinforcements in a large area, including several thousand LV grids. Therefore, the current state of research uses two different ways (Table 1): Most studies identify future grid restrictions in individually selected, representative grids based on load flow simulations. The selected grids' results are aggregated and scaled to the whole area of investigation (Section 2.1).

Table 1. Classification of recent studies according to their method to quantify total grid reinforcement costs for several thousand grids.

Method to Quantify Total Grid Reinforcement Costs	Studies
Simulation of representative grid structures and scaling of their results:	[5,7,10,19–25]
- synthetic grids modeled based on real-life grid data	[5,19,22–24]
- real-life grids selected from the area of investigation	[7,10,20,21,25]
- classification of grids into representative classes	[5,7,19,20]
Large-scale grid simulation of numerous real-life grid models	[6,10,26]

Others perform load flow simulations in all grids in the investigated area. The total amount of grid reinforcement measures equals the sum of all grids' results (Section 2.2). In the following, recent studies in this field are classified accordingly.

2.1. Simulation of Representative Grid Structures and Scaling of Their Results

In Austria, for example, future costs of grid extension measures have recently been estimated by Oesterreichs Energie [10]. Therefore, grid impacts on the LV level caused by integrating EVs (10 and 30% penetration) and PVMs (increase by factor seven) are identified. Fifteen Austrian DSOs (supplying 87% of Austrian grid customers) participate in this study. From those, a third chose to simulate individually selected, representative LV grids and scale their results to the whole service area. Finally, grid reinforcement costs of each participating DSO are aggregated and scaled to the whole of Austria. Based on this approach, this study predicts total grid reinforcement costs on the Austrian LV level between 0.8–2.2 billion euros by 2030 (in addition to regular capital expenditure).

Vu [19] developed a simulation and optimization model to quantify reinforcement costs on the LV level induced by renewable energy sources and EVs. Therefore, repre-

sentative LV grids are modeled based on typical real-life network characteristics and simulated. The total grid reinforcement costs (between 11.6–22.2 billion euros) are acquired by scaling simulated grids' results to the whole of Germany. The study performed by Agora [7] determines the required costs of grid extension measures triggered by a future energy transition in Germany. Therefore, this study assumes 6–45 million EVs and 13–17 GW installed power of electric HPs, supplied by renewable energy sources with 65–88% penetration. Real-life grid data of representative power grids are applied for load flow simulation. Finally, the results of representative grid structures are scaled to the entire area of Germany, which results in total grid reinforcement costs between 19–39 billion euros required on the LV level.

Similarly, two additional German studies performed by the German Energy Agency [20] and the German Ministry of Economics and Technology [5] investigate future grid reinforcement costs of German LV networks. For this purpose, both consider possible scenarios based on network development plans and the German federal states' objectives and projections. In these studies, grid reinforcement costs of representative grids are determined based on grid simulations to scale their results up to the national LV level: 3.6–4.2 billion euros till 2030 [20] and 4.0–9.6 billion euros till 2032 [5].

Matrose et al. [21] investigated grid reinforcement costs caused by EV charging in five countries. On both the medium-voltage (MV) and LV levels, most representative grids are chosen by experts for grid planning and operation. Grid reinforcement costs are determined using load flow simulations for each selected grid. Finally, the relation between required grid reinforcement costs and the grids' total grid value (representing an exchange of all grid assets) is determined and scaled to all five countries. About 2% (charging with 3.7 kW) or 3% (11 kW) of the total grid value must be invested in MV and LV grids to avoid grid congestions, considering an EV penetration of 30%

Pudjianto et al. [22] quantified future costs required to integrate PVMs in eleven countries in the EU by 2030 (e.g., Italy, UK). This study creates representative European MV and LV grids based on statistical grid data to perform load flow simulations. Finally, total grid reinforcement costs per generated energy (MV and LV level combined) are derived for each of the eleven countries from the simulated results: Between 9.6–13.4 €/MWh (Italy) and between 14.0 €/MWh (UK).

Similarly, Hartvigsson et al. [23] use statistical grid data to model synthetic LV grids, whose capacity for integrating PVMs is determined using grid simulations. The modeled grids' results are scaled to the whole of Sweden, the UK, and Germany, to quantify these countries' total hosting capacity on the LV level: 33 GW (Sweden), 63 GW (UK), 248 GW (Germany). However, this study excludes the calculation of required grid reinforcement costs. Durusut et al. [24] indicated that 15.5 billion £ (about 18.6 billion euros) must be invested in the UK power system (LV level only) until 2030 due to an extensive transition towards EVs (8.0 million) and HPs (6.8 million). Therefore, ten representative grid models are developed synthetically based on statistical grid data. Flinn et al. [25] determined the integration costs for PVMs in California, USA (up to 744 $ until 2026). Therefore, the authors selected and investigated 75 representative feeders and extrapolated their results to the rest of California (over 10,000 feeders).

While all the studies mentioned above simulate individually selected grids to scale their results to the area of investigation, they vary in the selection (Section 2.1.1) and the number of representative grids to be simulated (Section 2.1.2).

2.1.1. Selection of Representative Grids to Be Simulated

Studies quantifying total grid reinforcement costs by scaling representative grids' results use different approaches to acquire appropriate grids (Table 1). Four recent studies [5,19,22–24] synthetically model representative grids based on real-life grid data and apply them for simulation. Others [7,10,20,21,25] select real-life representative grids to be simulated from all grids in the area of investigation. Therefore, they rely on the experience and insights of experts in the operating and planning of grids.

However, recent studies analyzing total grid reinforcement costs in whole Germany [5,7,19,20] classify German LV grids into, e.g., eleven [20], 18 [5] or 238 [19], representative classes depending on their grid region, topology, or future trends towards renewable energy sources (Table 1). Thus, the scaling of simulated grids' results is initially done for each class to scale each class's results to the whole of Germany. Nevertheless, classifying several grids into representative classes requires time-consuming pre-processing, enormous amounts of data, and significant computing effort [15].

2.1.2. Number of Representative Grids to Be Simulated

From all the studies using the described scaling method, only five define the exact number of representative grids to be simulated: The German Ministry of Economics and Technology [5] modeled over two million representative grids synthetically to perform load flow simulations. Pudjianto et al. [22], Hartvigsson et al. [23], and Durusut et al. [24] simulated only 15, 373 and ten synthetically created LV grids, respectively.

In total (considering all representative grid classes), 177 representative LV grids are selected by the German Energy Agency [20] to perform load flow simulation. Matrose et al. [21] and Flinn et al. [25] performed grid simulations in 200 and 75 selected grids, respectively. The remaining works [7,10,19] did not provide this information.

2.2. Large-Scale Grid Simulation of Numerous Real-Life Grid Models

Studies in the second group each simulate several thousand real-life LV grids in the area of investigation to quantify its total grid reinforcement costs. Gupta et al. [6] determined grid impacts of future solar PVMs (20–70% penetration), HPs (up to 100%), and EVs (15–100%) on the LV level, considering the service area of one Swiss DSO. Therefore, the authors perform load flow simulations in 5879 MV/LV substations using GIS data. The authors conclude that by 2050 the total grid reinforcement costs can amount to 11.0 billion CHF (about 10.1 billion euros).

As described in Section 2.1, fifteen Austrian DSOs quantify their grid reinforcement costs by 2030 in the study by Oesterreichs Energie [10]. In contrast to the ones already described, six DSOs perform load flow simulations in all their LV grids to determine required grid reinforcement measures. Lemmens et al. [26] developed a large-scale grid simulation tool to quantify future grid reinforcement measures caused by three different penetrations of EVs and PVMs. Therefore, Flemish LV grids, including 60,000 km grid lines, are simulated and examined regarding voltage violations and thermal congestions. Considering penetrations of 14.4% (PVM), 7.7% (plug-in hybrid EV), and 6.7% (EV), 15,900 km of grid lines (26.5%), and 8% of all transformers must be exchanged.

2.3. Applied Approaches to Modeling Grid Customers' Load

Besides the applied quantification method, recent studies use different approaches to model future grid customers' loads as the basis for grid simulations (Table 2): Durusut et al. [24] neglected to specify the applied modeling approach. In only one study [22], grid customers' loads are taken into account using time series. Three recent studies [5,19,21] use the Monte-Carlo method to stochastically determine the power at each grid node based on statistical data. However, based on its stochastic nature, the Monte-Carlo method requires multiple iterations to be simulated [27]. In contrast to time series-based and Monte-Carlo simulations, static deterministic grid simulations analyze only one load case, which aims to represent the worst-case in terms of grid impacts [28,29]. Therefore, grid customers' loads are estimated using coincidence factors. Considering a defined number of grid customers (NoC), the coincidence factor represents the maximum of their aggregated electrical power (P_i) divided by the sum of their individual maximum power (Equation (1)) [6,28].

Table 2. Classification of recent studies according to their approach to modeling grid customers' load.

Applied Approach to Modeling Grid Customers' Load	Studies
No specification	[24]
Time series-based simulation	[22]
Monte-Carlo simulation	[5,19,21]
Deterministic grid simulations using coincidence factors:	[6,7,10,20,23,25,26]
- single, consistent coincidence factor	[20,25]
- single, grid-specific coincidence factor	[6,23,26]
- double, grid-specific coincidence factors	[7,10]

The coincidence factor takes temporal interdependences between grid customers' electrical loads into account. Thus, it also indicates the probability of simultaneously occurring electrical loads considering a defined number of grid customers: The higher the coincidence factor, the higher the probability of temporal aggregations between grid customers' loads. Naturally, the more customers are considered, the lower the probability of temporal peak load aggregations and the lower the coincidence factor [30]:

$$Coincidence\ factor(NoC) = \frac{\max\limits_{t}(\sum_{i=1}^{NoC} P_i(t))}{\sum_{i=1}^{NoC} \max\limits_{t}(P_i(t))} \quad (1)$$

Since it only requires one time step to be simulated, the application of coincidence factors allows much faster computation [27,31] than time series-based and Monte-Carlo simulations. That is why most studies analyzing many real-life grids [6,7,10,20,23,26] use this approach (Table 2).

However, since the coincidence factor depends on the number of considered customers, it must be adapted according to the grid element to be analyzed: Grid elements supplying numerous customers (e.g., the MV/LV substation) are characterized by low coincidence factors. In contrast, grid elements supplying few customers (e.g., grid lines at the end of feeders) are characterized by high coincidence factors. Nevertheless, recent studies use various approaches to applying grid customers' coincidence factors. Hence, they consider this aspect differently:

Hartvigsson et al. [23] and Gupta et al. [6] determined one single coincidence factor specifically for each grid based on the number of grid customers supplied by the MV/LV substation (Figure 1). This single value is applied to each grid customer to perform load flow simulations. The German Energy Agency [20] and Flinn et al. [25] also apply one single coincidence factor to each grid customer. Although, these studies use a consistent coincidence factor for each LV grid to be simulated, neglecting the grid's actual number of customers. Lemmens et al. [26] applied one single coincidence factor to each grid customer. Therefore, the number of customers supplied by the respective feeder's main line (Figure 1) is considered for each grid specifically.

In contrast to the previous works, the studies performed by Oesterreichs Energie [10] and Agora [7] apply two different coincidence factors to each grid customer depending on the grid element to be analyzed. The coincidence factor applied to analyze the MV/LV substation is determined based on the total number of customers the substation supplies. For a second load flow simulation, the number of customers supplied by each feeder's main line is used to define the coincidence factor for all remaining elements in the respective feeder. Both coincidence factors are varied for each LV grid specifically.

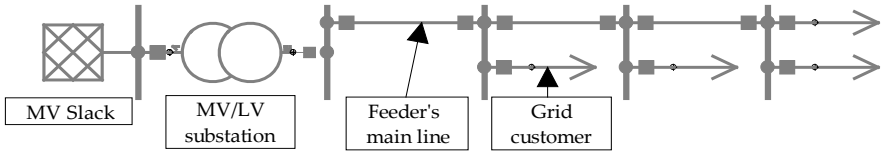

Figure 1. Typical grid topology of one low-voltage (LV) feeder supplying four grid customers.

In conclusion, recent studies' approaches to applying coincidence factors differ regarding the following aspects (Table 2): Firstly, the coincidence factor's variation in the analyzed grids (consistent or defined for each grid specifically). Secondly, the number of various coincidence factors applied to each grid (single or multiple). Thirdly, the grid element on the basis of which the coincidence factors are determined (MV/LV substation or each feeder's main line). By applying one single coincidence factor to each grid customer (e.g., defined based on the number of customers the MV/LV substation supplies), numerous grid elements might be examined using inappropriate coincidence factors. As a countermeasure, multiple coincidence factors must theoretically be applied to grid customers to analyze each grid element adequately. However, recent studies determining total grid reinforcement costs in several thousand grids include this aspect differently due to different approaches to applying coincidence factors.

2.4. Remaining Gap in the Current State of Research

Previous sections indicate different methods to quantify grid reinforcement needs (Sections 2.1 and 2.2) and model grid customers' electrical loads (Section 2.3) applied in recent studies. This broad spectrum of methods and simplifications impedes comparing recent works in this field and their results [32]. Indeed, Vu [19] demonstrated significant differences (about 21–45% concerning the total line length to be reinforced in Germany) between the presented study and the ones performed by the German Energy Agency [20] and the German Ministry of Economics and Technology [5].

Identifying the impact of the selected quantification method (scaling of representative grids' result or large-scale grid simulations) and the approach to model grid customers' electrical loads (consistent or grid-specific, single or multiple) would facilitate the comparison of studies in this field. To the authors' best knowledge, only one study addresses this issue: Eberl et al. [15] have analyzed different methods (e.g., [19,20]) to quantify grid reinforcement costs in a large area with several thousand grids. However, those methods are evaluated only qualitatively regarding the accuracy of results, assumptions and simplifications, and the required amount of data.

The shortage of applying only one single coincidence factor for all grid customers has been quantified in 13 LV grids by Ulffers et al. [33]. Nevertheless, the current state of research lacks a quantitative analysis of how recently applied methods and approaches can affect the calculated grid reinforcement costs in a large area with several thousand grids [32].

3. Open Research Questions and Structure of This Work

Based on the remaining gap in the current state of research (Section 2.4), the following research questions remain unsolved:

1) What is the potential error when simulating only a few individually selected LV grids and scaling their results to quantify grid reinforcement costs in a large area?
2) How many grids (in %) must be simulated to reach a certain degree of accuracy?
3) How to apply grid customers' coincidence factors to quantify grid reinforcement measures accurately (consistent or grid-specific; single or multiple; based on which grid element)?
4) What is the trade-off between the acquired simulation accuracy and required computing time?

5) How to quantify future grid reinforcement costs allowing both high accuracy and adequate computing time in the most optimal way?

Various quantification methods and approaches to applying coincidence factors, used in the current state of research, are analyzed to answer these research questions for one DSO's service area with several thousand LV grids. Therefore, an automated large-scale grid simulation tool is developed (Section 4.1) and applied to quantify future grid reinforcement needs using real-life grid data (Section 4.2). The investigated scenario regarding the penetration of EVs, PVMs, and HPs is described in Section 4.3. Sections 4.4 and 4.5 demonstrate the evaluated quantification methods and approaches to applying coincidence factors. Their impacts on the determined grid reinforcement measures and the required computing time are demonstrated in Section 5. Finally, Section 6 discusses this paper's results according to the presented research questions and provides an outlook on further work.

4. Materials and Methods

4.1. Automated Large-Scale Grid Simulation Tool: Quantification of Grid Extension Needs

The grid simulation tool developed in this study allows fully automated analysis of several thousand grid models, including evaluating potential grid reinforcement needs. Thereby, all LV grids in a DSO's service area can be simulated and examined in terms of grid restrictions. The tool's scheme applied for each grid model respectively is illustrated in Figure 2. The following sections describe each of these steps in detail. The parallelization of the presented scheme (Figure 2) using 32 CPUs (3 GHz, 128 GB RAM) in MATLAB allows the simulation of several grid models simultaneously (one grid model per CPU). Thereby, it enables an average computing time of 20.8 s per 1000 grid nodes, about 16 times faster compared to a sequential simulation.

4.1.1. Import and Processing of Original Grid Data

In the first step of the grid simulation tool, each grid's original grid data is imported into MATLAB. Therefore, we developed interfaces between commercial grid simulation tools (e.g., NEPLAN [34], PowerFactory [35]), database software (e.g., MS Access), and MATLAB, allowing fully automated and standardized data transfer. For a successful performance of the developed tool, each grid's data set must include the following information:

- Power lines and transformers**:** Maximum current, internal impedance (R', L', C'), and connected nodes
- Grid nodes**:** Type of node (Slack, PQ, or PV), nominal voltage as well as type (e.g., household, PVMs, EVs, and HPs), number, and installed power of connected grid customers

Each grid's topology is structured into feeders and feeder levels, as shown in Figure 3. The feeder level represents the distance of grid elements (transformers, nodes, and lines) from the MV slack: The higher the feeder level, the higher the distance. Transformers at the MV/LV substation and the connected LV bus bar are characterized by feeder level 1.

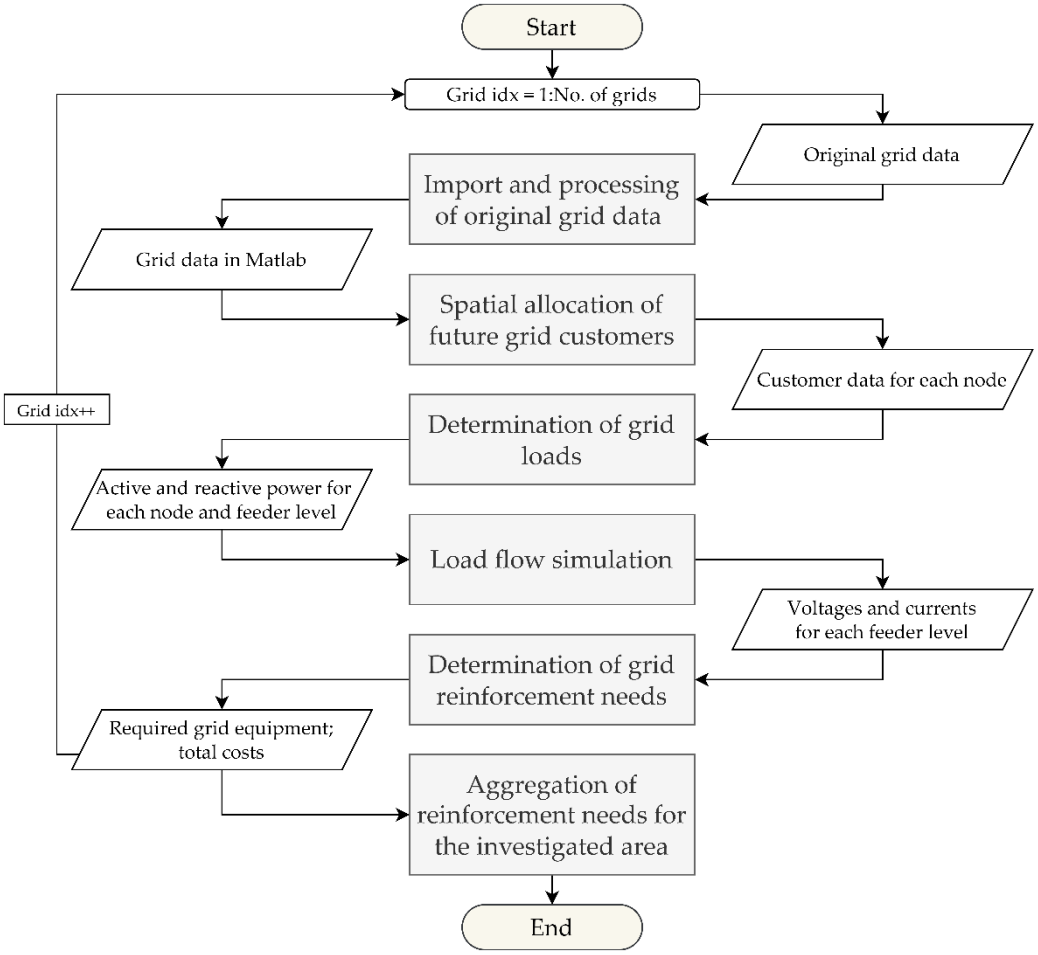

Figure 2. Scheme of the developed fully automated large-scale grid simulation tool.

Grid lines and nodes connected to the LV bus bar are assigned feeder level 2. This scheme is continued until all grid elements are assigned a particular feeder level (Figure 3).

Like recent studies simulating several thousand LV grids (Section 2.3), the developed tool uses coincidence factors to model grid customers' loads. However, the coincidence factor depends on the number of customers considered.

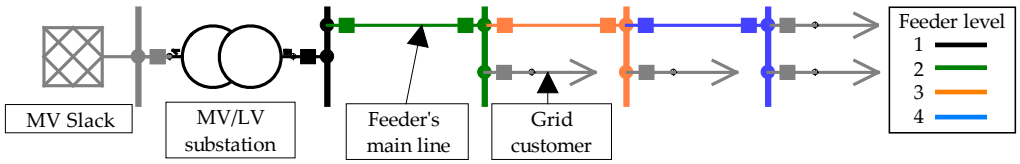

Figure 3. Structuring the grid topology into feeder levels.

Hence, it must be adapted according to the grid element to be analyzed. The implementation of feeder levels allows us to apply the appropriate coincidence factor to each grid customer depending on the grid element to be analyzed (described in detail in Section 4.1.3).

4.1.2. Spatial Allocation of Future Grid Customers

Besides existing grid customers, the automated large-scale grid simulation tool analyzes future EVs, PVMs, and HPs and their impacts on LV networks. Therefore, the total number of EVs, PVMs, and HPs in each LV grid is determined based on the analyzed penetrations (from 0–100%) and the total number of households (assuming maximally one

EV, PVM, and HP per household). While existing grid customers' location in the grid is documented in the imported grid data (Section 4.1.1), future customers' spatial allocation is, of course, unclear. The distribution of future grid customers significantly influences their grid impact and on resulting grid reinforcement costs [24]. Therefore, the spatial allocation of EVs, PVMs, and HPs can freely be selected using the automated large-scale grid simulation tool (e.g., stochastic or uniform). As relaxation of the problem, this study assumes a uniform placement of future customers to the grid's nodes (cf. Thormann et al. (2020) [8]). In the end, this step provides all relevant data regarding existing and future grid customers for each node, which is then applied to determine realistic grid loads (Section 4.1.3).

4.1.3. Determination of Grid Loads

Quantifying grid reinforcement measures requests the identification of critical grid loads and their impacts on the investigated grid. Since the automated large-scale grid simulation tool uses static deterministic grid simulation, critical grid loads are determined using coincidence factors (described in Section 2.3). Considering a certain number of customers (NoC), their aggregated power ($P_{aggregated}$) is calculated by multiplying the sum of their individual maximum powers ($Pmax_i$) by the respective coincidence factor (CF), according to Equation (2) [28]:

$$P_{aggregated}(NoC) = \left(\sum_{i=1}^{NoC} Pmax_i\right) \cdot CF(NoC) \quad (2)$$

The maximum power of existing customers is provided by original grid data (Section 4.1.1). In contrast, future customers' peak power is defined as follows: The possibility of charging EVs strongly depends on the type of housing, i.e., family houses or multi-apartment residential buildings. Analogously to Thormann et al. [8], this study classifies future EVs accordingly: EVs charged with high power (11 kW) at family houses and EVs charged with low power (3.7 kW) at multi-apartment residential buildings. Additional PVMs are integrated into the grid model with a maximum power of 5 kW (feeding into the grid). The load profile of electric HPs is characterized by increased starting current/power due to the compressor motor [36]. However, since starting currents last only few seconds, a base load of 3.0 kW (cf. [37–39]) is assumed for this customer type.

As described in Section 2.3, coincidence factors are applied for load flow simulations to take temporal interdependences between grid customers into account. Besides the number of grid customers, these interdependences depend on the customer types (e.g., households, EVs). While state-of-the-art coincidence factors neglect this aspect, novel coincidence factors have been modeled in the authors' previous work (Thormann et al. [8], Figure 4). It also describes the methodology applied for modeling these new coincidence factors.

Since the modeled coincidence factors combine different customer types, the coincidence factor at a certain aggregated number of customers varies depending on their distribution. For example, three households are characterized by a lower coincidence factor than one household with one EV and one HP (in total, three customers). In general, EVs and PVMs (near one) are characterized by high coincidence factors, whereas households and HPs are characterized by lower ones (Figure 4). As described in Section 2.3 and demonstrated in Equation (2), the coincidence factor (and the resulting aggregated power) depends on the number of considered customers. Hence, it must be adapted according to the grid element to be analyzed and its number of supplied customers. As a result, static deterministic load flow simulation (one time step only) using coincidence factors does not allow the accurate simulation of all grid elements at once.

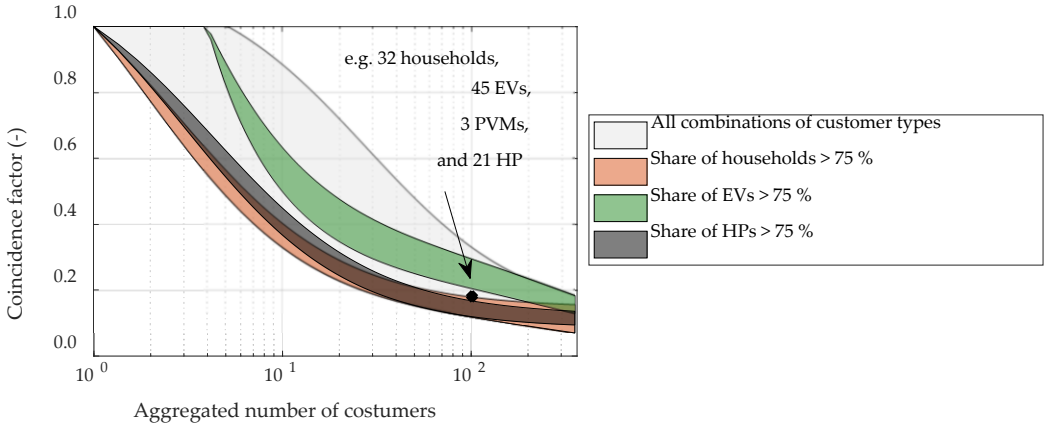

Figure 4. Novel coincidence factors considering temporal interdependences between various customer types: households, electric vehicles (EVs), photovoltaic modules (PVMs), and heat pumps (HPs).

Therefore, each LV grid is structured into several feeder levels, described in Section 4.1.1 (Figure 3). The coincidence factor defined at each customer depends on the analyzed grid element, hence, the respective feeder level (Figure 5): When analyzing the MV/LV substation in feeder level 1 (e.g., supplying three customers), the respective coincidence factor (e.g., 0.65) is applied to each connected customer. The aggregated power (13.0 kW), calculated using Equation (2), is distributed to grid customers (6.5, 2.6, and 3.9 kW) according to their maximum individual power (10.0, 4.0, and 6.0 kW).

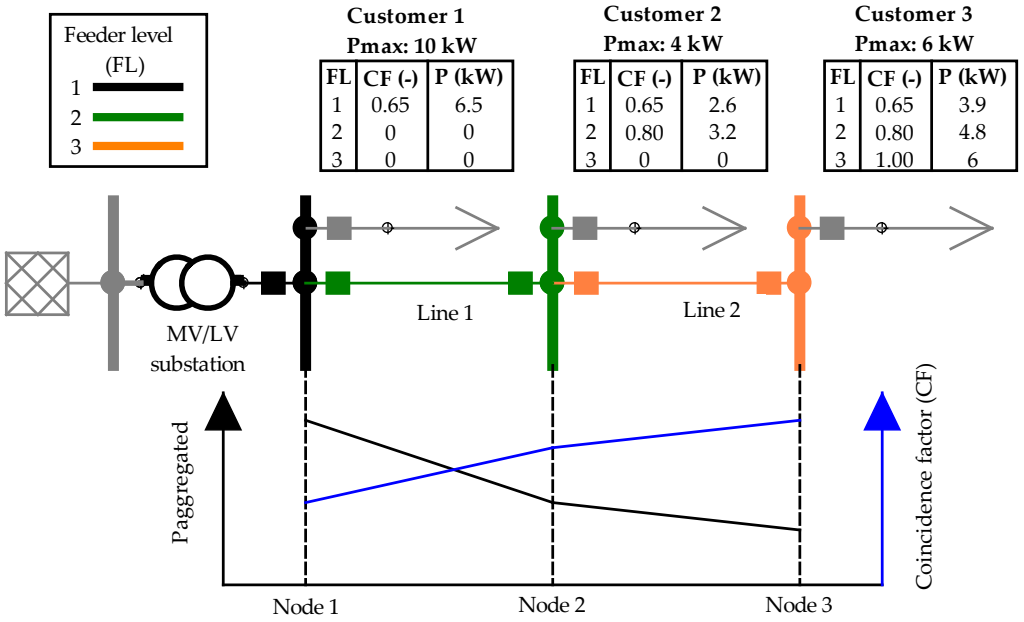

Figure 5. Exemplary allocation of coincidence factors (CF) and resulting power (P) to the grid's customers depending on the analyzed feeder level (FL).

Each feeder's main line (Line 1 in Figure 5) is evaluated, considering feeder level 2 (e.g., supplying two customers). Therefore, each connected customer is assigned the respective coincidence factor (e.g., 0.80), whereas non-relevant customers are neglected (coincidence factor of 0.0). This procedure is done for each feeder level. In the end, each customer is assigned one coincidence factor and one power value for each feeder level, respectively (Figure 5). After determining the active power for each grid customer and feeder level, reactive power is calculated by using the following power factors: 0.99 (leading) for EVs, 1.00 for PVMs, and 0.90 (lagging) [8,36,40,41].

4.1.4. Load Flow Simulation

In the next step, active and reactive power values of each customer and each feeder level are applied to analyze potential grid restrictions. Therefore, static load flow simulations are performed using the Newton-Raphson method. For each feeder level, one static load flow simulation is performed using the appropriate coincidence factor for each customer (Figure 5). All grid elements assigned to the same feeder level are analyzed simultaneously. Hence, the number of required load flow simulations equals the number of feeder levels assigned to each grid, respectively. However, the developed grid simulation tool allows users to define the number of simulated feeder levels to adapt to the available computing power. In this study, the number of simulated feeder levels is varied (Section 4.5) to investigate different approaches to applying coincidence factors and their impact on simulation accuracy.

As output data, the static load flow simulation provides each node's complex voltage ($\underline{V}_{Output}$; Figure 6a) and the thermal utilization of transformers and lines (Figure 6b) for each simulated feeder level. However, the actual results of individual elements (nodes, transformers, and lines) depend on their actual coincidence factor and, thereby, the assigned feeder level. Thus, the actual current of transformers and lines is retrieved from the output data (Figure 6b) according to their assigned feeder level, e.g., at feeder level 1 for the MV/LV substation or at feeder level 3 for Line 2 (Figure 5).

FL	Node 1	Node 2	Node 3
1	97.8 pu	96.7 pu	95.2 pu
2	98.1 pu	96.0 pu	93.3 pu
3	98.6 pu	97.1 pu	93.9 pu

(**a**)

FL	MV/LV substation	Line 1	Line 2
1	81 %	40 %	33 %
2	73 %	71 %	59 %
3	53 %	51 %	70 %

(**b**)

Figure 6. Exemplary output of static load flow simulations performed for three feeder levels (FL): Each node's voltage (**a**) and the thermal utilization of the MV/LV substation and lines (**b**).

The actual complex voltage of a node n ($\underline{V}_{n,actual}$) is calculated according to Equation (3), based on the actual complex voltage of the previous node ($\underline{V}_{n-1,actual}$) and their complex output voltages ($\underline{V}_{Output}$; Figure 6a) at the feeder level of node n (FL_n). The applied calculation of voltages can only be used for evaluating radial grid structures, not for mesh networks. However, considering radial grid structures on the LV level, this method has been validated by time series-based grid simulation in Thormann et al. [8]

$$\underline{V}_{n,actual} = \underline{V}_{n-1,actual} + \underline{V}_{Output}(FL_n, n) - \underline{V}_{Output}(FL_n, n-1) \quad (3)$$

In the end, the performed load flow simulations provide each node's actual voltage and the actual current of transformers and lines. The grid's actual voltages and currents are then applied to evaluate potential grid reinforcement needs (Section 4.1.5).

4.1.5. Determination and Aggregation of Grid Reinforcement Needs

In the final step of the automated large-scale grid simulation tool, required grid reinforcement measures induced by various grid customers (existing ones, EVs, PVMs, and HPs) and resulting costs are determined. Therefore, each grid's results are examined for voltage violations and thermal congestions (cf. [7,19,20]). The acceptable voltage range and the maximum thermal utilization of transformers and lines are defined freely by the user. The European standard EN 50160 [42] defines the acceptable voltage range of the LV and MV levels with ±10% of the nominal voltage. However, this voltage range is shared by both voltage levels conjunctly. According to the voltage range partitioning presented in [5,43], an acceptable voltage range of [104.5%; 93.5%] of the nominal voltage (0.4 kV) is used in this study. In addition, grid reinforcements are required if transformers or lines

exceed their allowed thermal utilization of 100%. Depending on the type of grid restriction, the following grid reinforcement measures are automatically executed in the grid model (cf. [7,20,44]):

- Thermal overload of the transformer(s) at the MV/LV substation**:** The developed tool initially examines whether the parallel installation of an additional transformer with the same nominal power as the existing one(s) is sufficient to prevent thermal overload. If not or the maximum number of parallel transformers is already reached (Table 3), existing transformers at the MV/LV substation are exchanged with new ones, providing sufficient nominal power.
- Thermal overload of individual lines**:** If individual grid lines are overloaded, additional lines are installed parallel until the maximum power can be transmitted or the maximum number of parallel lines (Table 3) is reached. Therefore, the cable type NAYY 4 × 150 mm² (cf. [7,20]) with a maximum current of 245 A is installed by default.
- Voltage violations**:** If one or more nodes show inadmissible voltages, the affected feeder is divided into two feeders at 2/3 of the total length from the MV/LV substation (cf. [20]).

As a result, this step provides the number and nominal power of additional transformers as well as the total length of additional grid lines to be installed in the grid. Grid reinforcement costs are estimated for each grid by applying specific construction- and material costs of additional transformers and grid lines. While the user can define specific costs freely, this study uses values listed in Table 3, including personnel-, planning- and construction costs [7,20,44].

Table 3. Parameters applied for determining required grid reinforcement costs [7,20,44].

Parameter	Applied Values
Max. number of parallel transformers (-)	2
Max. number of parallel lines (-)	4
Nominal power of additional transformers (MVA)	0.1, 0.25, 0.4, 0.63, 0.8, 1.0, 1.25
Material and installation costs of additional transformers (k€)	7.0, 17.3, 27.7, 29.6, 35.6, 38.0, 41.4
Specific construction costs of additional grid lines (€/km)	65,000
Specific material costs of additional grid lines (€/km)	10,000

In the current version of the developed grid simulation tool, measures of congestion management are excluded. However, they will be integrated into further versions of the tool. The developed automated large-scale grid simulation tool executes the workflow described in Section 4.1 (Figure 2) for each grid. All the grids' costs are aggregated to determine total grid reinforcement measures in the investigated area caused by a user-defined scenario (e.g., characterized by a specific EV-, PVM- and HP-penetration).

4.2. Grid Data Applied in This Study

This study evaluates various methods and approaches to quantify potential grid reinforcement needs based on 7114 real-life LV grids. The analyzed LV grids are operated by a major Austrian DSO whose service area is mainly characterized by suburban and rural regions. Figure 7 describes the analyzed LV grids by illustrating their frequency of occurrence and median regarding the installed transformer capacity, the number of nodes, the total line length, and the average number of customers per point of common coupling.

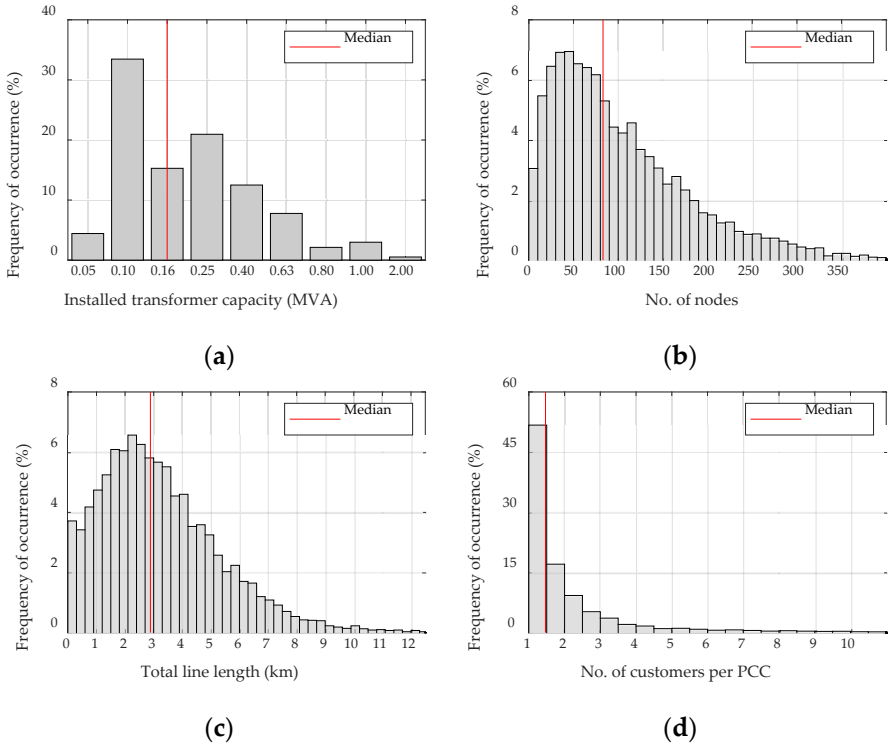

Figure 7. Frequency of occurrence of (**a**) the installed transformer capacity, (**b**) the number of nodes, (**c**) the total line length, and (**d**) the number of customers per point of common coupling (PCC) in the analyzed LV grids.

Most LV grids are supplied by a MV/LV transformer with a capacity of 0.10 (34%), 0.16 (15%, median), 0.25 (21%), or 400 MVA (13%). Only 13% of MV/LV substations are equipped with a higher transformer capacity (Figure 7a). In total, the investigated LV grids include about 740,400 nodes with a median of 83 nodes per grid (Figure 7b) and 23,000 km of grid lines with a median of 2.89 km (Figure 7c). All grids together supply 498,600 customers via 207,400 points of common coupling. The median of 1.47 customers per point of common coupling (Figure 7d) demonstrates a relatively low population density in the area of investigation.

Grid customers can be classified into 307,200 households (median: 43), 60,300 commercial businesses, 29,800 agricultural businesses, 83,100 electric water heaters, 2000 lighting systems and 16,200 existing PVMs. Each grid is structured as a radial network and supplied by the MV grid (represented by an MV slack node) via one or two MV/LV substations and transformers (Figure 3). In conclusion, the investigated LV grids show a high heterogeneity regarding the installed transformer capacity, the number of nodes, the total line length, and the number of customers per point of common coupling (Figure 7). However, this discrepancy between real-life LV grids has also been noticed in central Europe and the USA due to various grid planning approaches of DSOs and geographical differences [45–48]. In fact, the statistical distribution of the analyzed LV grids' parameters shows similarities to other studies (e.g., [49–51]).

4.3. Scenario Applied in This Study

Besides the quantification method and the approach to applying coincidence factors, recent studies differ concerning the considered scenarios. In contrast, this work compares those methods and approaches by applying one consistent scenario. Therefore, the future penetration of EVs, PVMs, and HPs is derived for 2030. According to the Environment Agency Austria [52], this study assumes an EV penetration of 27% in 2030. Furthermore, we assume that 30% of households will be equipped with domestic PVMs in 2030, according to Fechner [53]. The future penetration of electric HPs is estimated based on the study

by Fraunhofer [54], which predicts their penetration between 14–31% in 2030. Hence, this study uses the mean value of 23% to compare various quantification methods and approaches to applying coincidence factors.

4.4. Varying the Applied Method to Quantify Grid Reinforcement Measures

The presented study evaluates four different methods to quantify grid reinforcement costs (Table 4) in the area of investigation, including 7114 LV grids (Section 4.2). Those follow the methods applied by the current state of research and presented in Section 2. Thereby, they vary in the selection and number of grids to be simulated based on load flow simulations: The first method (Scaling of grid regions) performs load flow simulations selecting three representative LV grids, one per grid region (urban, suburban, and rural according to [55]). As in most recent studies (Section 2.1.1), representative grids are selected in consultation with the respective grid planners and based on their experience and know-how. The total grid reinforcement costs in the selected area are determined by simulating the selected grids and scaling their costs to the whole area (7114 grids) according to Equation (4):

$$Total\ grid\ reinforcement\ costs = \frac{\left(\sum_{i=1}^{No.of\ simulated\ grids} Costs_i\right) \cdot 7114}{No.of\ simulated\ grids} \quad (4)$$

The second quantification method (scaling of arbitrarily selected grids) randomly selects representative grids from the available grid data to perform grid simulations. Total grid reinforcement costs are then estimated by scaling the grids' results to the defined area (Equation (4)). This method's results strongly depend on the number of selected grids and the selected grids' structures. On this account, we vary the number of simulated grids between 1–7114 using this method (Table 4). For each number of simulated grids, the random selection and simulation of grids are repeated 1000 times to vary the analyzed grid structures as well. Since this method neglects the statistical distribution of grids' parameters (e.g., transformer capacity, number of nodes, number of customers, total line length), it represents a simplified approach to select grids for simulation.

Table 4. Evaluated methods to quantify future grid reinforcement costs.

	Quantification Method	Selection of Representative Grids to Be Simulated	No. of Simulated Grids
1	Scaling of grid regions	Based on the grid planner's expertise (one per region)	3
2	Scaling of arbitrarily selected grids	Randomly for 1000 iterations	Varied between 1–7114
3	Scaling of statistically selected grids	Based on statistical data	Varied between 1–7114
4	Simulation of all grids	-	7114

In contrast, the third quantification method (scaling of statistically selected grids) selects representative grids to be simulated based on statistical data (cf. [46,56]). Therefore, the root mean square relative deviation between each grid's parameters (installed transformer capacity, number of nodes, total line length, and the number of customers per point of common couplings) and the respective medians (demonstrated in Section 4.2) are calculated. Similar to method 2, the number of simulated grids is varied between 1–7114. For each number of simulated grids, those with the lowest root mean square relative deviation are selected for simulation. The total grid reinforcement costs are calculated by scaling their results to the whole area of investigation (Equation (4)). In the fourth quantification method (simulation of all grids), we simulate all 7114 LV grids in the investigated area, requiring no scaling or grid selection. Total grid reinforcement costs are determined by aggregating all grids' results.

The developed grid simulation tool (Section 4.1) is applied for each method, though different numbers of grids are simulated (Table 4). Furthermore, all feeder levels are simulated in each quantification method to consider each grid element's appropriate coincidence factor (approach 4 in Section 4.5).

4.5. Varying the Approach to Applying Coincidence Factors

As demonstrated in Section 2.3, studies quantifying future grid reinforcement costs in a large area vary regarding the following aspects:

- The coincidence factor's variation in the analyzed grids (consistent or grid-specific)
- The number of various coincidence factors applied per grid (single or multiple)
- The grid element on the basis of which the coincidence factors are determined (the MV/LV substation or each feeder's main line)

The presented study identifies these aspects' impact on the calculated total grid reinforcement costs. Therefore, four different approaches to applying coincidence factors (Table 5), following the current state of research (Section 2.3), are evaluated. With each approach, all 7114 LV grids (Section 4.2) are simulated using the developed large-scale grid simulation tool (Section 4.1).

Table 5. Evaluated approaches to applying coincidence factors (CF).

	CF-Variation in the Analyzed Grids	No. of Various CFs Applied per Grid	Grid Element as Basis of CF-Determination	Simulated Feeder Levels
1	Consistent	Single	MV/LV substation	Feeder level 1
2	Grid-specific	Single	MV/LV substation	Feeder level 1
3	Grid-specific	Double	MV/LV substation and each feeder's main line	Feeder level 1 and 2
4	Grid-specific	Multiple	Each grid element	All feeder levels

However, the applied tool is adjusted according to the approach to be investigated. Firstly, depending on how coincidence factors vary throughout the analyzed LV grids: In the first approach, one consistent coincidence factor is applied to each LV grid. Therefore, this study uses a coincidence factor of 0.26, selected from the calculated values (Figure 4) based on the average number of 43 households (Section 4.2) and the respective EV- (27%), PVM- (30%), and HP-penetration (23%), described in Section 4.3. This method neglects the actual number of customers in the analyzed grid. In contrast, approaches 2–4 determine the coincidence factor for each grid specifically depending on its number of grid customers.

Secondly, we vary the number of different coincidence factors applied per grid and the grid element on the basis of which these coincidence factors are determined. Both can be defined by the number of feeder levels to be analyzed (Section 4.1.3) using the developed large-scale grid simulation tool. In this study, the number of simulated feeder levels is adjusted according to the investigated approach to applying coincidence factors (Table 5): The first and second approaches apply a single coincidence factor to each grid customer, determined based on the number of customers the MV/LV substation supplies. Hence, only feeder level 1 is simulated in these approaches using the respective coincidence factors (consistent or grid-specific). In the third approach, feeder levels 1 and 2 are simulated to take two different coincidence factors at the MV/LV substation and each feeder's main line (Figure 3) into account for each grid customer. Finally, approach 4 determines the actual coincidence factors for each grid element to be analyzed depending on its number of connected customers. Therefore, multiple coincidence factors are applied to grid customers, and all feeder levels are simulated.

Using the developed large-scale grid simulation tool, the number of analyzed feeder levels equals the number of required load flow simulations. Thus, the approaches analyzed in this study differ in the number of performed load flow simulations.

5. Results

5.1. Comparing Different Quantification Methods

This work analyzes various methods (Table 4) to quantify the total grid reinforcement costs in the selected area, including 7114 LV grids. Due to data protection issues, the actual costs required in the investigated area must not be published. However, the actual costs are divided by a selected non-published reference value to compare various quantification methods. Thus, total grid reinforcement costs determined by the analyzed quantification methods are illustrated as per unit (pu) values depending on the number of simulated grids (Figure 8):

The simulation of one representative grid per grid region (urban, suburban, and rural—three grids in total) and the scaling of their results up to the total number of grids (Scaling of grid regions) reveals total grid reinforcement costs of 0.66 pu. The second method's results (Scaling of arbitrarily selected grids) strongly depend on the selected grids' structures. Consequently, this method shows a broad range of possible grid reinforcement costs, especially at a low number of simulated grids. When simulating, for example, 50 randomly chosen grids (0.7% of all grids) and scaling their results to the selected area, the total costs differ between 0.08 pu and 3.18 pu (Figure 8). However, with an increasing number of simulated grids, the spectrum of possible results narrows: Between 0.93–1.68 pu at 1000 simulated grids (14%); between 1.15–1.44 pu at 3500 grids (49%); between 1.23–1.36 pu at 6000 grids (84%).

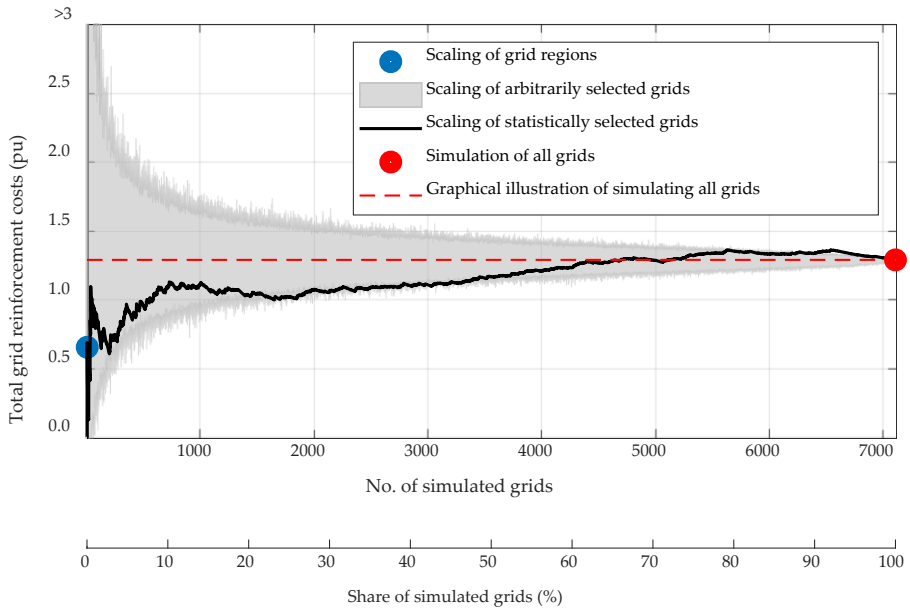

Figure 8. Comparison of different quantification methods regarding their detected total grid reinforcement costs depending on their number and share of simulated grids.

Total grid reinforcement costs determined by scaling statistically selected grids' results (method 3) also vary depending on the number of simulated grids. Only 54 of the statistically 500 most representative grids (7.0% of all grids), chosen according to the procedure depicted in Section 4.4, require grid reinforcements in the selected scenario. Scaling their results to the selected area reveals grid reinforcement costs of 1.02 pu. However, the simulation of more grids (and their scaling) leads to total grid reinforcement costs of 1.13 pu (1000 grids), 1.16 pu (3500), and 1.33 pu (6000). Based on the same approach to applying coincidence factors (approach 4: Grid-specific, multiple coincidence factors), quantification methods 2–4 all reveal total costs of 1.29 pu if all 7114 LV grids are simulated (Figure 8).

The results of simulating all LV grids are graphically illustrated in Figure 8 as a red dashed line to provide a better comparison to other quantification methods. The scaling of grid regions' representative grids (method 1) underestimates grid reinforcement costs by 49% compared to a detailed simulation of all grids (method 4). The scaling of arbitrarily selected and simulated grids (method 2) approaches the actual result (1.29 pu) the more grids are simulated. If LV grids are selected for simulation based on statistical data (method 3), the scaled grid reinforcement costs oscillate around all grids' aggregated costs (1.29 pu). In this method, all grids are ranked according to their statistical deviation from the "most representative" grid and selected for simulation. The statistically 4600 most representative grids (65%) in the selected area require on average lower grid reinforcement costs (1.7967×10^{-4} pu) than the overall average of all 7114 grids (1.8165×10^{-4} pu). Consequently, the scaling of their results underestimates the actual total costs required in the selected area. Simulating between 4601 and 5200 LV grids and scaling their results to the whole area of investigation provides similar (deviation between ±1.6%) results than simulating all grids. However, the simulation and scale of more grids (between 5201 and 7110) overestimate the actual demand of grid reinforcement costs (acquired by simulating all grids). These numbers demonstrate that the "most representative" LV grid in the investigated area shows a high capacity for integrating future customers. On the contrary, total grid reinforcement costs are triggered mainly by grids deviating from the median in the selected area.

5.2. Comparing Different Approaches to Applying Coincidence Factors

5.2.1. Required Grid Reinforcement Measures

Besides different quantification methods, this study examines various approaches to applying coincidence factors (Table 5) and their suitability for quantifying future grid reinforcement needs. The latter is divided into the total (all 7114 grids) transformer capacity and total length of lines additionally installed to overcome grid restrictions. Similar to costs (Section 5.1), both are divided by selected non-published reference values and illustrated as pu values to fulfill all data protection criteria (Figure 9):

A consistent, single coincidence factor determined based on the average number of customers supplied by the MV/LV substation and applied to each grid (approach 1) neglects the grid's actual number of customers and misjudges grid conditions in many analyzed grids. As demonstrated in Figure 4, the coincidence factor strongly correlates with the number of customers. Hence, this method overestimates the coincidence factor at the MV/LV substation in grids with considerably more households than the average grid (applied to calculate the coincidence factor in this method). Vice versa, it underestimates the coincidence factor at the MV/LV substation in grids with considerably fewer households. Consequently, the required transformer extensions determined by this method exceed all remaining approaches' results by 3.22 pu (4.00 pu in total). Since all the other approaches determine grid-specific coincidence factors for the MV/LV substation (feeder level 1), they indicate the same transformer reinforcements, i.e., 0.78 pu (Figure 9). However, the significant discrepancy between consistent and grid-specific coincidence factors (413%) demonstrates the importance of determining the actual coincidence factor at the MV/LV substation for each grid individually. Otherwise, potential grid restrictions are misjudged significantly.

The investigated approaches to applying coincidence factors also differ concerning their resulting line extension needs (Figure 9): Applying single coincidence factors, defined according to the number of customers the MV/LV substation supplies, reveals total line extensions of 0.66 pu (approach 1: Consistent) and 0.24 pu (approach 2: Grid-specific). A value of 0.63 pu is detected, considering grid-specific, double coincidence factors at the MV/LV substation and each feeder's main line (approach 3, feeder level 1 and 2). Simulating each feeder level, including grid-specific, multiple coincidence factors (approach 4), provides a total line extension of 1.20 pu.

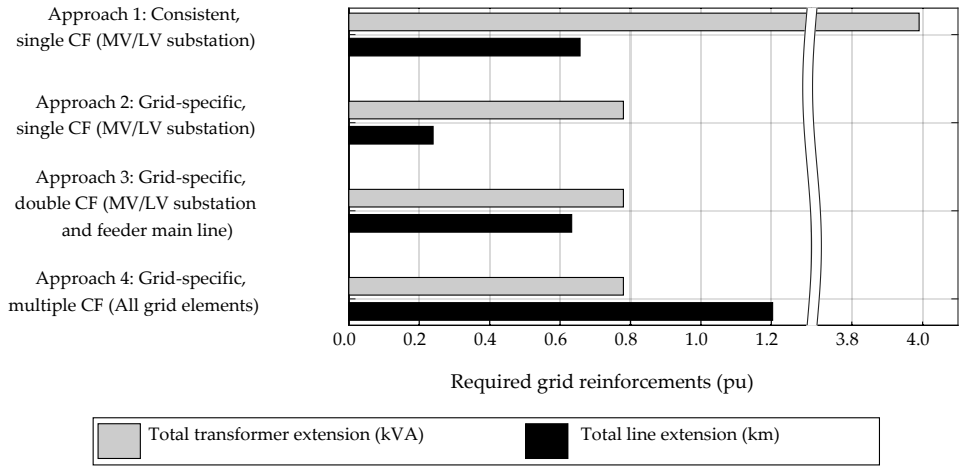

Figure 9. Comparison of different approaches to applying coincidence factors (CF) regarding the required transformer- and line extensions (7114 LV grids simulated).

These results demonstrate the importance of applying grid customers' coincidence factors appropriately: Considering single coincidence factors based on grid elements in feeder level 1 (MV/LV substation) underestimates grid loads at higher feeder levels since coincidence factors rise with lower numbers of customers (Figure 4). Hence, using these methods, the sum of indicated line extension measures in all 7114 LV grids is 45% (approach 1: Consistent) and 80% (approach 2: Grid-specific) lower than the exact consideration of all feeder levels (approach 4). As already mentioned, the consistent coincidence factor of 0.26 (applied in approach 1) overestimates the coincidence factor for many grids' MV/LV substation (feeder level 1). However, since the coincidence factor increases with an increasing feeder level (decreasing number of grid customers), it estimates grid loads at higher feeder levels and line congestions more appropriately (Figure 9).

Even the application of grid-specific, double coincidence factors (approach 3) according to the MV/LV substation and each feeder's main line (feeder level 1 and 2) underestimates the total length of additionally required lines (Figure 9): Only 53% of line reinforcement measures are indicated compared to considering grid customers' coincidence for each grid element in approach 4 (all feeder levels). This discrepancy demonstrates that in the investigated LV grids, a large part of grid reinforcements are required at higher feeder levels, i.e., grid elements distanced from the MV/LV substation.

5.2.2. Required Grid Reinforcement Costs

Similar to Section 5.1, the total grid reinforcement costs, determined using various approaches to applying coincidence factors, are divided by a non-published reference value and illustrated as pu values (Figure 10). This study uses the same cost parameters of transformer- and line reinforcements for each approach (Table 3). However, due to significant differences concerning the required grid reinforcement measures (Figure 9), the examined applications of coincidence factors evaluate total grid reinforcement costs differently. Consistent, single coincidence factors (approach 1) result in total grid reinforcement costs of 1.09 pu (Figure 10). Determining single coincidence factors (MV/LV substation) for each grid individually provides total grid reinforcement costs of 0.33 pu (approach 2). Considering each grid's coincidence factor at the MV/LV substation and each feeder's main line and applying both for load flow simulations increases the required costs to 0.72 pu (approach 3). Applying grid-specific, multiple coincidence factors depending on the grid element to be analyzed (approach 4) detects total costs of 1.29 pu, which are needed to prevent potential grid congestions in the analyzed scenario.

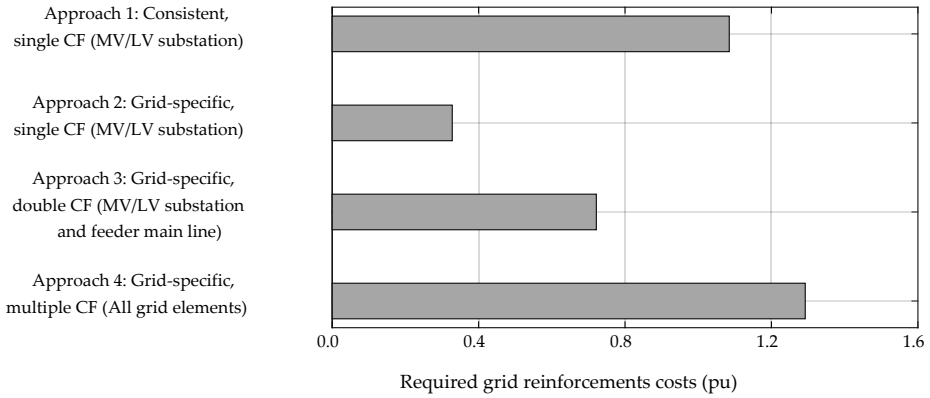

Figure 10. Comparison of different approaches to applying coincidence factors (CF) regarding the required grid reinforcement costs (7114 LV grids simulated).

The comparison of all approaches reveals the following insights: Applying consistent, single coincidence factors to each grid, the overestimation of required transformer extensions, and the underestimation of required line extensions partly balance each other out (Figure 9). Based on the specific cost parameters selected in this study (Table 3), the underestimation of required line extension measures more decisively affects total grid reinforcement costs. As a result, only 84% (−16%) of the grid reinforcement costs in approach 4 (1.29 pu) are also depicted using this simplified method (Figure 10). Compared to the application of one consistent coincidence factor to each grid (approach 1), grid-specific values (approach 2) misjudge required line extensions more decisively (Figure 9). Due to a more expensive reinforcement of grid lines (compared to transformers), total grid reinforcement costs deviate even more (−74%).

The consideration of grid-specific, double coincidence factors (approach 3), according to the MV/LV substation and at each feeder's main line, increases the detected costs. However, even this method misjudges total grid reinforcement costs substantially: Compared to grid-specific, multiple coincidence factors (simulating each feeder level), costs are underestimated by 44%.

5.2.3. Computing Time

Each approach to applying coincidence factors (Table 5) is tested with the same computing power (32 CPUs, 3 GHz, 128 GB RAM) using the developed large-scale grid simulation tool. However, since they vary in the number of simulated feeder levels, hence, load flow simulations, they show significant differences in the required computing time (Figure 11): Applying single coincidence factors to each grid customer (either consistent or grid-specific) requires one load flow simulation per grid (approaches 1–2). Thus, these methods allow the simulation of all 7114 LV grids in 0.24 h, which corresponds to 1.16 s per 1000 grid nodes (Figure 11).

Two load flow simulations per grid (approach 3), necessary to apply double coincidence factors to grid customers, increase the computing time to 0.45 h for all grids or 2.19 s per 1000 nodes.

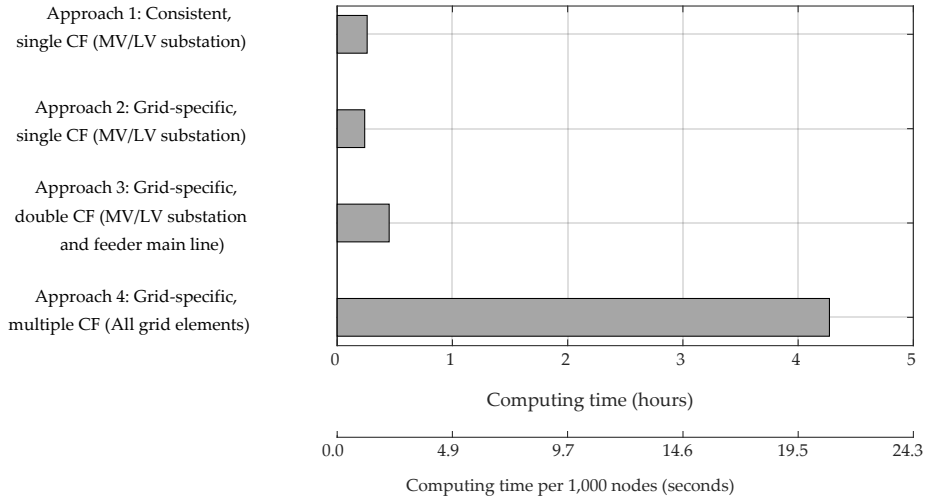

Figure 11. Comparison of different approaches to applying coincidence factors (CF) regarding the required computing time (7114 LV grids simulated).

Finally, individually considering grid customers' coincidence factor for each grid element to be analyzed (approach 4) requires 4.27 h in total or 20.77 s per 1000 nodes (Figure 11). The 17.8-times longer computing time, compared to the application of single coincidence factors, correlates with 16.2-times more feeder levels to be simulated on average per grid.

6. Discussion and Outlook

This section discusses the paper's results (Section 5) and its contribution to the current state of research. Furthermore, it provides an outlook on further work necessary in this field of research. Therefore, this section is divided according to the presented research questions unanswered by the current state of research (Section 3).

6.1. What Is the Potential Error When Simulating Only a Few Individually Selected LV Grids and Scaling Their Results to Quantify Grid Reinforcement Costs in a Large Area?

Present-day LV grids show high discrepancies regarding their maximum hosting capacity considering EVs, PVMs, and HPs [8]. This paper's results identify the impact of LV grids' heterogeneity on quantifying future grid reinforcement costs: Considering the analyzed grid area, simulating only a few individually selected grids and scaling their results leads to a broad spectrum of total grid reinforcement costs (Figure 8): If, for example, about 200 grids are selected for load flow simulation (cf. [20,21]), the total costs might deviate between -66% and +82% from the actual value. Assuming actual grid reinforcement costs of 42.5 billion euros [20], this equals a deviation between -28.0 and +34.9 billion euros. Using statistical data to select representative grids (in this work, the root mean square deviation to the median) only slightly decreases the potential error compared to an arbitrary selection of grids to be simulated (Figure 8).

If even fewer grids are simulated, the potential error increases significantly, and the selection of which grids to simulate becomes more crucial. Even if grids are classified depending on their grid region, the simulation of a few grids per region is insufficient to adequately determine overall grid reinforcement costs (Figure 8). However, while this study investigates only one grid per region, selecting other or more grids per region might increase this method's accuracy. Nevertheless, grid topologies at the LV level significantly fluctuate, even within the same region (urban, suburban, or rural) [48]. Thus, when simulating multiple grids per region, the question of which grids to simulate arises again.

6.2. How Many Grids (in %) Must Be Simulated to Assure a Certain Degree of Accuracy?

The more LV grids are analyzed using load flow simulations, the more accurate future grid reinforcement costs can be estimated (Figure 8). Though, considering the area investigated in this study, up to 5800 grids (82%) must be selected arbitrarily and simulated to enable accuracy of 95%. Decreasing the acceptable accuracy to 85% still requires the simulation of 2800 LV grids (39%).

As demonstrated in Figure 8, selecting representative grids based on statistical data only slightly increases the reliability of results: In some cases, for example, simulating the 4600 (or 5200) most representative grids in the investigated area, total grid reinforcement costs can be determined very accurately (100%). Nevertheless, the acquired results deviate to the same extent as randomly selecting grids. Consequently, the large-scale quantification of potential grid reinforcement costs with adequate accuracy requires simulating several thousand LV grids.

6.3. Impact of the Analyzed Grid's Variance

It has to be mentioned that this work compares the presented quantification methods only for one Austrian DSO and its LV grids (Section 4.2). Despite similarities to LV grids investigated in other studies (e.g., [49–51]), applying the presented insights to other DSOs, hence, different grid topologies and grid planning strategies, requires further investigations. For example, a DSO operating LV grids with similar topology as well as customer density and types may provide deviating results. On this account, we additionally analyze the impact of LV grids' variance on the share of recommended grids to be simulated. Therefore, similar LV grids are picked from all the LV grids (7114) based on statistical data to establish two classes with different variance: According to Levi et al. [46], Class 1 includes LV grids with a total line length within the 25%-(1.69 km) and 75%-quantile (4.41 km) of all grids. In addition to the total line length, the number of customers per point of common coupling is limited to the 25%-(1.25) and 75%-quantile (2.27) to further decrease the variance of LV grids in class 2. For each class, the share of selected, simulated, and scaled grids is varied between 0–100% (Figure 12).

Decreasing the variance of analyzed LV grids, hence, analyzing more similar grids, allows higher accuracy if simulating only a small share of all grids: Between 0–10% share of simulated grids, the average error is decreased to 13.8% (class 1) and 16.7% (class 2), compared to 32.6% when analyzing all 7114 LV grids (Figure 8). However, despite the lower variance in total line length and customers per point of common coupling, the potential error increases if simulating more grids (>10%): From a maximum error of 23% when analyzing all 7114 grids to 24% (class 1) and 28% (class 2) when analyzing more similar grids (Figure 12).

These results demonstrate that even if the analyzed LV grids show a lower variance, their required reinforcement costs due to future customers might deviate substantially. Consequently, the potential error when simulating representative grids and scaling their results to the whole area of investigation grids must not be neglected.

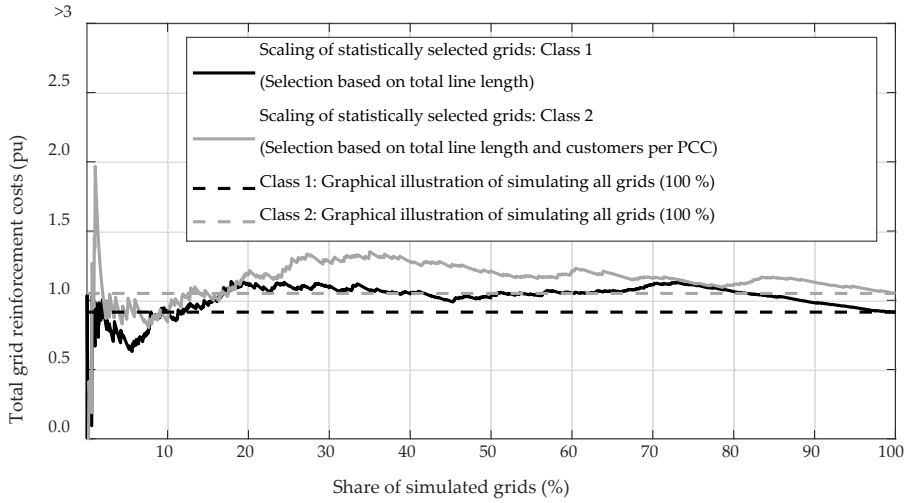

Figure 12. Comparison of scaling statistically selected LV grids' results for two grid classes, classified according to the total line length and the number of customers per point of common coupling (PCC).

As illustrated in Figure 12, LV grids vary significantly even within the same class. Hence, the same question arises when classifying grids into representative classes (cf. [5,7,19,20]). Only if grids are classified finely enough, and multiple grids are simulated per class, the scaling of grid reinforcement costs enables adequate accuracy. On the other hand, this approach requires lengthy pre-processing, with huge time- and computation effort [15]. In fact, recent studies using this approach (e.g., [5,20]) analyze all grids of Germany, which justifies time-consuming pre-processing. Since this study investigates one particular service area, including 7114 LV grids, this approach (including pre-processing) would require more time than the simulation of all grids. How to apply grid customers' coincidence factors to quantify grid reinforcement measures accurately (consistent or grid-specific; single or multiple; based on which grid element)?

Besides the necessity to simulate several thousand grids, this paper's results (Section 5.2) illustrate another crucial aspect to quantify required grid reinforcements adequately: The appropriate application of grid customers' coincidence factors. Therefore, this section provides relevant guidelines to accomplish that. While the question of which coincidence factors to use has already been answered in Thormann et al. [8], these guidelines focus on how to apply them for simulating numerous grids:

Firstly, assuming one consistent coincidence factor for each grid (approach 1) is inappropriate to identify grid conditions in several thousand LV grids. This method misjudges both required transformer (overestimated) and line extensions (underestimated) significantly (Figure 9). While in this study, both errors partly balance each other out regarding total grid reinforcement costs (Figure 10), this effect strongly depends on the selected cost parameters. Applying, for example, higher specific transformer costs might increase this method's error. Thus, each grid's coincidence factor must be specifically defined depending on its number of supplied customers to overcome this problem.

However, determining single coincidence factors according to the number of customers supplied by the MV/LV substation (approaches 1–2) misjudges grid elements at higher feeder levels, i.e., nodes, transformers, or lines more distanced to the MV/LV substation. The application of double coincidence factors, based on the number of customers supplied by the MV/LV substation and each feeder's main line (Figure 3), only slightly increases the accuracy of results (approach 3). Consequently, grid customers' actual coincidence factor must be defined individually for each grid element depending on the number of supplied customers (approach 4). Only then, future grid reinforcement measures and resulting costs can be calculated accurately. As demonstrated in Section 2.3, the current state

of research, using coincidence factors [6,7,10,20,23,26], neglects these guidelines. Consequently, their estimated grid reinforcement costs due to future EVs, PVMs, and HPs, might be even higher.

Nevertheless, discrepancies between the analyzed approaches to use coincidence factors apply to the investigated service area with primarily suburban and rural LV grids. Considering grid customers' coincidence only at the MV/LV substation or each feeder's main line might be more accurate if applied to urban LV grids, often characterized by fewer grid nodes. Furthermore, due to the selected cost parameters (Table 3), line extensions more significantly affect total grid reinforcement costs than the installation of additional transformers. Cost deviations between the analyzed approaches might be lower, applying higher transformer costs. On this account, the impact of various grid topologies, grid planning strategies, and cost parameters on this issue will be analyzed in further studies.

6.4. What Is the Trade-Off between the Acquired Simulation Accuracy and Required Computing Time?

As demonstrated in Section 4.1.3, the coincidence factor of each grid customer can be considered accurately by simulating multiple feeder levels (Section 4.1.3). While this measure increases the accuracy of grid simulations (Figure 9), it increases the required computing time (Figure 11). However, what is the trade-off between the results' accuracy and required computing time? In other words: How many feeder levels must be simulated to determine grid reinforcement costs adequately? To answer this question, we vary the number of simulated feeder levels from one (determining single coincidence factors) to all feeder levels (determining multiple coincidence factors, according to the grid element to be analyzed) when simulating all 7114 LV grids. Furthermore, we compare the determined total grid reinforcement costs and the required computing time (Figure 13).

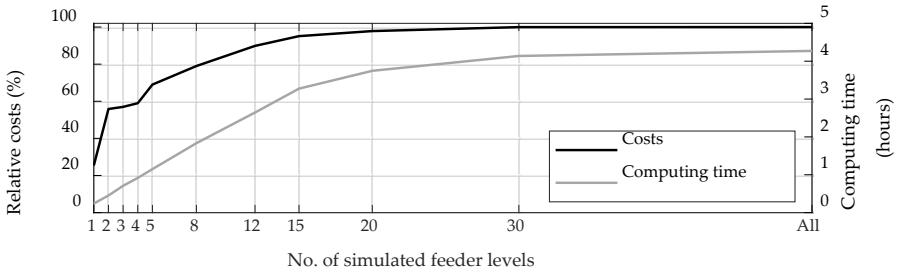

Figure 13. Grid reinforcement costs (relative to the simulation of all feeder levels) and required computing time depending on the number of simulated feeder levels.

This time, costs are referred to the value of 1.29 pu (Figure 10), acquired by the most accurate application of coincidence factors (simulation of all feeder levels). As demonstrated in Section 5.2, the simulation of one or two feeder levels allows fast computation (0.24 and 0.45 h). Though, it results in lower costs (26% and 56%) than the simulation of all feeder levels. Despite twice the computing time (0.90 h), a further increase to four feeder levels to be simulated only slightly increases accuracy (+3%). This effect is because only a few customers are connected between feeder levels 2 and 4, inhibiting a more accurate consideration of customers' coincidence. However, at least 95% accuracy requires the simulation of at least 15 feeder levels (Figure 13), which requires 3.3 h of computation. Since not all LV grids are characterized by more than 15 feeder levels, the simulation of all feeder levels only slightly enhances the accuracy of results (+5%). Though, it extends the required computing time by one hour (+23%).

6.5. How to Quantify Future Grid Reinforcement Costs Allowing Both High Accuracy and Adequate Computing Time in the Most Optimal Way?

While Section 5.1 highlights the need for large-scale grid simulations to quantify future grid reinforcement costs, Section 5.2 demonstrates two criteria they should comply with: Applying grid customers' coincidence factors appropriately depending on the grid element to be analyzed and keeping the required computing time adequate. Both criteria are fulfilled using the developed large-scale grid simulation tool (Section 4.1). The former is tackled by simulating multiple feeder levels and adapting grid customers' coincidence factors accordingly. Thereby, temporal interdependences between existing (e.g., households) and future customers (EVs, PVMs, and HPs) are accounted for accurately.

Despite the simulation of multiple feeder levels, the required computing time remains reasonable: 20.8 s per 1000 grid nodes. Assuming 104 nodes per grid on average (Section 4.2), about 1600 LV grids can be simulated per hour. In conclusion, the developed tool enables the fast quantification of future grid reinforcement measures and costs with high accuracy. Thereby, it helps to avoid the misjudgment of future power grid investments caused by poor grid selection and inadequate applications of coincidence factors.

Besides classic grid reinforcements (e.g., exchange of transformers or grid lines), grid congestions caused by future customers can be limited or even be prevented by grid-relieving measures. Grid restrictions on the LV level triggered by future EVs can successfully be reduced by demand-side measures, e.g., the adaption of charging power based on appropriate user tariffs [57–62]. Furthermore, the conventional power system's transition towards a power electronics-based power system promotes the provision of grid ancillary services, such as active- or reactive power control. Recent studies [63–68] demonstrated these measures' potential to mitigate grid overloads. Based on their grid-relieving impact, these measures can save investment costs of the DSO by delaying the upgrade of LV infrastructure, such as adding new cables [69,70]. According to Durusut et al. [24], demand-side measures, for example, can reduce the required grid reinforcement costs by 7% in the UK.

However, the potential of grid-relieving measures to mitigate grid restrictions strongly depends on the investigated grid and its region [71]: While urban LV grids are rather characterized by thermal overload, suburban and rural ones are more likely to face voltage violations [8]. Consequently, the quantification of future grid reinforcement costs implementing these measures in a large area will once again require the simulation of numerous grids. Since this paper focuses on comparing different methods to quantify grid reinforcement costs (and not the determined costs themselves), grid-relieving measures are neglected in this work. Nevertheless, the authors will further develop the presented automated large-scale grid simulation tool and implement various flexibility options (e.g., demand-side management, active- and reactive power control, energy storage systems). Thereby, various grid-relieving measures as a countermeasure to classic grid reinforcements can be evaluated considering a large area with several thousand grids.

In addition, the developed large-scale grid simulation tool is restricted in its current version to static deterministic load flow simulations. On the one hand, those provide significant advantages regarding the required computing time when simulating several thousand LV grids. On the other, they inhibit the consideration of time-related effects, crucial to investigate the duration of grid restrictions (e.g., the long-term of thermal overloads) and the potential of flexibility options (e.g., the implementation of energy storages or demand-side measures).

The authors' following works will further extend the grid simulation tool to allow both fast computation and the consideration of time-related effects: Static deterministic grid simulations are initially performed for several thousand grids to identify potentially endangered grids (based on worst-case conditions). Endangered grids are further examined based on time series-based load flow simulations regarding the duration of grid ele-

ments and the potential for implementing grid-relieving measures. Furthermore, the developed tool will be provided as open-source MATLAB code (e.g., GitHub, MATLAB File Exchange) to allow its free application by the scientific community and grid planners.

7. Conclusions

In the analyzed service area operated by an Austrian distribution system operator, low-voltage grids differ significantly in topology and grid customers. As a result, the applied quantification method (scaling of simulated grids' results or simulating all grids) has a significant influence on quantifying future grid reinforcement costs: The simulation of only a few grids and the scaling of their grid reinforcement costs to the whole service area strongly depends on the selected grids. In case of a poor grid selection, total grid reinforcement costs in the analyzed area might be misjudged significantly using this quantification method. The classification of low-voltage grids in the analyzed area according to their region or grid parameters (e.g., number of customers, total line length) only slightly increases the reliability of results. Consequently, large-scale grid simulations are crucial to quantify grid reinforcement costs triggered by future electric vehicles, photovoltaic modules and electric heat pumps. By varying the approach to applying coincidence factors, this work additionally highlights the importance of accurate grid simulations when quantifying grid reinforcement costs: Simplified approaches, often applied in the current state of research, require only one or two load flow simulations per grid and allow a fast investigation of several thousand grids. Nevertheless, their misjudgment of grid customers' coincidence factor when evaluating remaining grid elements underestimates required grid reinforcement measures and costs. As a countermeasure, multiple coincidence factors must be applied to grid customers, according to the grid element to be analyzed. While this measure moderately increases the total computing time, it decisively enhances the acquired simulation accuracy.

Knowing the substantial influence of the applied quantification method and the application of coincidence factors helps classify recent studies in this field and their results. Furthermore, the large-scale grid simulation tool developed in this study enables additional analyses by investigating several thousand low-voltage grids with reasonable computing effort. In contrast to recently published grid simulation tools, grid customers' coincidence factors are accurately considered. Thereby, future grid reinforcement costs due to electric vehicles, photovoltaic modules, or electric heat pumps can accurately be determined while keeping the required computing time adequate.

Author Contributions: Conceptualization, B.T. and T.K.; Data curation, B.T.; Formal analysis, B.T.; Funding acquisition, T.K.; Investigation, B.T.; Methodology, B.T. and T.K.; Project administration, T.K.; Resources, B.T. and T.K.; Software, B.T.; Supervision, T.K.; Validation, B.T. and T.K.; Visualization, B.T.; Writing—original draft, B.T.; Writing—review & editing, T.K. All authors have read and agreed to the published version of the manuscript.

Funding: This research received no external funding.

Conflicts of Interest: The authors declare no conflict of interest.

References

1. European Commission. *Communication from the Commission to the European Parliament, the European Council, the Council, the European Economic and Social Committee and the Committee of the Regions*: *The European Green Deal*; European Commission: Brussels, Belgium, 2019.
2. Austrian Federal Government. Government Program 2020–2024: Out of a Sense of Responsibility for Austria. Available online: https://www.bmoeds.gv.at/Ministerium/Regierungsprogramm.html (accessed on 31 January 2020).
3. European Parliament; Council. *Directive 2010/31/EU of the European Parliament and of the Council of 19 May 2010 on the Energy Performance of Buildings*; EUR-Lex: Luxembourg, 2010.
4. Mulenga, E.; Bollen, M.H.; Etherden, N. A review of hosting capacity quantification methods for photovoltaics in low-voltage distribution grids. *Int. J. Electr. Power Energy Syst.* **2020**, *115*, 105445. https://doi.org/10.1016/j.ijepes.2019.105445.

5. Büchner, J.; Katzfey, J.; Flörcken, O.; Moser, A.; Schuster, H.; Dierkes, S.; van Leeuwen, T.; Verheggen, L.; Uslar, M.; van Amelsvoort, M. Moderne Verteilnetze fuer Deutschland. Verteilernetzstudie, 2014. Available online: www.bmwi.de/Redaktion/DE/Publikationen/Studien/verteilernetzstudie.html (accessed on 18 August 2021).
6. Gupta, R.; Pena-Bello, A.; Streicher, K.N.; Roduner, C.; Farhat, Y.; Thöni, D.; Patel, M.K.; Parra, D. Spatial analysis of distribution grid capacity and costs to enable massive deployment of PV, electric mobility and electric heating. *Appl. Energy* **2021**, *287*, 116504. https://doi.org/10.1016/j.apenergy.2021.116504.
7. Agora Verkehrswende; Agora Energiewende. Regulatory Assistance Project (RAP). Verteilnetzausbau für die Energiewende–Elektromobilität im Fokus. 2019. Available online: https://www.agora-verkehrswende.de/veroeffentlichungen/studie-verteilnetzausbau-fuer-die-energiewende (accessed on 12 February 2021).
8. Thormann, B.; Kienberger, T. Evaluation of Grid Capacities for Integrating Future E-Mobility and Heat Pumps into Low-Voltage Grids. *Energies* **2020**, *13*, 5083. https://doi.org/10.3390/en13195083.
9. Salah, F.; Ilg, J.P.; Flath, C.M.; Basse, H.; van Dinther, C. Impact of electric vehicles on distribution substations: A Swiss case study. *Appl. Energy* **2015**, *137*, 88–96. https://doi.org/10.1016/j.apenergy.2014.09.091.
10. Association of Austrian Electricity Companies. Netzberechnungen Österreich-Einfluss der Entwicklungen von Elektromobilität und Photovoltaik auf das österreichische Stromnetz. Available online: www.oesterreichsenergie.at/die-welt-des-stroms/stromnetze/studie-netzberechnungen-oesterreich.html (accessed on 5 January 2021).
11. Horowitz Kelsey, A.W.; Ding, F.; Mather, B.; Palmintier, B. The Cost of Distribution System Upgrades to Accommodate Increasing Penetrations of Distributed Photovoltaic Systems on Real Feeders in the United States. Available online: www.nrel.gov/docs/fy18osti/70710.pdf (accessed on 3 November 2021).
12. Li, G.; Zhang, X.-P. Modeling of Plug-in Hybrid Electric Vehicle Charging Demand in Probabilistic Power Flow Calculations. *IEEE Trans. Smart Grid* **2012**, *3*, 492–499. https://doi.org/10.1109/TSG.2011.2172643.
13. Grainger, J.J.; Stevenson, W.D. *Power System Analysis*; McGraw-Hill: New York, NY, USA, 1994; ISBN 0-07-113338-0.
14. Werth, T. *Netzberechnung mit Erzeugungsprofilen*; Springer Fachmedien Wiesbaden: Wiesbaden, Germany, 2016; ISBN 978-3-658-12727-5.
15. Eberl, T.; Hufendiek, K.; Wiest, P.; Rudion, K. Integrale Modellierung von Verteilnetzen und Verteilter Erzeugung. 2014. Available online: www.ieh.uni-stuttgart.de/forschung/forschungsprojekte/integrale-modellierung-von-verteilnetzen-und-verteilter-erzeugung (accessed on 1 April 2021).
16. Navarro-Espinosa, A.; Mancarella, P. Probabilistic modeling and assessment of the impact of electric heat pumps on low voltage distribution networks. *Appl. Energy* **2014**, *127*, 249–266. https://doi.org/10.1016/j.apenergy.2014.04.026.
17. Torres, S.; Durán, I.; Marulanda, A.; Pavas, A.; Quirós-Tortós, J. Electric vehicles and power quality in low voltage networks: Real data analysis and modeling. *Appl. Energy* **2022**, *305*, 117718. https://doi.org/10.1016/j.apenergy.2021.117718.
18. Tie, C.H.; Gan, C.K.; Ibrahim, K.A. The impact of electric vehicle charging on a residential low voltage distribution network in Malaysia. In *Proceedings of the 2014 IEEE Innovative Smart Grid Technologies-Asia (ISGT Asia) Conference, Kuala Lumpur, Malaysia, 20–23 May 2014*; IEEE: Piscataway, NJ, USA, 2014; pp 272–277.
19. Vu, T. *A Stochastic Methodology to Determine Reinforcement Cost of Power Distribution Grid for Integrating Increasing Share of Renewable Energies and Electric Vehicles*; IEEE: Piscataway, NJ, USA, 2018; pp. 1–5. https://doi.org/10.1109/EEM.2018.8469890.
20. Agricola, A.; Höflich, B.; Richard, P.; Völker, J.; Rehtanz, C.; Greve, M.; Gwisdorf, B.; Kays, J.; Noll, T.; Schwippe, J.; et al. Dena-Verteilnetzstudie. Ausbau- und Innovationsbedarf der Stromverteilnetze in Deutschland bis 2030. Energiesysteme und Energiedienstleistungen: Berlin, Germany. 2012. Available online: https://www.dena.de/themen-projekte/projekte/energiesysteme/dena-verteilnetzstudie/ (accessed on 1 April 2021).
21. Matrose, C.; Helmschrott, T.; Godde, M.; Szczechowicz, E.; Schnettler, A. Impact of different electric vehicle charging strategies onto required distribution grid reinforcement. In *Proceedings of the 2012 IEEE Transportation Electrification Conference and Expo. (ITEC), Dearborn, MI, USA, 18–20 June 2012*; Staff, I., Ed.; IEEE: Piscataway, NJ, USA, 2012; pp 1–5.
22. Pudjianto, D.; Djapic, P.; Dragovic, J.; Strbac, G. Grid Integration Cost of Photovoltaic Power Generation. Available online: https://helapco.gr/pdf/PV_PARITY_D44_Grid_integration_cost_of_ (accessed on 14 January 2022).
23. Hartvigsson, E.; Odenberger, M.; Chen, P.; Nyholm, E. Estimating national and local low-voltage grid capacity for residential solar photovoltaic in Sweden, UK and Germany. *Renew. Energy* **2021**, *171*, 915–926. https://doi.org/10.1016/j.renene.2021.02.073.
24. Durusut, E.; Slater, S.; Strbac, G.; Pudjianto, D.; Djapic, P.; Aunedi, M. *Infrastructure in a Low-Carbon Energy System to 2030. Transmission and Distribution: Final Report*; Imperial College London: London, UK, 2014.
25. Flinn, J.; Webber, C.; Tong, N.; Cox, R. *Customer Distributed Energy Resources Grid Integration Study: Residential Zero Net Energy Building Integration Cost Analysis*; California Public Utilities Commission: San Francisco, CA, USA, 2017.
26. Lemmens, J.; Macharis, B.; Gys, R.; Vonken, D. *Data-Driven Asset Management with the NGIN Analytics Platform: Assessing EV and PV Impact on the Flemish LV Grid*; CIRED: Liège, Belgium, 2019.
27. Rothrock, L.; Narayanan, S. *Human-in-the-Loop Simulations*; Springer London: London, UK, 2011; ISBN 978-0-85729-882-9.
28. Willis, H.L. *Power Distribution Planning Reference Book*, 2. ed.; CRC Press: Boca Raton, FL, USA, 2004; ISBN 0824748751.
29. Resch, M.; Bühler, J.; Klausen, M.; Sumper, A. Impact of operation strategies of large scale battery systems on distribution grid planning in Germany. *Renew. Sustain. Energy Rev.* **2017**, *74*, 1042–1063. https://doi.org/10.1016/j.rser.2017.02.075.
30. Bielecki, S. Estimation of maximum loads of residential electricity users. *E3S Web Conf.* **2019**, *137*, 1006. https://doi.org/10.1051/e3sconf/201913701006.

31. Wahl, M.; Hein, L.; Moser, A. Fast Power Flow Calculation Method for Grid Expansion Planning. In Proceedings of the 2019 21st European Conference on Power Electronics and Applications (EPE '19 ECCE Europe), Genova, Italy, 3–5 September 2019; pp. 1–7.
32. Scheidler, A.; Braun, M.; Kraiczy, M. Automated Grid Planning for Distribution Grids with Increasing PV Penetration. In Proceedings of the 6th Solar Integration Workshop, Vienna, Austria, 14–15 November 2016.
33. Ulffers, J.; Scheidler, A.; Töbermann, J.-C.; Braun, M. Grid Integration Studies for eMobility Scenarios with Comparison of Probabilistic Charging Models to Simultaneity Factors. In Proceedings of the 2nd E-Mobility Power System Integration Symposium, Delft, The Netherlands, 10 October 2018.
34. NEPLAN AG. NEPLAN.; Küsnacht, Switzerland. Available online: https://www.neplan.ch/?lang=de (accessed on 14 February 2022)
35. DIgSILENT GmbH. PowerFactory.; Gomaringen, Germany. Available online: https://www.digsilent.de/de/powerfactory.html (accessed on 14 February 2022)
36. Fox, B.; Morrow, J.D.; Akmal, M.; Littler, T. Impact of heat pump load on distribution networks. *IET Gener. Transm. Distrib.* **2014**, *8*, 2065–2073. https://doi.org/10.1049/iet-gtd.2014.0056.
37. Protopapadaki, C.; Saelens, D. Heat pump and PV impact on residential low-voltage distribution grids as a function of building and district properties. *Appl. Energy* **2017**, *192*, 268–281. https://doi.org/10.1016/j.apenergy.2016.11.103.
38. Widén, J.; Wäckelgård, E.; Paatero, J.; Lund, P. Impacts of distributed photovoltaics on network voltages: Stochastic simulations of three Swedish low-voltage distribution grids. *Electr. Power Syst. Res.* **2010**, *80*, 1562–1571. https://doi.org/10.1016/j.epsr.2010.07.007.
39. Pflugradt, N. Online Load Profile Generator. Available online: https://www.loadprofilegenerator.de (accessed on 8 December 2021).
40. Heffernan, W.; Watson, N.R.; Buehler, R.; Watson, J.D. Harmonic performance of heat-pumps. *J. Eng.* **2013**, *2013*, 31–44. https://doi.org/10.1049/joe.2013.0012.
41. Kusch, W.; Stadler, I.; Bhandari, R. Heat pumps in low voltage distribution grids by energy storage. In Proceedings of the 2015 International Energy and Sustainability Conference (IESC), Farmingdale, NY, USA, 12–13 Novermber 2015; pp. 1–6. https://doi.org/10.1109/IESC.2015.7384386.
42. UNE. *Voltage Characteristics of Electricity Supplied by Public Electricity Networks*; EN 50160; Beuth: Berlin, Germany, 2011.
43. Laribi, O.; Rudion, K. Optimized Planning of Distribution Grids Considering Grid Expansion, Battery Systems and Dynamic Curtailment. *Energies* **2021**, *14*, 5242. https://doi.org/10.3390/en14175242.
44. Scheffler, J. *Verteilnetze auf dem Weg zum Flächenkraftwerk*; Springer: Berlin/Heidelberg, Germany, 2016. https://doi.org/10.1007/978-3-642-55297-7.
45. Cloteaux, B. Limits in Modeling Power Grid Topology. In Proceedings of the 2013 IEEE 2nd Network Science Workshop (NSW), West Point, NY, USA, 29 April–1May 2013. https://doi.org/10.1109/NSW.2013.6609189.
46. Levi, V.; Strbac, G.; Allan, R. Assessment of performance-driven investment strategies of distribution systems using reference networks. *IEE Proc. Gener. Transm. Distrib.* **2005**, *152*, 1. https://doi.org/10.1049/ip-gtd:20041109.
47. Traupmann, A.; Kienberger, T. Test Grids for the Integration of RES—A Contribution for the European Context. *Energies* **2020**, *13*, 5431. https://doi.org/10.3390/en13205431.
48. Postigo Marcos, F.; Mateo Domingo, C.; Gómez San Román, T.; Palmintier, B.; Hodge, B.-M.; Krishnan, V.; de Cuadra García, F.; Mather, B. A Review of Power Distribution Test Feeders in the United States and the Need for Synthetic Representative Networks. *Energies* **2017**, *10*, 1896. https://doi.org/10.3390/en10111896.
49. Scheffler, J. Bestimmung der Maximal Zulässigen Netzanschlussleistung Photovoltaischen Energiewandlungsanlagen in Wohnsiedlungsgebieten. Ph.D. Thesis, Technischen Universität Chemnitz, Düsseldorf, Germany, 2004.
50. Pagani, G.A.; Aiello, M. Towards Decentralization: A Topological Investigation of the Medium and Low Voltage Grids. *IEEE Trans. Smart Grid* **2011**, *2*, 538–547. https://doi.org/10.1109/TSG.2011.2147810.
51. Strunz, K.; Fletcher, R.H.; Campbell, R.; Gao, F. Developing benchmark models for low-voltage distribution feeders. In Proceedings of the 2009 IEEE Power & Energy Society General Meeting, Calgary, AB, Canada, 26–30 July 2009; pp. 1–3. https://doi.org/10.1109/PES.2009.5260227.
52. Umweltbundesamt GmbH. Elektromobilität in Österreich: Szenario 2020 und 2050. REP-0257, 2010. Available online: https://www.umweltbundesamt.at/fileadmin/site/publikationen/REP0257.pdf (accessed on 18 July 2021).
53. Fechner, H. Ermittlung des Flächenpotentials für den Photovoltaik-Ausbau in Österreich: Welche Flächenkategorien sind für die Erschließung von Besonderer Bedeutung, um das Ökostromziel Realisieren zu Können, Vienna. 2020. Available online: https://oesterreichsenergie.at/downloads/publikationsdatenbank/detailseite/photovoltaik-ausbau-in-oesterreich (accessed on 25 December 2021).
54. Fraunhofer IWES/IBP. Wärmewende 2030: Schlüsseltechnologien zur Erreichung der mittel- und Langfristigen Klimaschutzziele im Gebäudesektor. Available online: https://www.agora-energiewende.de/fileadmin/Projekte/2016/Sektoruebergreifende_EW/Waermewende-2030_WEB.pdf (accessed on 30 July 2021).
55. European Commision. Degree of Urbanisation (DEGURBA)-Local Administrative Units. Available online: https://ec.europa.eu/eurostat/ramon/miscellaneous/index.cfm?TargetUrl=DSP_DEGURBA (accessed on 26 June 2020).
56. Kadam, S. Defintion and Validation of Reference Feeders for Low-Voltage Networks. Ph.D. Thesis. Available online: https://repositum.tuwien.at/handle/20.500.12708/7709 (accessed on 18 August 2021).

57. Shao, S.; Pipattanasomporn, M.; Rahman, S. Demand Response as a Load Shaping Tool in an Intelligent Grid with Electric Vehicles. *IEEE Trans. Smart Grid* **2011**, *2*, 624–631. https://doi.org/10.1109/TSG.2011.2164583.
58. Faddel, S.; Mohammed, O.A. Automated Distributed Electric Vehicle Controller for Residential Demand Side Management. *IEEE Trans. Ind. Appl.* **2019**, *55*, 16–25. https://doi.org/10.1109/TIA.2018.2866255.
59. Brinkel, N.; Schram, W.L.; AlSkaif, T.A.; Lampropoulos, I.; van Sark, W. Should we reinforce the grid? Cost and emission optimization of electric vehicle charging under different transformer limits. *Appl. Energy* **2020**, *276*, 115285. https://doi.org/10.1016/j.apenergy.2020.115285.
60. Richardson, P.; Flynn, D.; Keane, A. Local Versus Centralized Charging Strategies for Electric Vehicles in Low Voltage Distribution Systems. *IEEE Trans. Smart Grid* **2012**, *3*, 1020–1028. https://doi.org/10.1109/TSG.2012.2185523.
61. Clement-Nyns, K.; Haesen, E.; Driesen, J. The Impact of Charging Plug-In Hybrid Electric Vehicles on a Residential Distribution Grid. *IEEE Trans. Power Syst.* **2010**, *25*, 371–380. https://doi.org/10.1109/TPWRS.2009.2036481.
62. García-Villalobos, J.; Zamora, I.; Knezović, K.; Marinelli, M. Multi-objective optimization control of plug-in electric vehicles in low voltage distribution networks. *Appl. Energy* **2016**, *180*, 155–168. https://doi.org/10.1016/j.apenergy.2016.07.110.
63. Geth, F.; Leemput, N.; van Roy, J.; Buscher, J.; Ponnette, R.; Driesen, J. Voltage droop charging of electric vehicles in a residential distribution feeder. In *Proceedings of the 2012 3rd IEEE PES Innovative Smart Grid Technologies Europe (ISGT Europe 2012), International Conference and Exhibition, Berlin, Germany, 14–17 October 2012*; IEEE: Piscataway, NJ, USA, 2012; pp 1–8.
64. Ireshika, M.A.S.T.; Lliuyacc-Blas, R.; Kepplinger, P. Voltage-Based Droop Control of Electric Vehicles in Distribution Grids under Different Charging Power Levels. *Energies* **2021**, *14*, 3905. https://doi.org/10.3390/en14133905.
65. Al-Awami, A.T.; Sortomme, E.; Asim Akhtar, G.M.; Faddel, S. A Voltage-Based Controller for an Electric-Vehicle Charger. *IEEE Trans. Veh. Technol.* **2016**, *65*, 4185–4196. https://doi.org/10.1109/TVT.2015.2481712.
66. Zecchino, A.; Marinelli, M. Analytical assessment of voltage support via reactive power from new electric vehicles supply equipment in radial distribution grids with voltage-dependent loads. *Int. J. Electr. Power Energy Syst.* **2018**, *97*, 17–27. https://doi.org/10.1016/j.ijepes.2017.10.034.
67. Knezović, K.; Marinelli, M. Phase-wise enhanced voltage support from electric vehicles in a Danish low-voltage distribution grid. *Electr. Power Syst. Res.* **2016**, *140*, 274–283. https://doi.org/10.1016/j.epsr.2016.06.015.
68. Thormann, B.; Braunstein, R.; Wisiak, J.; Strempfl, F.; Kienberger, T. Evaluation of grid relieving measures for integrating electric vehicles in a suburban low-voltage grid. In *CIRED Conference Proceedings 2019*; CIRED: Liège, Belgium, 2019.
69. UK Power Networks. Network Impacts of Supply-Following Demand Response: Report A6. Available online: https://innovation.ukpowernetworks.co.uk (accessed on 14 February 2022).
70. Aigner, M.; Schmautzer, E.; Friedl, B.; Bliem, M.; Haber, A. Synergetic effects for DSOs and customers caused by the integration of renewables into the distribution network-Influences on business and national economics. In *CIRED Conference Proceedings 2015*; CIRED: Liège, Belgium, 2015.
71. Turton, H.; Moura, F. Vehicle-to-grid systems for sustainable development: An integrated energy analysis. *Technol. Forecast. Soc. Chang.* **2008**, *75*, 1091–1108. https://doi.org/10.1016/j.techfore.2007.11.013.

10.4 CIRED 2019

Evaluation of Grid Relieving Measures for Integrating Electric Vehicles in a Suburban Low-Voltage Grid

EVALUATION OF GRID RELIEVING MEASURES FOR INTEGRATING ELECTRIC VEHICLES IN A SUBURBAN LOW-VOLTAGE GRID

Bernd Thormann
Montanuniversitaet Leoben-Austria
bernd.thormann@unileoben.ac.at

René Braunstein
Energienetze Steiermark GmbH-Austria
rene.braunstein@e-netze.at

Johannes Wisiak
Energienetze Steiermark GmbH
johannes.wisiak@e-netze.at

Franz Strempfl
Energienetze Steiermark GmbH
franz.strempfl@e-netze.at

Thomas Kienberger
Montanuniversitaet Leoben
thomas.kienberger@unileoben.ac.at

ABSTRACT

Within this study the impacts of future electric vehicle penetrations on the low-voltage level are analyzed. Therefore, the need for grid expansions is prematurely identified based on a suburban grid, operated by the Austrian distribution system operator Energienetze Steiermark GmbH. The future development of electromobility-induced grid effects is demonstrated by simulating several electric vehicle penetration rates. Additionally, grid restrictions are counteracted by analyzing grid- and user-controlled measures.
The investigated suburban low-voltage grid could face inadmissible voltage range deviations per EN 50160 at an EV-penetration of only 10 %. Moreover, an increased share of electric vehicles leads to critical voltage unbalances (around 40 % EV) and thermal overloads (around 20 % EV). This study shows in addition, that voltage deviations are reduced significantly by several measures. Furthermore, grid expansions can be avoided by a charging infrastructure equipped with voltage-dependent active power control, or switching to three-phase charging with reduced power. These measures prevent inadmissible voltage range deviations and voltage unbalances as well as critical thermal conditions even at an 80 % electromobility penetration.

INTRODUCTION

The amount of traffic-related greenhouse gases in Austria increased by 67% between 1990 and 2016, triggered by higher mileage of passenger cars and trucks [1]. As a countermeasure, Austria's climate and energy strategy for 2030 aims for a carbon-free traffic sector by 2050, and accordingly, for an expansion of electric mobility in the upcoming years [2]. The rapid development of electric vehicles (EV) in Norway [3], a role model with respect to the implementation of electromobility, demonstrates the potential of how EV-incentives can help to increase the share of electrified vehicles. Austria's plan to increase the number of EV by monetary (funding for purchasing an EV, taxation benefits) and non-monetary (parking benefits) incentives [4, 5] should promote electromobility in a similar way. According to the Austrian Federal Environment Agency, the number of battery electric vehicles will reach 210,000 in 2020, when providing ideal political and environmental framework conditions [6].
The last years illustrated, that most charging processes take place at household charging stations [7]. As a result of little private charging possibilities in urban areas combined with a lacking implementation of public and semi-public charging infrastructure, the future change to electrified vehicles will specially take place in suburban and rural areas [8]. Consequently, distribution system operators (DSO) will be faced with new challenges due to rising numbers of electric vehicles in the upcoming years [5], especially in suburban and rural low-voltage (LV) grids. Despite Austria's early stage of e-mobility (0.39 % battery electric vehicle penetration rate in 2018 [2]), these upcoming challenges should be identified prematurely. The integration of future EV-penetrations in existing distribution grids can of course be established by classic grid expansion measures. Due to high costs for excavation, new grid lines and new substations, DSOs are interested in more cost-efficient alternatives [5]. For this reason, this study analyzes future impacts of private charged electric vehicles on a suburban low-voltage grid with respect to voltage range deviations, voltage unbalance and thermal conditions. Based on the identification of critical grid elements, the potentials of several grid relieving measures are also analyzed. This paper provides the methodology behind the executed simulations, the results for a range of EV-penetrations from 10 % to 100 % and a conclusion with key-insights.

METHODOLOGY

Simulations are performed as co-simulations in MATLAB and NEPLAN in order to determine the effects of projected EV numbers on a suburban low-voltage grid. Scenario-dependent grid impacts are analyzed by long-term load flow simulations in NEPLAN. The modelling of the analyzed grid, the modelling of consumer- and EV load profiles and considered control strategies for grid relieving measures are described in the following chapters.

Grid specifications and -modelling

The potentials of grid-oriented measures that may reduce

EV-caused grid restrictions are demonstrated on the basis of a suburban low-voltage grid operated by Energienetze Steiermark GmbH. The grid topology is characterised by a 250 kVA-substation, supplying radially located feeders via cable (91 %) and overhead lines (9 %). Real grid data enables highly accurate grid modelling (NEPLAN) and thereby the identification of grid impacts with a high level of detail. In the grid model, the upper voltage side of the LV substation is connected to a constant voltage source (slack), which means that voltage deviations in the medium-voltage level won't be considered. The permitted voltage range of ± 10 % of the nominal value in accordance with EN 50160 [9] is shared by the medium- and low-voltage level conjunctly. However, only 6.5 % are available for voltage drops at the substation and the LV grid pursuant to the voltage range partitioning in [10]. Therefore, the nominal voltage on the upper voltage side of the LV substation is set to 0.965 pu. This takes the maximal voltage drop caused by medium-voltage loads into account.

Modelling of consumer load profiles

Modelling of consumer loads is separated into a two-step procedure: In the first step, industrial and agricultural consumers are modelled by phase-symmetrical standard load profiles in accordance with [11]. The behavior-based load profile generator by Pflugradt [12] is used in the second step to create highly resolved long-term power profiles for various household structures. This provides phase-asymmetrical synthetic household load profiles, which enables unbalanced load conditions to be considered. All types of consumer load profiles (symmetrical industrial- and agricultural loads as well as asymmetrical household loads) are scaled by the specific customer's annual energy consumption, provided by Energienetze Steiermark GmbH, and aggregated for each grid connection node. Finally, this aggregated load profiles are calibrated by real data. Therefore, long-term active- and reactive power profiles are measured at the LV substation.

Modelling of EV load profiles

EV-caused grid impacts are evaluated by means of an EV reference scenario, considering state of the art charging technology and -distribution: single- and multi-phase charging with 3.7 kW - 22 kW charging power (Figure 1). EV load profiles are modeled for several EV-penetrations (10 % - 100 %) by the use of measured charging data of 21 different EV-models [13] including active- and reactive power profiles. A time resolution of one minute allows the consideration of short-term peak loads. In addition, realistic charging behavior of EV users charging at private charging stations is taken into account. Therefore, the following parameters are determined by statistical data and random numbers for each vehicle, according to the probabilistic approach from Razee et al [14]: driving type (EV or ICE), EV-model (battery capacity, electric consumption, technically feasible charging power),

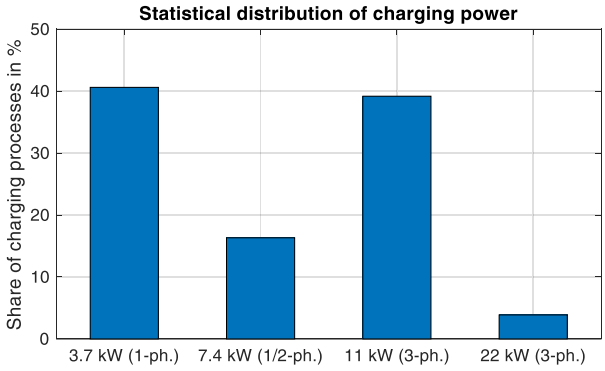

Figure 1: Statistical distribution of charging power for an EV-penetration of 40 %

installed charging power as well as the required amount of energy and time of charging based on traffic analyses. While the described probabilistic approach enables the modelling of realistic charging patterns, it also risks excluding critical grid conditions. Consequently, this modelling approach was done for a number of iterations. Finally, the iteration which includes the highest number of charging processes is selected for each EV-user and prepared for load flow simulations. Based on this methodology, charging processes with 3.7 kW (40.6 %) and 11 kW (39.2 %) are represented with a high share within the simulated period (Figure 1). Charging with 7.4 kW and 22 kW is considered with a share of 16.3 % and 3.9 % respectively, which results in an average charging power of 7.9 kW within the reference scenario. All the single-phase charging EV are connected to the same grid phase in order to consider the most critical case with respect to power unbalance.

Control strategies

On the basis of identified grid restrictions provided by the reference scenario, measures for reducing, or rather avoiding the future need for grid expansions, should be examined. Therefore, a range of grid- (A-E) and user-controlled (F) strategies (listed in Table 1) are investigated. Grid controlled measures are characterized by voltage measurements at defined grid nodes. The regulation of scenario-dependent parameters (active power, phase connection between grid and charging station, tap changer) is executed with a time interval of five minutes corresponding to the lowest phase voltage value.

Table 1: List of analyzed grid relieving measures

Scen.	Measure
A	Remote control at distribution substation (RC)
B	Local control at distribution substation (LC)
C	Remote control at critical feeders
D	Voltage-controlled phase selection
E	Voltage-controlled active power regulation - P(V)
F	Three-phase charging with reduced power (3.7kW)

For analyzing grid-controlled measures (A-E), the EV-user behavior and thereby EV load profiles of the reference scenario are considered. Existing technological- (voltage measurement, power control, communication system) and legal frameworks, required for grid control strategies are assumed. The following chapters provide a detailed description of the considered control strategy for each measure.

Voltage-controlled tap changer at the substation (A, B) or rather at critical feeders (C)

Within these scenarios (A-C), EV-caused voltage deviations should be limited to admissible limits according to EN 50160 [9] by the implementation of transformers equipped with on-load tap changers. Voltage-controlled tap changer adjustment at the distribution substation is analyzed by means of two control strategies: remote control based on voltage measurements at defined grid connection nodes in critical feeders (scen. A) and local control based on the voltage measurement at the lower-voltage side of the substation (scen. B). If the measured voltage exceeds the defined voltage control bandwidth (± 0.05 pu for scenario A and ± 0.02 pu for scenario B), the tap changer is adjusted within nine taps ([-2, 6]) with a tap range of 0.01 pu. Scenario C is defined by the installation of variable transformers (voltage-dependent remote control analogically to scenario A) not at the substation but in critical feeders.

Voltage-controlled phase selection (D)

Each charging station in scenario D is equipped with a voltage-controlled phase-switch. The application of this feature enables load-balancing of asymmetrical loads, for example single-phase charging EV. Therefore, grid phases with minimal and maximal voltage values are detected for each grid connection node with a time interval of five minutes. Finally, phase connections between grid and EV-load are switched accordingly in the grid model in case of voltage values lower than 0.95 pu.

Voltage-controlled active power regulation (E)

In contrast to uncontrolled charging of electric vehicles (reference scenario and scenario F), a voltage-controlled regulation of available charging power is analyzed within this scenario. Therefore, each charging station is equipped with an active current/voltage regulation in accordance with the characteristic in Figure 2 in order to avoid critical voltage deviations. Regarding higher charging power, an adaptation of the control characteristic may be necessary.

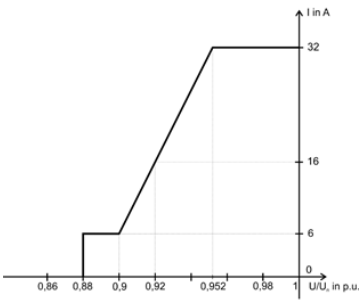

Figure 2: I-u-characteristic of active power control [5]

Three-phase charging with reduced power (F)

This scenario covers a change to three-phase charging with a reduced charging power of 3.7 kW, which can be considered as the optimal charging scenario concerning the prevention of peak loads and power unbalances. Furthermore, this scenario considers area-wide phase-balancing of several single-phase chargers. EV load profiles for scenario F are modelled analogously to the described approach in the reference scenario, considering a charging power of 3.7 kW.

RESULTS

Evaluation of critical grid elements

The need for grid extension measures on the low-voltage level caused by increasing EV numbers is derived by the number of critical grid elements for a certain penetration rate of electric vehicles. Therefore, the following criteria are considered for contrasting with the simulated results of grid nodes and grid lines:

1) Permissible voltage deviation per EN 50160 [9]: 95 % of all 10-minute mean values of one week have to be within ± 10 % of the nominal voltage
2) Permissible voltage unbalance per EN 50160 [9]: Within one week, 95 % of all 10-minute mean values of the relation between negative and positive sequence voltage must be lower than 2 %
3) Thermal line utilization within the line-specification

The examination of voltage range compliance (criteria 1) is based on the determination of the 5 %- and the 100 %-quantiles of all 10-minute mean values within one week for each grid node. Criteria 2 is verified by means of the 95 %-quantile of the relation between negative and positive sequence voltages (10-minute mean values). Critical grid lines are identified accordingly to the maximal thermal utilization within the simulated period.

Identification of grid expansion needs (reference scenario)

The future development of EV-induced grid impacts on the low-voltage level is derived by the simulation of several electromobility penetration rates (10 – 100 %). However, an EV-penetration of 10 % already can result in inadmissible voltage range deviations according to EN 50160 [9] in a number of grid nodes. Figure 3 illustrates the 5 %- and 100 %-quantiles of all 10-minute mean voltage values of each grid node for a 10 %-penetration. The nominal voltage of 0.965 pu as well as the lower voltage limit of 0.9 pu (EN 50160) is marked by a red line. Temporal aggregations of household- and EV-loads, trigger inadmissible voltage decreases in 19 grid nodes. These are located at the end of long feeders, which are characteristic for radially arranged low-voltage grids in suburban and rural areas. In contrast, the considered grid shows no inadmissible voltage unbalance or thermal overload at an EV-penetration of 10 % (Figure 3).

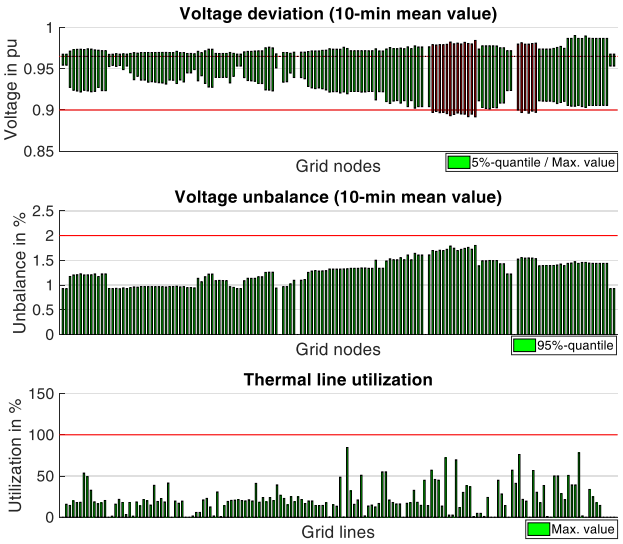

Figure 3: Voltage range deviations, unbalances and thermal utilizations for a 10 %-EV-penetration (reference scenario)

Nevertheless, the described charging pattern (Figure 1) with a high share of single-phase chargers can lead to critical voltage unbalances at future penetrations of around 40 %. Thermal overloads on the other hand are caused by simultaneously charging electric vehicles with high charging power, connected on the same feeder. Therefore, such overloads can occur already at low EV-penetrations (around 20 %). Based on the probabilistic modelling of EV-load profiles, the proportion of critical grid elements does not increase necessarily with higher penetration rates (Figure 4). Therefore, the fitted expectation values of critical grid elements (reference scenario) with respect to voltage deviations, unbalance and thermal overload are added to Figure 4. In other words, a certain share of electrified vehicles (e.g. 40 %, Figure 4) triggers critical voltage characteristics without showing thermal overloads. The reason for that is the probabilistic selection and spatial distribution of single- and multi-phase chargers (with various charging power) by the use of random numbers and statistical data which result in the charging-pattern shown in Figure 1. The further increase of electric vehicles (up to 80 % EV-penetration) raises the share of endangered grid elements for the considered grid and charging-pattern to 41 % (voltage deviation), 39 % (unbalance) and 3 % (thermal overload). These results clarify, that critical voltage characteristics represent the limiting factor for integrating future EV into the analyzed LV grid.

Potentials of grid relieving measures (scen. A-F)

The verified grid relieving measures aim especially for a decrease of inadmissible voltage range deviations and voltage unbalance according to EN 50160. The proportions of endangered grid nodes and grid lines (Figure 4) are therefore illustrated for each strategy (scenario A-F) and contrasted to the reference scenario. Voltage-controlled tap changer adaptations at transformers in dependence of critical grid nodes (remote control) can reduce inadmissible voltage drops even at high EV-penetrations. The use of remote control at the substation (scen. A) or rather the use at critical feeders (scen. C) can reduce the share of voltage range deviations to 0 % or rather 1 %, considering an 80% penetration (Figure 4). In case of critical voltage characteristics in isolated feeders, these two measures (scen. A and C) must be compared with respect to cost-efficiency. Implementing local voltage control at the lower voltage side of distribution substations (scen. B) has lower influence on critical grid nodes compared to remote control: critical voltage conditions will occur continuously with higher EV-penetrations (40-80 %). These results clarify the relevance of the chosen control strategy using a variable distribution substation.

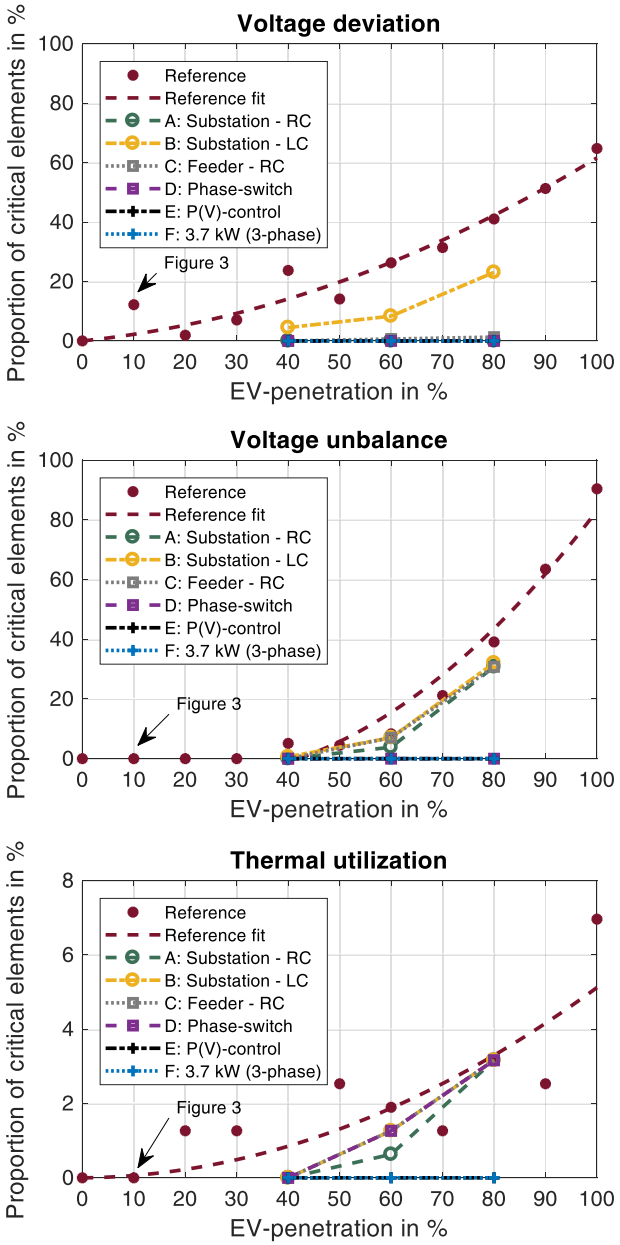

Figure 4: Potential of analyzed strategies with respect to voltage deviations, voltage unbalance and thermal utilization

Beside the reduction of voltage range deviations, scenario A, B and C show little potential for avoiding thermal overload and unbalanced voltage conditions. In contrast, the voltage-controlled allocation of EVs on grid-phases (scen. D) even allows the implementation of EV penetrations up to 80 % without critical voltage characteristics (Figure 4). Similar to the scenarios A-C, the impact on thermal utilization is low: an EV-penetration of 80 % triggers critical conditions in 3 % of all grid lines. Within analyzed grid relieving measures (scen. A-E), the voltage-controlled regulation of available active charging power (scen. E) represents the most effective strategy that integrates high numbers of EV in the considered LV grid. Even at an EV-penetration of 80 %, impermissible voltage range deviations, critical voltage unbalance and thermal overload are avoided (Figure 4) by an extended implementation of P(V)-control. Additionally, EV-induced grid-impacts can as well be prevented by an area-wide adaptation of charging parameters. The limitation of available charging power to 3.7 kW (uniformly phase-distributed) allows for large EV installation capacity and avoids critical voltage- and thermal conditions at high EV-penetrations. This scenario demonstrates, that even poorly developed low-voltage grids are capable of supplying future electromobility, if vehicles are charged three-phase with reduced power. Due to low charging demand in daily life [6] and high duration of parking at home, the comfort of EV-users wouldn't be affected by this measure.

CONCLUSION

Regarding state of the art charging technology (charging with up to 22 kW), the investigated LV grid shows limited capacity for integrating electric vehicles. EV-penetrations of 10 - 20 % could already result in inadmissible voltage range deviations and thermal overload. Furthermore, the local accumulation of single-phase charging EV could lead to critical grid conditions with respect to voltage unbalance at a 40 % penetration. In addition, these grid restrictions are counteracted by the simulation of several grid relieving measures. The relevance of the selected control strategy using a variable distribution transformer is illustrated by the comparison between remote and local control. The tap changer adjustment based on local voltage control shows little potential for avoiding critical voltage deviations at high EV-penetrations. In contrast, EV-induced voltage drops can be reduced by remote control at the substation, and by variable transformers installed in endangered feeders using remote control. Moreover, the implementation of charging infrastructure equipped with voltage-dependent phase-switches represents an effective measure that avoids inadmissible voltage conditions. Beside positive effects on voltage characteristics, the mentioned measures are not capable of adequately reducing the thermal utilization of grid elements. Nevertheless, thermal overload and inadmissible voltage characteristics can be avoided by voltage-controlled active power regulation as well as an area-wide change to three-phase charging with reduced charging power even for an 80 % EV-penetration. Consequently, charging at home during night enables the use of low charging power and provides thereby high potential for reducing the need for grid expansions without any loss of EV-user comfort.

ACKNOWLEDGMENTS

The authors acknowledge the support of the Austrian Federal Ministry of Transport, Innovation and Technology within the project "move2grid". In addition, this study was instructed and supported by Energienetze Steiermark GmbH and Energie Steiermark Technik GmbH.

REFERENCES

[1] Environment Agency Austria, "Greenhouse gases – traffic sector", retrieved November 2018

[2] Federal Ministry of Sustainability and Tourism, 2018, „#mission2030: Austrian Climate and Energy Strategy", Vienna

[3] Norsk Elbilforeningen, "Number of electric cars and plug-in hybrids in Norway from 2010 to 2017", Statista, retrieved November 16, 2018

[4] Austrian Ministry for Transport, Innovation and Technology, 2016, „Final report about the implementation plan Electromobility in and from Austria"

[5] Oesterreichs Energie, 2018, „Leitfaden: Aktuelle und zukünftige Anforderungen an Ladeeinrichtungen für Elektrofahrzeuge" (Present and future requirements to the charging infrastructure for electric vehicles)

[6] Environment Agency Austria, 2010, „Electromobility in Austria: Scenario 2020 and 2050"

[7] Deutsches Dialog Institut GmbH, 2017, „Showcase Regions for Electric Mobility: Final report of parallel impact research"

[8] German National Platform for Electric Mobility, 2011, "Second Progress Report"

[9] ISO EN 50160, 2011, „Voltage Characteristics in Public Distribution Systems"

[10] Federal Ministry for Economic Affairs and Energy, Germany, 2014, "Moderne Verteilernetze für Deutschland" (Modern distribution grids for Germany)

[11] E-Control, „Electricity Market Code – Chapter 6"

[12] N. Pflugradt, Online-Load-Profil-Generator, www.loadprofilegenerator.de, retrieved June 2018

[13] A. Sulzenbacher, 2016, "Niederfrequente Netzrückwirkungen von Elektrofahrzeugen", (Low-frequency grid effects of electric vehicles), Graz, University of Technology

[14] S. Rezaee, E. Farjah, B. Khorramdel, 2013, "Probabilistic Analysis of Plug-In Electric Vehicles Impact on Electrical Grid Through Homes and Parking Lots", *IEEE Transactions on Sustainable Energy 4*, Nr. 4, S. 1024–1033

10.5 NEIS 2019

Grid-friendly Integration of Future Public Charging Infrastructure by Flywheel Energy Storage Systems (FESS)

Grid-friendly Integration of Future Public Charging Infrastructure by Flywheel Energy Storage Systems (FESS)

Bernd Thormann, Thomas Kienberger
Montanuniversitaet Leoben, Chair of Energy Network Technology, Leoben, Austria

Abstract

An area-wide electrification of the transport sector requires, in addition to private charging at home, the implementation of public charging infrastructure. However, the aggregation of private- and public-charging loads could push existing distribution grids to their limits, considering future electric vehicle penetration prospections. In this regard, potential grid impacts of private- and public EV charging on an urban low-voltage grid are evaluated for several charging scenarios and various electromobility penetrations. Furthermore, it is investigated if EV related grid restrictions can be counteracted by the implementation of flywheel energy storage systems. Finally, this study demonstrates the potential of locally generated photovoltaic energy for supplying electric vehicle charging demands based on decentralized storage systems.

Keywords – Electric Vehicle, Grid Restrictions, Low-Voltage Level, Flywheel Energy Storage System

1 Introduction

Increasing numbers of zero-emission vehicles integrated into Austria's road transport system should ensure a CO_2-neutral transport sector by 2050 [1]. For this purpose, monetary incentives are supposed to advance electromobility in Austria into the next stage. The Austrian Ministry for Transport, Innovation and Technology and the Ministry for Sustainability and Tourism (in cooperation with OEMs) provide e-mobility funding measures in the extent of 93 million Euros for 2019 and 2020 [2] to private and commercial users. Combined with future price reducing effects, triggered by technological developments, these and even more efficient measures in other countries [3] will increase electric vehicle (EV) numbers not only for private use, but also in several other fields of application (electric busses, electric taxis, etc.). Besides positive aspects with regard to a decarbonisation of the traffic sector, new challenges for distribution system operators arise [4-6].

1.1 Energy Storage Systems for EV Charging Purposes

Besides other measures, these future challenges might be counteracted by the integration of energy storage systems (ESS) into the EV charging infrastructure. Several types of ESSs and their potential for various EV user groups have already been analyzed by means of theoretical- [7-9] and prototype-applications [10-12]. The reduction of grid exchange by implementing a local lithium-ion battery energy storage system (BESS) into an EV charging point has been demonstrated by Chandra Mouli et al. [7]. In addition, Ding et al. have examined the decrease of network integration costs by ESSs. Therefore, fast charging stations for electric busses equipped with lithium-ion battery systems have been tested. [8] An approach for designing the optimal size of a flywheel energy storage system (FESS), supporting fast charging stations, has been published by Negarestani et al. [9]. In contrast to these theoretical applications, demand side management strategies have been demonstrated by Makohin et al. [10], based on test bed conditions including a fast charging station, a lithium-ion BESS and a PV-generation system. Similarly, Novoa et al. verified a small-scale power system for EV charging purposes. In this context, several ESS-control strategies have been analyzed in a test environment including PV-supply, EV charging points as well as a lithium-ion BESS. [11] In addition, the study by Zhao et al. [12] demonstrates an intelligent energy management, using an EV charging station supplied by PV-generation and a lithium-ion BESS. Most of the mentioned research focus on battery energy storage systems. Though, when it comes to the support of EV charging infrastructure, FESSs show several advantages compared to BESSs. While BESSs have lower costs per kWh [9], they are characterized by significantly shorter lifetime [9, 13]. As a result, FESSs provide lower life-cycle costs [13] combined with higher charging- and discharging efficiency [9].

1.2 Project FlyGrid

In this regard, the project "FlyGrid" deals with the future grid impacts triggered by various e-mobility use-cases and their counteracting by FESSs. Therefore, high-performance FESSs are integrated into fast-charging stations in order to investigate grid-friendly EV-charging. The cooperation with the Austrian distribution system operator Energienetze Steiermark GmbH allows detailed grid analyses based on real grid- and consumer data, provided in an anonymous form and in compliance with data protection regulations. The project "FlyGrid" is funded by the Austria Research Promotion Agency FFG.
Recent studies show: Electric vehicles should preferably be charged at private charging points at home with low power.

Nevertheless, the future integration of EVs into the traffic sector will depend significantly on the extent of available public charging possibilities - besides incentive measures and lower investment costs. [14] An area-wide implementation of a public charging infrastructure provides the change to electrified vehicles for a broader audience, especially in urban areas, where on-street parking prevails. Consequently, grids in these areas could possibly benefit from the integration of FESSs charged with local photovoltaic (PV) energy.
Therefore, this paper provides first project insights by regarding one of the project's use-cases: Public charging of electric vehicles and its impacts on an urban low-voltage (LV) grid located near the city center. Besides public EV-charging, private charging at home is taken into account in order to investigate the aggregation of these two user groups.

2 Methodology

Future grid effects occurring from private- and public EV-charging and their counteracting by the integration of FESSs are investigated based on co-simulations. Time resolved consumer loads (2.1), EV loads (2.2), PV-generation and FESS-profiles (2.3) are modelled in MATLAB. Detailed grid analyses of an urban LV-grid (2.4) are executed by means of long-term load flow simulations in NEPLAN, using a time resolution of one minute.

2.1 Modelling of Consumer Loads

Consumers supplied by the analyzed LV-grid can be divided, in accordance with Austrian Grid Codes [15], into 76 commercial grid customers and 333 households. In this work, commercial customers are modelled by phase-balanced, standardized load profiles pursuant to [15]. Additionally, we use the load profile generator by Pflugradt [16], in order to model highly-resolved, phase-unbalanced load profiles for various household structures. Both, commercial- and household load profiles, are scaled by the real consumer's annual energy consumption. In each point of common coupling (PCC), all connected consumer loads are aggregated and prepared for unbalanced load flow simulations.

2.2 Modelling of EV Loads

For analyzing future grid impacts on an urban LV-grid, the following electric vehicle user groups are taken into account:

1) Private chargers at home (PCH): EVs charged at private charging points installed in underground parking areas of domestic apartment buildings
2) Public on-street chargers (POC): EV-users who are forced to park their vehicles on the street due to missing private parking possibilities

Table 1 EV charging scenarios

EV-scenario	Considered charging types
A	PCH
B	PCH and POC with 3.7-22 kW
C	PCH and POC with 44 kW

Interactions between these types of EV-users are investigated on the basis of three EV-scenarios (Table 1): While scenario A deals with private chargers exclusively, scenarios B and C demonstrate the aggregation of private and public EV charging in an urban area with a high population density. Within all scenarios, PCHs are charged with 3.7 kW (66.6 % of charging processes), 7.4 kW (8.2 %) and 11 kW (25.2 %), uniformly distributed to all grid phases (scenario A, Figure 1). In contrast, POCs are implemented with charging powers of 3.7 – 22 kW (scen. B) and 44 kW (scen. C) exclusively. Single-phase charging POCs are all connected to the same grid phase in order to consider the most critical case in terms of power unbalance. The accumulation of all charging processes including both EV user groups results in a high share of 3.7 kW-chargers (Figure 1), even in scenario B and C. This demonstrates different numbers of PCHs (303 parking lots) and POCs (37) in the considered area. For both user-groups, realistic mobility- and charging patterns are taken into account, applied by stochastic modelling of EV loads according to Rezaee et al. [17]. Thereby, the following parameters are determined by statistical data and random numbers for each vehicle: Drive train (EV or ICE), EV-model (battery capacity, electric consumption), as well as the required amount of energy and time of charging. The latter two are provided by the Austrian traffic planer verkehrplus GmbH [18] for typical Austrian driving patterns. Measured charging data of 21 different EV-models enable the consideration of real active- and reactive power profiles. Finally, these measured charging profiles in combination with determined charging patterns are used to create long-term unbalanced EV load profiles for each point of common coupling (PCC) depending on the charging scenario. The future development of EV-induced grid impacts is analyzed based on the simulation of various EV-penetration rates (0 – 80 %), which define the degree of extended charging infrastructure.

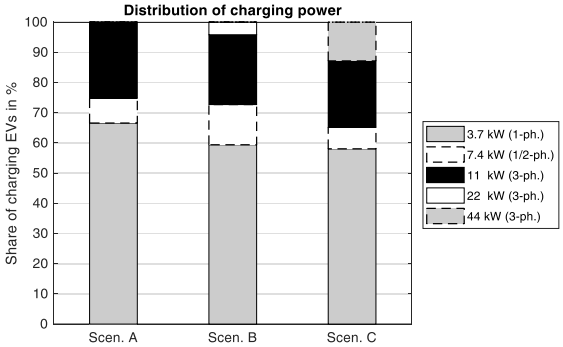

Figure 1 Scenario-dependent distribution of charging power

For example, half the private and public parking lots are equipped with charging points at an EV-penetration of 50 %. By means of this approach, future events regarding e-mobility, e.g. an (drastic) increase of EV, can be demonstrated in an easy way. Furthermore, certain PCH- and POC-penetrations and their impacts on existing grid structures might be investigated.

2.3 FESS-Implementation and PV-Modelling

Based on the scenario-dependent identification of critical grid elements, FESSs are implemented into public charging points. Thereby, classic grid extension measures should be prevented by covering POC-caused peak loads. Therefore, FESS-charging (supplying POCs) is investigated with two various strategies: Grid- and PV-charging. The former one is characterized by FESS-charging during off-peak periods [9, 11] in order to avoid the aggregation of EV- and FESS-charging. Therefore, FESSs are immediately charged with 5 kW (phase-balanced) when no EV is connected to the grid, aiming for a complete charge as soon as possible. Considering strategy "PV-charging", FESSs are supplied exclusively by locally generated PV-energy. Hence, FESSs are charged phase-balanced during sunny periods when local PV-generation exceeds EV charging demands (1).

$$P_{FESS}(t) = P_{PV}(t) - P_{POC}(t) \qquad (1)$$

Otherwise, POC-charging is directly supplied by local PV-generation [12]. For that purpose, PV-generation profiles are modelled based on real weather data from the Austrian Central Institute for Meteorology and Geodynamics (ZAMG) [19] combined with data from a solar-roof register [20]. The applied approach determines the direct and diffuse share of global radiation based on the Perez model [21]. Furthermore, the correlation between temperature and PV-module-efficiency as well as the correlation between load and inverter-efficiency are derived by previous projects. The investigated urban LV-grid supplies solely apartment buildings characterized by flat roofs. Hence, an azimuth of 0 ° (south) and a tilt angle of 35 ° is assumed for all potential PV-areas [22]. For charging FESSs by renewable energy, the whole PV-potential within the urban LV-grid is considered, which represents a complete expansion of PV-modules. Regardless of the charging strategy, FESSs are discharged in case of POC loads exceeding certain power limits. These limits are defined in accordance with grid line specifications, aiming for the prevention of thermal overloads. Furthermore, real-time detection of POC loads enables a phase-unbalanced compensation of POC charging demands by FESSs including a variable power factor. For analyzing the influence of FESS's available energy content, each charging strategy is tested applying capacities of 5 kWh and 10 kWh (Table 2) per FESS-module (compare to [4]). Assuming an average energy consumption of current electric passenger models of

Table 2 FESS-specifications applied for grid simulation

FESS-parameter per module	Value
Energy capacity	5 and 10 kWh
Max. discharging power	100 kW
Charging power	5 kW / PV-dependent
Depth of discharge	100 %
Charging efficiency	90 %
Discharging efficiency	90 %
Max. stand-by losses	0.5 kW(100 % SOC)
Power factor: Charging	1

14.9 kWh/100 km (New European Driving Cycle) [23], an amount of 5 kWh equals to a covered distance of 33.6 km. Based on statistics about mobility patterns in Austria [24], 92.4 % of motorized, individual trips can be covered by this amount of energy (10 kWh considering round trips). Further FESS-parameters (Table 2) – maximal discharging power, depth of discharge, charging- and discharging efficiency, maximal stand-by losses and power factor of charging – are specified within the project FlyGrid and applied for FESS-simulations. Therefore, each extended public charging point (depending on EV penetration rates) is equipped with one FESS-module, characterized by the mentioned specifications.

2.4 Grid Topology and -Modelling

The analyzed LV-grid is operated by Energienetze Steiermark GmbH and located in an urban area near the city center with high population density. Moreover, it is characterized by ring network structures (Figure 2) openly operated under normal grid conditions. Two parallel 630 kVA-substations supply consumers and electric vehicles via 21 PCCs. Real grid data enables highly accurate grid modelling (NEPLAN) and thereby the identification of grid impacts with a high level of detail.
Private- and public charging points are assumingly supplied by existing grid infrastructure. Hence, all types of grid loads (conventional consumers, PCHs and POCs) are aggregated for each PCC and integrated as one load module. Additionally, scenario-dependent PV-modules and FESSs are integrated three-phase into the grid model (Figure 2) as a measure of EV-penetration.

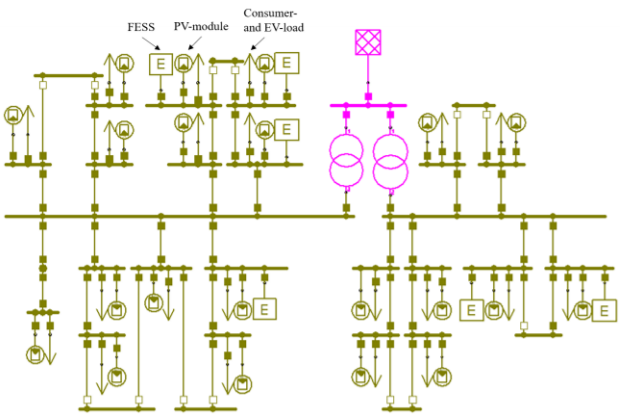

Figure 2 Grid topology of the analyzed, urban LV-grid

In the grid model, the distribution substation's high-voltage side is connected to a constant voltage source (slack) with a nominal voltage of 1 per unit (pu). As a result, voltage deviations in the medium-voltage level are excluded. This aspect is taken into account when contrasting simulation results to specified grid limits.

3 Results

3.1 Evaluation of EV-induced grid restrictions

Three EV-charging scenarios (A - C) and their consequences for existing grid structures are investigated by long-term (one week), 1-minute resolved load flow simulations. The need for grid extension measures is derived by the number of critical grid elements at certain EV-penetration rates (0 – 80 %). Therefore, voltage characteristics (voltage deviation and voltage unbalance) of all grid nodes are compared with limits according to EN 50160 [25]. The permitted voltage range of ± 10 % is shared by the medium- (MV) and low-voltage level conjunctly. However, only a limited voltage range between -6.5 pu and +4.5 pu is available for voltage deviations at the MV/LV-substation and in the LV-grid, pursuant to the voltage range partitioning in [26]. Thus, the maximum- (1.045 pu) and minimum voltage (0.935 pu) are defined accordingly, in order to take maximum voltage deviations in the medium-voltage level into account. In addition to voltage deviations, voltage unbalance, determined by the relation between negative and positive sequence voltage, is limited to 2 % [25]. These defined thresholds have to be complied by 95 % of all 10-minute means (deviation and unbalance) within one week. Besides voltage characteristics, critical grid lines as well as the transformers' capacities are verified based on their thermal utilization according to equipment specifications. EV-induced voltage deviations, voltage unbalance and thermal utilizations are compared to a reference scenario, in which neither electric vehicles nor photovoltaic modules are connected to the grid.

The analyzed, urban LV-grid shows high capacity for integrating future electric vehicles in terms of voltage characteristics per EN 50160. Although already 40 % electric vehicles trigger minimal 10-minute voltage means below the limit of 0.935 pu (scen. B and C), the 95 %-criteria is fulfilled for each grid node (Figure 3). Furthermore, single-phase charging POCs (scen. B) cause increased voltage unbalance in several grid nodes, compared to balanced, three-phase charging within scenario C (Figure 3). Nevertheless, voltage deviations as well as voltage unbalances are ranged within admissible limits, despite high numbers (70 %) of private- and public charging EVs (scen. B and C). Within this study, the implementation of FESSs aim specifically for a reduction of short-term thermal line utilizations by peak shaving of POC loads. As a result, voltage characteristics will be affected positively by this measure as well.

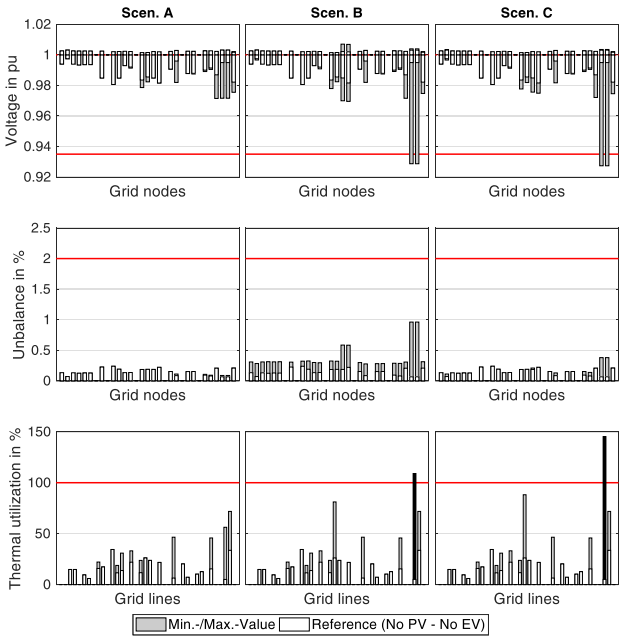

Figure 3 Scenario-dependent grid impacts considering an EV-penetration of 40 %

On this account, further results focus exclusively on thermal overloads, while disregarding voltage characteristics. Considering charging of private parkers at home (scen. A), even an EV-penetration of 60 % (Figure 4) can be supplied without grid restrictions, due to phase-balanced charging with low power (3.7 – 11 kW). In contrast, the aggregation of PCHs and POCs triggers short-term overloads in one single grid line at penetrations of 40 % (scen. B) and 20 % (scen. C). Moreover, further increases of EV numbers (80 %) could result in critical thermal utilizations in two (scen. A), three (scen. B) and four (scen. C) grid lines (Figure 4).

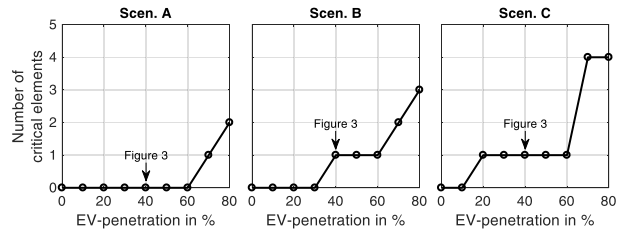

Figure 4 Number of thermally overloaded grid lines in dependence of charging scenario and EV-penetration

Nevertheless, these results demonstrate the urban grid's little need for grid extension measures: Future electromobility can be integrated by focussing on few grid lines, either by line extension (more or less within the scope of normal grid planning), the integration of FESSs or alternative measures.

3.2 Prevention of grid extensions by FESSs

Based on identified grid impacts, the equipment of public on-street chargers with FESSs is simulated by means of two FESS-charging scenarios (grid-charging and PV-

charging) as well as two FESS-capacities (5 kWh and 10 kWh).

3.2.1 Grid-charging

Assuming POC-charging with 3.7 – 22 kW (scen. B), the selected FESS-specification shows no influence on the line-conditions (Figure 5): Even FESS-capacities of 5 kWh allow a "delay" of thermal overloads until a 50 % EV-penetration. In contrast, charging of public on-street parkers with 44 kW (scen. C) requires higher FESS-capacities for sufficient grid support. Considering the same power limits triggering FESS-interference as well as the same charging behaviour, high-power charging POCs (scen. C) force significantly increased FESS-interferences, compared to low-power charging: 131.6 kWh in scenario B and 305.0 kWh in scenario C are provided by the implemented FESS (10 kWh) within one week. Hence, the potential of FESSs with a capacity of 5 kWh for supplying high-power charging POCs are limited due to a shortened state of charge (SOC) during peak periods. Though, even 60 % of high-power charging POCs can be integrated without grid restrictions by increasing the available FESS-capacity to 10 kWh (Figure 6, scenario C). Furthermore, an EV-penetration of 60 % illustrates the temporal aggregation of low-power charging PCHs and low-power charging POCs (scen. B). Therefore, the simultaneity of charging is determined by the relation between accumulated EV load profiles $P_i(t)$ and the sum of EV-specific power peaks (2) [27], and compared between scenario B and C (Figure 6).

$$Simultaneity(t) = \frac{\Sigma_i \ P_i(t)}{\Sigma_i \ \max(P_i(t))} \qquad (2)$$

Assuming consistent charging behavior (time of arrival and amount of energy), the simultaneity of charging differs with various charging powers: As a result of longer charging processes, low-power charging of POCs (scen. B) causes higher simultaneity (0.45) than charging with 44 kW (0.39) in scenario C (Figure 6).

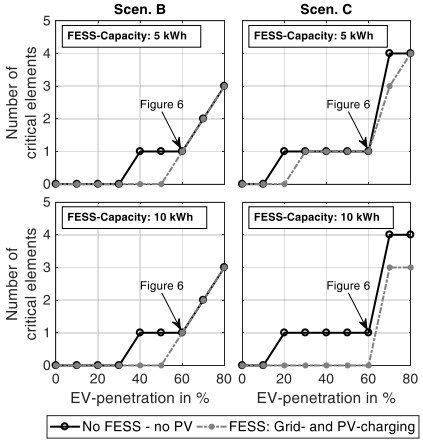

Figure 5 Number of thermally overloaded grid lines in dependence of FESS-charging strategy and FESS-capacity

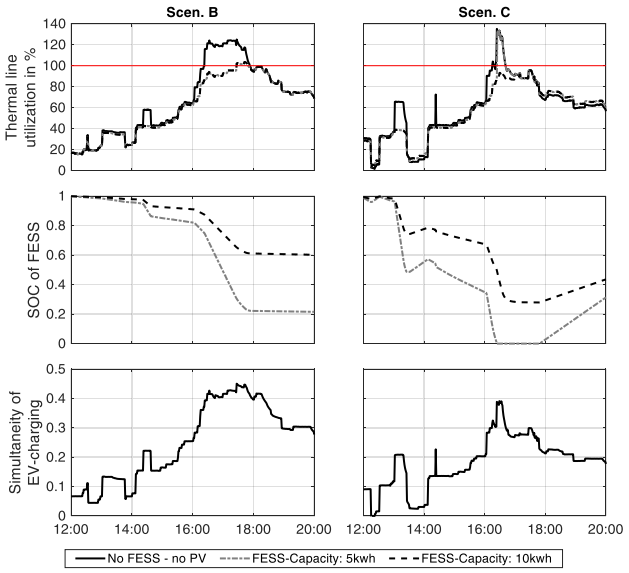

Figure 6 Thermal line utilization, state of charge (FESS) and simultaneity of EV-charging considering the limiting grid line at an EV-penetration of 60 %

According to the same power limits (2.3) and independent to FESS-interference, low-power POC-charging (scenario B) is characterized by longer charging periods, compared to scenario C. Consequently, even FESS-reduced POC-loads temporally overlap with private charging loads, which triggers short-term overloads despite FESS-application.
In contrast, short-term charging of POCs with high power (scen. C) prevents the aggregation with PCH-loads. Furthermore, load peaks still occurring can easily be covered by the implementation of FESSs avoiding critical thermal conditions.

3.2.2 PV-charging

Besides grid-charging, a complete supply of FESSs by locally generated renewable energy is examined. Therefore, a full extension of PV-areas is assumed, generating a total energy amount of 5.8 MWh per week (summer period). However, in the considered urban grid situation, even a full PV-extension covers neither the present consumer demands (21.6 MWh per week) nor future electromobility demands (20.1 MWh (scen. A), 22.9 MWh (scen. B) and 23.1 MWh (scen. C) per week; EV-penetration: 50 %). Nevertheless, in the considered urban grid situation local PV-generation enables the charging of decentralized FESSs, guaranteeing same grid relieving potentials as grid supply (Figure 5): EV-induced grid restrictions can be prevented until high EV-penetrations by the implementation of FESSs, even though charged exclusively by local PV-generation.

4 Conclusions

The analyzed low-voltage grid located in an urban area with a high population density shows high capacity for integrating future electric vehicle numbers. Even a

penetration of 70 %, considering private- and public charging EVs, can be supplied without inadmissible voltage characteristics according to EN 50160. Additionally, only one grid line faces critical thermal conditions, when up to 60 % of both EV user groups are electrified (Figure 4). Besides normal grid extension as solution to tackle overload-situations, also the integration of FESSs into public charging points can prevent them: Considering public charging with 3.7 – 22 kW, even FESSs with a capacity of 5 kWh provide the sufficient reduction of peak loads until a 50 %-penetration. In contrast, high-power charging with 44 kW requires at least 10 kWh-storage units, supplying this share of electric vehicles. Furthermore, the application of FESSs enable the temporal bridging between PV-generation and EV-demands. Thereby, even high electromobility numbers can be supplied by locally generated renewable energy, avoiding grid extension measures.

5 Literature

[1] *#mission2030: Austrian Climate and Energy Strategy*, Austrian Federal Ministry for Sustainability and Tourism, Vienna, Austria, 2018

[2] *#mission2030 E-Mobilitätsoffensive*, Austrian Federal Ministry for Transport, Innovation and Technology, May 2019. [Online]. Available: http://www.bmvit.gv.at/verkehr/elektromobilitaet/foerderungen/emoboffensive

[3] O. H., Hannisdahl, H. V., Malvik, G. B., Wensaas, "The future is electric! The EV revolution in Norway - Explanations and lessons learned," *Proc. 27th International World Electric Vehicle Symposium and Exposition (EVS 27)*, Barcelona, Spain, 2013

[4] L., Pieltain Fernandez, T., Gomez San Roman, R., Cossent, C., Mateo Domingo, P., Frias, "Assessment of the Impact of Plug-in Electric Vehicles on Distribution Networks," *IEEE Trans. Power Syst.*, vol. 26, no. 1, pp. 206–213, 2011, doi: 10.1109/TPWRS.2010.2049133.

[5] A. G., Anastasiadis, G. P., Kondylis, A., Polyzakis, G., Vokas, "Effects of Increased Electric Vehicles into a Distribution Network," *Energy Procedia*, vol. 157, pp. 586–593, 2019, doi: 10.1016/j.egypro.2018.11.223.

[6] K., Clement-Nyns, E., Haesen, J., Driesen, "The Impact of Charging Plug-In Hybrid Electric Vehicles on a Residential Distribution Grid," *IEEE Trans. Power Syst.*, vol. 25, pp. 371–380, 2010, doi: 10.1109/TPWRS.2009.2036481.

[7] G. R., Chandra Mouli, P., Bauer, M., Zeman, "System design for a solar powered electric vehicle charging station for workplaces," *Applied Energy*, vol. 168, pp. 434-443, 2016, doi: 10.1016/j.apenergy.2016.01.110.

[8] H., Ding, Z., Hu, Y., Song, "Value of the energy storage system in an electric bus fast charging station," *Applied Energy*, vol. 157, pp. 630–639, 2015, doi: 10.1016/j.apenergy.2015.01.058.

[9] S., Negarestani, M., Fotuhi-Firuzabad, M., Rastegar, A., Rajabi-Ghahnavieh, "Optimal Sizing of Storage System in a Fast Charging Station for Plug-in Hybrid Electric Vehicles," *IEEE Trans. Transp. Electrific.*, vol. 2, no. 4, pp. 4433-453, 2016, doi: 10.1109/TTE.2016.2559165.

[10] D., Makohin, F. V., Jordan, V. S., Zeni, K. H. M., Lemos, C., Pica, M. A., Gianesini, "Use of lithium iron phosphate energy storage system for EV charging station demand side management," *Proc. IEEE 8th International Symposium on Power Electronics for Distributed Generation Systems (PEDG)*, 2017, doi: 10.1109/PEDG.2017.7972528.

[11] L., Novoa, J., Brouwer, "Dynamics of an integrated solar photovoltaic and battery storage nanogrid for electric vehicle charging," *Journal of Power Sources*, vol. 399, pp. 166–178, 2018, doi: 10.1016/j.jpowsour.2018.07.092.

[12] H., Zhao, A., Burke, "An intelligent solar powered battery buffered EV charging station with solar electricity forecasting and EV charging load projection functions," *Proc. IEEE International Electric Vehicle Conference (IEVC)*, Florence, Italy, 2014, doi: 10.1109/IEVC.2014.7056169.

[13] A., Buchroithner, H., Wegleiter, B., Schweighofer, "Flywheel Energy Storage Systems Compared to Competing Technologies for Grid Load Mitigation in EV Fast-Charging Applications," *Proc. IEEE 27th International Symposium on Industrial Electronics (ISIE)*, Cairns, Australia, 2018, doi: 10.1109/ISIE.2018.8433740.

[14] F., Kley, „Expansion strategy for electric vehicle charging infrastructure based on driving behavior," (in German: Ladeinfrastruktur für Elektrofahrzeuge - Entwicklung und Bewertung einer Ausbaustrategie auf Basis des Fahrverhaltens), Fraunhofer-Institut für System- und Innovationsforschung ISI, Karlsruhe, Germany, 2011

[15] E-Control: Electricity Market Code – Chapter 6

[16] *Online Load Profile Generator*, N., Pflugradt, June 2018. [Online]. Available: http://www.loadprofile-generator.de

[17] S., Rezaee, E., Farjah, B., Khorramdel, "Probabilistic Analysis of Plug-In Electric Vehicles Impact on Electrical Grid Through Homes and Parking Lots," *IEEE Trans. Sustain. Energy*, vol. 4, pp. 1024–1033, 2013, doi: 10.1109/TSTE.2013.2264498.

[18] verkehrplus (2017): Traffic analyses as data basis for grid simulations within the scope of the FFG-Project "Move2Grid"

[19] *Temperature- and global radiation data from Austria*, Zentralanstalt für Meteorologie und Geodynamik, 2014, Vienna, Austria

[20] *Solar roof register for the province of Styria*, Federal State of Styria, 2019. [Online]. Available: http://www.graz.at/cms/beitrag/10295929/8115447/Online_Karte_Solardachkataster.html

[21] B., Böckl, J., Vopava, L., Kriechbaum, T., Kienberger, „Limitations of integrating photovoltaic energy into municipal grids excluding and including storage systems," *Proc. 6th Solar Integration Workshop*, 2016

[22] M., Hartner, A., Ortner, A., Hiesl, R., Haas, "East to west – The optimal tilt angle and orientation of photovoltaic panels from an electricity system perspective," *Applied Energy*, vol. 160, pp. 94–107, 2015, doi: 10.1016/j.apenergy.2015.08.097.

[23] *Factsheet #12 - Charging duration and charging type*, Austrian Mobile Power, January 2019. [Online]. Available: https://www.austrian-mobile-power.at

[24] R., Tomschy, M., Herry, G., Sammer, R., Klementschitz, S., Riegler, R., Follmer, D., Gruschwitz, F., Josef, S., Genasasz, R., Kirnbauer, T., Spiegel, „Final report about the Austrian traffic analysis Österreich unterwegs 2013/2014," (in German: Ergebnisbericht zur österreichweiten Mobilitätserhebung Österreich unterwegs 2013/2014), Austrian Federal Ministry for Transport, Innovation and Technology, Vienna, Austria, 2016

[25] Voltage Characteristics in Public Distribution Systems, ISO EN 50160, 2011

[26] J., Büchner, J., Katzefey, O., Flörcken, A., Moser, H., Schuster, S., Dierkes, T., von Leeuwen, L., Verheggen, M., Uslar, M., van Amelsvoort, „Modern distribution grids for Germany," (in German: Moderne Verteilernetze für Deutschland), Federal Ministry for Economic Affairs and Energy, Germany, 2014

[27] A., Probst, „Impacts of electromobility on energy supply networks based onprobabilistic grid design," (in German: Auswirkungen von Elektromobilität auf Energieversorgungsnetze analysiert auf Basis probabilistischer Netzplanung), Ph.D. dissertation, Dept. Informatics, Electrical Eng. and Information Technology, University of Stuttgart, 2013, doi: 10.1109/TSTE.2013.2264498

10.6 IEWT 2021

FlyGrid – Integration of Energy Storage Systems into EV Fast Charging Infrastructure

FlyGrid – Integration of Energy Storage Systems into EV Fast Charging Infrastructure

Bernd Thormann[1] (1), René Braunstein (2), Thomas Kienberger (1)

(1) Montanuniversität Leoben, Lehrstuhl für Energieverbundtechnik, Franz-Josef-Straße 18, 8700 Leoben, +43 3842 402 5409, bernd.thormann@unileoben.ac.at
(2) Energie Steiermark Technik GmbH, Leonhardgürtel 10, 8010 Graz, rene.braunstein@e-steiermark.com

Abstract:

An increasing number of electric vehicles will challenge the present-day power system, especially on the low- and medium-voltage level. Energy storage systems might have the potential to mitigate grid loads substantially. Hence, in the project "FlyGrid," energy storage systems are integrated into electric vehicle charging infrastructure. Furthermore, the required design of these systems is determined in detail, considering numerous electric vehicle use cases. This work presents the project's previous results and conclusions acquired so far: The required specifications of energy storage systems strongly depend on the electric vehicle application, including its charging power and the number of installed charging points. However, even storage units with low capacity and moderate discharging power enable significant grid relief for the local power grid in most cases.

Keywords: Electric vehicle, distribution system, peak load shaving, energy storage system

1 Introduction

On both the European [1] and the national level [2], climate-neutrality shall be realized, inter alia, by transitioning towards clean electric mobility. However, future electric vehicle (EV) numbers will also challenge existing distribution systems [3]. On this account, new innovative solutions must be found to avoid costly grid expansions yet fulfilling the EV user's mobility needs. The integration of energy storage systems (ESSs) into EV charging infrastructure represents one of them. Nevertheless, integrating decentralized ESSs into future grid planning processes certainly requires detailed knowledge about their required specifications depending on the supplied EV use case. The research project "FlyGrid" [4] tackles this problem by identifying ESS specifications required for covering short-term charging peak loads of various e-mobility use cases.

1.1 Project FlyGrid and structure of this work

The project "FlyGrid" [4] is funded by the Austrian "Klima- und Energiefonds" via the Austrian Research Promotion Agency (FFG) program "Leuchttürme eMobilität". Within the project, high-performance ESSs are integrated into (fast-) charging stations as follows (Fig. 1): Distribution system, ESS, and charging infrastructure are connected to a DC voltage link via AC/DC,

[1] Jungautor

DC/AC or DC/DC inverters, comparable with Dragicevic et al. (2014) [5] and Yan et al. [6]. Future EV charging demands are either supplied by the distribution system, the ESS (in case of available energy capacity), or both.

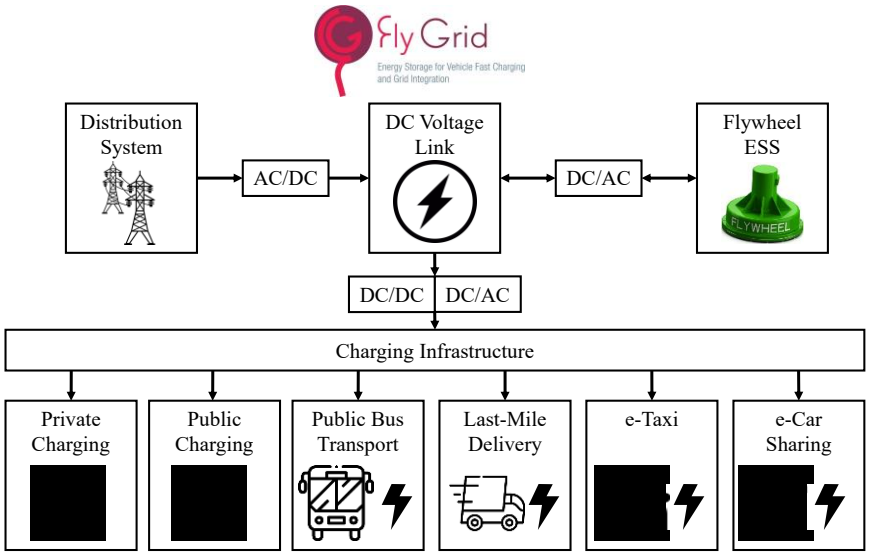

Figure 1: Scheme of the project "FlyGrid": Grid integration of future e-mobility use cases by implementing a flywheel energy storage system (ESS) [4]

Notwithstanding the above, both AC and DC power can be provided by the charging point. Hence, even at the low-voltage level, high charge-power can be reached while at the same time stabilizing the grid. Regarding the short-term supply of high-power EV charging, flywheel ESS provide substantial benefits compared to battery ESS [7–10]: High life cycle number, high power density, fast access time, low maintenance effort, small environmental impact, and the independency of power and energy content. In addition, flywheel ESSs allow lower investment and operation costs compared to supercapacitors [5,11]. As a result, flywheel ESSs are selected as energy storage technology in the project "FlyGrid". However, the project's results and conclusions are also applicable to other storage technologies. Before testing the application of a flywheel ESS based on real-life demonstrations, the project "FlyGrid" identifies its specifications required for supplying future e-mobility in detail. Therefore, e-mobility use cases (Table 1) with significant environmental and economic importance are selected for investigation.

Table 1: E-mobility use cases and their respective charging power considered in the project "FlyGrid"

	EV Use Case	**Charging power (kVA)**
1	Charging at public parking lots	3.7 – 44.0
2	EV car sharing	3.7 – 100.0
3	Highway fast charging	50.0 – 350.0
4	Public charging at shopping centers	3.7 – 100.0
5	Electrified busses	100.0 – 600.0
6	Electrified taxies	3.7 – 100.0
7	Electrified last-mile delivery trucks	100.0 – 350.0

Parts of the project's previous results have already been published in Thormann et al. (2019) [12], considering use case 1, and in Thormann et al. (2021) [13], considering use cases 3, 5, and 7. This work describes the methodology (Section 2) applied in the project "FlyGrid", and summarizes all use cases' results (Section 3). Finally, Section 4 provides the most significant conclusions from the project acquired so far and an outlook regarding further research questions.

2 Methodology

In the project "FlyGrid", realistic charging patterns and loads are modeled based on real-life mobility data (Section 2.1). These charging loads of EVs are integrated into existing distribution networks to identify potential grid impacts of EV charging. Based on identified grid restrictions, ESS specifications required for counteracting them are determined in detail (Section 2.2).

2.1 Modeling of realistic charging loads

In the first step of the project, realistic annual time-series (1 min. temporal resolution) of EV charging loads are modeled stochastically for each of the pre-defined EV use cases (Table 1). Therefore, the following aspects are taken into account:

- The spatial distribution of charging points
- Individual mobility patterns (time of charging and covered distance)
- EV model specifics (battery capacity, specific energy consumption, and charging efficiency)
- Charging power (Table 1)

The spatial distribution of charging grids is derived from real-life locations of public parking lots (Use case 1), car-sharing terminals (2), highway service stations (3), shopping centers (4), bus stations (5), taxi terminals (6) and hubs of last-mile delivery vehicles (7). The time of charging and the distance covered before charging are both determined stochastically using statistical data [14–17] (in the form of cumulative distribution functions) and random numbers (Fig. 2).

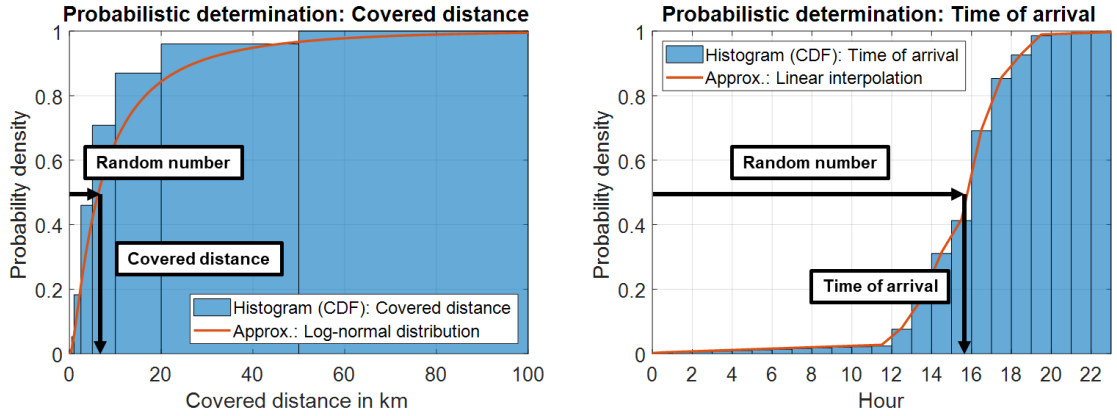

Figure 2: Probabilistic determination of the covered distance (left) and the time of arrival (right) using the cumulative distribution function (CDF) and random numbers

Besides temporal mobility patterns, the timely-resolved modeling of EV loads requires the consideration of the state-of-the-art EV model specifics. Battery capacities, specific energy consumptions, and charging efficiencies applied in this project are described in Thormann et al. (2020 and 2021) [13,18]. For analyzing potential grid impacts caused by EV charging,

numerous scenarios regarding various charging powers are analyzed for each use case. Based on these four aspects, EV charging profiles are modeled for each use case, either by using measured charging data [18] or rectangular charging curves with constant charging power during the charging process.

2.2 Determining required ESS specifications

The modeled EV charging loads are then virtually integrated into grid models of existing real-life distribution power grids, operated by Energienetze Steiermark GmbH. Long-term (one year) load flow simulations are performed to identify thermal grid restrictions of lines or transformers triggered by future EV use cases. In the next step, the capacity and power of decentralized ESSs required to counteract these thermal grid restrictions are determined in detail. Therefore, the apparent power available in the power grid ($S_{Available}$) is calculated in each time step *t* using the nominal power of grid elements ($S_{max,therm}$) and the grid elements' initial load without EVs ($S_{initial}$) according to Eq. 1.

$$S_{Available}\,(t) = S_{max,therm} - S_{initial}\,(t) \tag{1}$$

$$S_{ESS}(t) = S_{available}\,(t) - S_{EV}(t) \tag{2}$$

$$Energy_{ESS}(t) = Energy_{ESS}(t-1) + \int_{t-1}^{t} P_{FESS} * dt \tag{3}$$

$$required\ ESS\ discharging\ power = \frac{\min(S_{ESS}(t))}{\eta_{Discharging}} \tag{4}$$

$$required\ ESS\ capacity = \min(Energy_{ESS}(t)) \tag{5}$$

Each ESS's apparent power (S_{ESS}) is determined by subtracting the EV charging load from the available capacity at the particular power grid location (Eq. 2). Thus, ESSs are discharged ($S_{ESS} < 0$) when EV charging loads exceed the available capacity of the grid. After discharging triggered by peak shaving needs, the supplied amount of energy is recharged ($S_{ESS} > 0$) into the ESS during off-peak periods, when the available grid capacity exceeds EV charging demands. Furthermore, the amount of energy stored in the ESS ($Energy_{FESS}$) is calculated in each time step *t* using Eq. (3): The amount of energy stored in the ESS decreases during ESS-discharging and increases during ESS-charging. Furthermore, we limit the energy stored in the ESS with [-∞; 0] to ensure that ESSs only recharge the amount of energy they have provided during previous peak shaving services. Since flywheels are selected as storage technology in this study, the following characteristics are applies specifically for this storage technology: A charging and discharging efficiency of 90 % [19] is applied to model realistic operation of the flywheel ESS. Furthermore, a linear approximation between dissipation losses and the state of charge of the flywheel ESS is implemented [20]. Hence, dissipation losses vary between 0.5 kW (100 %) and 0.0 kW (0 %), depending on the flywheel's state of charge. Finally, the required ESS discharging power and capacity are identified for each use case and each charging power (Table 1) using Eq. (4) and (5).

3 Results

This section provides the ESS discharging power and capacity per charging point required to cover short-term EV charging loads and prevent local grid restrictions. Regardless of the

supplied use case, both – power rating and energy content - strongly depend on the actual EV charging power: The higher the EV charging power, the higher the capacity and discharging power requested by the ESS per charging point. Of course, the actual ESS specifications depend on the particular distribution grid and its local load conditions. Furthermore, the required ESS specifications correlate with the number of supplied charging points. The more charging points are supplied by the ESS, the more energy must be stored per charging point to counteract local grid overloads. Similarly, the required ESS discharging power per charging point increases the more charging points are installed.

Based on these correlations, the applied design method identifies a broad spectrum of required ESS specifications for each use case, illustrated in Fig. 3 (ESS capacity) and Fig. 4 (ESS power). Considering low-power charging use cases (1, 2, 4, and 6), the required ESS capacity (Fig. 3) varies between 0.5 and 158 kWh per charging point, with medians between 0.5 (Use case 2) and 1.5 kWh (Use Case 4). Furthermore, integrated ESSs must provide a discharging power between 0.25 and 53 kVA per charging point to supply these use cases (Fig. 4).

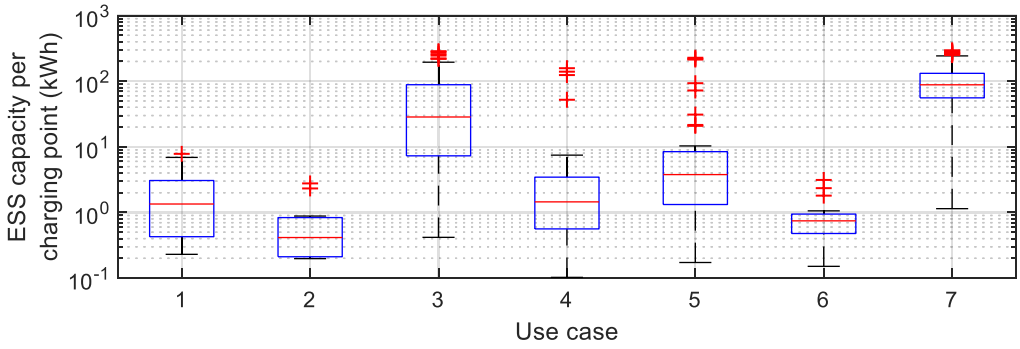

Figure 3: Spectrum of ESS capacity per charging point supplying various EV use cases

For example, a ESS integrated into an electric taxi charging station with six charging points and charging power of 22 kVA each requires at least a capacity of 2.2 kWh and a discharging power of 24.6 kVA. The supply of high-power charging EV uses cases (3, 5, and 7), one the other hand, requires a ESS capacity (Fig. 3) between 0.17 and 295 kWh, with a median between 4 (Use case 5) and 88 kWh (Use case 7).

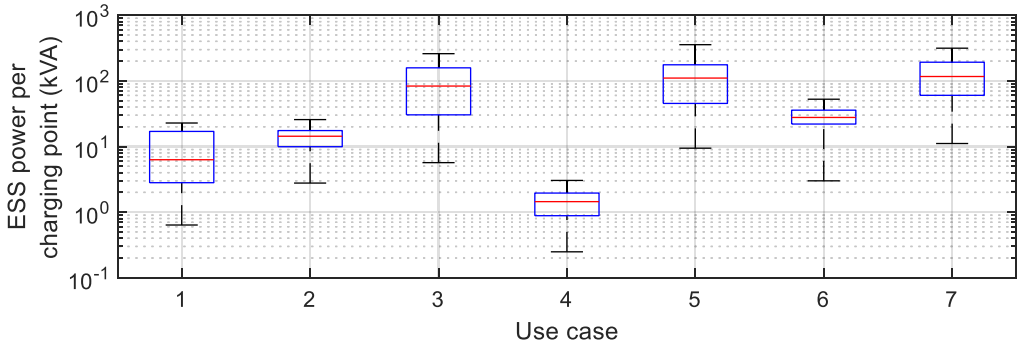

Figure 4: Spectrum of ESS power per charging point supplying various EV use cases

The short-term covering of peak loads requests ESS discharging power (Fig. 4) between 6 and 356 kWh per installed charging point, with medians of 83 (Use case 3), 110 (5), and 117 kVA (7). Despite the broad spectrum of ESS specifications, most charging demands of future EV

use cases can be supplied by integrating a ESS with relatively low capacity (e.g., 5 kWh) and moderate power (e.g., 100 kVA) per charging point. This tendency correlates with the fact that most (95.1 %) individual trips are shorter than 50 km [14], corresponding to an energy demand of about 10 kWh. However, EV applications requiring higher ESS capacity and discharging power may be supplied either by larger ESSs, or a modular approach of several ESS units.

4 Conclusions and Outlook

The modeling of timely-resolved charging profiles based on accurate mobility data demonstrates crucial differences in the charging behavior of varying EV use cases. When applying these realistic charging profiles, even numerous charging points can be integrated into existing low- and medium-voltage grids considering EV charging with moderate charging power (up to 44 kVA). Furthermore, the project's previous results confirm that any kind of energy storage can severely mitigate potential grid congestions in many cases. However, the required ESS specifications depend significantly on the individual EV use case, EV charging power, and the grid location. The demonstrated discrepancies between EV use cases inhibit the design of one single ESS unit suitable for all considered applications. Nevertheless, most EV cases can entirely be supplied by the ESS specifications of 100 kVA discharging power and 5 kWh capacity per ESS module. Considering flywheel ESSs, for example, e-mobility use cases with higher energy- and power demands may require a modular approach of several flywheel units. Thereby, even high-power charging EV applications, e.g., opportunity charging of electric busses, can be supplied in a grid-friendly way considering a moderate number of charging points and moderate charging power.

Of course, the application of ESSs must also be evaluated in terms of the total investment and operation costs. Therefore, future work should compare the integration of different ESS technologies with demand-side measures or classic grid reinforcements in terms of overall costs. Flywheel ESS, for example, can provide significant economic benefits when supplying high-power EV charging demands characterized by numerous, though short, charging processes (e.g., electric busses), demonstrated in Thormann et al. (2021) [13].

5 Acknowledgments

This work is part of the project "FlyGrid" (www.flygrid.tugraz.at), funded by the Austrian "Klima- und Energiefonds" via the Austrian Research Promotion Agency (FFG) program "Leuchttürme eMobilität" (grant number 865447).

6 References

[1] Communication from the Commission to the European Parliament, the European Council, the Council, the European Economic and Social Committee and the Committee of the Regions: The European Green Deal, 2019.

[2] Austrian Federal Government. Government program 2020-2024: Out of a Sense of Responsibility for Austria. Available online: https://www.bmoeds.gv.at/Ministerium/Regierungsprogramm.html (accessed on 31 January 2020).

[3] Association of Austrian Electricity Companies. Netzberechnungen Österreich - Einfluss der Entwicklungen von Elektromobilität und Photovoltaik auf das österreichische Stromnetz. Available online: www.oesterreichsenergie.at/die-welt-des-stroms/stromnetze/studie-netzberechnungen-oesterreich.html.

[4] Joos, G.; Freige, M. de; Dubois, M. Design and simulation of a fast charging station for PHEV/EV batteries. Electrical Power and Energy Conference (EPEC), August 25-27, 2010, Halifax, NS, Canada

[5] Gabbar, H.A.; Othman, A.M. Flywheel-Based Fast Charging Station – FFCS for Electric Vehicles and Public Transportation. 2nd International Conference on Green Energy Technology (ICGET 2017), 18–20 July 2017, Rome, Italy.

[6] Fahad, A.H.; Gabbar, H.A. Wireless Flywheel-Based Fast Charging Station (WFFCS). 2018 IEEE International Conference on Renewable Energy and Power Engineering (REPE 2018), November 24-26, 2018, Toronto, Canada.

[7] Amiryar, M.; Pullen, K. A Review of Flywheel Energy Storage System Technologies and Their Applications. Applied Sciences 2017, 7, 286, doi:10.3390/app7030286.

[8] Khodaparastan, M.; Mohamed, A. Flywheel vs. Supercapacitor as Wayside Energy Storage for Electric Rail Transit Systems. Inventions, 4(4), 62 2019, doi:10.3390/INVENTIONS4040062.

[9] Dragicevic, T.; Sucic, S.; Vasquez, J.C.; Guerrero, J.M. Flywheel-Based Distributed Bus Signalling Strategy for the Public Fast Charging Station. IEEE Trans. Smart Grid 2014, 5, 2825–2835, doi:10.1109/TSG.2014.2325963.

[10] Offcial Site of the FlyGrid project. Available online: https://www.tugraz.at/en/projekte/flygrid/home/ (accessed on 28 July 2020).

[11] Yan, Y.; Wang, H.; Jiang, J.; Zhang, W.; Bao, Y.; Huang, M. Research on Configuration Methods of Battery Energy Storage System for Pure Electric Bus Fast Charging Station. Energies 2019, 12, 558, doi:10.3390/en12030558.

[12] Thormann, B.; Kienberger, T. Grid-friendly Integration of Future Public Charging Infrastructure by Flywheel Energy Storage Systems (FESS). NEIS 2019 - Conference on Sustainable Energy Supply and Energy Storage Systems.

[13] Thormann, B.; Puchbauer, P.; Kienberger, T. Analyzing the suitability of flywheel energy storage systems for supplying high-power charging e-mobility use cases. Journal of Energy Storage 2021, 39, 102615, doi:10.1016/j.est.2021.102615.

[14] Austrian Federal Ministry of Transport, Innovation and Technology: Ergebnisbericht zur österreichweiten Mobilitätserhebung „Österreich unterwegs 2013/2014“, Vienna, 2016.

[15] Deutsche Bahn Connect GmbH. Archive data of Flinkster car sharing bookings. Available online: https://data.deutschebahn.com/dataset/data-flinkster.html.

[16] Autobahnen- und Schnellstraßen-Finanzierungs-Aktiengesellschaft. Location-based traffic count data, 2019. Available online: https://www.asfinag.at.

[17] Fraunhofer Institute for Systems and Innovation Research. REM 2030 Driving Profiles, 2019. Available online: https://www.rem2030.de/rem2030-de/REM-2030-Driving-Profiles.php.

[18] Thormann, B.; Kienberger, T. Evaluation of Grid Capacities for Integrating Future E-Mobility and Heat Pumps into Low-Voltage Grids. Energies 2020, 13, 5083, doi:10.3390/en13195083.

[19] Buchroithner, A.; Wegleiter, H.; Schweighofer, B. Flywheel Energy Storage Systems Compared to Competing Technologies for Grid Load Mitigation in EV Fast-Charging Applications. 2018 IEEE 27th International Symposium on Industrial Electronics (ISIE), 13 - 15 June, 2018, Cairns, Australia.

[20] A. Buchroithner, C.V. Enabling Flywheel Energy Storage for Renewable Energies - Testing of a low-cost, low-friction bearing configuration. 12. VDI-Fachtagung Gleit- und Wälzlagerungen.

11 APPENDIX B: ADDITIONAL CONFERENCE PROCEEDINGS AND SCIENTIFIC ARTICLES

Buchroithner, A., Preßmair, R., Haidl, P., Wegleiter, H., **Thormann, B.**, Kienberger, T., et al., *Grid Load Mitigation in EV Fast Charging Stations Through Integration of a High-Performance Flywheel Energy Storage System with CFRP Rotor*, In: IEEE Green Energy and Smart Systems Conference proceedings, November 2021, Long Beach, CA, USA

Thormann, B., Purgstaller, W., Kienberger, T., *Evaluating the potential of future e-mobility use case for providing grid ancillary services*, In: CIRED 2021 conference proceedings, September 2021, Geneva, Switzerland

Thormann, B. & Kienberger, T., Comparison of electromobility-impacts on the low-voltage level in different grid regions, In: 2nd E-Mobility Power System Integration Symposium proceedings, October 2018, Stockholm, Sweden

Thormann, B., Vopava, J., Braunstein, R. & Kienberger, T., Auswirkungen einphasiger Ladevorgänge von Elektrofahrzeugen auf städtische Niederspannungsnetze, In: EnInnov 2018 proceedings, February 2018, Graz, Austria

Vopava, J., Kienberger, T., Hammer, A., **Thormann, B.**, Kriechbaum, L., Sejkora, C., et al., *Move2Grid - Umsetzung regionaler Elektromobilitätsversorgung durch hybride Kopplung*, Finaler Endbericht, 2018

Vopava, J., Sejkora, C., **Thormann, B.** & Kienberger, T., *Nachhaltige Versorgung regionaler Elektromobilität aus regionalen erneuerbaren Ressourcen*, In: WING-Business, 2018

Vopava, J., **Thormann, B.** & Kienberger, T., *Development of a Model for Power Grids Based on the Cellular Approach for an Optimum Integration of Electric Charging Infrastructure*, In: 1st E-Mobility Power System Integration Symposium proceedings, October 2017, Berlin, Germany